STRUCTURE, SEISMICITY AND TECTONICS OF THE PORTER'S PASS-AMBERLEY FAULT ZONE, NORTH CANTERBURY, NEW ZEALAND.

A thesis
submitted in partial fulfilment
of the requirements for the Degree
of

Doctor of Philosophy

in the
University of Canterbury

by

Hugh Allister Cowan

University of Canterbury
1992

La dernière chose qu'on trouve en faisant
un ouvrage, est de savoir celle qu'il faut mettre la première.

The last thing one knows in constructing a work is what to put first.

Blaise Pascal (1623-1662)

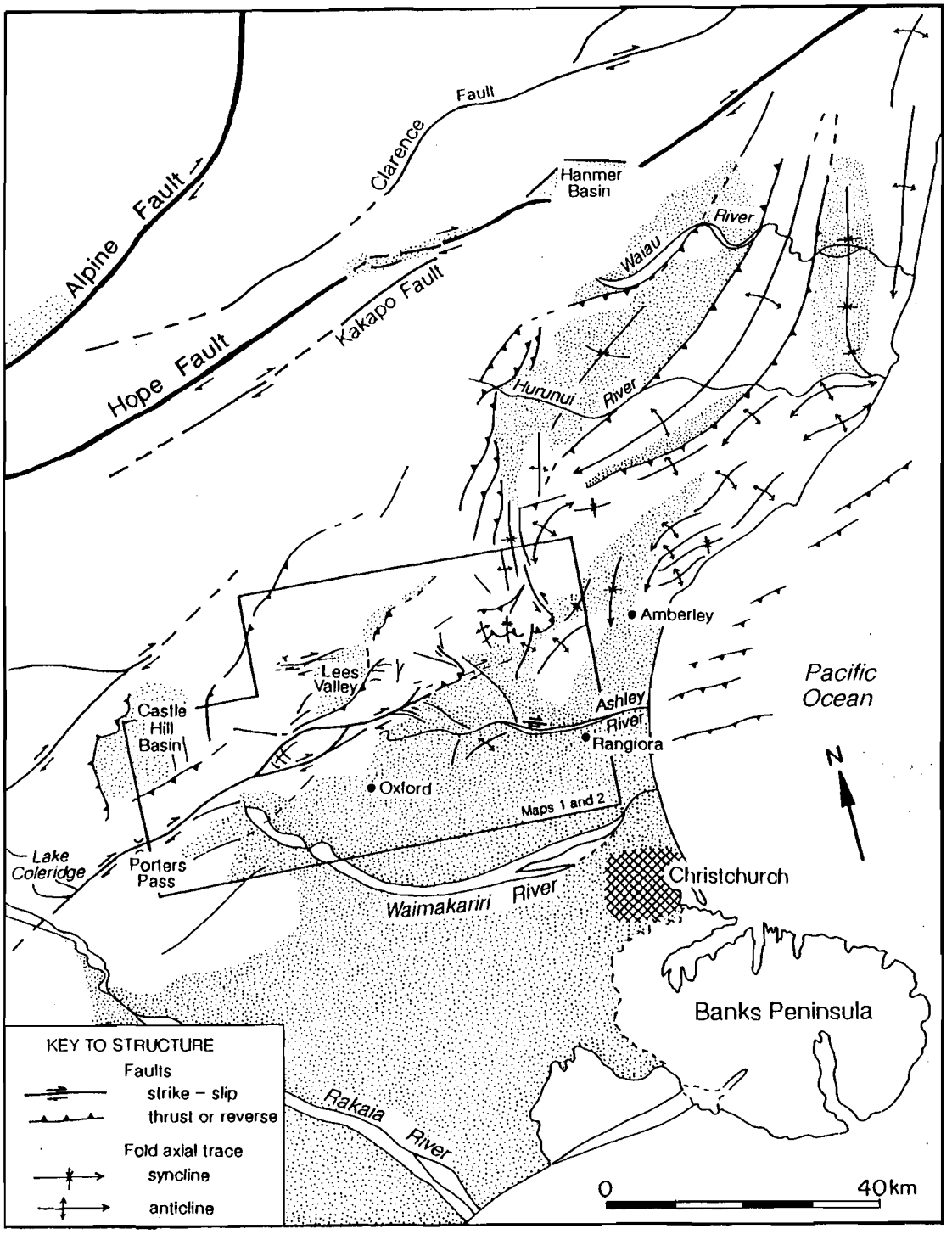

Frontispiece 1. Landsat image and accompanying line drawing of North Canterbury, South Island, showing major structural elements, geographic features and the area mapped in this study. Stipple pattern corresponds to areas of Late Quaternary alluvium. Landsat image processed by NZ DSIR Division of Information Technology (1991). Geological structure from Gregg (1964); Nicol (1991); R. Mould (pers.comm. 1992); and this study. Preliminary offshore structure (P. Barnes pers.comm. 1992).

MAPS 1 & 2

Frontispiece 2. View northwest across metropolitan Christchurch (pop. 285,000) and the Canterbury Plains, to the eastern ranges of the Southern Alps. The forested Ashley Range and snow-capped Puketeraki Range have been uplifted since the middle Pleistocene, and are traversed by the Porter's Pass-Amberley Fault Zone, of which the Cust Anticline (back-lit by morning sun) is an active element within 35 km of central Christchurch.


Cust Anticline

Frontispiece 3. Oblique aerial view northeast across accordant summits of the Ashley and Okuku Ranges, along the northern margin of the Canterbury Plains. Embayments in the range-front represent synclinal cross-folds, developed in basement perpendicular to the strike of the Porter's Pass-Amberley Fault Zone, which defines the leading edge of the plate boundary deformation front in North Canterbury.

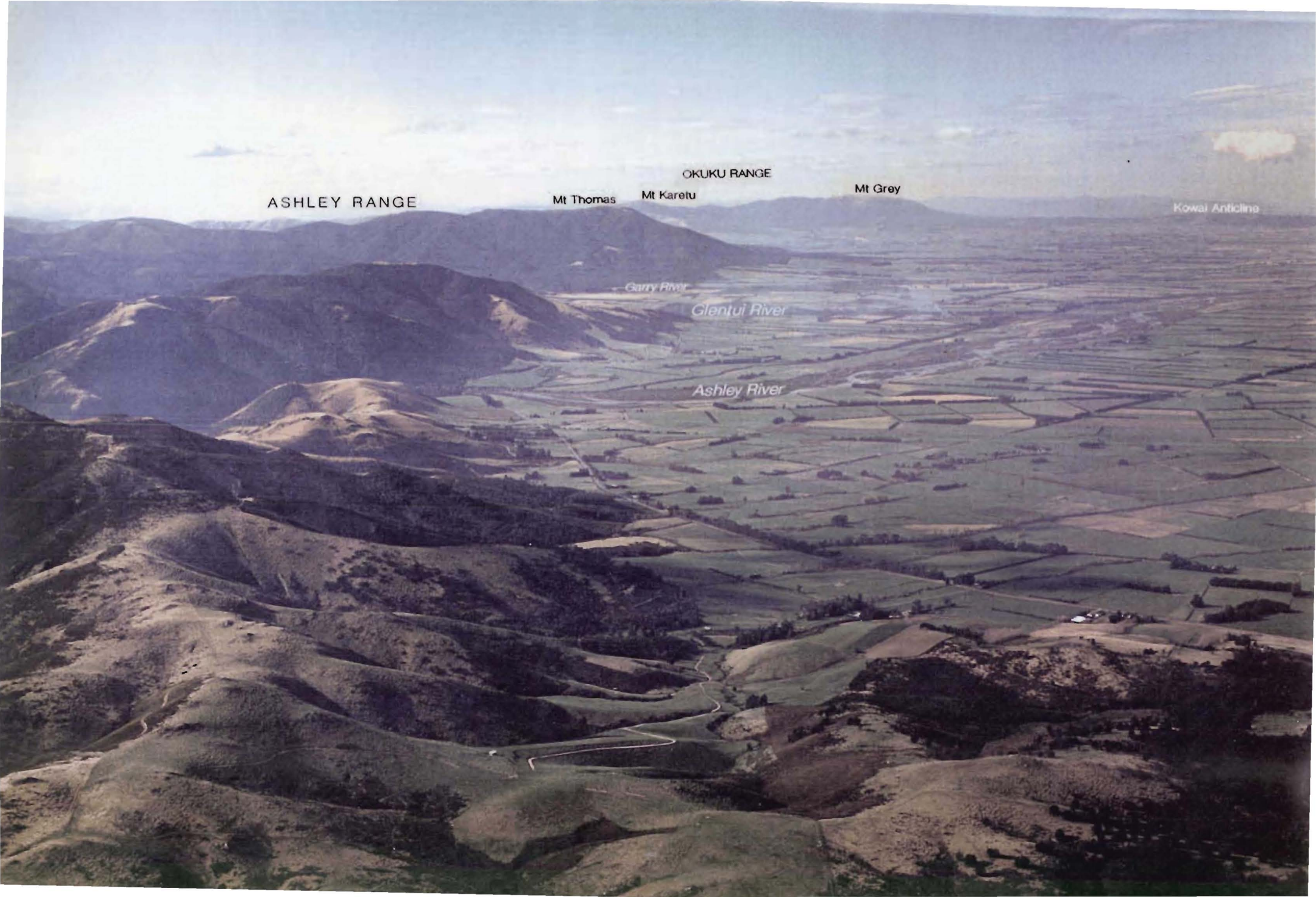
ASHLEY RANGE
Mt Thomas
Mt Karetu
OKUKU RANGE
Mt Grey
Kowai Anticline
Garry River
Glentui River
Ashley River

ABSTRACT

The Porter's Pass-Amberley Fault Zone (PPAFZ) is a complex zone of anastomosing faults and folds bounding the southeastern edge of the transition from subducting Pacific Plate to continental collision on the Australia Plate boundary. This study combines mapping of a 2000 km^2 zone from the Southern Alps northeast to the coast near Amberley, 40 km north of metropolitan Christchurch, with an analysis of seismicity and a revision of regional seismic hazard.

Three structural styles: 1) a western strike-slip, and 2) a more easterly thrust and reverse domain, pass into 3) a northwest verging fold belt on the northern Canterbury Plains, reflecting the structural levels exposed and the evolving west to east propagation. Basal remnants of a Late Cretaceous-Cenozoic, largely marine sedimentary cover sequence are preserved as outliers that unconformably overlie Mesozoic basement (greywacke and argillite of the Torlesse terrane) in the mountains of the PPAFZ and are underlain by a deeply leached zone which is widely preserved. Structure contouring of the unconformity surface indicates maximum, differential uplift of c.2600 m in the southwest, decreasing to c.1200 m in the coastal fold belt to the northeast. Much lower rates (or reversal) of uplift are evident a few kilometres southeast of the PPAFZ range-front escarpment.

The youngest elements of the cover sequence are basement-derived conglomerates of Plio-Pleistocene age preserved on the SE margin. The source is more distant than the intervening mountains of the PPAFZ, probably from the Southern Alps, to the west and northwest. The absence of another regional unconformity on Mesozoic basement, older than Pleistocene, indicates that this uplift is post-Pliocene. Late Pleistocene (<100 kyr) differential uplift rates of c.0.5-2.7 m/kyr from uplifted marine terraces at the east coast, and rates of 2.5-3.3 m/kyr for tectonically-induced river-downcutting further west, suggest that uplift commenced locally during the last 1 Ma, and possibly within the last 0.5 Ma, if average rates are assumed to be uniform over time.

Analysis of seismicity, recorded during a 10 week regional survey of microearthquakes in 1990, identified two seismic zones beneath North Canterbury: 1) a sub-horizontal zone of activity restricted to the upper crust (≤12 km); and 2) a seismic zone in the lower crust (below a ceiling of ≤17 km), that broadens vertically to the north and northwest to a depth of c.40 km, with a bottom edge which dips 10°N and 15°NW, respectively. No events were recorded at depths between 12 km and 17 km, which is interpreted as a relatively aseismic, mid-crustal ductile layer.

Marked differences (up to 60°) in the trend of strain axes for events above and below the inferred ductile layer, are observed only north of the PPAFZ. A fundamental, north-to-south increase in the wavelength of major geological structures occurs across the PPAFZ, and is

interpreted as evidence that the upper crust beneath the Canterbury Plains is coupled to the lower crust, whereas the upper crust further north is not. Most of the recorded microearthquakes <12 km deep beneath the PPAFZ have strike-slip mechanisms. It is probable that faults splay upward into the thrusts and folds at the surface as an evolving transpression zone in response to deep shear in basement.

There have been no historic surface ruptures of the PPAFZ, but the zone has been characterised historically by frequent small earthquakes. Paleoseismic data (dated landslides and surface ruptures) compiled in this study, indicate a return period of 1500-1900 years between the last two M>7-7.5 earthquakes, and 500-700 years have elapsed since the last. The magnitudes of these events are estimated at c.M7.5, which represents a probable maximum magnitude for the PPAFZ. There are insufficient data to determine whether or not the frequency of large earthquakes conforms to a recognised model of behaviour, but comparison of the paleoseismic data with the historic record of smaller earthquakes, suggests that the magnitudes of the largest earthquakes in this zone are not exponentially distributed. A seismicity model for the PPAFZ (Elder et al., 1991) is reviewed, and a b-value of 1.0 is found to be consistent with the newly acquired paleoseismic data. This b-value reduces the predicted frequency of large earthquakes ($M \geq 7.0$) in this zone by a factor of 3.5, while retaining a conservative margin that allows for temporal variations in the frequency of large events and the possibility that the geological database is incomplete, suggesting grounds for revising the hazard model for Christchurch.

TABLE OF CONTENTS

CHAPTER 1. INTRODUCTION 1
1.1 BACKGROUND TO THE STUDY 1
1.2 PURPOSE AND SCOPE 4
1.2.1 Introduction 4
1.2.2 Field mapping 6
1.2.3 Microearthquake study 6
1.3 OUTLINE OF NORTH CANTERBURY GEOLOGY 8
1.3.1 Introduction 8
1.3.2 Basement rocks 11
1.3.3 Cretaceous-Cenozoic Cover Sequence 14
1.4 PHYSIOGRAPHY OF THE STUDY AREA 16
1.5 THESIS ORGANISATION 16

CHAPTER 2 PRINCIPLES AND METHODS 17
2.1 INTRODUCTION 17
2.2 FIELD WORK 17
2.2.1 Logistics 17
2.2.2 Rationale 17
2.2.3 Mapping base 18
2.3 MAPPING 18
2.4 MAP PRODUCTION 19
2.4.1 Use of colour 19
2.5 MICROEARTHQUAKE STUDY 20
2.5.1 Network design and instrumentation 20
2.5.2 Field servicing 22
2.5.3 Data Processing 22
2.5.4 Magnitudes 25
2.5.5 Epicentral plots, cross sections and focal mechanisms 25

CHAPTER 3. STRUCTURE AND TECTONICS OF THE PORTER'S PASS-AMBERLEY FAULT ZONE 27
3.1 INTRODUCTION 27
3.2 CRITERIA FOR THE RECOGNITION OF ACTIVE STRUCTURES . 27
3.3 STRUCTURAL ELEMENTS OF THE STRIKE-SLIP DOMAIN 29
3.3.1 Porter's Pass Fault: Porters Pass to Waimakariri River 29
3.3.2 Mt Oxford Duplex: Townshend Fault Zone 29
3.3.3 Mt Oxford Duplex: Coopers Creek Fault Zone 31
3.3.4 Mt Oxford Duplex: Cross-faults 31
3.3.5 Glentui Fault Zone 33
3.3.6 Porters Pass Fault : Woodstock to Oxford 33
3.3.7 Whistler Fault Zone 35
3.4 STRUCTURAL ELEMENTS OF THE THRUST AND REVERSE FAULT DOMAIN 36
3.4.1 Lees Valley Fault 36
3.4.2 Okuku River to South Branch Waipara River 36
3.4.3 Mt Thomas Fault Zone 40
3.4.4 Mt Karetu-Mt Grey Fault Zone 42
3.5 NORTHWEST-VERGING FOLD DOMAIN 42
3.5.1 Introduction 42
3.5.2 Kowai Anticline 44
3.5.3 Cust Anticline 44
3.5.4 Cust Fault 44
3.5.5 Ashley Fault 45
3.6 TIMING OF DEFORMATION IN THE PPAFZ 45
3.6.1 Evidence for Tertiary deformation 45
3.6.2 Quaternary inception of the PPAFZ 46

3.7 KINEMATICS OF QUATERNARY FAULTING IN THE PPAFZ 47
3.7.1 Thrust and reverse fault domain 47
3.7.2 Strike-slip domain 49
3.7.3 Holocene slip-rates 49
3.8 FOLDING AND QUATERNARY UPLIFT IN THE PPAFZ 50
3.9 RATE AND TIMING OF UPLIFT 58
3.9.1 Uplift rate for the Ashley Range 58
3.9.2 Uplift rates from Pleistocene marine terraces at the east coast 59
3.10 SUMMARY 62

CHAPTER 4. KINEMATICS OF CRUSTAL DEFORMATION IN NORTH CANTERBURY FROM MICROEARTHQUAKES 66
4.1 INTRODUCTION 66
4.2 DATA 66
4.3 HYPOCENTRAL LOCATIONS (Appendix 4.4) 67
4.3.1 Regional seismicity 67
4.3.2 Porter's Pass-Amberley Fault Zone 67
4.4 FAULT-PLANE SOLUTIONS 73
4.4.1 Introduction 73
4.4.2 Upper seismic zone 73
4.4.3 Lower seismic zone 78
4.5 CONTRACTIONAL STRAIN AXES 78
4.6 TENSILE STRAIN AXES 78
4.8 SLIP VECTORS 85
4.9 DISCUSSION 85
4.9.1 Regional seismicity 85
4.9.2 Seismicity and geological structure of the PPAFZ . 88
4.10 SUMMARY 91

CHAPTER 5. SEISMIC HAZARD ASSESSMENT FROM FAULT RUPTURE AND LANDSLIDES ALONG THE PORTERS PASS-AMBERLEY FAULT ZONE 94
5.1 INTRODUCTION 94
5.2 TIMING OF SURFACE RUPTURES 94
5.2.1 Porters Pass Fault 94
5.2.2 Cust Anticline and Ashley Fault 98
5.2.3 Mt Grey Fault 101
5.3 LANDSLIDES 103
5.4 RELATIONSHIP BETWEEN SURFACE RUPTURES AND LANDSLIDES . . . 106
5.5 MAGNITUDES 106
5.6 DISCUSSION 113
5.6.1 Implications for recurrence of large earthquakes . 113
5.6.2 Implications for seismic hazard assessment 115
5.7 CONCLUSIONS 116

CHAPTER 6. SYNTHESIS AND CONCLUSIONS 119
6.1 INTRODUCTION 119
6.2 CRUSTAL STRUCTURE IN NORTH CANTERBURY: THE TRANSITION FROM SUBDUCTION TO CONTINENTAL COLLISION 121
6.2.1 Crustal structure from earthquake hypocentres . . 121
6.2.2 Strain axes and evidence for a mid-crustal detachment beneath North Canterbury 121
6.2.3 Geological evidence for a mid-crustal detachment . 122
6.3 SEISMICITY, STRUCTURE AND QUATERNARY TECTONICS OF THE PORTER'S PASS-AMBERLEY FAULT ZONE 124
6.3.1 Structural domains and kinematics of near-surface deformation 124
6.3.3 Relationship between seismicity and geological structure of the PPAFZ 125
6.3.2 Amount and rate of Quaternary uplift 126

6.4 SEISMIC HAZARD 128
6.4.1 Proximity of seismogenic structures to Christchurch 128
6.4.2 Proximity of seismogenic faults to towns on the northern Canterbury Plains 129
6.4.3 Maximum magnitudes 130
6.4.4 Seismicity model for PPAFZ 130
6.5 FINAL STATEMENT AND RECOMMENDATIONS FOR FUTURE WORK . . . 131

REFERENCES 135

APPENDICES 152

ABSTRACT i

LIST OF TABLES vi

LIST OF FIGURES vii

LIST OF APPENDICES xi

LIST OF SHEETS IN MAP POCKET xii

ACKNOWLEDGEMENTS xiii

LIST OF TABLES

5.1 Data of prehistoric surface ruptures in the Porter's Pass-Amberley Fault Zone .....96 and 97

5.2 Dated landslides of the Porter's Pass-Amberley Fault Zone.....107

5.3 Inferred magnitudes for prehistoric earthquakes in the Porter's Pass-Amberley Fault Zone.....110

LIST OF FIGURES

1.1 Elements of the Australia-Pacific plate-boundary in New Zealand . 2

1.2 Historic North Canterbury earthquakes responsible for shaking of MMV or greater at Christchurch 3

1.3 Seismicity (M≥3) in central South Island: 1964-1991 5

1.4 Map of known tectonic structure in North Canterbury prior to this study 7

1.5 Map showing station and shot locations for the 1990 North Canterbury Microearthquake Network 9

1.6 Map of the New Zealand Seismograph Network, showing stations used to supplement the 1990 North Canterbury Network 10

1.7 Mesozoic terrane map of South Island, showing principal constituents of the Torlesse terrane basement in North Canterbury 12

1.8(a) Photo example of indurated, alternating sandstone-siltstone of the Rakaia subterrane (greywacke-argillite basement) in the study area 13

1.8(b) Photo example of pervasively sheared greywacke of the Esk Head Melange in the eastern part of the study area . 13

1.9 Nomenclature and correlation diagrams for the Cretaceous-Cenozoic cover sequence in Central and North Canterbury 15

2.1 Sample seismograms and first-motions of an event recorded on the North Canterbury Microearthquake Network 24

3.1 Enlargement of LANDSAT photograph of the Porter's Pass-Amberley Fault Zone (PPAFZ) showing areas of contrasting structural styles 28

3.2 Oblique aerial photo, view NE along strike of PPAFZ from Waimakariri River Gorge 30

3.3 Photo of crushed basement associated with the Porter's Pass Fault in the lower reaches of Coal Creek, Waimakariri River Gorge . . 32

3.4 Late Quaternary fault offset exposed in the west branch of Cooper's Creek, south side of Mt Oxford Duplex 32

3.5 Quartz-mineralised fault breccia associated with NW-SE trending cross-faults of the Mt Oxford Duplex 34

3.6 Oblique aerial view SE across Lees Valley, to Mt Oxford and Townshend Valley 37

3.7 Crushed basement associated with the Lees Valley Fault, thrust NW over Lower Tertiary sandstone, SE side of Lees Valley . . . 38

3.8 View northeast along sinuous surface trace of the Lees Valley Fault 38

3.9 Oblique aerial view NE along Holocene surface trace associated with the eastern end of the Lees Valley Fault 39

3.10 Oblique aerial view NE to Mt Karetu and Mt Grey, showing folded strike-ridge of Lower Miocene limestone, and geomorphology of surrounding area 41

3.11 View SE from lower slopes of Mt Karetu to Mt Thomas and Hillside Anticline, Okuku River 43

3.12 Photo example of Kowai Formation conglomerate 43

3.13 Photo example of angular, locally-derived fan debris unconformably overlying Kowai Formation of Fig.3.12 43

3.14 Photo example of coarse, angular debris that forms a large and deeply-dissected fan on the slopes of Mt Karetu 48

3.15(a) Remnant, high-level strath terraces in the Ashley River Gorge, Lees Valley Road 51

3.15(b) Ashley River Gorge and river-bed viewed from the Lees Valley Road 51

3.15(c) Saw-cut gorge of the GlentuiRiver 51

3.16(a) Strongly leached basement beneath the Late Cretaceous unconformity, Field Road, Ashley Forest 52

3.16(b) Strongly leached basement beneath the Late Cretaceous unconformity, Horsford Downs Road, Ashley Forest 52

3.17 Structure contour map of the Late Cretaceous unconformity surface in the study area 53

3.18 The inferred fold-depression of the Bald Hills-Garry River area 54

3.19 Photo view west across the Late Cretaceous unconformity surface at Round Hill, Okuku River 55

3.20 Remnants of the unconformity surface back-lit by morning light on the southern slopes of Mt Karetu 55

3.21 Cartoon showing how the total differential Quaternary uplift in the study area is estimated from the thickness of cover sequence and height of the Late Cretaceous unconformity surface 57

3.22 Late Pleistocene aggradation terrace surface in the Ashley Gorge 60

3.23 Marine terrace terminology 60

4.1 Map showing station locations of the 1990, North Canterbury Microearthquake Network and epicentres for all recorded events 68

4.2 Epicentres for all shallow (<12 km) events within the North Canterbury Network 69

4.3 Epicentres for all deep (>17 km) events within the North Canterbury Network 69

4.4 Map showing epicentres for all events within the North Canterbury Network and azimuths for cross-sections 70

4.5(a) SW-NE regional cross-section all events (azimuth 050°) . 71

4.5(b) NW-SE regional cross-section all events (azimuth 140°) . 71

4.6(a) SW-NE cross-section of events in the PPAFZ (azimuth 060°) 72

4.6(b) NW-SE cross-section of events in the PPAFZ (azimuth 150°) 72

4.7 Map of fault-plane solutions for shallow (<12 km) events within the North Canterbury Network 74

4.8 Highest quality fault-plane solutions for sub-set of shallow (<12 km) events 75

4.9 Locations and fault-plane solutions for all shallow events in the PPAFZ 76

4.10 Map of principal faults of the Castle Hill Basin, west end of study area, showing locations and fault-plane solutions of two pure thrust events beneath the Craigeburn Range 77

4.11(a) Fault-plane solutions for all deep (>17 km) events in the North Canterbury Network 79

4.11(b) Highest quality fault-plane solutions for sub-set of deep (>17 km) events 79

4.12(a) P-axes for all shallow events 80

4.12(b) P-axes for all deep events 80

4.13 P-axes for all shallow events in the PPAFZ 81

4.14(a) T-axes for all shallow events 82

4.14(b) T-axes for all deep events 82

4.15 T-axes for all shallow events in the PPAFZ 83

4.16 Comparison of P-axes (a & b), and T-axes (c & d), for a subset of shallow and deep events 84

4.17 Slip-vectors for highest quality fault-plane solutions of shallow events in the PPAFZ 86

4.18 Slip-vectors for all shallow events in the PPAFZ 87

4.19 Fault-plane solution for Ms 5.8 event recorded in 1965, beneath the North Chatham Slope, offshore North Canterbury 89

4.20 Fault-plane solutions for shallow events in the PPAFZ combined with epicentres of historic events located by the National Seismograph Network 90

5.1 Major structural elements of the PPAFZ and locations of prehistoric landslides 95

5.2 Trench log showing cross-cutting relationships between faults and buried soils in the crushed zone of the Porter's Pass Fault at Porter's Pass 99

5.3 Oblique aerial view, west along the Ashley River and northern limb of the Cust Anticline 100

5.4 Articulated lower leg and toe bones of a *Diornis giganteus*, recovered from a landslide on the northern limb of the Cust Anticline . . 102

5.5 The surface trace of the Mt Grey Fault at Onepunga Station, east flanks of Mt Grey 104

5.6 Trench log of cross-cutting relationships between the Mt Grey Fault and a series of debris flow deposits 105

5.7 Temporal clustering of landslides and surface ruptures in the PPAFZ compared with landslides from the Southern Alps 108

5.8 Comparison of relationship between landsliding and earthquake magnitude for three historic earthquakes in northern South Island, and that of global compilation by Keefer (1984) 111

5.9 Spatial distribution of dated landslides by age group, in the PPAFZ and Southern Alps 112

5.10 Comparison of the relationship between recurrence-frequency distribution for historic (instrumental) seismicity of the PPAFZ, and that of prehistoric (late Holocene) earthquakes identified in this study 117

LIST OF APPENDICES

3.1 Locations of strongly leached basement beneath the Late Cretaceous unconformity in the Porter's Pass-Amberley Fault Zone.....153

4.1 Station and shot locations for the 1990 North Canterbury Microearthquake and Crustal Structure study.....156

4.2 Summary of the technical performance of the North Canterbury Microearthquake Network.....158

4.3 Derivation of the seismic velocity model from inversion of explosion travel-times and earthquakes.....161

4.4 Hypocentre listing of events recorded on the North Canterbury Microearthquake Network: September 01 - November 15, 1990.....162

4.5 Fault-plane solutions.....167

4.6 Listing of events for fault-plane solutions.....170

4.7 Lower hemisphere projections of P-wave first-motions for fault-plane solutions listed in Appendix 4.6.....172

5.1 Regression analysis of the relationship between landsliding and earthquake magnitude for three historic earthquakes in northern South Island.....178

5.2 Derivation of parameters for a Porter's Pass-Amberley Fault Zone seismicity model.....180

LIST OF SHEETS IN MAP POCKET

MAP 1 Active tectonic structure of the Porter's Pass-Amberley Fault Zone: **Geology and Structure.** . . . . . .

MAP 2 Active tectonic structure of the Porter's Pass-Amberley Fault Zone: **Topography and structure.** . . . . . .

MAPS 3 & 4 Geomorphology of the Cust Anticline and Ashley Fault, northwestern Canterbury Plains. . . . . .

Geological cross-sections of the Porter's Pass-Amberley Fault Zone (1 Sheet).

Geological Map of New Zealand, SHEET 18 "HURUNUI" : Gregg, D.R. (1964)

ACKNOWLEDGEMENTS

This thesis represents the product of a three year study at the University of Canterbury, where I held a University Grants Committee Postgraduate Scholarship. The project was conceived by Jarg Pettinga and Jocelyn Campbell (University of Canterbury), and Martin Reyners (DSIR Geology & Geophysics). Without their foresight, experience and hard work, neither the funds nor technical resources necessary to support this project would have materialised. At the same time, I have enjoyed the freedom to set research priorities within broad parameters, for which I am particularly grateful.

The material costs of research were met by the Earthquake and War Damages Commission (EQC), with additional sponsorship from DSIR (Geology & Geophysics) and the Institute of Geophysics, Victoria University of Wellington (V.U.W.), for the North Canterbury microearthquake study. I gratefully acknowledge this support, and the opportunity it provided to work with and interact among a wide group of scientists.

Andy Nicol was advanced in his study of late Cenozoic deformation in the Waipara area when I commenced this study, and I have been fortunate to work closely with him. We mapped the Mt Grey block together - between the east branch of Grey River and Boby's Creek (Maps 1 and 2: pocket). Our most recent collaborative work (Cowan and Nicol, in prep.), is encapsulated in Chapter 5 of this thesis.

With respect to Chapter 5, I also thank Phil Tonkin, Brian Molloy and Neville Moar for providing unpublished radiocarbon dates and trench logs, relating to prehistoric ruptures of the Porter's Pass Fault; and staff of Soils and Foundations Ltd for pre-prints of their seismic hazard analysis for Christchurch: Elder et al. (1991). The revision in this study, of elements of their work relating specifically to the Porter's Pass-Amberley Fault Zone, arises naturally from the consideration of new data and should not to be interpreted as a negative criticism of their work.

Malcolm Laird (DSIR Geology & Geophysics) allowed me to refer to numerous unpublished measured sections of the North Canterbury cover sequence, and Mike Broadbent and Roly Jenkins (DSIR Geology & Geophysics) provided unpublished gravity and seismic refraction data from the Waimakariri Gorge area. Len Brown (DSIR Geology & Geophysics) provided tables and diagrams from a pre-print on borehole data in the Christchurch area. The Department of Survey and Land Information (Wellington), permitted me to reproduce their topographic maps.

Discussion with Rick Herzer (DSIR Geology & Geophysics) on the evolution of ideas about the Porter's Pass-Amberley Fault Zone was very helpful. Rick also went to considerable trouble to try and locate (for re-processing),

unpublished petroleum industry data from seismic reflection surveys of the Canterbury Plains.

Phil Barnes and Keith Lewis (DSIR Oceanographic Institute) provided valuable discussion on the nature of late Cenozoic deformation off the shore of North Canterbury. Two research cruises with them, on the R.V. Rapuhia (April 1990 and July 1991), were memorable experiences that greatly expanded our knowledge (and uncertainties) about crustal structure in this region.

Apart from the Mt Grey block (defined above) I mapped the PPAFZ single-handedly, but the results are proportional to the encouragement and feedback received from colleagues and advisors on different occasions. In this context I acknowledge: Andy Nicol, Jarg Pettinga, Jocelyn Campbell, Phil Tonkin, Bill Bull, John Crowell, Phil Barnes, Rose Fitzgerald, Richard Garlick, Richard Mould, Alan Hull, Mark Yetton, John Berrill, Steve Weaver, Jane Newman, John Bradshaw, David Nobes and Rod Muir.

On occasions in the field I enjoyed good company with sharp eyes and keen minds (not just extra hands). Day-trips with Jocelyn, Jarg, Andy, and John Crowell were both enjoyable and helpful. My wife, Jeanine Keller accompanied me during some of the most arduous mapping of the Whistler catchment and Puketeraki Range, and Dave Connelly and Viktor Hunkeler did the same on different occasions in the Townshend and Waimakariri Valleys, respectively. I acknowledge and thank Graham Mehrtens of View Hill for his skill in negotiating the Waimakariri River Gorge by jet-boat, while ferrying me into inaccessible parts of the Puketeraki Range, and Stuart Cooper; for organising and piloting an aircraft for aerial photography at very short notice. His skilful flying in violent turbulence above the Torlesse Range was reassuring, and might have prevented me from falling from the open door (I later discovered my harness had released in flight).

The study of microseismicity in North Canterbury (and particularly the PPAFZ) was complementary to the field studies of the surface faults, and I am privileged to have been offered a new apprenticeship in seismology. Martin Reyners, John Taber and Tim O'Neill provided instruction during the deployment and operation of the seismograph network. I thank all of the landowners who gave permission to deploy seismographs on their properties.

No landowner refused me permission to enter private property, and during the field mapping several offered welcome respite from foul weather. In this respect, I thank the high-country farmers of Lees Valley and particularly the Le Cren family of Mt Pember Station. Thanks also to Marty Thompson (Department of Conservation, Mt Thomas) for occasional free use of huts, and Bill Balderstone of Carter Holt Harvey Ltd, for providing gate-keys to locked areas of plantation forests.

Seismicity data were processed at the Institute of Geophysics (V.U.W.), and DSIR Geology & Geophysics (Kelburn) where the work environment was exceptionally positive. I am pleased to acknowledge instruction and advice, given freely by: John Taber, Ken Gledhill, Mark Chadwick, Wayne Richardson, Alister Gorman, Jim Ansell, Jim Miller and Pauline Galea (V.U.W.); and Martin Reyners, Helen Anderson, Russell Robinson, Alan Cresswell and the late George Eiby (DSIR).

The "writing-up" has taken place between March and July, 1992 and the task has been a demanding one. It would have been more so, were it not for the willingness of many people to review drafts at short notice, and to assist with various aspects of compilation. Thanks to Albert Downing for reproducing prints from colour slides, to Kelvin MacMillan for providing the negative for Frontispiece 2, and to Richard Garlick for several photos from Lees Valley. Jarg Pettinga and Andy Nicol reviewed all chapters twice, and additional reviews by Jocelyn Campbell (Chapter 1); Martin Reyners, John Taber and Jim Ansell (Chapters 2 and 4); John Bradshaw and Brad Pillans (Chapter 3); and Mauri McSaveney (Chapter 5), have improved the expression and rigour of this thesis. Naturally, I remain responsible for all errors in fact or interpretation.

Finally, I thank Lee Leonard for her skill and patience in draughting and editing many of the diagrams, particularly the large geological maps; Jeanine Keller for many hours spent colouring those maps; and Joan McTurk and Tracy Robinson for assistance with type-setting.

CHAPTER 1. INTRODUCTION

1.1 BACKGROUND TO THE STUDY

North Canterbury is located on the east side of South Island, New Zealand within a zone of active continental deformation, associated with oblique convergence between the Australian and Pacific Plates (Fig. 1.1). A transition from oceanic to continental crust of the Pacific Plate at the southern end of the Hikurangi Trough (c.2000 m isobath) is matched by a transition from westward subduction of oceanic Pacific Plate, to collision and thickening of continental crust juxtaposed across the Alpine Fault and central Southern Alps (Fig. 1.1).

The subducted Pacific Plate is defined seismically by a NW-dipping zone of earthquakes that extend to a depth of more than 200 km beneath northwestern South Island (Robinson, 1991). Seismicity is widespread in the overlying continental crust (Reyners, 1989) and several large, shallow earthquakes ($M>6.5$; depth ≤ 15 km) have occurred since 1850 A.D., including three in North Canterbury (Eiby, 1968; Elder et al. 1991; Fig.1.2). Structure of the upper crust is dominated by east-northeast trending faults and associated folds, that accommodate the transfer of plate motion between the Hikurangi subduction zone and the Alpine Fault. Principal structures include elements of the Marlborough Fault System and further south, the Porters Pass-Amberley Fault Zone (Fig. 1.1; Frontispiece 1).

Many faults in North Canterbury are associated with late Quaternary surface traces (Gregg, 1964: Sheet 18, map pocket), but only one historic earthquake was accompanied by large fault displacements documented at the surface (Hope Fault, 1888: McKay, 1890; Cowan, 1991), and no large earthquakes have occurred here since 1929 (Eiby, 1968; Dibble et al., 1980; Cowan and Pettinga, 1990). However, recent studies (Marden, 1976; Yousif, 1987; Coyle, 1988) have confirmed the youthful but complex character of tectonic deformation in North Canterbury, highlighting the need for more comprehensive and systematic studies.

In 1988, an Active Tectonics Research Group was established in the Department of Geology at University of Canterbury, and several projects since have been completed (Cowan, 1989; McMorran, 1991; Syme, 1991; Nicol, 1991; Garlick, 1992; Mould, 1992).

The first project to be completed under the umbrella programme (Cowan, 1989), involved a detailed re-evaluation of the historic (1888) Hope Fault rupture (Frontispiece 1), a study in which the kinematics and rate of slip on the ruptured (Hope River) segment were defined, and the

Figure 1.1. Elements of the Australia-Pacific plate boundary zone in New Zealand, adapted from Walcott (1984, 1987). The 2000 m isobath defines the transition up-slope from oceanic to continental crust. Arrows denote the velocities of the Pacific with respect to the Australia Plate. Major features of the plate boundary include:

1) subduction of Pacific Plate beneath North Island and northern South Island, accompanied by imbricate thrusting in the east and back-arc spreading and active volcanism in central North Island and offshore further north;

2) N-NE trending strike-slip faults in continental crust of North Island (North Island Shear Belt) and northern South Island (Marlborough Fault System) that accommodate predominately right-lateral displacement between the Hikurangi subduction zone and the Alpine Fault;

3) a zone of continent-continent collision along the Alpine Fault in southern South Island, characterised by crustal thickening and uplift of the Southern Alps;

4) eastward subduction of Australia Plate along the Puysegur Trench and beneath crystalline continental rocks of southwest South Island;

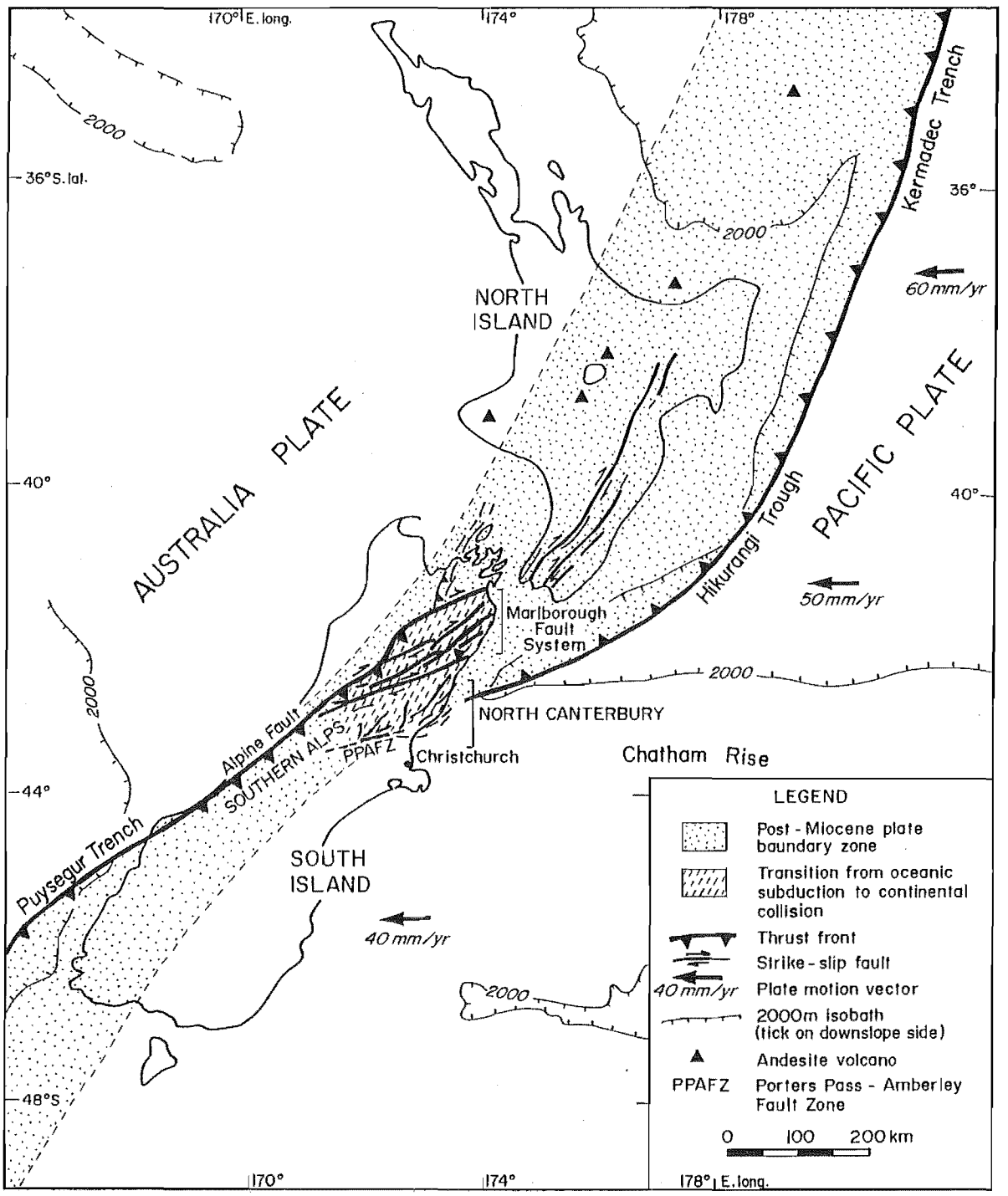
170° E. long.
174°
178°
36° S. lat.
36°
40°
40°
44°
48° S
2000
2000
2000
2000
2000
Kermadec Trench
60 mm/yr
NORTH ISLAND
AUSTRALIA PLATE
PACIFIC PLATE
Hikurangi Trough
50 mm/yr
Marlborough Fault System
NORTH CANTERBURY
Alpine Fault
SOUTHERN ALPS
PPAFZ
Christchurch
Chatham Rise
Puysegur Trench
SOUTH ISLAND
40 mm/yr
LEGEND
Post - Miocene plate boundary zone
Transition from oceanic subduction to continental collision
Thrust front
Strike - slip fault
40 mm/yr
Plate motion vector
2000m isobath (tick on downslope side)
Andesite volcano
PPAFZ
Porters Pass - Amberley Fault Zone
0
100
200 km
170°
174°
178° E. long.

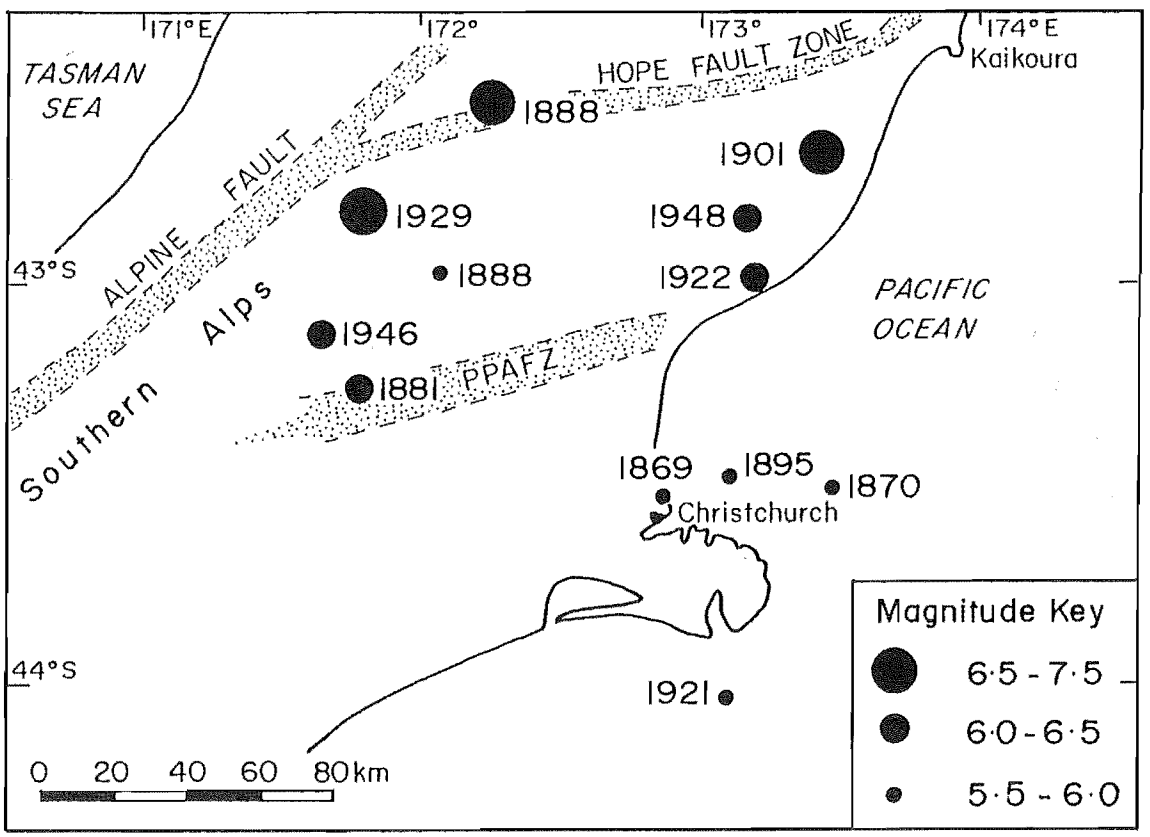

Figure 1.2. Historic (post-1850 A.D.) North Canterbury earthquakes that generated shaking intensities greater than MM V in Christchurch (after Elder et al. 1991). Locations are based largely on felt reports compiled by Eiby (1968); Dibble et al.(1980) and Cowan (1991). Locations for events smaller than M<6.5, are indicative at best.

coseismic rupture history extended into the prehistoric period (Cowan, 1990, 1991; Cowan and McGlone, 1991). The results suggest that the Hope River segment of the Hope Fault and the neighbouring Kakapo Fault (Frontispiece 1) are highly active (14 ±3 m/kyr and 7 ±2 m/kyr, respectively) and represent significant seismic hazards in North Canterbury. Nicol (1991; in press, 1992) demonstrated that southeast of the Hope Fault, deformation is complex and characterised predominately by shortening, with two orthogonal sets of faults and folds developed in basement and cover; both sets are younger than early Pleistocene. This PhD thesis represents the culmination of a three year study of structure, seismicity and tectonics of the Porter's Pass-Amberley Fault Zone.

1.2 PURPOSE AND SCOPE

1.2.1 Introduction

The Porter's Pass-Amberley Fault Zone (PPAFZ) extends northeast, from the Rakaia Valley in the Southern Alps to Amberley near the Pacific coast. The PPAFZ comprises anastomosing faults and block-folded mountains, that traverse the northwestern Canterbury Plains, within 35 km of metropolitan Christchurch (Frontispiece 2, 3).

Several elements of the PPAFZ were identified during early surveys of geology in North Canterbury (e.g. Haast, 1872; Speight and Wild, 1918; Speight, 1924, 1938; Mason, 1941), but only the Porter's Pass Fault (west of Waimakariri River), and Ashley Fault (west of Rangiora) have been reported widely (e.g. Wellman, 1953; Berryman, 1979; Officers of the New Zealand Geological Survey, 1983). Previous interest has focussed on the relationship of the Porter's Pass Fault to the Marlborough Fault System further north (Scholz et al. 1973), and its role of accommodating a southward migration of deformation associated with subduction along the Hikurangi Margin (Rynn & Scholz, 1978; Carter & Carter, 1982; Herzer & Bradshaw, 1985).

There have been no historic ruptures of the PPAFZ, but the zone is better defined seismically than most surface faults in New Zealand (Reyners, 1989; Fig.1.3), and evidence of repeated surface rupture within the last 7000 years has previously been gathered from one locality, on the youngest trace of the Porter's Pass Fault (P. Tonkin and B.J. Molloy unpublished data). In addition, three landslides have been identified and dated adjacent to that fault, the ages tending to corroborate the inference of recent surface rupture (Coyle, 1988).

Figure 1.3. Seismicity in central South Island, 1964-1991. The Porter's Pass-Amberley Fault Zone (delineated by events of magnitude $M \leq 5.3$) is better defined seismically than most surface faults in New Zealand (Reyners, 1989). Data courtesy of the Seismological Observatory, N.Z. DSIR, Wellington.

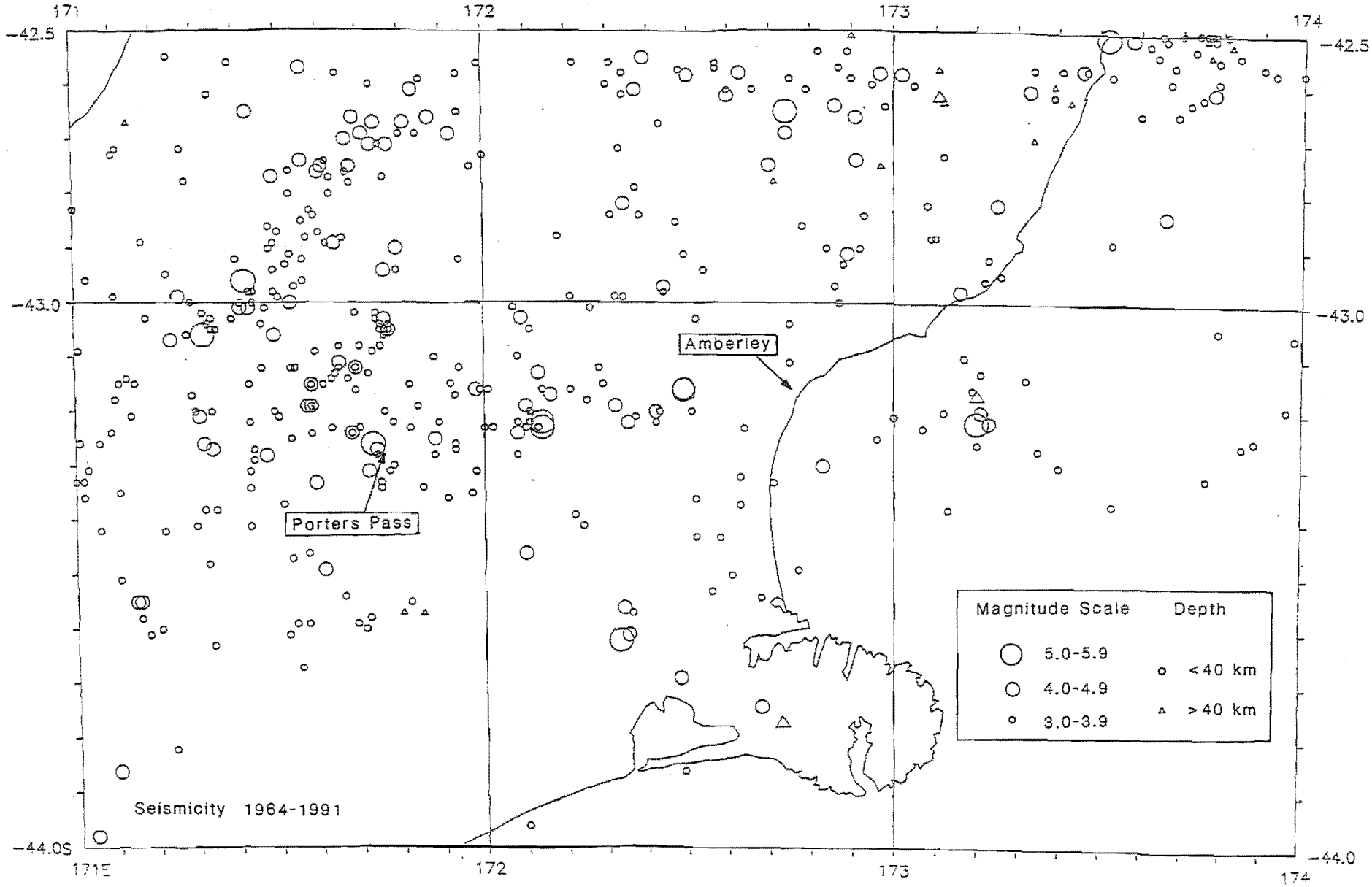
171
172
173
174
-42.5
-43.0
-44.0S
171E
Amberley
Porters Pass
Magnitude Scale
5.0-5.9
4.0-4.9
3.0-3.9
Depth
<40 km
>40 km
Seismicity 1964-1991

1.2.2 Field mapping

It is only recently that the contribution of the PPAFZ to regional seismic hazard has been discussed (Cowan and Pettinga, 1990; Elder et al. 1991). Several faults have late Quaternary displacements (Wilson, 1963; Gregg, 1964; Berryman, 1979; Coyle, 1988; Wilson, 1989), but only a small proportion of the active faults had been mapped prior to this study (see Sheet 18 and Fig.1.4). Thus, a fundamental aim of this study was to systematically document the geometry and spatial extent of the Porter's Pass-Amberley Fault Zone, as a pre-requisite to developing a better understanding of the displacement history of the zone. This necessitated that a large area be mapped, between the Waimakariri River and Mt Grey (Frontispiece 1). Maps 1 and 2 (map pocket) encompass an area of c.2800 km^2 of which approximately 2000 km^2 has been mapped as part of this study. Study objectives were defined as follows:

1) to document the geological structure of the area between Waimakariri River and Mt Grey;

2) to define the geometry and kinematics of Quaternary deformation within the PPAFZ;

3) to quantify ages and rates of deformation of different elements within the zone; and,

4) to determine the timing of prehistoric fault ruptures, and infer the magnitudes and return periods for large earthquakes.

1.2.3 Microearthquake study

Although this PhD research commenced as a geological and geomorphological investigation of surface faults and folds of the PPAFZ, an opportunity arose to conduct a regional survey of microseismicity and crustal structure, in collaboration with DSIR Geology & Geophysics (Kelburn Centre), and the Institute of Geophysics (Victoria University of Wellington). Twenty-four portable, digital seismographs were deployed throughout North Canterbury for 12 weeks during 1990 (1 September - 15 November), for the purpose of recording small earthquakes (Fig.1.5). The data recorded by the portable network were supplemented by that of seven National Network stations, located at larger distances from North Canterbury (Fig.1.6).

These data are the first of their kind to be obtained in this part of South Island, and the recorded hypocentres and earthquake mechanisms provide insight into the character of faulting in the crust. In this aspect of the study I was guided by experienced co-workers, but was

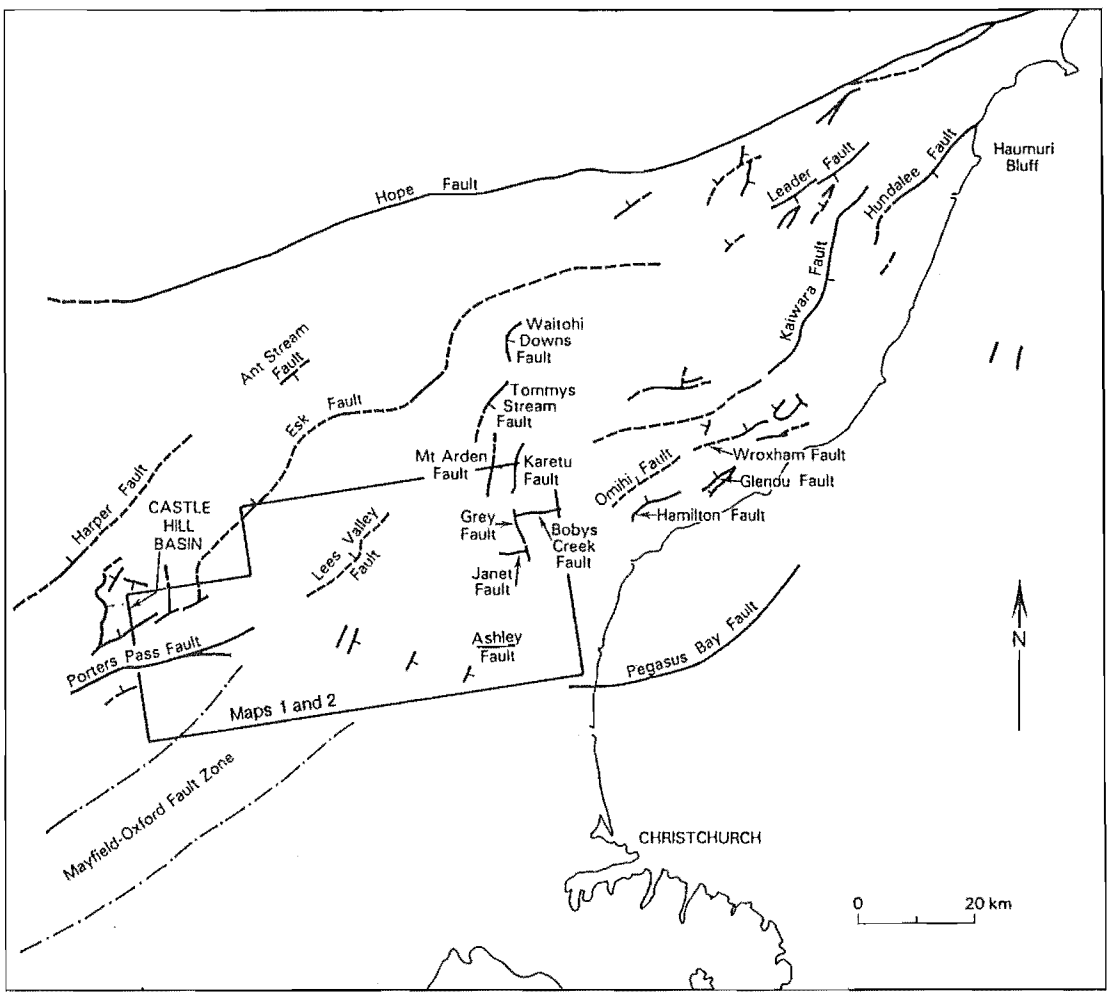

Figure 1.4. Map adapted from Field et al. (1989) comprising a synthesis of structural data available from various sources prior to this study. The box indicates the area of Maps 1 and 2 (this study).

jointly responsible for deploying the network and solely responsible for maintaining and withdrawing it, as well as processing and analysing the data.

A concurrent and complementary study of crustal structure (Reyners & Cowan, in prep.), involved the inversion of travel times for three explosions and a subset of the recorded earthquakes, to develop a seismic velocity model for the North Canterbury crust (Appendix 4.3). This model was used to locate local earthquake hypocentres and determine focal mechanisms for the recorded events (see Chapter 4). Thus, the scope of this thesis was broadened to encompass additional goals:

1) to accurately locate small earthquakes beneath the surface faults of the PPAFZ, and compare the kinematics of faulting at seismogenic depths, with cumulative displacements at the surface;

2) to acquire microseismic data on the kinematics of faulting throughout North Canterbury, for the purpose of understanding the structure and tectonics of the transition between subduction in the northeast, and continental collision to the west; and,

3) to assess the current status of the PPAFZ and its relationship to other elements of the Australia-Pacific plate boundary zone.

1.3 OUTLINE OF NORTH CANTERBURY GEOLOGY

1.3.1 Introduction

The most recently published regional geological map of North Canterbury is that of Gregg (1964: hereafter "Sheet 18" in map pocket). Revised stratigraphic nomenclature of more recently published work is adopted here. Regional stratigraphy consists of **basement** (quartzo-feldspathic greywacke and argillite of Mesozoic age); and **cover sequence** (a c.750-2000 m thick, largely marine succession of clastic, calcareous and detrital sediments, locally interbedded with mafic igneous rocks, ranging in age from late Cretaceous to early Quaternary).

The principal studies of basement rocks in North Canterbury include: Bradshaw (1972); Botsford (1983); Silberling et al. (1988) and Bradshaw (1989). Elements of the formerly widespread cover sequence have been described in detail by numerous authors during the last 100 years. Browne & Field (1985) and Field and Browne (1986) re-measured stratigraphic sections and rationalised local nomenclature. Field et al.

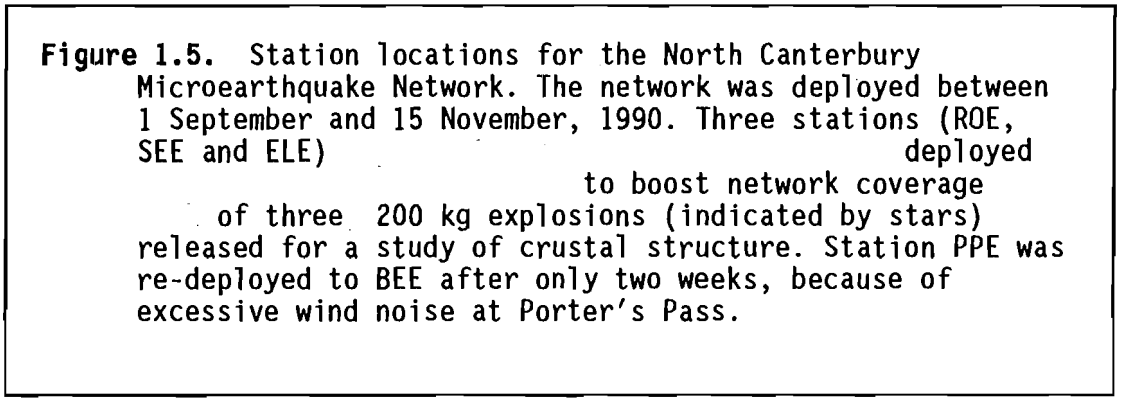

Figure 1.5. Station locations for the North Canterbury Microearthquake Network. The network was deployed between 1 September and 15 November, 1990. Three stations (ROE, SEE and ELE) deployed to boost network coverage of three 200 kg explosions (indicated by stars) released for a study of crustal structure. Station PPE was re-deployed to BEE after only two weeks, because of excessive wind noise at Porter's Pass.

COE
FHE
PPE
BEE
WDR
MPE
ROE
CHR
LPE
ORR
SHR
BHE
OPE
NDE
CCR
SEE
EWR
SFE
LTZ
PVR
WKE
SDE
IHE
MCR
MOE
KHZ
RQR
ELE
MQZ
GHR
OBE
CHRISTCHURCH

Portable RATS seismograph 1-component (z) ● GHR

Portable EARSS seismograph 3-component (z,n,e) ▲ MOE

National Network seismograph 3-component (z,n,e) ✕ LTZ

Location of explosions used for velocity inversion ★

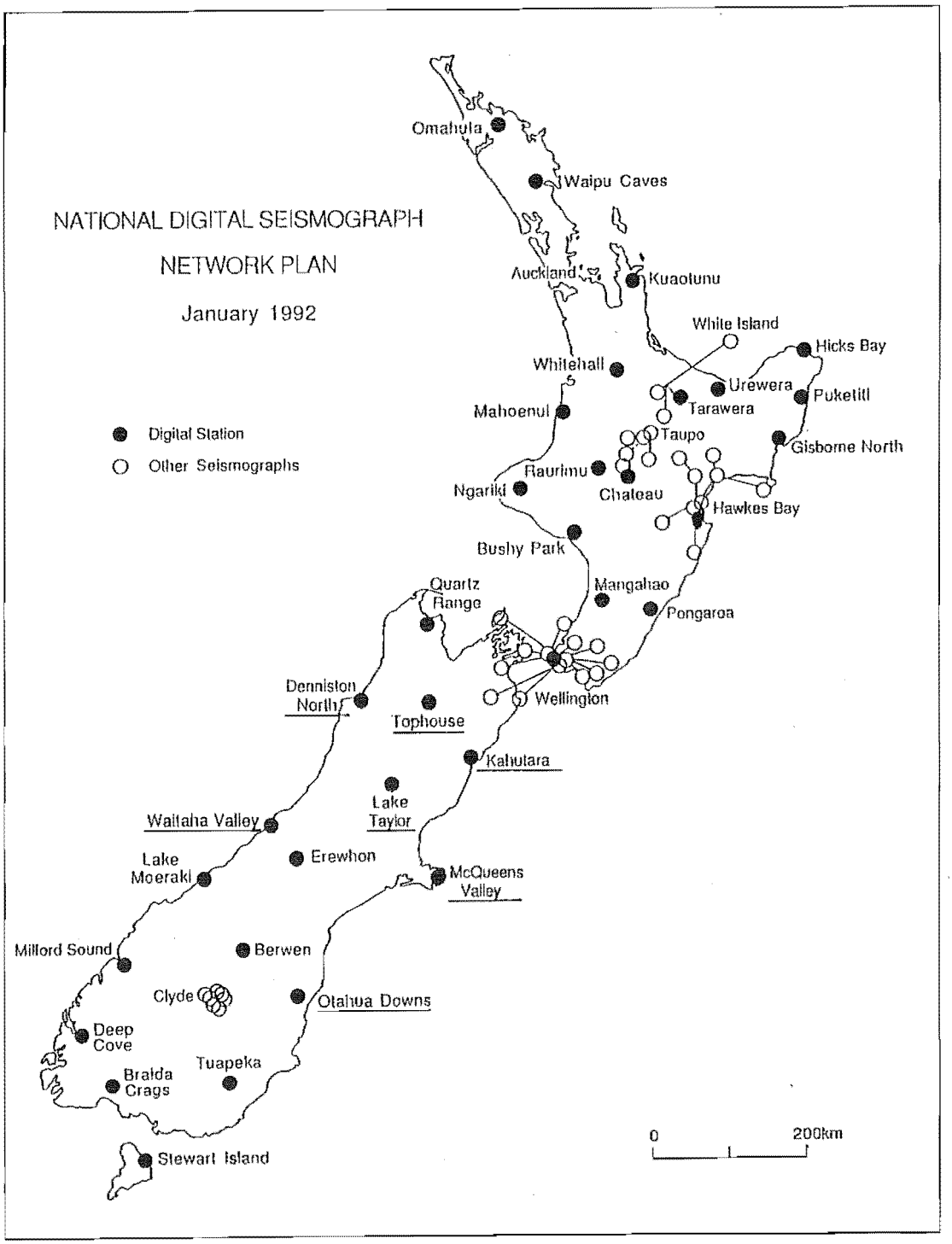

Figure 1.6. Station locations for the New Zealand Seismograph Network. Stations from which data were collected to supplement the North Canterbury Microearthquake Network are underlined.

(1989) provided a synthesis of these and other data as part of a regional study of Cretaceous-Cenozoic sedimentary basins by NZ DSIR Geological Survey; their revised stratigraphic nomenclature for the cover sequence is adopted here.

1.3.2 Basement rocks

Basement rocks in North Canterbury have been assigned to the Torlesse terrane (Bradshaw et al., 1981), which is composed dominantly of quartzo-feldspathic greywacke and argillite of submarine-fan facies. The Torlesse terrane represents the most easterly of several Permian and Mesozoic terranes in New Zealand, believed to have been accreted to the Pacific-facing Gondwana margin. Torlesse Terrane comprises three major belts of rocks, the Rakaia and Pahau subterranes separated by the Esk Head Melange (Fig.1.7).

Esk Head Melange is a 10-20 km wide belt of tectonic melange and broken formation, which forms a diffuse tectonic contact between Permian to late-Triassic, Rakaia subterrane in the west and latest Jurassic and Early Cretaceous, Pahau subterrane to the east. The melange contains material derived from both adjacent subterranes, but exhibits generally a greater diversity of lithologies, including various kinds of limestone, bedded chert-argillite, tuffaceous mudstone and basalt. Except in the hanging-walls of Quaternary thrust faults, the stratigraphic layering in all elements of the Torlesse terrane is steep, and parallel to the local shear fabric which strikes broadly NW-SE.

The tectonic fabric of the Esk Head melange varies from cleaved argillite and stretched (boudinaged) sandstone (where bedding remains recognisable), to blocks of tectonically rounded sandstone 'floating' in a sheared matrix of argillite and tuffaceous mudstone. Interspersed within the strongly disrupted zones of mixed lithology are essentially intact blocks of well-bedded greywacke that are indistinguishable (on field characteristics), from the Rakaia and Pahau subterrane rocks to the west and northeast, respectively (cf. Figs.1.8a, 1.8b).

Within this thesis study area the Esk Head Melange has been mapped in the Okuku and Waipara rivers by Botsford (1983), who described the lithologic associations and Mesozoic tectonic fabrics in detail. Map coverage of basement rocks has been extended considerably in this study, and observed variations in stratigraphic layering provide an additional tool for interpreting late Cenozoic structural trends. Esk Head Melange is defined by zones of high strain and mixed lithologies, and is differentiated from areas of substantially intact greywacke/argillite on

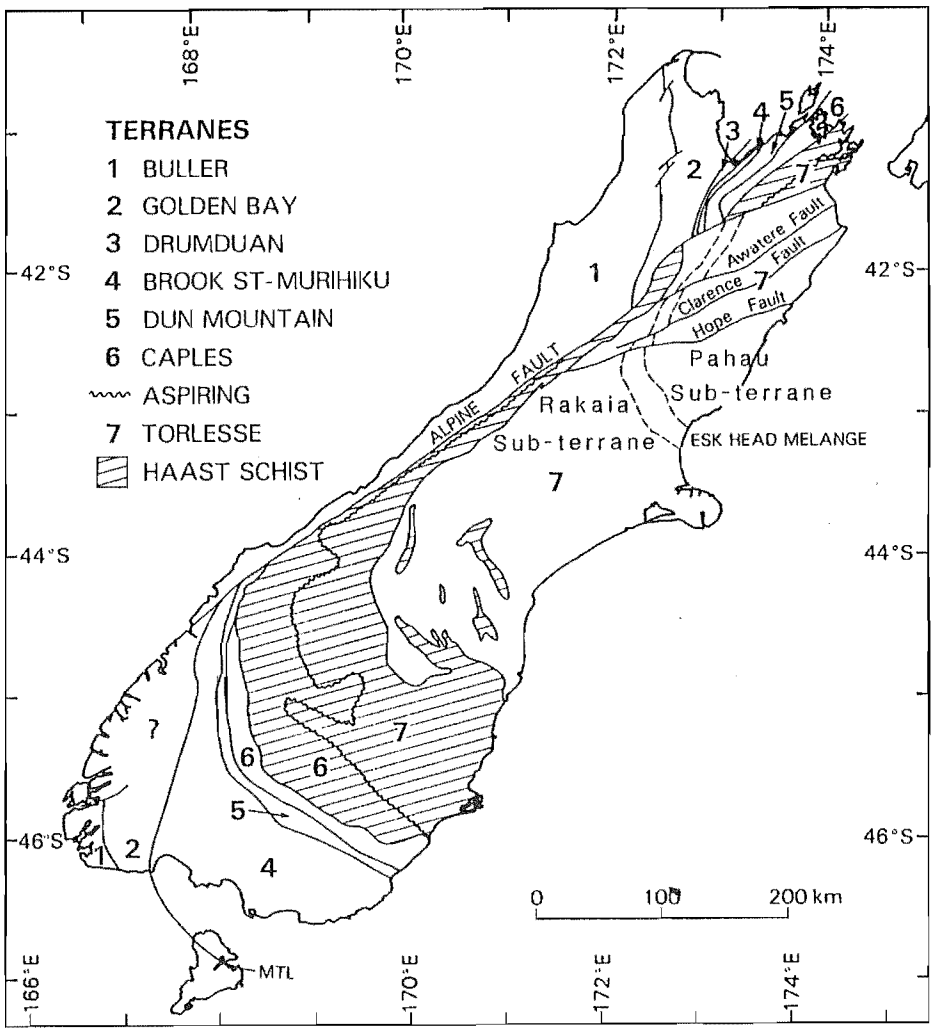

Figure 1.7. Mesozoic terrane map showing the distribution of Torlesse terrane in South Island, and gross relationships between its constituents in North Canterbury: the Rakaia and Pahau subterranes and Esk Head Melange. Adapted from Field et al. (1989) after Bishop et al. (1985) and Norris and Craw (1987).

Figure 1.8(a). Indurated and coherent, centimetre to decimetre-bedded, alternating sandstone and siltstone (quartzofeldspathic greywacke) of the Rakaia subterrane, exposed in a farm track on hills northwest of Oxford. Locality reference: L34/.2439800,5773200.

Figure 1.8(b). Exposure of pervasively sheared greywacke with a bedding-parallel shear fabric characteristic to numerous, annealed and oxidised crushed zones in Esk Head Melange. This outcrop is a cutting on Horsford Downs Road, Ashley Forest (M34/.2469300,5787000). Note that here, bedding is defined only by phacoids of sandstone. Rapid lateral variations in the degree of deformation are common, and in many exposures the rocks are indistinguishable from the generally less-disrupted rocks of Rakaia subterrane to the west.

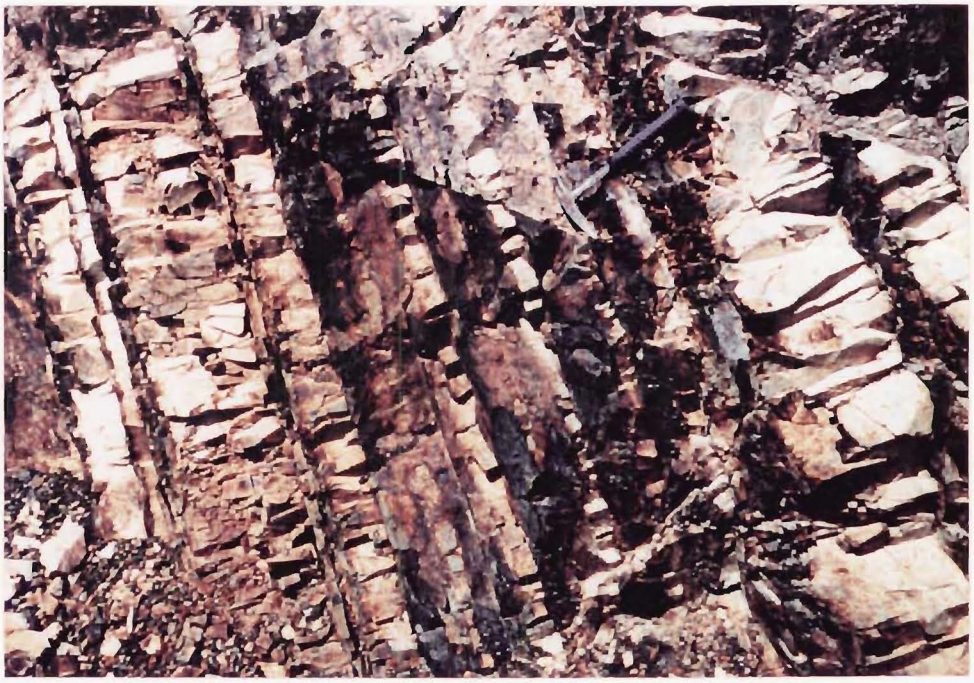

a.

b.

Maps 1 and 2 (map pocket).

1.3.3 Cretaceous-Cenozoic Cover Sequence

A c.750-2000 m thick, largely marine sedimentary succession unconformably overlies basement in North Canterbury and records a cycle of Upper Cretaceous-Lower Tertiary marine transgression, associated with opening of the Tasman Sea; followed by marine regression since the Miocene, that accompanied propagation of a convergent plate boundary through the New Zealand continental block.

Marine sedimentary and minor interbedded submarine igneous rocks of Upper Cretaceous-Lower Tertiary age are included in the Eyre Group and rocks of the ensuing regressive phase are assigned to the Motunau Group. The Burnt Hill Group is a lateral correlative of part of the Motunau Group in the Oxford district and comprises volcaniclastic and flow rocks, and some detrital sand units (Field and Browne, 1986; Fig.1.9).

The basal (Eyre Group) deposits generally comprise quartzose coal measures and are succeeded by several formations of quartz-rich sandstone, glauconitic sandstone and mudstone, overlain by Oligocene limestones. Pillowed, tholeiitic basalt was erupted in the Oxford district during the Palaeocene and Lower Eocene (View Hill Volcanics: Sheet 18), and tuffs of similar age have been described from drillholes more than 100 km to the southeast (Field et al. 1989). Submarine, sub-alkaline basalts were erupted in the Oxford district and Castle Hill Basin during the Oligocene and early Miocene (K-Ar ages: 30 Ma and c.23 Ma (McClennan and Weaver, 1984; Sewell and Gibson, 1988, respectively). The volume erupted in these areas was small, but the volume of correlatives in Marlborough further north (Cookson Volcanics: Sheet 18), may exceed 100 km^3 (Coote, 1987).

Volcanism was absent from Marlborough during the late Miocene, but more sub-alkaline to tholeiitic basalt was erupted in the Oxford district between 16 Ma and 10.5 Ma (Burnt Hill Group), and the large Banks Peninsula volcanoes (Frontispiece 1) were constructed between 11 and 5.8 Ma (Weaver and Smith, 1989).

The Neogene, (Motunau Group) is dominated by terrigenous sediments: Miocene-Pliocene calcareous siltstones and sandstones, that intercalate locally with lenses of coarse, bioclastic limestone and occasional Torlesse-derived conglomerate. Moderately to deeply weathered, late Pliocene and Pleistocene conglomerates cap most of the sequence, but are unconformably overlain by slightly to moderately weathered, late Pleistocene conglomerates and loess.

Figure 1.9. Cretaceous-Cenozoic cover stratigraphy in the Porter's Pass-Amberley Fault Zone (from Field et al. 1989, after Browne and Field, 1985; Field and Browne, 1986). The listed formation names are followed by suffixes in brackets that correspond to New Zealand chronostratigraphic Series (upper case), and Stages (lower case). Correlation diagrams constructed relative to the mid-late Oligocene regional unconformity, show: a) stratigraphic thicknesses, and b) intervening time-breaks (vertical lines), relative to the area mapped in this study.

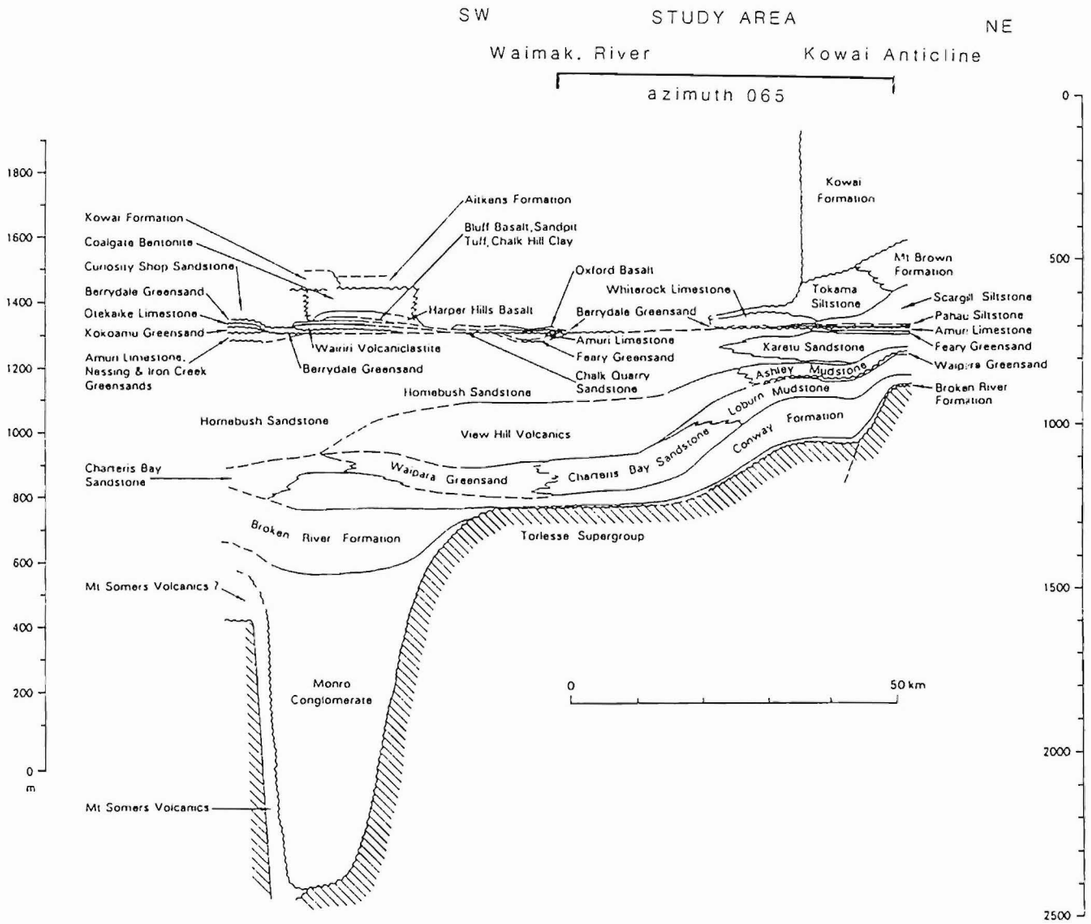

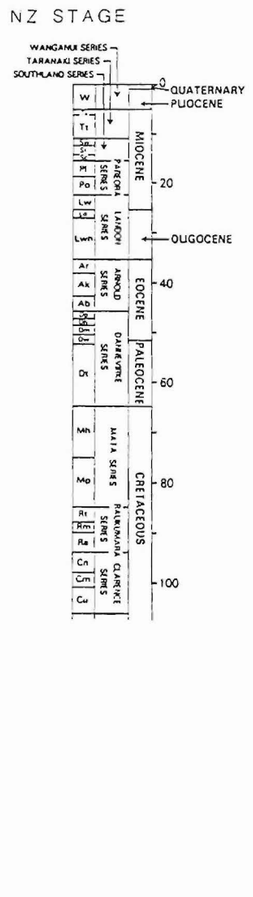

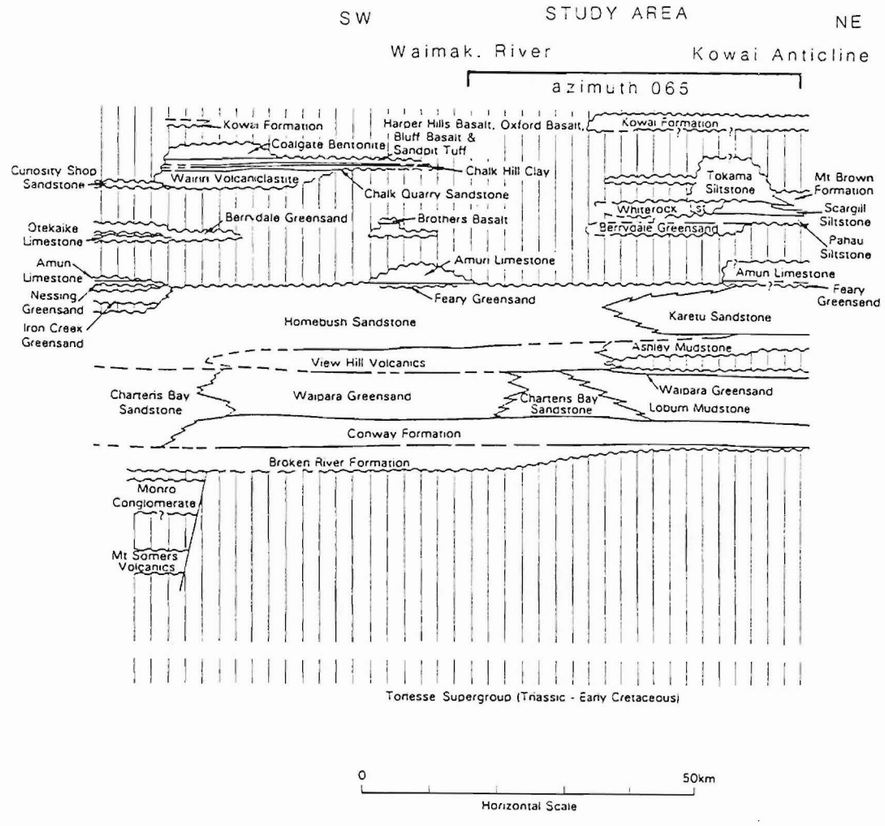

STUDY AREA (west)

BURNT HILL GROUP	Kowai Formation (W)
	Coalgate Bentonite (Tl-k)
	Harper Hills Basalt (Tl)
	Bluff Basalt (Tl)
	Sandpit Tuff (Sw-Tl)
	Chalk Hill Clay (Sw-Tl)
	Chalk Quarry Sandstone (Sw)
	Wairiri Volcaniclastite (Pl-Sw)
MOTUNAU GROUP	Omihi Formation (Ld-w)
	Berrydale Greensand member
EYRE GROUP	Homebush Sandstone (?Dh-?Ar)
	View Hill Volcanics (Dl-Dh)
	Waipara Greensand (Dl)
	Conway Formation (Mh-Dl)
	Broken River Formation (Mh)

STUDY AREA (east)

MOTUNAU GROUP	Kowai Formation (Wo-m)
	Tokama Siltstone (Pl-Sw)
	Mt Brown Formation (Po-Sw)
	Whiterock Limestone Member
	Waikari Formation (Lw-Po)
	Scargill Siltstone member
	Pahau Siltstone member
	Omihi Formation (Lwh-w)
	Berrydale Greensand member
(unassigned)	Amuri Limestone (Lwh)
EYRE GROUP	Feary Greensand (Ar)
	Karetu Sandstone (Ab-Lwh)
	Homebush Sandstone (Ab?)
	Ashley Mudstone (Dw-Ar)
	Waipara Greensand (Dl)
	Loburn Mudstone (Mh-Dl)
	Conway Formation (Mh-Dl)
	Broken River Formation (Mh-Dl)

NORTHEAST OF STUDY AREA

MOTUNAU GROUP	Greta Formation (Sl-c)
	Mt Brown Formation (Po-Sw)
	Waikari Formation (Lw-Po)
	Glenesk Sandstone Member
	Spy Glass Formation (Ld-Po)
(unassigned)	Amuri Limestone (Ar-Lwh)
EYRE GROUP	Ashley Mudstone (Dm-Ab)
	Waipara Greensand (Dl-w)
	Conway Formation (Mh-Dl)

1.4 PHYSIOGRAPHY OF THE STUDY AREA

The topography of the study area varies from that of an open pastoral landscape along the inner margin of the Canterbury Plains, to steep mountains of the Torlesse, Puketeraki, Ashley and Okuku Ranges - the latter known colloquially as the "Canterbury foothills" (Frontispiece 1 and 2). The Torlesse and Puketeraki Ranges exceed 1900 metres and are deeply dissected. In contrast, the height of the Ashley and Okuku Ranges averages between 800 and 1200 m and the majority of summits are flat and locally accordant. However, the rivers draining these lower ranges are deeply incised within saw-cut gorges; much of the area is heavily forested, accessible only on foot and is physically demanding to traverse.

1.5 THESIS ORGANISATION

Chapter 1 outlined the purpose and scope of this thesis and provided a brief introduction to the geology and tectonic setting of North Canterbury, a description of the study area and a summary of the principal objectives.

Chapter 2 describes the principal methods used to collect, process and analyse data from field mapping and the microearthquake study.

Chapter 3 presents the results of field mapping with reference to accompanying maps and cross-sections, and a synthesis of available geological data from published and unpublished sources. Kinematic styles and rates of Quaternary deformation are presented and discussed.

Chapter 4 presents the results of seismicity data from the 1990 microearthquake study. The regional pattern of seismicity is presented in a series of epicentral maps and hypocentral cross-sections, followed by similar maps and cross-sections of seismicity in the PPAFZ. Fault-plane solutions are presented and discussed in the context of the relationship between surface faults and seismicity.

Chapter 5 presents data relating to prehistoric fault ruptures in the PPAFZ. Data from fault ruptures and landslides are used to estimate recurrence intervals for large ($M>7.0$) earthquakes, and evaluate the validity of frequency-magnitude seismicity models based on the catalogue of historic seismicity.

Chapter 6 provides a synthesis of the principal conclusions of the thesis and includes recommendations for future work.

CHAPTER 2 PRINCIPLES AND METHODS

2.1 INTRODUCTION

The purpose of this chapter is to provide a brief summary of the rationale and methods adopted to achieve the desired aims of the study. The thesis embodies results of two, complementary projects: one based on field mapping and analysis of late Quaternary deformation in the PPAFZ; the other, a survey of microseismicity associated with the PPAFZ and North Canterbury region.

2.2 FIELD WORK

2.2.1 Logistics

Access to the northeastern part of the study area is facilitated by 4WD tracks through farms and plantation forests. A metalled public road provides access to Okuku and Lees Valleys, and rougher tracks extend from this road short distances into the Townshend, Whistler, upper Ashley and Lillburn Valleys.

Rivers, streams, ridges and road-cuttings were mapped systematically, with an emphasis on stratigraphic layering, shear fabrics, discrete faults, zones of crushed rock and macroscopic folds. The topography is rugged and west of Okuku River, densely forested. Two-thirds of the mapped area can be reached only on foot, mainly via rivers and streams and occasionally by foot-tracks. Water-courses provide the best geological exposure, but commonly are punctuated by waterfalls 5-30 m high, deep pools, debris dams and bounded by thick vegetation that renders travel slow and physically demanding.

2.2.2 Rationale

One of the important psychological barriers to be broken during this work was the partially received preconception, that mapping in basement might be a hopelessly unrewarding activity, because of the complexity of deformation in Torlesse rocks. In fact, the degree of success in mapping basement depended upon the definition of pertinent mapping objectives.

Observations made at each outcrop, included: 1) the average attitude of stratigraphic layering, with, or more commonly without facing direction; 2) the attitude of the local shear fabric; 3) the presence or

absence of crushed rock, fault gouge, fault breccia and particularly, whether the fabric of such rocks was annealed or not. The results (Map 1, Map 2: map pocket) indicate that away from the major faults, bedding attitudes in basement often are relatively uniform over a wide area, and provide a frame of reference for analysis of localised disruption of stratigraphic layering by elements of the PPAFZ.

2.2.3 Mapping base

New Zealand Map Series 260: Sheets L35; M35; L34; M34 (Department of Survey and Land Information, 1983, 1984, 1990, 1991, respectively), provided up-to-date cultural and topographic detail at a scale of 1:50,000, essential for accurate positioning in the field. Enlargements of these (1:25,000) were used as field sheets, supplemented by air-photos, where available. At the end of each field day or trip, data were plotted on 1:25,000 scale, contours-only maps of the New Zealand Map Series 270 (referenced on Map 1 and Map 2). Exceptions to this format are maps of the Cust Anticline and Ashley Fault (Map 3 and Map 4), that were drawn in the field on enlargements of vertical aerial photographs. N.B. ALL GRID REFERENCES IN THIS THESIS ARE FOR N.Z. GEODETIC DATUM 1949 (metres); prefixed by the N.Z. Topographical Map Series 260 (1:50,000) Sheet number - (e.g. L34/. Grid reference).

2.3 MAPPING

Contours-only maps have been used for final map reproduction so as to convey maximum information on the relationship between structure and topographic relief, without the clutter of biological and cultural detail. Sufficient cultural detail has been included to permit comparisons with published maps of the area (e.g. Sheet 18: map pocket).

Faults and associated zones of proto-cataclasite have been drawn to show their true extent in basement, which typically much wider than represented by existing geological maps. Geology and the geometry of planar surfaces (mainly bedding and faults), have been extrapolated only a few hundred metres each side of recorded measurements of strike and dip, in a deliberate attempt to reduce the ratio between inference and observation. Consequently, gaps between data are accorded equivalent emphasis, and the absence of a structure or pattern on the maps does not confirm its absence on the ground, merely that it was not observed.

The previously published lithostratigraphic map (Sheet 18), conveys information about aspects of the geology which for clarity have been

excluded from, or suppressed on maps compiled in this study. Sheet 18 encompasses an larger area and is complementary; a copy is included as a reference guide to elements of discussion in this thesis (map pocket).

2.4 MAP PRODUCTION

2.4.1 Use of colour

It is traditional to use colour to illustrate the different ages and/or types of rock on geologic maps. This approach has been used to good effect on the Geological Map of New Zealand (1:250 000) series, of which Sheet 18 is an example. However, the maps compiled in this study have been drawn to emphasise structural patterns of Quaternary deformation, rather than sequence stratigraphy, so in a departure from the standard format, colour has been used to emphasise the relationship between: 1) geology and structure (Map 1); and 2) topography and structure (Map 2).

Highly strained rocks and mixed lithologies of the Esk Head Melange in the study area are differentiated from well-bedded sequences of greywacke, which are more characteristic of Rakaia subterrane. This simple subdivision means that areas of well-bedded and largely intact greywacke in the principal area of Esk Head Melange, are mapped in the same colour as Rakaia subterrane. This is justified on the grounds that it is more important to discriminate areas of unequivocal melange from those of relatively undisrupted and homogeneous lithology, than it is to discriminate ages, when in fact, the provenance of such blocks of greywacke cannot be determined from field characteristics alone.

The Cretaceous-Cenozoic cover sequence is differentiated from basement rocks, and stratigraphic markers in the cover sequence, such as igneous dykes and sills, and limestone beds are discriminated from otherwise rather featureless sedimentary formations. The cover sequence has been coloured as if it were a single entity, but authentic stratigraphic contacts are shown where these have been determined. Most of the major tectonic structures identified as active in this study,

probably are younger than the youngest elements of the Tertiary cover (Nicol, 1991; in press), and variations in the attitude of bedding within the cover sequence depend primarily on proximity to structures, not age.

Quaternary sediments are almost ubiquitous, typically forming a veneer of colluvial debris on slopes, in addition to extensive fluvial terraces in areas of low relief. For sake of clarity these are discriminated only locally, and are not coloured on Map 1. At the Ashley Fault and Cust Anticline, a finer subdivision of Quaternary surfaces is warranted to illustrate the displacement history of underlying structures (Map 3 and Map 4).

2.5 MICROEARTHQUAKE STUDY

2.5.1 Network design and instrumentation

The 1990 microearthquake survey involved the temporary field deployment of 14 three-component and 10 single-component digital seismographs, at an average spacing of 15-20 km, between Banks Peninsula, Lake Coleridge and Waiau (Fig.1.5). Data from this network were supplemented by that from seven National Network seismographs, from Denniston in the north to Oamaru in the south (Fig.1.6). Ten days during August 1990 were spent locating suitable sites for the instruments, and these were subsequently deployed on geology which varied from greywacke basement and Tertiary basaltic volcanics, to weakly consolidated alluvium and loess. Care was taken to find quiet sites, and only two instruments were subsequently relocated to eliminate excessive wind noise. Seismometers deployed on hard-rock sites were plastered onto a levelled substrate, and the connecting cables were immobilised by large rocks. Those deployed at sites underlain by alluvium or loess were buried about half to one metre below the ground surface.

The two types of instruments used during this survey, were

developed by NZ DSIR Geophysics Division for regional and local earthquake detection and analysis. The design and operation of this equipment has been described by Robinson (1988) and Gledhill et al. (1991), and only a brief outline of the main features and servicing requirements is summarised here.

The single-component 'RATS' (Record Arrival Time System) records the arrival time, amplitude and first-motion direction of an earthquake, on a small RAM memory chip. The earthquake detection and timing algorithm utilises a frequency domain event detector, as well as a time domain arrival timer. RATS is optimized for recording impulsive local earthquakes, and will not trigger on emergent events or on teleseisms. The recorded data are played back at the field site through a serial interface to a lap-top computer. The system can operate unattended for up to 30 days.

The EARSS digital seismograph (Equipment for the Automatic Recording of Seismic Signals), has three input channels (for a three-component seismometer), and utilises a frequency domain detection algorithm. Both EARSS and RATS instruments incorporate an internal clock, and a radio which is tuned to a station that broadcasts hourly time pips (in New Zealand these are AM-long wave stations, operated by the Broadcasting Corporation of N.Z.). The time pips are monitored and used to apply a time correction to compensate for clock drift. The EARSS takes 4 hours before making its first calculation of time correction, but does it hourly thereafter. The EARSS only applies a time correction when the clock drifts ± 1 second. The time correction is applied to both EARSS and RATS data during data processing.

EARSS allow complete digital seismograms of detected events to be recorded on a magnetic tape cartridge. The total number of events per tape is a function of event-length, and because EARSS is an event-triggered seismograph, the number of useful earthquakes recorded will depend on the false detection rate, which is a function of site location.

A noisy (poorly selected) site may result in a high rate (say, more than 50%) of false event detection.

A portable EARSS requires two large car batteries wired in parallel to provide approximately 10-14 days of power. Variations in the operating life of each instrument were dependent principally on climatic conditions, particularly temperature. Low temperatures, which accompanied bad weather on several occasions during the survey, resulted in increased tape-drive errors and depressed battery voltages (refer to Appendix 4.2).

2.5.2 Field servicing

During the survey, all EARSS stations were serviced fortnightly, and RATS stations every three weeks. Servicing of EARSS involved changing the batteries and tape cartridges, and running a series of checks on all operational aspects of the system. Each check included a review and retrieval of system log-files, and if necessary or desirable, a change in detection parameters. The system check was performed using 'EARSS Talk', a user-friendly interface developed by Ken Gledhill and Mark Chadwick (Gledhill, 1991) that operates on an IBM lap-top PC running MS-DOS. Servicing of RATS involved a similar procedure, but in addition to down-loading system log-files, data also were retrieved.

2.5.3 Data Processing

The recorded data were processed at the Institute of Geophysics, Victoria University of Wellington, between each round of field servicing. Processing of EARSS data involved reading the data from magnetic tapes into a PC-based system, and sorting the resulting files into discrete events which combined data from all seismograph stations. This was done using VUWEARTH (Victoria University of Wellington Earthquake analysis system), a series of interactive programs developed by Gledhill (1992)

specifically for analysis of RATS and EARSS data.

The VUWEARTH seismograms were stored in event directories in binary files labelled: HHMMSS.STN (e.g. 093627.OPE), where HH is the hour, MM the minute, SS the second, and STN the station code. Each event directory contained an internal phase pick-file, an external phase pick-file (for merged RATS data), and an earthquake location file. Two more files essential for sorting and analysis of the seismograms were located in the main directories: 1) a list of seismograph station codes and their locations in decimal degrees, and; 2) parameters of a velocity model used for locating earthquakes.

Having read the tape image onto the PC hard disk, the tape block headers and time corrections calculated by EARSS were checked. Any bad bytes identified were corrected, then tape images were sorted into event directories on the PC hard disk, using the directory structure of MS-DOS. At this stage RATS data were merged and events recorded on fewer than three stations were subsequently deleted.

The seismograms for each event were then viewed, and a decision would be made whether or not to retain a given event for further processing. An event could be too small to warrant interest, or might consist of noise recorded simultaneously at several stations - with a little experience it is possible to quickly discriminate real from spurious events, on the basis of frequency characteristics. Distant events (i.e. those occurring outside the network) were either deleted, or stored if they were sufficiently well recorded to be of interest in future studies.

The arrival times and amplitudes of P and S phases were picked for all events within the network that were recorded on at least 3 stations (Fig.2.1). Locations were computed at the Seismological Observatory (NZ DSIR, Kelburn) using the earthquake location program MICRO (Smith, 1979), and the final velocity model (Reyners and Cowan, in prep.; Appendix 4.3).

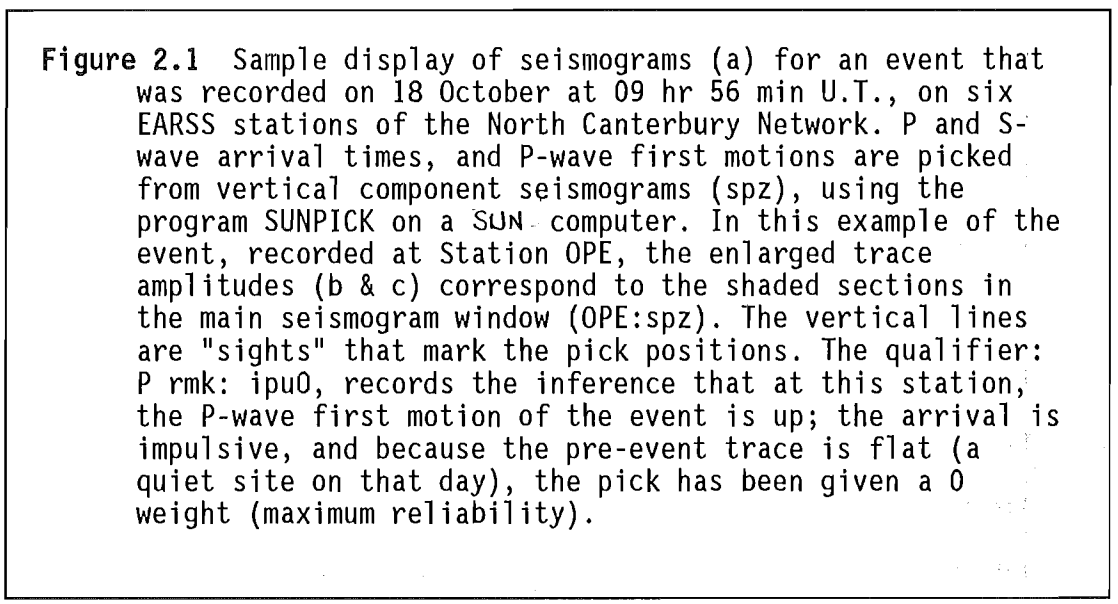

Figure 2.1 Sample display of seismograms (a) for an event that was recorded on 18 October at 09 hr 56 min U.T., on six EARSS stations of the North Canterbury Network. P and S-wave arrival times, and P-wave first motions are picked from vertical component seismograms (spz), using the program SUNPICK on a SUN computer. In this example of the event, recorded at Station OPE, the enlarged trace amplitudes (b & c) correspond to the shaded sections in the main seismogram window (OPE:spz). The vertical lines are "sights" that mark the pick positions. The qualifier: P rmk: ipu0, records the inference that at this station, the P-wave first motion of the event is up; the arrival is impulsive, and because the pre-event trace is flat (a quiet site on that day), the pick has been given a 0 weight (maximum reliability).

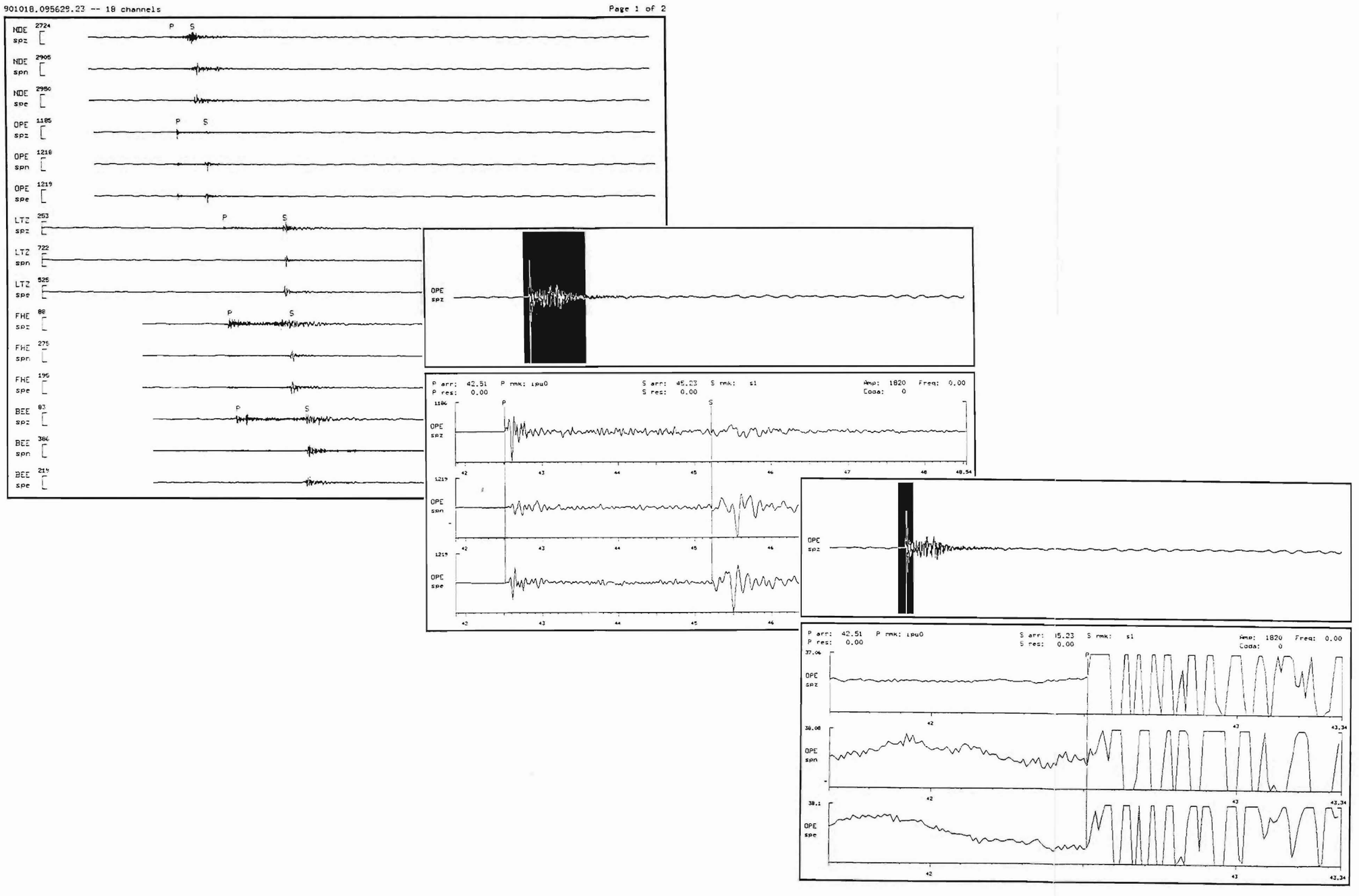
901018.095629.23 -- 18 channels
Page 1 of 2
NDE spz
NDE spn
NDE spe
OPE spz
OPE spn
OPE spe
LTZ spz
LTZ spn
LTZ spe
FHE spz
FHE spn
FHE spe
BEE spz
BEE spn
BEE spe
P arr: 42.51 P rmk: ipu0
P res: 0.00
S arr: 45.23 S rmk: s1
S res: 0.00
Amp: 1820 Freq: 0.00
Coda: 0
42
43
44
45
46
47
48
48.54
37.06
38.08
38.1
43.34

2.5.4 Magnitudes

Earthquake magnitudes were calculated using the formula developed by Robinson (1987), namely:

$$M = \log A + 1.0 \log R + 0.0029R + K$$

where A is the maximum P-wave amplitude, R is the slant distance from the earthquake focus to the station (in km) and K is a station correction allowing for the instrument gain and site variability. The constant K has been determined for the National Network station LTZ (Lake Taylor), so the resulting magnitude is consistent with the local magnitude scale used by the Seismological Observatory. Hence magnitudes for earthquakes recorded in this study were determined from the maximum amplitude at LTZ when this was available. For the 23 events which were not recorded at LTZ, magnitudes were determined using the stations LPE (Lees Pass), FHE (Flock Hill), MPE (Mt Pember) and WKE (Waikari). Magnitude corrections for these stations relative to LTZ were determined using a subset of the recorded earthquakes.

2.5.5 Epicentral plots, cross sections and focal mechanisms

One of the principal aims of the microearthquake survey was to obtain better information about the kinematics of faulting in North Canterbury, from the spatial distribution of events and analysis of their focal mechanisms. To this end, all phase and final location files were loaded onto SUN computers at the Institute of Geophysics, VUW, where a variety of programs were used to generate maps, showing station locations, earthquake epicentres for different depth ranges, and cross-sections of earthquake hypocentres.

Numerous events were recorded outside the network, especially to the west (Appendix 4.4). These data were retained for analysis in future

studies, but only those events which occurred within the North Canterbury network were used to generate cross-sections of hypocentres and focal mechanisms. Fault plane solutions and P and T strain axes, were derived from the P-wave first-motion polarities recorded at the respective stations using the conventions of Aki and Richards (1980) (Appendix 4.5). Fault-plane solutions (Appendix: 4.6, 4.7) were assigned to one of three categories of confidence based on how tightly the nodal planes are constrained by the recorded first motions. The higher quality mechanisms are illustrated separately in discussion in Chapter 4.

CHAPTER 3. STRUCTURE AND TECTONICS OF THE PORTER'S PASS-AMBERLEY FAULT ZONE

3.1 INTRODUCTION

This chapter describes the location and geometry of late Quaternary faults and associated fold structures within the mapped area of the Porter's Pass-Amberley Fault Zone (PPAFZ) and sets out the geological and geomorphological evidence from which inferences are made about the kinematics of deformation within the zone. On the basis of geological mapping three structural domains have been identified, in which the geometry and kinematic style of late Quaternary deformation differ at the surface (Fig.3.1). The domains are defined as follows:

1) a **strike-slip domain** encompassing the area of Rakaia subterrane basement, between the Waimakariri, Whistler and Glentui rivers, and centred on Mt Oxford;

2) a **thrust and reverse fault domain** that extends east and southeast of Lees Valley, encompassing the landmark peaks of the Ashley and Okuku Range - Mt Thomas, Mt Karetu and Mt Grey, and encompassing the area of basement mapped as Esk Head Melange; and

3) a **northwest-verging fold belt** on the northern Canterbury Plains between Amberley and Cust, in which Quaternary conglomerates are folded, and Holocene surfaces are offset by faults. The subdivision is to some extent arbitrary because some of the structures are demonstrably interconnected across the domain boundaries (discussion in Chapter 4), but for descriptive purposes it is appropriate to introduce the structural geometries in this way. This chapter should be read in conjunction with the accompanying maps and cross-sections (Maps 1,2,3,4: map pocket).

3.2 CRITERIA FOR THE RECOGNITION OF ACTIVE STRUCTURES

Where late Quaternary elements of the cover succession and topography are disrupted by faulting or folding, a late Quaternary age of deformation is unequivocal. In the absence of such features, other criteria are required to corroborate this inference and two lines of evidence are used:

1) zones of crushed rock that are not annealed and are commonly characterised by soft fault gouge, are the same (senu lato) as those which pass up through basement and offset the cover sequence, and those

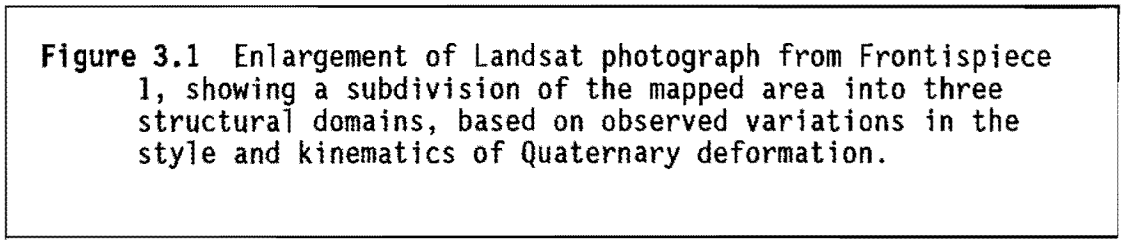

Figure 3.1 Enlargement of Landsat photograph from Frontispiece 1, showing a subdivision of the mapped area into three structural domains, based on observed variations in the style and kinematics of Quaternary deformation.

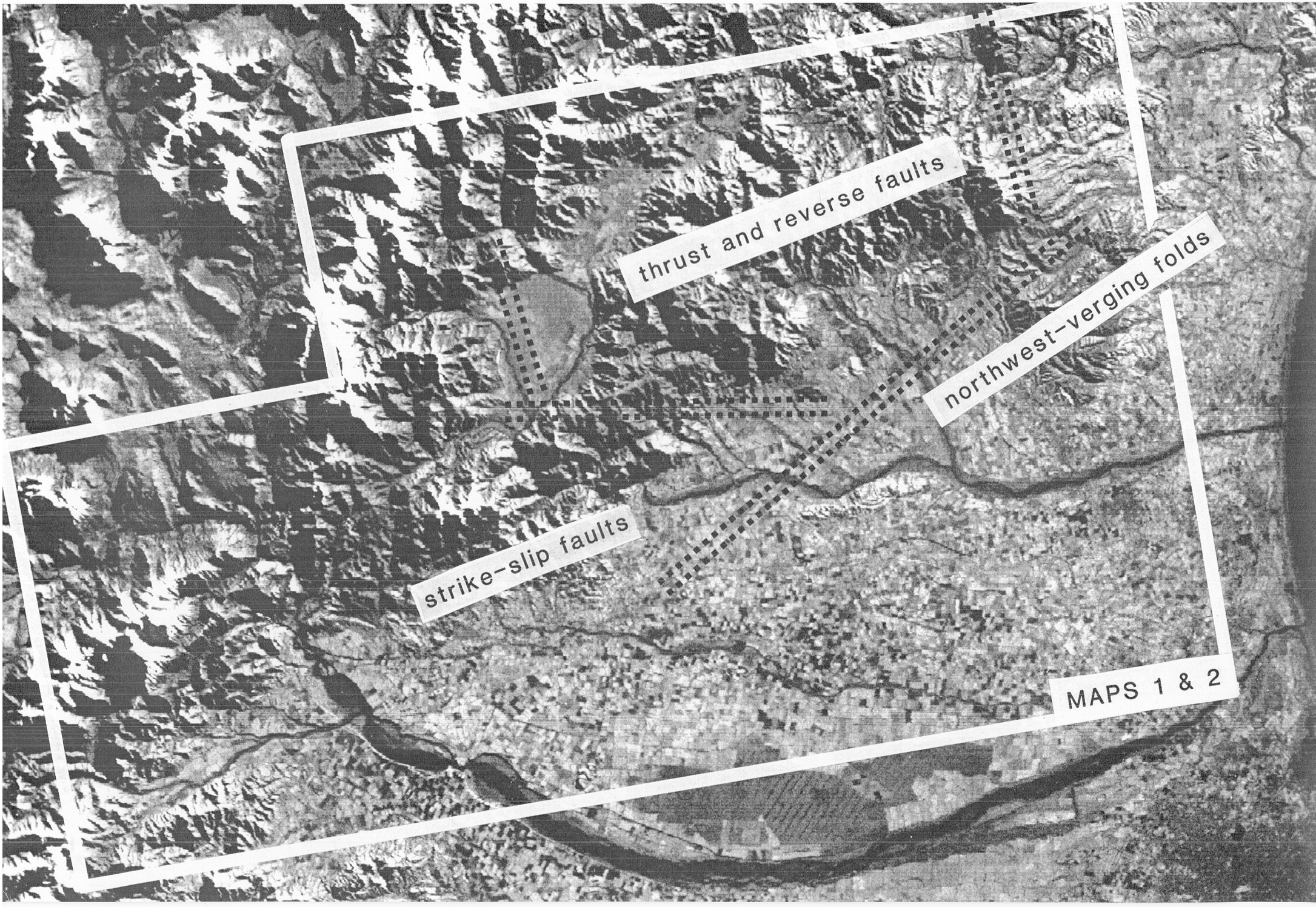
thrust and reverse faults
northwest-verging folds
strike-slip faults
MAPS 1 & 2

associated with zones of known prehistoric and historic surface rupture elsewhere (e.g. Hope Fault: Freund, 1971; Frontispiece 1);

2) the locations of several shallow (5-10 km deep) earthquakes recorded during the 1990 microearthquake survey, are consistent with on-going activity at seismogenic depths beneath the crushed zones.

3.3 STRUCTURAL ELEMENTS OF THE STRIKE-SLIP DOMAIN

3.3.1 Porter's Pass Fault: Porters Pass to Waimakariri River

At Porter's Pass a surface fault trace traverses the slopes of the Torlesse Range to the east of State Highway 73. This is the 'type locality' of the Porter's Pass Fault, from which inferences have been made about the gross kinematics of faulting along the PPAFZ (e.g. Scholz et al., 1973). The Porter's Pass Fault extends northeast into the Kowhai and Rubicon river catchments, where it is has been studied by Coyle (1988). The fault is defined by a series of discontinuous surface traces, and zones of pervasively crushed rock which generally possess a sub-vertical shear fabric. Mapping by Coyle (1988) and Wood (in Wilson, 1989) has identified a number of discrete splays of the fault, and evidence of late Quaternary displacement has been recorded at several localities including Porter's Pass (discussion in Chapter 5).

At the Waimakariri River (Fig.3.2) a zone of crushed rock more than 400 m wide is exposed in the walls of a narrow peninsula that bissects a large meander loop (Horseshoe Bends: Map 1). This crushed zone encompasses the principal slip surfaces of the Porter's Pass fault. A few hundred metres further east the crushed zone is well-exposed in the lower reaches of Coal Creek, where pervasively sheared basement has been thrust over ?late Pleistocene alluvium of the Waimakariri River (Fig.3.3). At this locality the crushed zone bifurcates to form the principal bounding elements of a major strike-slip duplex, that encompasses the Mt Oxford block to the east (Fig.3.2).

3.3.2 Mt Oxford Duplex: Townshend Fault Zone

A major zone of crushed rock extends from the Porter's Pass fault at Waimakariri River, northeast along Coal Creek and across the headwater divide into the catchment of the Townshend River. Preserved within the crushed zone are large blocks of well-bedded greywacke which have been rotated about sub-vertical axes, relative to bedding exposed in the adjacent valleys of Fosters Stream and Eyre River to the west and east,

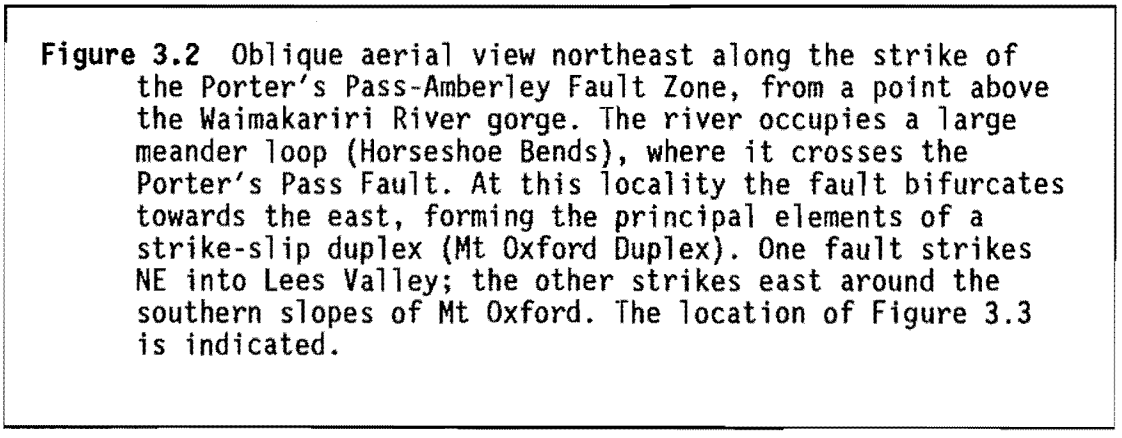

Figure 3.2 Oblique aerial view northeast along the strike of the Porter's Pass-Amberley Fault Zone, from a point above the Waimakariri River gorge. The river occupies a large meander loop (Horseshoe Bends), where it crosses the Porter's Pass Fault. At this locality the fault bifurcates towards the east, forming the principal elements of a strike-slip duplex (Mt Oxford Duplex). One fault strikes NE into Lees Valley; the other strikes east around the southern slopes of Mt Oxford. The location of Figure 3.3 is indicated.


Mt Oxford
Lees Valley
Coopers Creek
Fosters Stream
Coal Creek
Eyre River
crushed basement
Fig 3.3
Waimakariri River

respectively (Map 1).

The crushed zone narrows at the drainage divide, where an outlier of basal cover sequence (Broken River Formation) is preserved in sedimentary contact with strongly leached basement (locality 2: Appendix 3.1). East of the divide the crushed zone broadens to more than one kilometre wide in the middle Townshend valley, where it merges with a second, narrower crushed zone (strike 300°/dip 72°N) which has been traced northwest to the Waimakariri River (Map 1). In the middle of the main zone, faults dip steeply. Near the northern limits of the zone, however, in the upper Townshend Valley and Shifton Stream, the dips are lower (30-55° S and SE) and appear to characterise by a outward fanning wedge of faults (cross-section A-B).

In the lower Townshend valley, the crushed zone bifurcates: half of the zone maintains an easterly strike across the top entrance to the Ashley River gorge in Lees Valley, where its dip decreases to a range of 15-50° S; the other half of the zone bounds the northeast margin of the Mt Oxford Duplex, and strikes at 105° through the middle of the Ashley Range along a seam of bedded, red and green chert and argillite. The dip of this element of the zone is vertical at Townshend Valley, and reduces to 72°N at Raspberry Gully, where the principal slip surface is associated with a surface trace.

3.3.3 Mt Oxford Duplex: Coopers Creek Fault Zone

At the Waimakariri River, the southerly splay of the crush zone that is associated with the main trace of the Porter's Pass fault, strikes east across the Eyre Valley into the upper catchment of the west and east branches of Cooper's Creek (Fig.3.2). A dip of 72°N was measured on the inferred principal slip surface in the west branch of Coopers Creek, where ?late Pleistocene alluvium is offset across the fault (Fig.3.4). From the headwaters of the east branch of Cooper's Creek, this element of the Mt Oxford Duplex strikes 055° to Raspberry Gully, where it merges with the Townshend Fault Zone and forms the Glentui Fault Zone east through the Ashley Gorge to Glentui River (Map 1).

3.3.4 Mt Oxford Duplex: Cross-faults

Within the block of basement that forms Mt Oxford, narrow and generally steeply-dipping zones of crushed rock strike 320-340°, at 45-90° to the principal bounding faults of the duplex. These cross-faults are sub-parallel to the strike of Torlesse bedding which is steeply

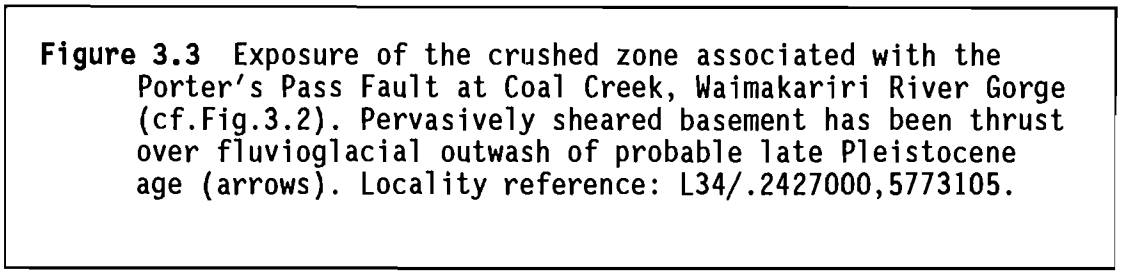

Figure 3.3 Exposure of the crushed zone associated with the Porter's Pass Fault at Coal Creek, Waimakariri River Gorge (cf.Fig.3.2). Pervasively sheared basement has been thrust over fluvioglacial outwash of probable late Pleistocene age (arrows). Locality reference: L34/.2427000,5773105.

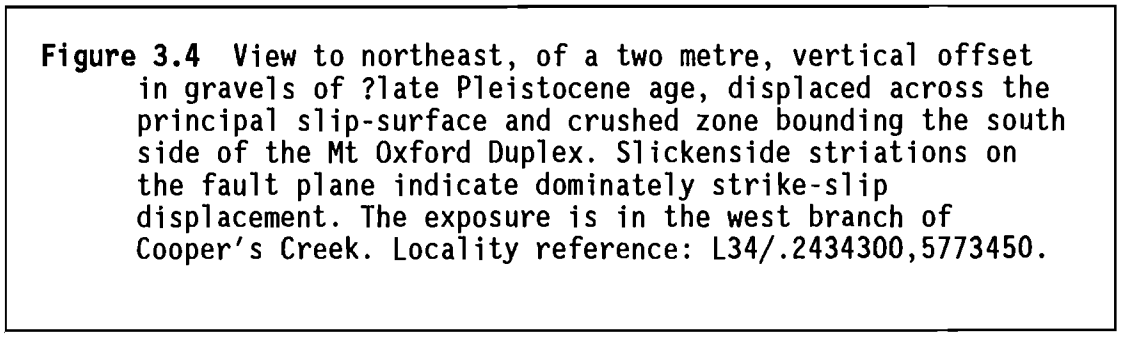

Figure 3.4 View to northeast, of a two metre, vertical offset in gravels of ?late Pleistocene age, displaced across the principal slip-surface and crushed zone bounding the south side of the Mt Oxford Duplex. Slickenside striations on the fault plane indicate dominately strike-slip displacement. The exposure is in the west branch of Cooper's Creek. Locality reference: L34/.2434300,5773450.

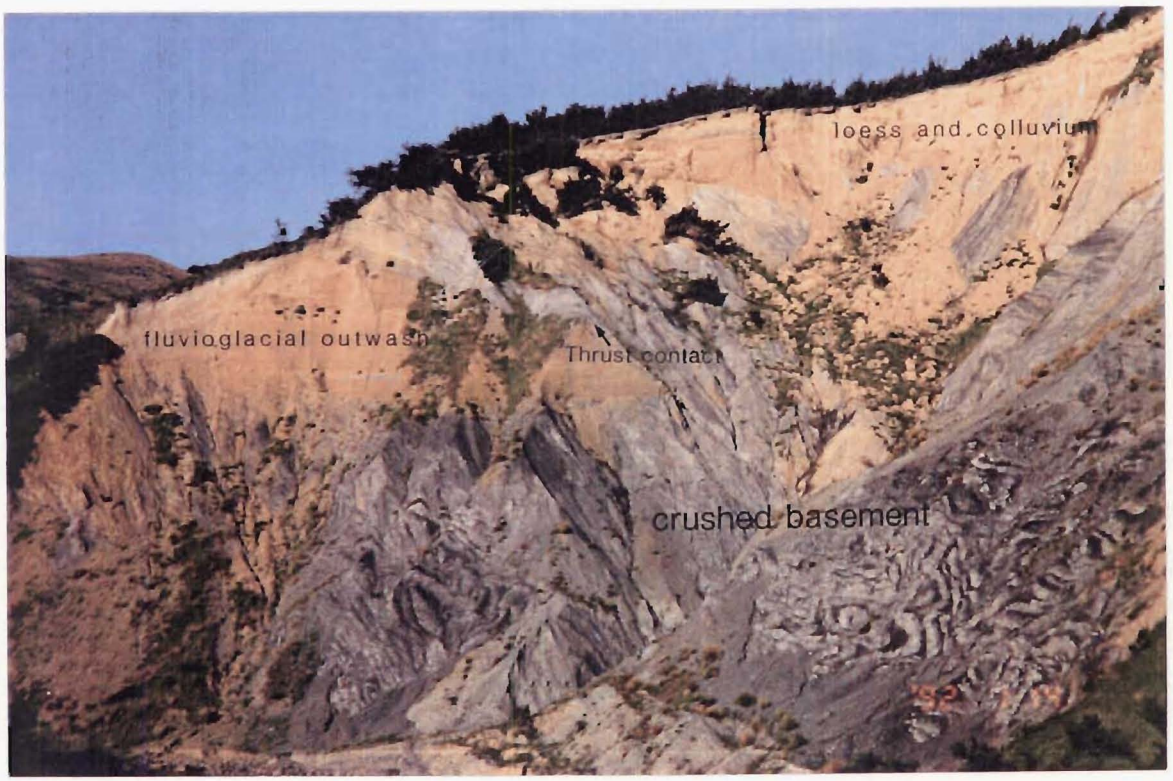
loess and colluvium
fluvioglacial outwash
Thrust contact
crushed basement

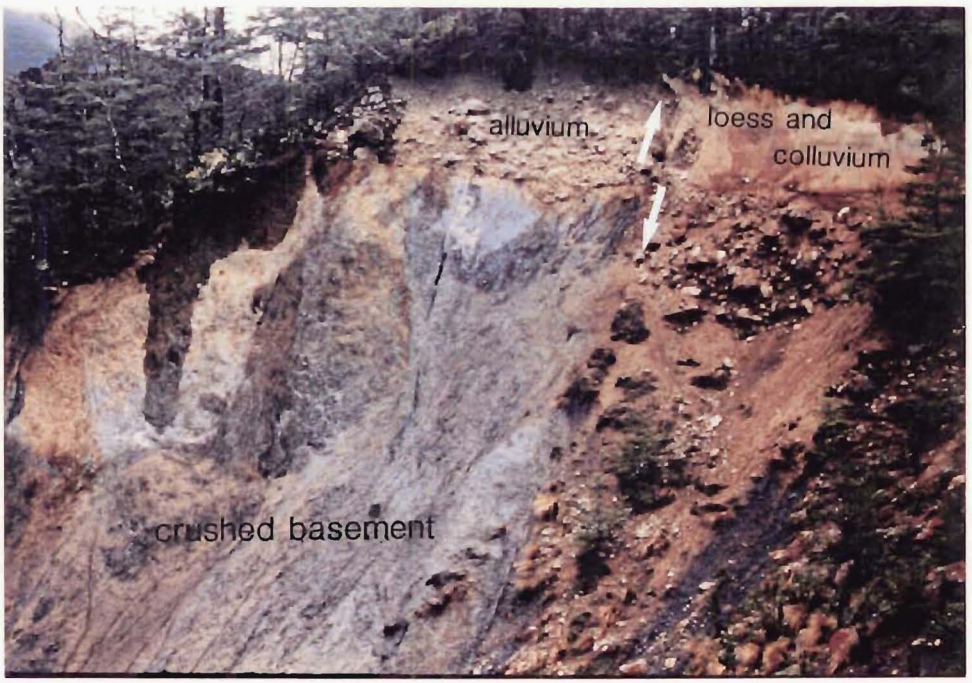
alluvium
loess and
colluvium
crushed basement

dipping, but not greatly disrupted or rotated. The sense of relative displacement on the cross-faults (inferred from slickenside striations) is locally ambiguous or contradictory. The cross-faults are expressed topographically by low saddles and ridge-line steps, but are best exposed in the Eyre River, Coal Creek and Moody's Stream, where they are marked by zones of shattered rock, fault gouge, and occasional quartz-mineralised fault breccia (Fig.3.5).

3.3.5 Glentui Fault Zone

East of the Mt Oxford Duplex, the zone of crushed greywacke and red and green argillite strikes east through the Ashley Range to the Glentui River. Here, the crushed zone broadens into a series of splays that strike to the east and southeast (120-140/90) across the Bald Hills, and parallel to the Glentui River. The contact between basement and the cover sequence is a crushed zone and Lower Tertiary cover beds and igneous dykes adjacent to the fault are tilted 50-77°S.

3.3.6 Porters Pass Fault : Woodstock to Oxford

West of the Waimakariri River, near Woodstock, a surface trace of the Porter's Pass fault has been mapped in Joyces Stream (Gregg, 1964; Wilson, 1989). This fault either dies out at the Waimakariri River, or possibly continues to the east, beneath the southern margin of the exposed cover sequence. There is no evidence for such a fault at the surface, but northeast of Oxford township, the range-front escarpment is bounded by a fault zone that is cryptically expressed at the surface by warped and dissected alluvial fans and lines of springs (Frontispiece 2; Map 1) and as an offset in basement identified on seismic reflection profiles (Kirkaldy & Thomas, 1963; Field et al., 1989).

West of Oxford, in the Eyre River and Cooper's Creek, several minor faults splay southeast from the Coopers Creek Fault Zone, but these zones of crushed rock are only a few metres wide and the faults cannot be traced reliably into adjacent streams. Between one and three kilometres south of the Coopers Creek Fault Zone, the cover sequence outcrops extensively (Map 1) and the contact with basement is sedimentary; bedding attitudes in cover, describe the middle limb of a monoclinal fold that dips 15-25° to the southeast.

The cover sequence is bounded at its eastern margin by a SE-facing topographic escarpment and crushed basement, in which the shear fabric is parallel to the strike of the escarpment (McLennan, 1981; Map 1). The

Figure 3.5 Quartz-mineralised fault breccia associated with cross-faults of the Mt Oxford Duplex, exposed in Coal Creek. Locality reference: L34/.2428400,5774450.

crushed zone was not found in Coopers Creek to the northeast, but the projected position of this fault to the southwest would separate exposures of basement from Quaternary alluvium in the Waimakariri River. A steep gradient in isostatic gravity anomalies (increasingly negative to the northwest), and an estimated 500 m vertical offset of basement (NW side down) detected from seismic refraction surveys have been observed across the projected strike of the fault (M. Broadbent, pers.comm. 1992; R.Jenkins and M. Reyners pers.comm. 1990, respectively). Projection of this structure further west would coincide with the Kowai Fault which bounds the base of the Russell Range (Speight, 1924).

3.3.7 Whistler Fault Zone

The Whistler Valley is a drainage catchment on the eastern flank of the Puketeraki Range, northwest of Lees Valley and 10 km north of the Townshend Valley. Along its middle reach the Whistler River flows east from the foot of Chest Peak, along a crushed zone exposed in basement to a height of approximately 150-200 m above the valley floor. The crushed zone strikes east beyond the entrance of the Whistler Valley, and bounds the northern margin of Lees Valley where it has been traced as far east as the Ashley River (Map 1).

The Whistler Fault Zone is up to 1 km wide and consists of an anastomosing network of predominately vertical faults, within 10->100 m wide belts of crushed greywacke which include igneous dykes of unknown, but probable Tertiary age, and hydrothermally altered basement. The dip of the crushed zone is vertical in the Whistler Valley, where slickenside-striations indicate predominately horizontal movement associated with the last increment of displacement. Further east, at the base of the Kingsdown Hills the dip of the crushed zone is 50-70°N. The Whistler Fault Zone is either absent or concealed beneath late Quaternary fan deposits on the floor of Lees Valley.

On ridges south of Whistler River the location and strike of faults is marked by accordant topographic steps (slumps or ridge-rents), but the crushed zone does not out-crop on the upper slopes of Chest Peak. The Whistler Fault Zone passes west beneath folded basement of the Puketeraki Range, but may approach the surface in the vicinity of Red Saddle, the lowest point in the range.

3.4 STRUCTURAL ELEMENTS OF THE THRUST AND REVERSE FAULT DOMAIN

3.4.1 Lees Valley Fault

The Lees Valley Fault (Gregg, 1964) is an element of the thrust and reverse fault domain, and bounds the southeast side of Lees Valley, representing a northeastward continuation of the Townshend Fault Zone (Fig.3.6). For much of its length the Lees Valley Fault is concealed beneath the active floodplain of the Ashley River and beneath late Quaternary fan deposits, derived from the steep slopes to the southeast.

The fault zone is well exposed in cliffs near the entrance to the Ashley Gorge, and at the eastern margin of Lees Valley where south to southeast-dipping (15-50°) faults have accommodated the thrusting of crushed basement, onto Tertiary marine sediments and Quaternary fan deposits (Fig.3.7; cross-section C-D). Several splays diverge to the north and east from this locality. The splays to the north are low-angle, southeast-dipping thrusts that are exposed at Ashley-river level but have only a weak topographic expression on the ridge separating the upper and lower basins of Lees Valley. In the upper Lees Valley, faults break out to form surface traces with scarps up to 6 m high (Fig.3.8). The surface traces displace several young (Holocene) fan surfaces, and have steep faces and sharp crests implying recent surface rupture. A detailed study of the geometry and geomorphology of this section of the fault zone is currently in progress (Garlick, 1992).

The splays to the east and southeast of the principal fault in Ribbonwood Stream have steep-to-vertical dips, and are marked topographically by saddles on the crest of the Ashley Range although the crushed zones are not exposed at the surface. These splays extend into the upper catchment of the Garry River and Pioneer Stream, where they terminate in a narrow, but complex zone of north-south striking, steeply dipping faults (Map 1).

3.4.2 Okuku River to South Branch Waipara River

The central element of the Lees Valley Fault zone extends NE along the axis of Ribbonwood Stream into the uppermost Garry River catchment, but further east in the south branch of the Okuku River the geomorphic and geological expression of faulting is diffuse. The continuation of the Lees Valley Fault to the northeast may be inferred from a topographic low between Lees Valley and the Waipara River (Map 2), but the surface traces associated with this fault zone in Lees Valley have not been observed

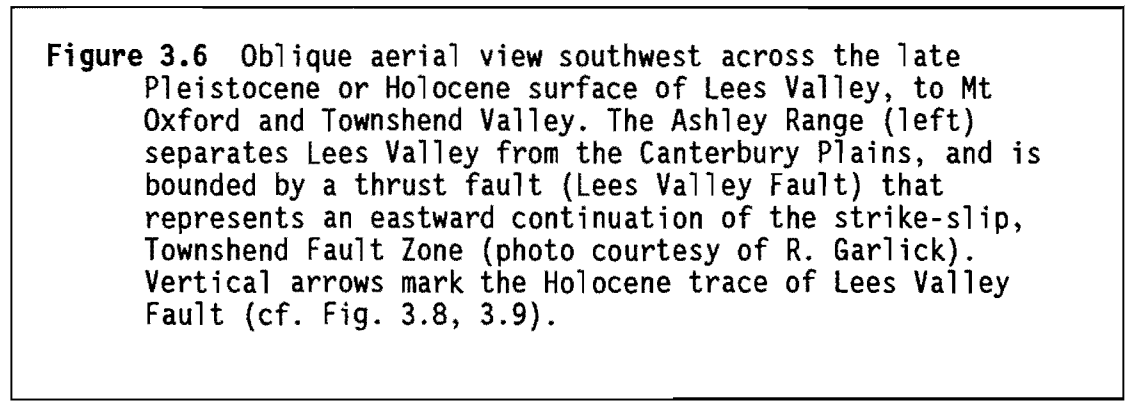

Figure 3.6 Oblique aerial view southwest across the late Pleistocene or Holocene surface of Lees Valley, to Mt Oxford and Townshend Valley. The Ashley Range (left) separates Lees Valley from the Canterbury Plains, and is bounded by a thrust fault (Lees Valley Fault) that represents an eastward continuation of the strike-slip, Townshend Fault Zone (photo courtesy of R. Garlick). Vertical arrows mark the Holocene trace of Lees Valley Fault (cf. Fig. 3.8, 3.9).


Canterbury Plains
Mt Oxford
Townshend Valley
Fig 3.7
Ashley River
Lees Valley

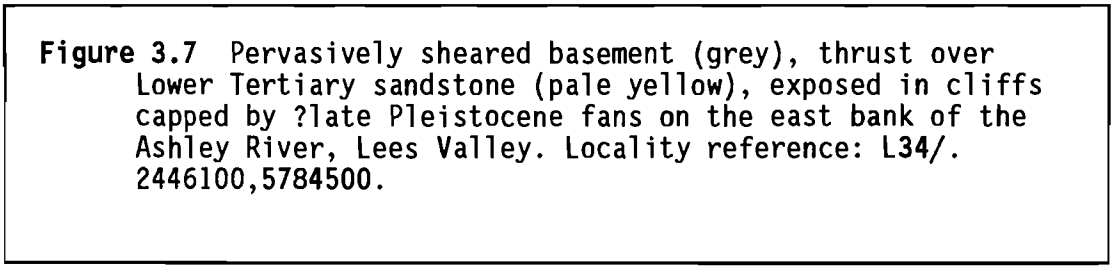

Figure 3.7 Pervasively sheared basement (grey), thrust over Lower Tertiary sandstone (pale yellow), exposed in cliffs capped by ?late Pleistocene fans on the east bank of the Ashley River, Lees Valley. Locality reference: L34/. 2446100,5784500.

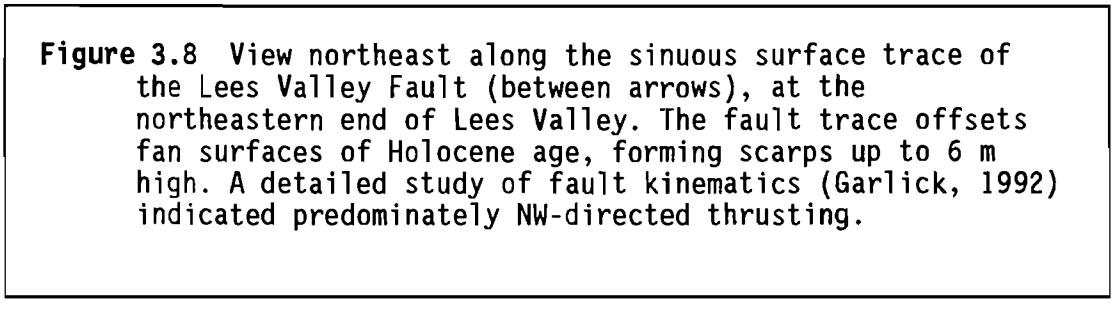

Figure 3.8 View northeast along the sinuous surface trace of the Lees Valley Fault (between arrows), at the northeastern end of Lees Valley. The fault trace offsets fan surfaces of Holocene age, forming scarps up to 6 m high. A detailed study of fault kinematics (Garlick, 1992) indicated predominately NW-directed thrusting.


fan deposits
crushed basement
thrust contact
tertiary sandstone

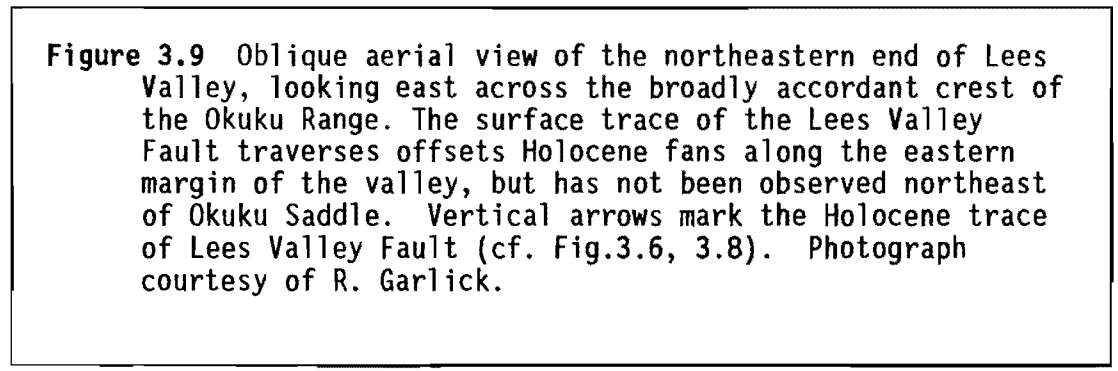

Figure 3.9 Oblique aerial view of the northeastern end of Lees Valley, looking east across the broadly accordant crest of the Okuku Range. The surface trace of the Lees Valley Fault traverses offsets Holocene fans along the eastern margin of the valley, but has not been observed northeast of Okuku Saddle. Vertical arrows mark the Holocene trace of Lees Valley Fault (cf. Fig.3.6, 3.8). Photograph courtesy of R. Garlick.


Culverden Basin
Lees Pass
Okuku Hill
Okuku Saddle
Lees Valley

east of Okuku Saddle (Fig.3.9).

At depth, the fault zone probably continues northeast, to connect with a series of major north-striking and east-verging, reverse faults and thrusts that bound the McDonald Anticline (Nicol, 1991) and western margin of Culverden Basin (R. Mould pers.comm. 1992). The diffuse nature of surface faulting possibly reflects the change in basement rheology, from the homogeneous and relatively coherent greywacke of the Rakaia subterrane in the west, to the heterogeneous, mud and volcanogenic-rich and highly-strained rocks of the Esk Head Melange further east. The few active faults in the Okuku Range are short and narrow (typically less than four kilometres long, and 20-50 metres wide), and strike perpendicular to (less commonly, parallel to) the Esk head Melange fabric.

3.4.3 Mt Thomas Fault Zone

On the south side of the Ashley Range, between the Glentui River and Bald Hills, the Glentui Fault Zone passes eastward into moderate-to-low angle (10-45°), southeast and south verging thrusts, which are best exposed in the Garry River and in deeply eroded ravines on the west and southeast flanks of Mt Thomas. The thrusts loop around the eastern flank of Mt Thomas, where they become narrow zones of moderate-to-steeply dipping crushed rock, inferred to represent tear faults, that strike northwest and splay to the NNE.

In streams on the southeast side of Mt Thomas, at the base of the escarpment, a steeply dipping crushed zone represents an eastward continuation of the shear zone associated with the Glentui Fault Zone. This crushed zone presumably continues northeast between Mt Thomas and Mt Grey, but is concealed beneath cover sediments in which a series of gently plunging, upright assymmetric anticline-syncline pairs have developed (Map 1). The fold limbs are well expressed by a strike-ridge of Lower Miocene limestone (Whiterock Limestone) (Fig.3.10), but the steepest dips are recorded in Plio-Pleistocene conglomerates of the Kowai Formation, exposed on the flanks of the Hillside Anticline (Fig.3.11). A fault is exposed in the core of the anticline and forms a short (c.500 m long) surface trace (Mt Lawry Fault) across a ?Holocene terrace between Okuku and Karetu Rivers (Map 1).

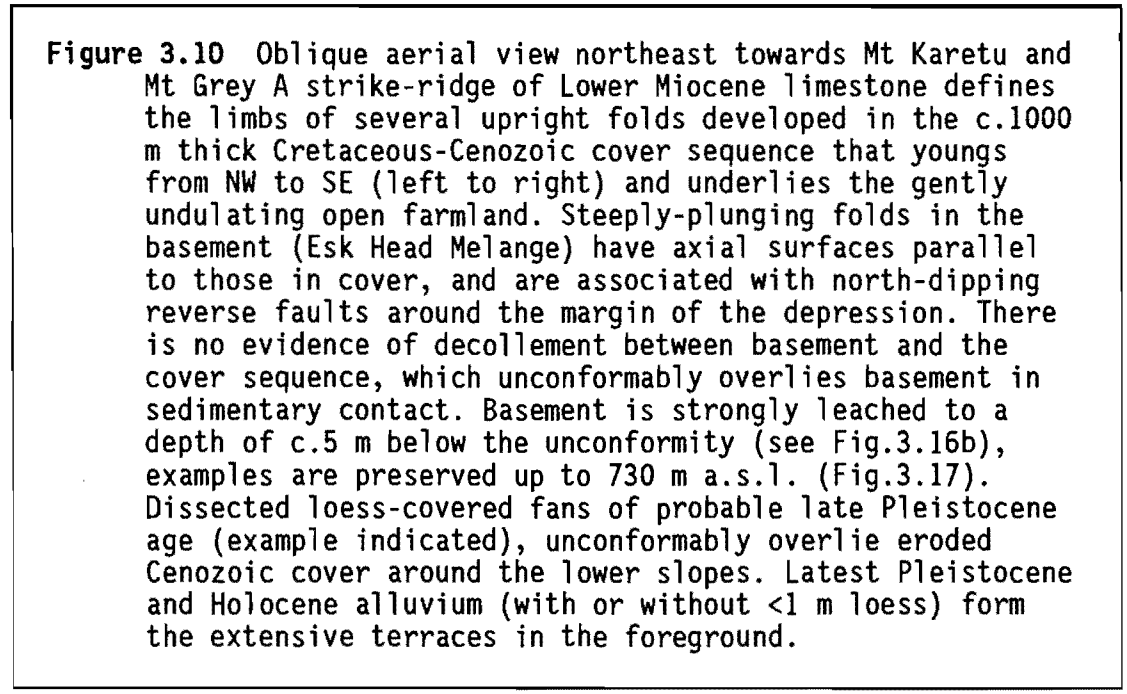

Figure 3.10 Oblique aerial view northeast towards Mt Karetu and Mt Grey A strike-ridge of Lower Miocene limestone defines the limbs of several upright folds developed in the c.1000 m thick Cretaceous-Cenozoic cover sequence that youngs from NW to SE (left to right) and underlies the gently undulating open farmland. Steeply-plunging folds in the basement (Esk Head Melange) have axial surfaces parallel to those in cover, and are associated with north-dipping reverse faults around the margin of the depression. There is no evidence of decollement between basement and the cover sequence, which unconformably overlies basement in sedimentary contact. Basement is strongly leached to a depth of c.5 m below the unconformity (see Fig.3.16b), examples are preserved up to 730 m a.s.l. (Fig.3.17). Dissected loess-covered fans of probable late Pleistocene age (example indicated), unconformably overlie eroded Cenozoic cover around the lower slopes. Latest Pleistocene and Holocene alluvium (with or without <1 m loess) form the extensive terraces in the foreground.


Mt Karetu
Mt Grey
Pleistocene fan

3.4.4 Mt Karetu-Mt Grey Fault Zone

With the exception of the Mt Lawry Fault there are few signs of active faulting to the north and immediately east of the Okuku River. Late Cenozoic deformation at this locality evidently has been accommodated by folding in the cover sequence, but exposures of crushed basement around the northern margin of the basin and in the west branch of the Grey River show evidence of reverse displacement; two pods of basal cover sequence have been displaced from the main body of cover rocks, several hundred metres upstream from the previously mapped unconformity (Browne and Field, 1985). The outliers are located on the hanging-wall of the faults, and the structurally highest (but stratigraphically lowest) one is preserved in sedimentary contact with leached basement (locality 21: Appendix 3.1). The crushed zones extend west and east into the highly strained rocks of the Esk Head Melange, and form bedding-parallel reverse faults (dip 50-75°N) which bound the southern slopes of Mt Karetu and Mt Grey, and are inferred to converge at depth with a south-dipping reverse fault zone that bounds the north side of Mt Karetu. The faults are associated with steeply plunging folds whose axial surfaces are sub-parallel to those of the cover sequence (Map 1), providing evidence of late Cenozoic folding of basement which explains the absence of evidence for a decollement between basement and cover.

To the east, in the east branch of the Grey River the reverse faults dip 80°N beneath the south side of the Mt Grey block (Janet Fault of Mason 1941), but the dip of this zone decreases to 31°N in a small ravine west of Lake Janet, where basement has been thrust over Kowai Formation. At Lake Janet the fault strikes north and bifurcates, forming a west-dipping, reverse-left-lateral fault associated with a surface trace in basement (Grey Fault: Wilson, 1963; Gregg 1964), and a second crushed zone at a slightly lower topographic elevation, against which the Tertiary sequence is locally overturned.

3.5 NORTHWEST-VERGING FOLD DOMAIN

3.5.1 Introduction

Plio-Pleistocene conglomerates (Kowai Formation), and late Pleistocene aggradation gravels and associated loess cover beds occur as a series of inliers on the northern Canterbury Plain. The inliers represent the surface expression of a young fold belt, which extends northeast from the Cust Anticline, to the Kowai Anticline west of

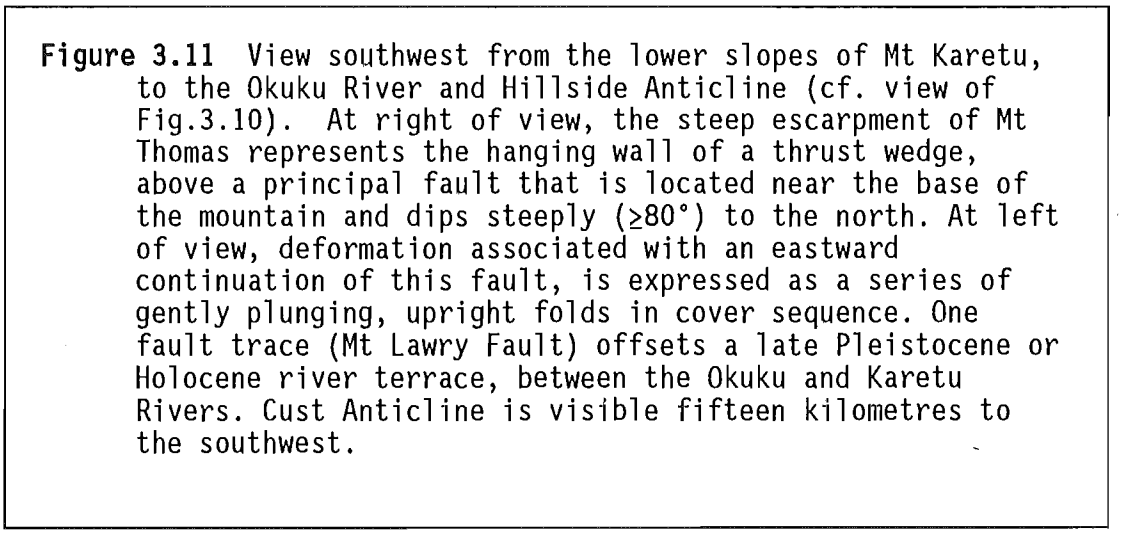

Figure 3.11 View southwest from the lower slopes of Mt Karetu, to the Okuku River and Hillside Anticline (cf. view of Fig.3.10). At right of view, the steep escarpment of Mt Thomas represents the hanging wall of a thrust wedge, above a principal fault that is located near the base of the mountain and dips steeply (≥80°) to the north. At left of view, deformation associated with an eastward continuation of this fault, is expressed as a series of gently plunging, upright folds in cover sequence. One fault trace (Mt Lawry Fault) offsets a late Pleistocene or Holocene river terrace, between the Okuku and Karetu Rivers. Cust Anticline is visible fifteen kilometres to the southwest.

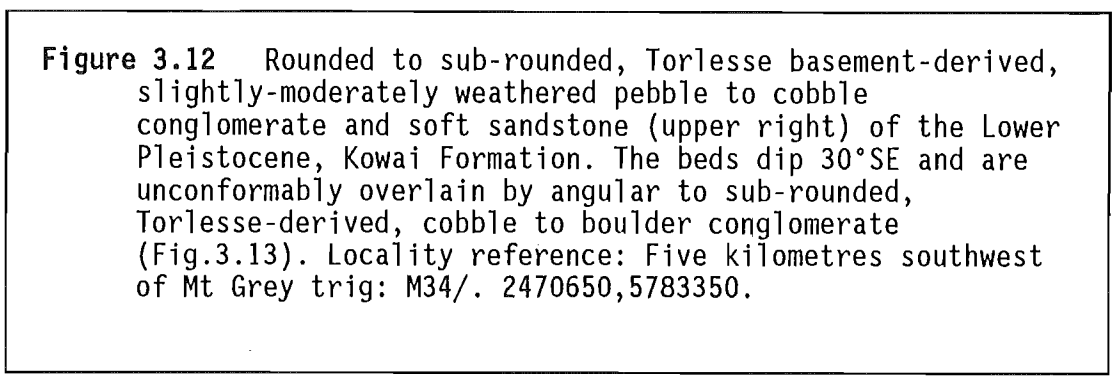

Figure 3.12 Rounded to sub-rounded, Torlesse basement-derived, slightly-moderately weathered pebble to cobble conglomerate and soft sandstone (upper right) of the Lower Pleistocene, Kowai Formation. The beds dip 30°SE and are unconformably overlain by angular to sub-rounded, Torlesse-derived, cobble to boulder conglomerate (Fig.3.13). Locality reference: Five kilometres southwest of Mt Grey trig: M34/. 2470650,5783350.

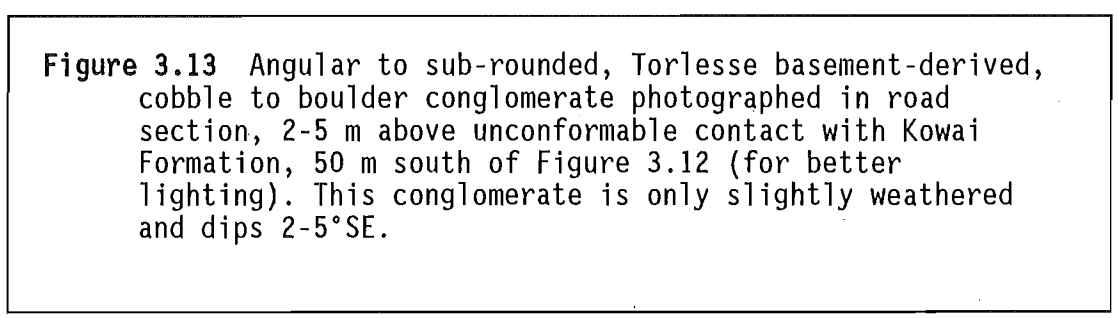

Figure 3.13 Angular to sub-rounded, Torlesse basement-derived, cobble to boulder conglomerate photographed in road section, 2-5 m above unconformable contact with Kowai Formation, 50 m south of Figure 3.12 (for better lighting). This conglomerate is only slightly weathered and dips 2-5°SE.

Fig.3.11

Fig.3.12

Fig.3.13

Amberley. The fold belt extends northeast beyond the mapped area, into the coastal hills north of Amberley (Wilson, 1963; Yousif, 1987), and offshore across the continental shelf (Carter and Carter, 1982; Barnes, pers.comm, 1990).

The amplitude of the folds above the surrounding Canterbury Plain and the depth to which the cover sequence has been unroofed, increases from southwest to northeast. The inferred uppermost part of marine (late Pliocene-early Pleistocene) Kowai Formation is exposed in the core of the Cust Anticline; fossiliferous marine (Pliocene) Kowai Formation is exposed in the core of the Kowai anticlines, and basement is exposed at the core of the Cass Anticline (Sheet 18).

3.5.2 Kowai Anticline

The northeast-southwest trending Kowai Anticline is an inclined, asymmetric fold, with a doubly-plunging axis and a "tear drop" geometry (Map 1). Northwest vergence is indicated by dip-slopes of 5-10° on the southeast limb and 30-60° on the northwest limb. A NW-SE oriented seismic reflection profile, located northeast of Kowai Anticline (Vax Line 1A, Kirkaldy & Thomas 1963), and the results of drilling (Hoolihan, 1978; Katz, 1982) indicate northwest-verging reverse or thrust faults in cover, at depths of a few hundred metres. Basement is at a depth of c.1400 m below ground surface (c.1200 m below sea-level).

3.5.3 Cust Anticline

The Cust Anticline is located on the northern Canterbury Plains and encompasses the elevated topography of the Mairaki and Cust Downs, south of the Ashley River (Map 1, Map 3). The Cust Anticline has a broadly similar geometry and wavelength to the Kowai Anticline but a smaller topographic amplitude and a more easterly strike. It is capped by an extensive late Pleistocene aggradation surface and more than 6 m of loess in places; and two lower terraces, the lowest of which represents a ancestral channel of the Ashley River, of probable Holocene age (Map 3).

3.5.4 Cust Fault

A 1.5 km long fault trace defines the surface expression of a fault, against which the west limb of Cust Anticline is terminated. The fault coincides with a large (c.500 m) offset in basement (NW-side up) (Vax Line 2: Kirkaldy & Thomas, 1963). This fault (herein named the Cust

Fault) has uplifted the western limb of the anticline, and impeded drainage where the ancestral Ashley River channel crosses the margin of the fold (Map 3).

3.5.5 Ashley Fault

The Ashley Fault is one of few active fault traces identified in the PPAFZ prior to this study and offsets Pleistocene and Holocene terraces of the Okuku River, between Okuku and Makerikeri Rivers (Brown, 1973; Berryman, 1979) (Maps 1, Map 4). The fault has a trace-length of 4.5 km and is down-thrown to the south. The fault swings in strike from 115° at its eastern end, to approximately 090° at Okuku River. No strike-slip offsets that could be regarded as unequivocal were observed in this study. High-resolution, low altitude air photographs of the Ashley Fault have been obtained by N.Z. DSIR Geology & Geophysics (P.R. Wood, pers.comm., 1989), but were not available for use in this study.

The projected trend of the Ashley Fault west of Okuku River coincides with the active floodplain of the Ashley River, and the base of the escarpment that defines the northern limb of the Cust Anticline. There is a clear contradiction between the throw on the Ashley Fault and the vergence and development of the Cust Anticline, implying that the former structure probably is an oblique-slip, tear-fault.

Along much of its length the north limb of the Cust Anticline has collapsed, as a series of large landslides which together with other data provide constraints on the timing of probable coseismic rupture on the Ashley Fault, and growth of the Cust Anticline (discussion in Chapter 5).

3.6 TIMING OF DEFORMATION IN THE PPAFZ

3.6.1 Evidence for Tertiary deformation

At least one fault in the area (Boby's Creek Fault: Sheet 18; Maps 1 and 2) shows evidence of activity associated with late Cretaceous rifting (Wilson, 1963; Field et al. 1989; Nicol, 1991). Volcanism was ubiquitous in North Canterbury at different times throughout the Tertiary, and several occurrences of igneous rocks are located close to Quaternary faults (e.g. Kowai and Lees Valley Faults: Map 1). But there is no evidence to suggest that Tertiary volcanism was accompanied by widespread faulting. Localised uplift and mild folding occurred during the late Oligocene (Wilson, 1963; Gage, 1970; McLennan and Bradshaw, 1984; Nicol, 1991), and is synchronous with evidence for widespread

volcanism in northeastern South Island (Weaver and Smith, 1989).

Miocene tectonic deformation was widespread (Wilson, 1963; Kirkaldy and Thomas, 1963; Andrews, 1968; Bradshaw, 1975; Field et al. 1989), and the entire pre-Miocene cover sequence was stripped from parts of northern North Canterbury at that time (Sheet 18). However, despite widespread active volcanism the intensity of Miocene deformation must have been weak in the south (this study area) because here, no unconformities on basement older than Pleistocene have been identified (refer to Fig.1.9). Consequently, in this study the age of the PPAFZ is defined as the period of time during which the presently oriented system of interconnected faults and related folds developed, and mountains within the zone were uplifted.

3.6.2 Quaternary inception of the PPAFZ

Widespread deposition of Torlesse-derived conglomerates in South Island during the Pliocene (e.g. Cutten, 1979; Field et al. 1989), indicates erosion of basement accompanying the uplift of the Southern Alps. In the study area, these deposits are included in the Kowai Formation (Fig.1.9) which comprises c.75-100 m of basal shallow-marine sediments (fossiliferous siltstone, fine sandstone and round pebble conglomerate), overlain by more than 500 m of conglomerate that coarsens up-section and become progressively more angular (Field and Browne, 1986). Kowai Formation unconformably overlies Early-Middle Miocene sediments in the Mt Grey area (Okuku, Grey and Kowai Rivers), and late Miocene sediments to the southwest (Field and Browne, 1986; and Carlson et al., 1980, respectively). Wilson (1963) and Browne and Field (1985) inferred that deposition of Kowai Formation was contemporaneous with fold growth, because at the type section (the core of the Kowai Anticline) the beds dip at progressively more gentle angles up-sequence.

The problem with this interpretation is that Kowai Anticline (among other folds in North Canterbury: Katz, 1982; Nicol, 1991), is strongly asymmetric and bedding attitudes for the basal and upper beds cannot be measured at the same points on the fold, because exposure is poor. The dip of upper beds is low (5-10°) on the eastern flank of the Kowai Anticline, but increases to 30-60° on the steep NW limb (Map 1). Elsewhere, upper beds of Kowai Formation are inclined to 64° (Hillside Anticline: Fig.3.11), or as little as 2° (in the hinge of McDonald Syncline: Nicol, 1991), which suggests that the variations are spatial, not temporal.

Although the upper Kowai conglomerate beds are coarser and more

angular than those near the base, they are considerably more rounded and finer-grained than the overlying, locally-derived late Pleistocene and Holocene deposits (cf. Figs 3.12, 3.13), which implies that the Kowai conglomerates were transported from a more distant source (probably the Southern Alps), prior to the uplift of the intervening Ashley and Okuku Ranges. The exact timing of uplift is poorly constrained: the top of the Kowai Formation is inferred to be Nukumaruan (c.1.5-2 Ma) (Field and Browne, 1986), but most sections are poorly dated and in the PPAFZ the top may be missing. At all localities examined during this study (also Nicol, 1991), Kowai Formation underlies a Holocene erosion surface (e.g. on the crest of Cust Anticline and Kowai Anticline: Maps 1 and 3), or is unconformably overlain by dissected fans of coarse, locally derived conglomerate capped by loess, indicative of a late Pleistocene age (e.g. Figs 3.10; 3.14).

3.7 KINEMATICS OF QUATERNARY FAULTING IN THE PPAFZ

3.7.1 Thrust and reverse fault domain

At Mt Grey, between one and two kilometres of SE-directed post-Pliocene thrusting may be inferred from offset strike-ridges of Amuri and Whiterock Limestone (AM and WR: Maps 1 and 2), and the presence of ?basal Kowai Formation beneath the thrust, west of Lake Janet. At Mt Thomas, E-SE directed thrusting may be inferred from fault geometries (Maps 1 and 2; cross-section E-F) but there are no structural markers to constrain the amount of displacement.

Further west, the distribution of Tertiary igneous rocks on either side of the Lees Valley Fault (Map 1) indicates right-lateral offset across that fault of, at most 4 km and possibly less than 1 km (Map 1). Vertical displacement of the same order across the Lees Valley Fault is implied by the juxtaposition of mineralogically equivalent but texturally different igneous rocks, of probable Lower Tertiary age: a lava flow or shallow sill of vesicular olivine basalt is a near-surface equvalent of a feeder dyke now exposed in cliffs formed in the hanging wall of the Lees Valley Fault, a few hundred metres to the south (Maps 1 and 2). The dyke comprises microgabbro, displaying a granophyric texture of quartz-feldspar intergrowths indicative of confinement pressures probably attained at a depth shallower than 5 km (R. Muir, pers.comm. 1991).

Figure 3.14 Angular to sub-angular, Torlesse basement-derived, cobble to boulder conglomerate exposed beneath a dissected Pleistocene fan which unconformably overlies basal cover sequence in sedimentary contact with leached basement. Locality reference (refer to Fig.3.10): Four kilometres southwest of Mt Karetu trig: M34/. 2465500,5784800.

3.7.2 Strike-slip domain

The total strike-slip offset across the central, Porter's Pass-Mt Thomas element of the PPAFZ is difficult to assess due to a lack of stratigraphic or geomorphic markers. Distinctive lithologies characteristic of Esk Head Melange (red and green chert and argillite) are common within the Glentui Fault Zone and abundant at Glentui River, which is c.15 km west of the nearest occurrence of Esk Head Melange. However, although such lithologies have not been observed in basement surrounding the Glentui Fault Zone, they are not unknown in basement further west (e.g. Sheet 18; Coyle, 1988). A right-lateral offset of c.15 km therefore is equivocal and must represent an upper bound.

Further west, a right-lateral offset of approximately 3 km across the Porter's Pass Fault may be inferred, where the Waimakariri River is deflected from its north-to-south trend and flows along the strike of the Porter's Pass Fault (Fig.3.2, Maps 1 and 2). The outlet of the Waimakariri River to the Canterbury Plains is a narrow corridor (<5 km wide) 1000 m below the crest of the Torlesse and Puketeraki Ranges (Map 2), so it is probable that the gorge is antecedent. Consequently, the c.3 km right-lateral offset may be indicative of the total strike-slip displacement on the Porter's Pass Fault, which is consistent with the inferred offsets on the oblique-slip, Lees Valley and Mt Grey Faults.

The available data suggest that the PPAFZ has accommodated perhaps less than 4 km of right-lateral displacement on any one element since the late Pliocene. This estimate represents one-fifth or less, of the right-lateral displacement of the Hope Fault to the north (c.20 km total right-lateral offset: Freund, 1971).

3.7.3 Holocene slip-rates

At sites between Porters Pass and Kowai River, Coyle (1988) measured right-lateral offsets of up to 53 m on stream channels displaced by the Porter's Pass Fault. Coyle proposed a Holocene slip-rate of 5-10 m/kyr for that fault, which is somewhat higher than the one published estimate of 4 m/kyr, inferred from a site just west of Porters Pass (Berryman, 1979). If accepted, Coyle's estimate of Holocene slip-rate for the Porters Pass Fault probably represents a minimum rate for the wider PPAFZ, and a total between 20% and 50 % that of the Hope Fault to the north (20-25 m/kyr: Van Dissen and Yeats, 1991), which is the presently the most active element of the Marlborough fault system, accommodating 50-60% of the total relative plate motion across southern Marlborough

(cf. Frontispiece 1 and Fig.1.1).

3.8 FOLDING AND QUATERNARY UPLIFT IN THE PPAFZ

Evidence that Tertiary tectonic deformation in the PPAFZ was mild is supported by the absence of unconformities on basement, older than Plio-Pleistocene (Fig.1.9). The morphometry of the Ashley and Okuku Ranges also is indicative of a young landscape: summit surfaces are broad and accordant; the drainage density is high, and rivers and streams presently are incised within deep, saw-cut gorges (Figs 3.15 a,b,c; Map 2).

The relatively uniform thickness of basal cover sequence in the study area (Fig.1.9) suggests that the unconformity surface originally was sub-planar. In the Mt Grey and Waipara areas, Wilson (1963) reported a c.5 m thick, severely weathered zone in basement beneath the unconformity. Smale (1989) concluded that this feature represents the product of intense leaching, resulting from the circulation of pore fluids beneath the Cretaceous coal measures of the Broken River Formation. Elsewhere in eastern South Island, similar features have been documented where the Torlesse-Cretaceous unconformity forms an extensive, exhumed peneplain (Cotton, 1917; Gair, 1967; Stirling, 1990).

In this study, many new localities where remnants of the leached unconformity surface are preserved, have been documented (Appendix 3.1; Maps 1 and 2), including several from which the Cretaceous-Cenozoic cover sequence has been removed (e.g. Fig.3.16 a,b). These data have been contoured to place constraints on total, post-late Cretaceous uplift within the PPAFZ and elucidate the relationship between topography and structure (Fig.3.17 cf. Map 2). The contoured unconformity surface corresponds closely to flat or gently inclined surfaces (ridge-crests and depressions) north and west of Mt Thomas (Figs 3.18, 3.19), and north and south of Mt Karetu (Map 2 and Figs 3.10, 3.20, respectively). The topographic depressions are interpreted as folds in the unconformity surface (wavelength c.6-8 km and amplitude c.400-600 m) which have developed in the weak rocks of the Esk Head Melange. Corroborative evidence of a mechanism for folding include the reverse faults and shorter-wavelength folds, developed in Esk Head Melange around the southern slopes of Mt Karetu (Map 2). Slopes surrounding the topographic depressions rise to the broadly accordant summits of between 900 and 1000 m (Frontispiece 3; Map 2), that extend west to the Ashley River Gorge and define a surface which is inferred to closely reflect the original

Figure 3.15(a) View northwest into Ashley Gorge, where remnant strath terraces attest to floodplain-widening, during a period of relative equilibrium: reduced stream power accompanying cold-climate aggradation, or perhaps a pause in tectonic uplift. The absolute strath ages are unknown, but they are higher than the inferred latest Pleistocene (c.14 kyr) aggradation terrace in the gorge. The Ashley River presently flows within a saw-cut gorge 60 metres below the lowest strath indicated on this Figure (see also Fig.3.15b). Observer location: Lees Valley Road L34/. 2445050,5774100.

Figure 3.15(b) Ashley River viewed from the Lees Valley Road. Note the absence of terraces above the riverbed. Canoeists for scale. Observer location: L34/. 2444100,5775100.

Figure 3.15(c) One of several saw-cut gorges of the Glentui River, incised into indurated basement (sandstone beds of Rakaia subterrane), upstream from the Glentui Fault Zone. The gorge is c.2 m wide at water-level. Locality reference: L34/. 2449250,5778250.

a.

b.

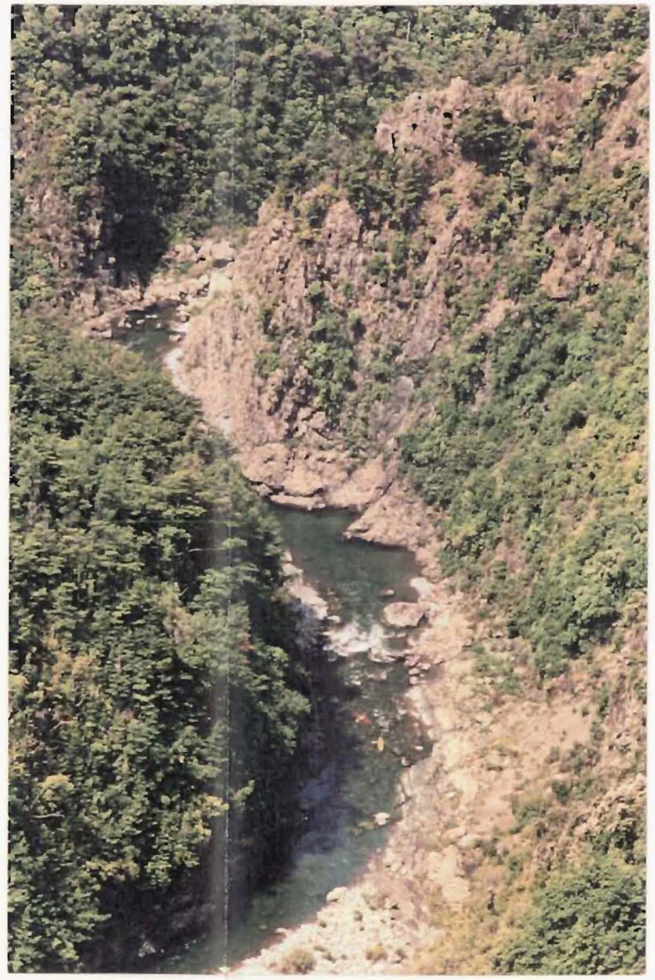

c.

Figure 3.16(a) Strongly leached basement below the Late Cretaceous unconformity. The rock can be crumbled by hand and at first glance is easily mistaken for basal cover sequence. This exposure is locality 29 (of Appendix 3.1), northwest of Mt Karetu: M34/.2462900,5794450.

Figure 3.16(b) Strongly leached basement analogous to that of Fig.3.16(a), but more oxidised. This exposure (locality 20:Appendix 3.1) is in a road-cut on the crest of a ridge, 560 m above sea-level and c.2 km southeast of the Mt Karetu trig. Locality reference: M34/. 2469050,5787400.

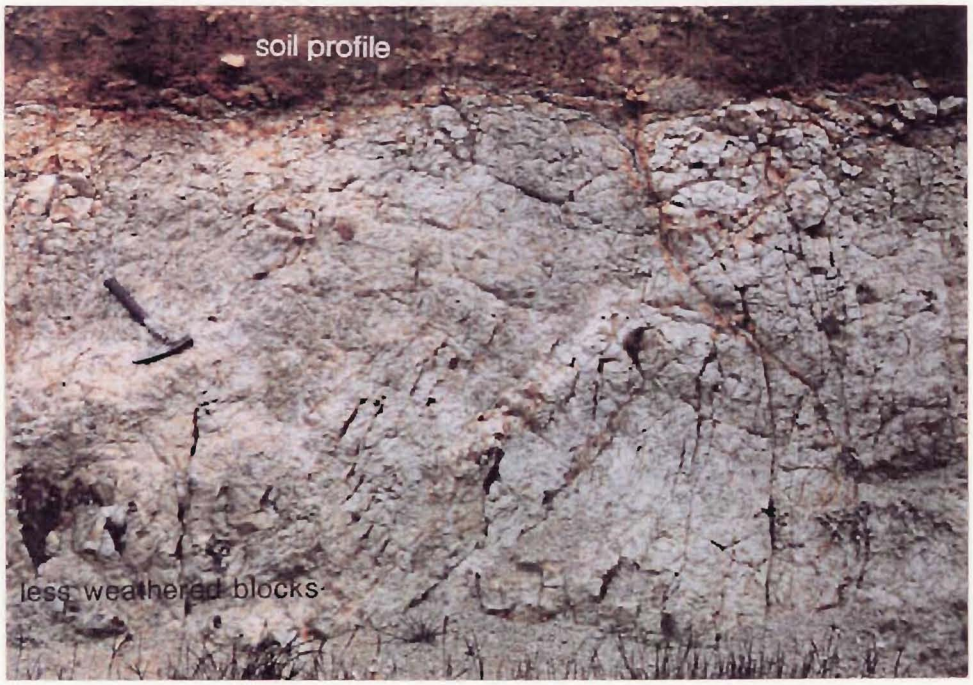
soil profile
less weathered blocks

a.


relict joints
less weathered block

b.

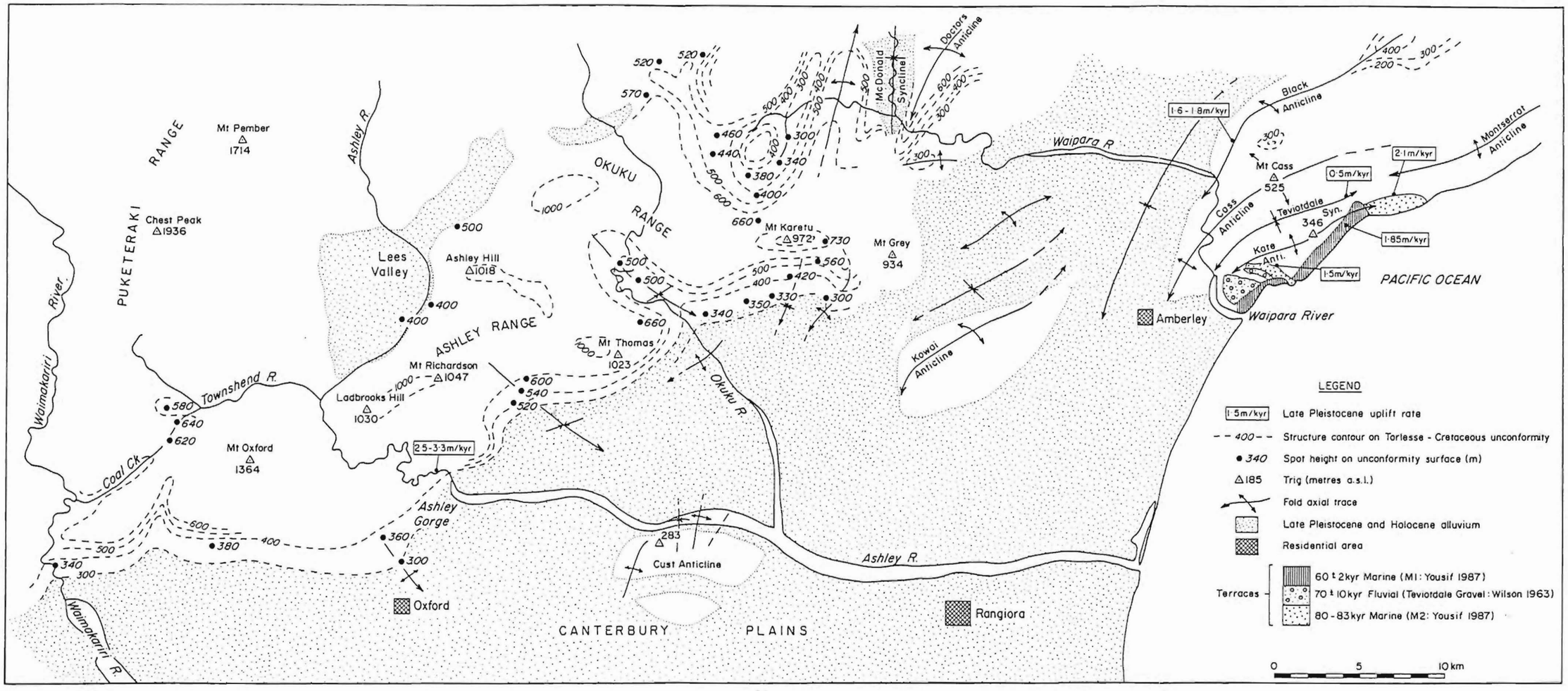

Figure 3.17 Map showing structure contours on the Torlesse-Cretaceous unconformity surface, constrained by spot-heights tabulated in Appendix 3.1. Axial traces of principal folds are shown, but faults are omitted for clarity. Differential uplift rates have been derived from offset fluvial terraces inland and uplifted marine terraces at the east coast (see text for explanation).

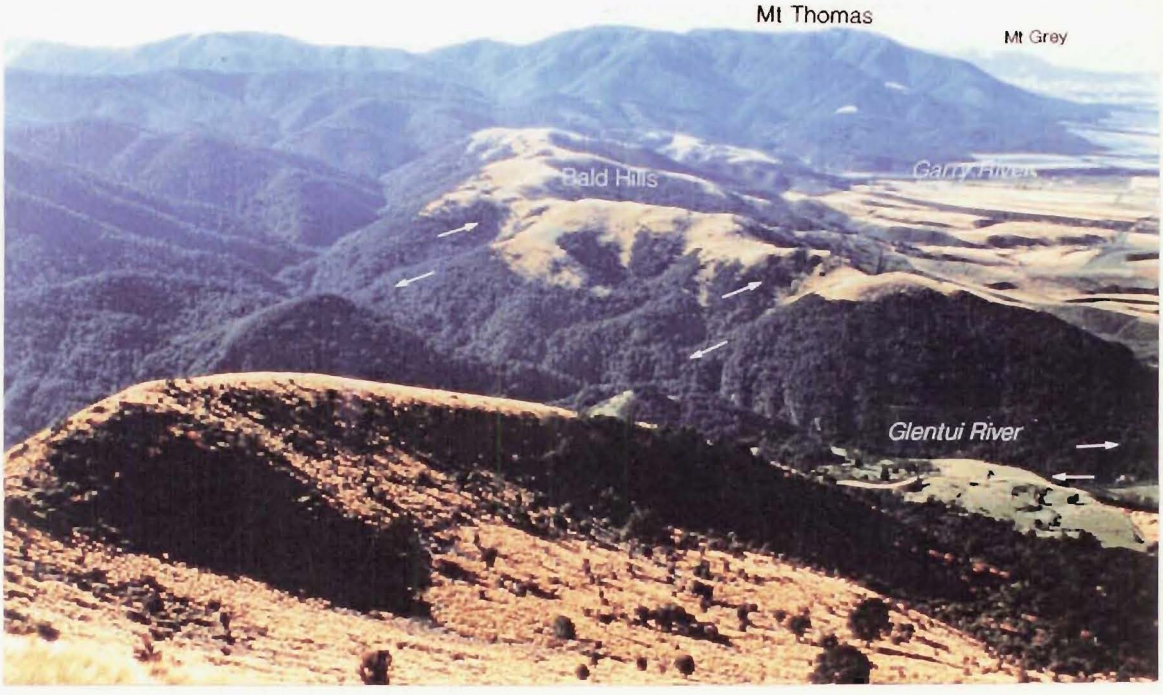

Figure 3.18 View east towards Mt Thomas along the strike of the Glentui Fault Zone across Glentui River and Bald Hills (arrows indicate location of principal faults and sense of relative displacement). Deeply weathered basement crops out on the Bald Hills, defining points on the Torlesse-Cretaceous unconformity surface which rises to the north (left) from beneath Quaternary cover of the Canterbury Plains, to 1000 m at the crest of the Ashley Range. The crest of Mt Thomas also is inferred to represent the unconformity surface, and the elevation difference at the range-front is attributed to cross-folding about sub-horizontal, NW-SE trending axes.

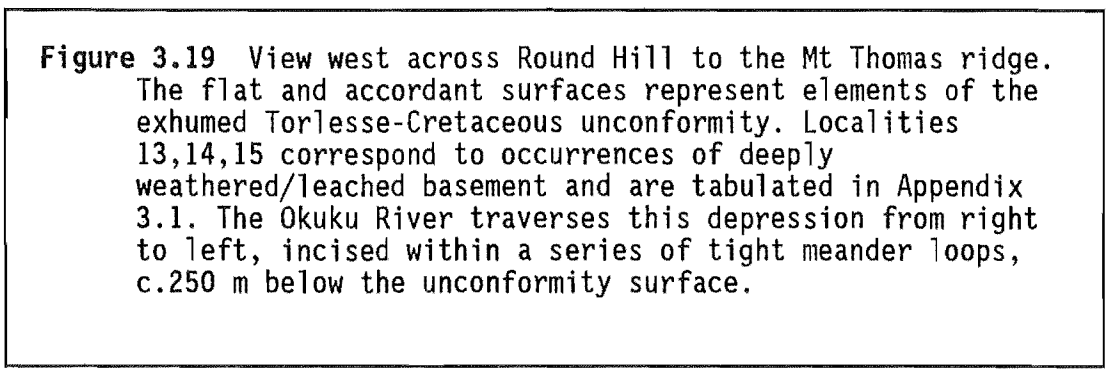

Figure 3.19 View west across Round Hill to the Mt Thomas ridge. The flat and accordant surfaces represent elements of the exhumed Torlesse-Cretaceous unconformity. Localities 13,14,15 correspond to occurrences of deeply weathered/leached basement and are tabulated in Appendix 3.1. The Okuku River traverses this depression from right to left, incised within a series of tight meander loops, c.250 m below the unconformity surface.

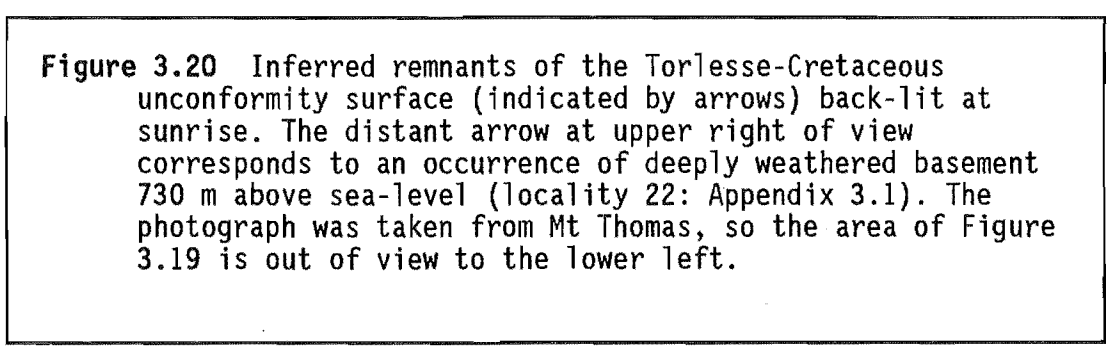

Figure 3.20 Inferred remnants of the Torlesse-Cretaceous unconformity surface (indicated by arrows) back-lit at sunrise. The distant arrow at upper right of view corresponds to an occurrence of deeply weathered basement 730 m above sea-level (locality 22: Appendix 3.1). The photograph was taken from Mt Thomas, so the area of Figure 3.19 is out of view to the lower left.

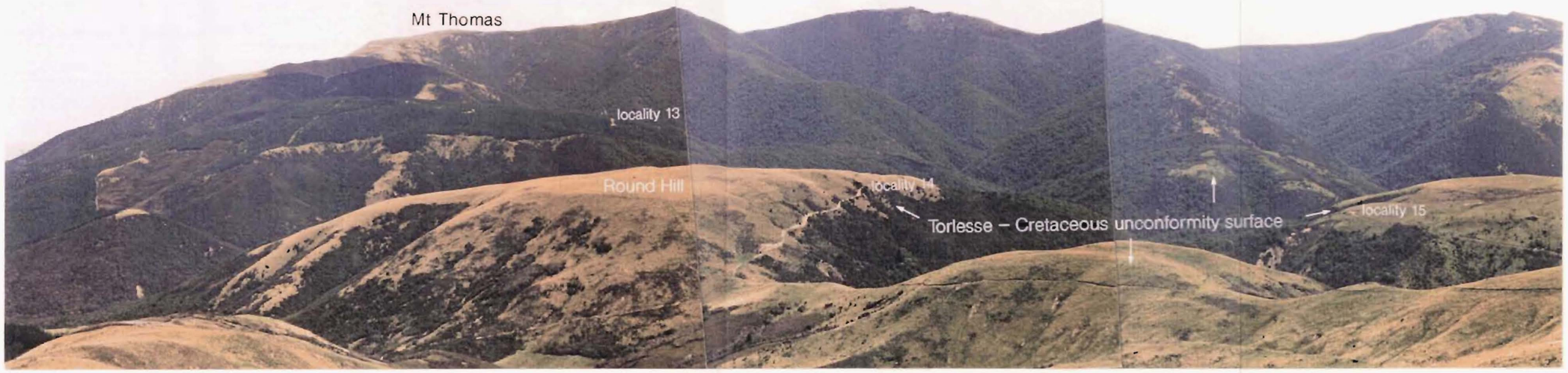

Fig.3.19

Fig.3.20

Torlesse-Cretaceous unconformity.

Along the margin of the Canterbury Plains, east of Waimakariri River and the western margin of the Culverden Basin as far north as Waiau River (Frontispiece 1), the unconformity surface lies between 300 and 400 m (Fig.3.17; R. Mould pers.comm. 1992; Syme, 1991). Above the hanging-wall of the range-bounding faults the unconformity surface rises to c.500-600 m in the fold depressions of the uplifted Ashley and Okuku Ranges, and 800-1000 m at the accordant range-crests if the analogy is accepted. The uniform elevation of the unconformity along the margins of the uplifted blocks and at higher elevations within the blocks, suggests that regional and differential uplift has been relatively uniform in these parts of North Canterbury.

It has been argued (Section 3.6.3) that conglomerates of the Plio-Pleistocene Kowai Formation were derived from a source more distant than the slopes of the modern Ashley and Okuku Ranges. Paleocurrent indicators in the Kowai Formation are sparse, but the most probable source regions are the Southern Alps to the west and northwest, where mountains rise to more than 1900 m and are deeply dissected (Frontispiece 1). Conglomerates derived from those areas would have been transported across the area now occupied by the Ashley and Okuku Ranges, so a first-order estimate of Pleistocene differential uplift in the PPAFZ is given by the equation:

$$\text{uplift } (U) = (T) + (H) \qquad (1)$$

where (T) is the thickness of cover sequence above the Torlesse unconformity, and (H) is the topographic offset of the unconformity surface above the youngest elements of Kowai Formation on the footwall of the range-bounding faults (Fig.3.21).

The thickness of cover sequence between the Torlesse-Cretaceous unconformity and the basal (marine) part of the Kowai Formation is 430 m thick in the Kowai-1 drillhole at Kowai Anticline (Map 2; Hoolihan, 1978); approximately 480 m thick in the west branch of the Grey River (Browne and Field, 1985, this study), and probably a similar thickness beneath the Cust Anticline further west (Vax Line 2, Kirkaldy and Thomas, 1963). In the Mt Grey area, basal Kowai beds are overlain by c.500-600 m of conglomerate. Sections elsewhere, including drillholes offshore, suggest a representative thickness for Kowai Formation of c.600 m (Field and Browne, 1986).

Kowai Formation comprises alternating marine and non-marine intervals, that are poorly constrained, but the upper-most interval west of Mt Grey is inferred to be non-marine. The inferred total thickness of

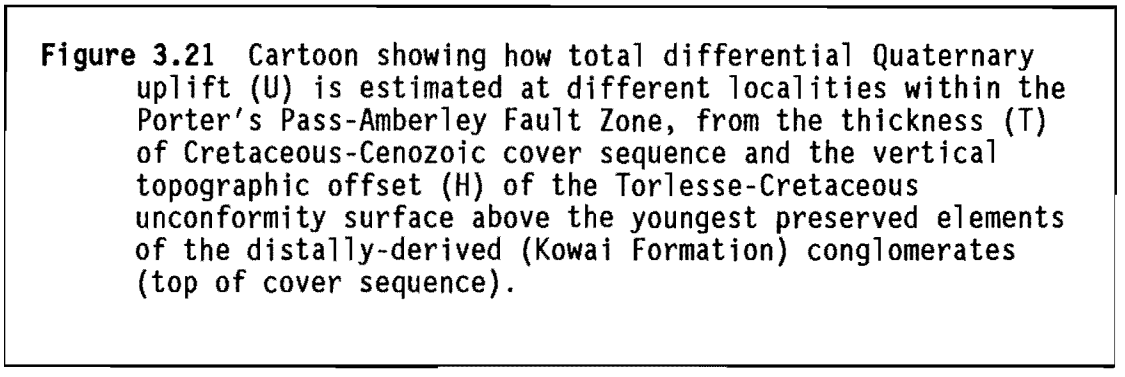

Figure 3.21 Cartoon showing how total differential Quaternary uplift (U) is estimated at different localities within the Porter's Pass-Amberley Fault Zone, from the thickness (T) of Cretaceous-Cenozoic cover sequence and the vertical topographic offset (H) of the Torlesse-Cretaceous unconformity surface above the youngest preserved elements of the distally-derived (Kowai Formation) conglomerates (top of cover sequence).

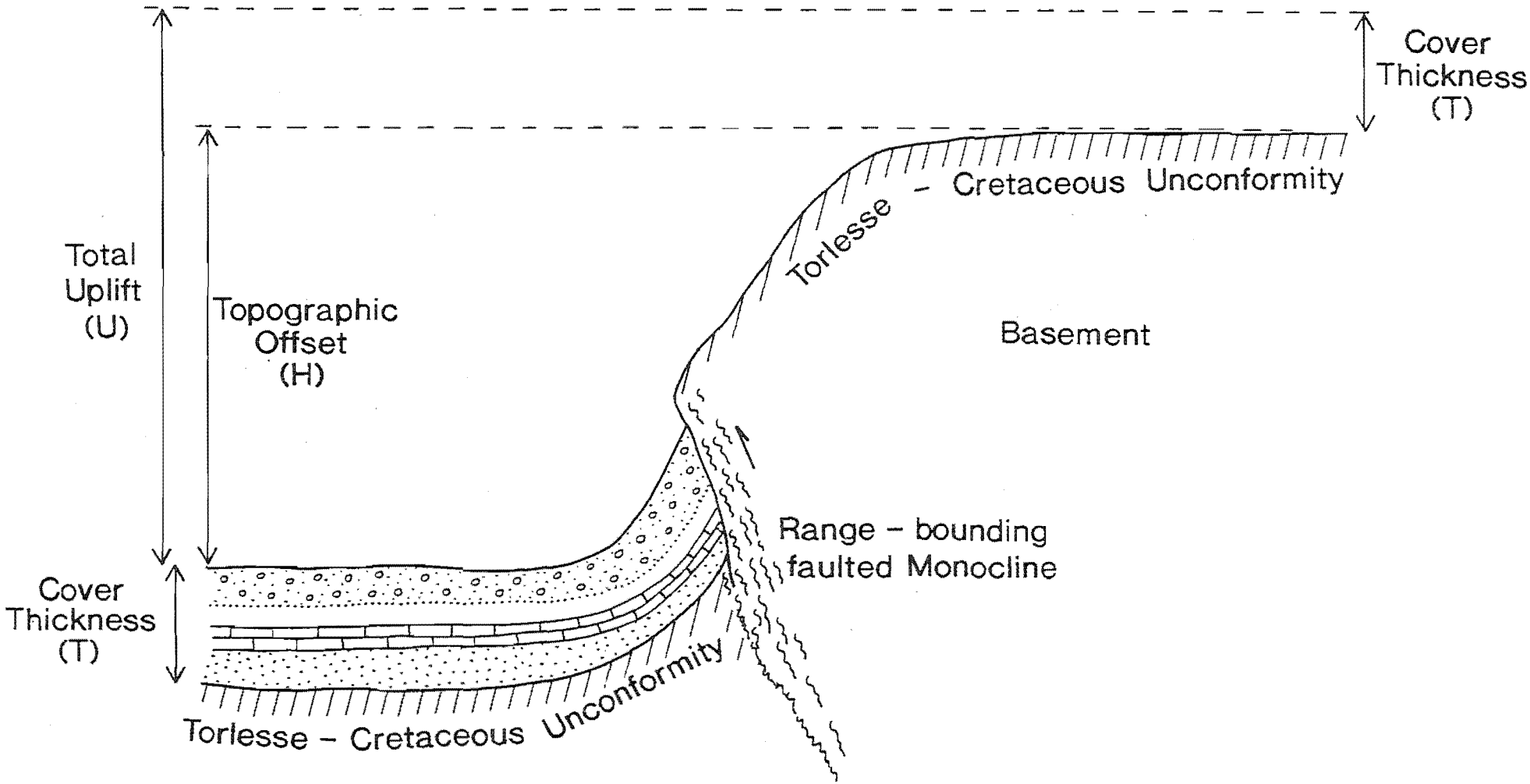
Cover
Thickness
(T)
Torlesse – Cretaceous Unconformity
Total
Uplift
(U)
Topographic
Offset
(H)
Basement
Range – bounding
faulted Monocline
Cover
Thickness
(T)
Torlesse – Cretaceous Unconformity

cover sequence is c.1000 m. The present elevation of the unconformity is constrained by data in Appendix 3.1 and Figure 3.17. At Waimakariri River the Torlesse-Cretaceous unconformity outcrops at 340 m above sea-level and only the Lower Tertiary elements of the cover sequence are preserved. The projected location of the top of the sequence (calculated from bedding dips in the preserved section) would be c.2-2.5 km downstream from the unconformity, at an elevation of c.300 m. In Castle Hill Basin to the northwest, the unconformity outcrops at 900 m (Field et al. 1989; Map 1). The crest of the intervening Torlesse and Puketeraki Ranges exceeds 1900 m, so from Equation 1 the minimum uplift (U) above the mountains is: (1000 m) + (1600 m) = 2600 m.

In contrast, uplift above the Ashley Range northeast of Ashley Gorge is (1000 m) + (700 m) = 1700 m, and above the Okuku Range uplift varies from: (1000 m) + (0 m) = 1000 m (in the fold depressions); to (1000 m) + (450-550 m) = 1450-1550 m along the crest of the range. Northeast of the study area, basement is exposed at the core of all major folds (Sheet 18), but much less uplift has occurred in the south (near Amberley) and the Torlesse-Cretaceous unconformity is exposed only in the core of the Cass Anticline (Fig. 3.17). From Equation 1, maximum uplift in this area is estimated at: (1000 m) + (200 m) = 1200 m.

Preservation of the leached late Cretaceous unconformity surface in the Ashley and Okuku Ranges, and the presence of locally-derived and only partially dissected fan deposits at high levels in the topography provide qualitative evidence of recent uplift and unroofing of basement in the study area. The abrupt decrease in topographic relief from northwest to southeast across the Puketeraki and Torlesse Ranges and the contrasting morphometry of the Ashley and Okuku Ranges, is consistent with an eastward migration of uplift previously inferred from facies and textural variations between late Miocene-Pleistocene stratigraphic sections in the west, and those of equivalent age intersected by drillholes offshore to the southeast (Field et al. 1989).

3.9 RATE AND TIMING OF UPLIFT

3.9.1 Uplift rate for the Ashley Range

The inception of uplift in the PPAFZ is younger than Lower Pleistocene, because the youngest ages obtained from Kowai Formation so far are Nukumaruan Stage (c.2-1.5 Ma) (Browne and Field, 1985); just how much younger the commencement of uplift is, is problematical to resolve because of a lack of age control on Pleistocene surfaces and deposits.

A differential uplift rate for the Ashley Range can be estimated at one locality in the lower Ashley River Gorge, where the strath of an aggradation terrace (Fig.3.22) presently is c.40 m higher than its inferred downstream correlative - a late Pleistocene aggradation surface of the Canterbury Plains (Frontispiece 3), mapped as Burnham Formation (Sheet 18; Wilson, 1989) and attributed a latest-Pleistocene age. Wilson (1989) suggests an age of 15-27,000 years for Burnham Formation, but his map indicates a younger limit of c.10,000 which marks the base of the post-glacial Springston Formation, and spans the interval 14-10,000 formerly represented by St Bernard Formation (Gage, 1958: refer to Sheet 18).

The end of the latest Pleistocene glaciation in New Zealand was accompanied by rapid withdrawal of ice and river incision at about 14,000 years ago in many parts of South Island, including North Canterbury (Suggate, 1965, 1988). Ashley River presently flows within a saw-cut gorge incised below the strath of the late Pleistocene aggradation terrace. No degradational strath or fill-terraces are preserved at intermediate levels, so it is reasonable to infer that the river has incised without pause since the aggradation terrace was abandoned. Consequently, the age of the aggradation terrace probably is latest-Pleistocene and for estimating a differential uplift rate at this locality, upper and lower bound ages of 16 kyr and 12 kyr, respectively, are surmised for the commencement of down-cutting below the terrace strath. From these ages, an uplift of 2.5-3.3 m/kyr is inferred. It may be unwarranted to assume that this indirect estimate of uplift represents a long-term average rate, but as a first approximation the total vertical offset of cover sequence above the Ashley Range east of Ashley Gorge (c.1700 m), suggests that initial uplift could have occurred within the range (1700/0.0025 m/yr = 680,000 years) to (1700/0.033 m/yr = 515,000 years).

3.9.2 Uplift rates from Pleistocene marine terraces at the east coast

At the northeastern end of the PPAFZ, Pleistocene marine terraces have been uplifted along the Pacific coast, on the flanks of folds that constitute eastern elements of the northwest-verging fold belt (cf. Fig.3.1 and Frontispiece 1). The topography of the coastal fold belt is several hundred metres lower than the Ashley and Okuku Ranges, and marine terraces represent wave-cut platforms, formed during Pleistocene interglacial and interstadial periods of high sea-level (within a few metres of present sea-level).

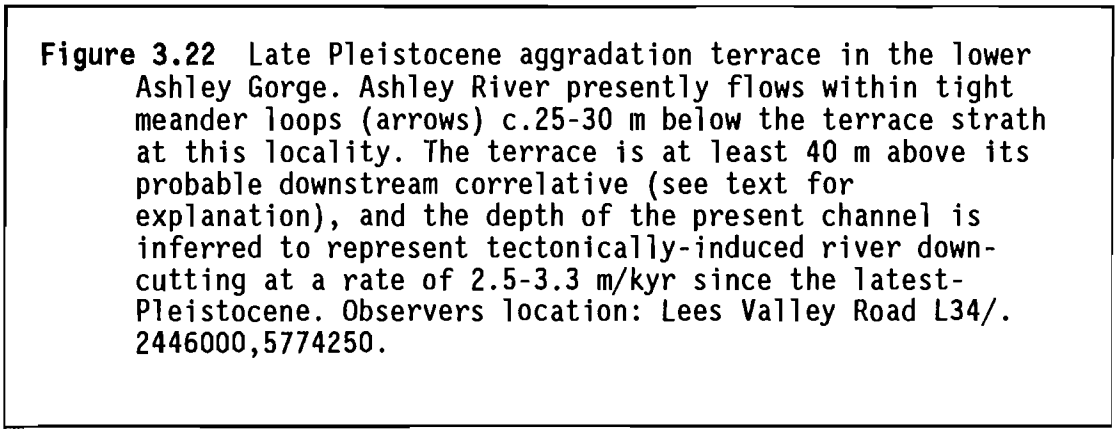

Figure 3.22 Late Pleistocene aggradation terrace in the lower Ashley Gorge. Ashley River presently flows within tight meander loops (arrows) c.25-30 m below the terrace strath at this locality. The terrace is at least 40 m above its probable downstream correlative (see text for explanation), and the depth of the present channel is inferred to represent tectonically-induced river down-cutting at a rate of 2.5-3.3 m/kyr since the latest-Pleistocene. Observers location: Lees Valley Road L34/. 2446000,5774250.

Figure 3.23 Marine terrace terminology (from Pillans, 1990).


aggradation terrace

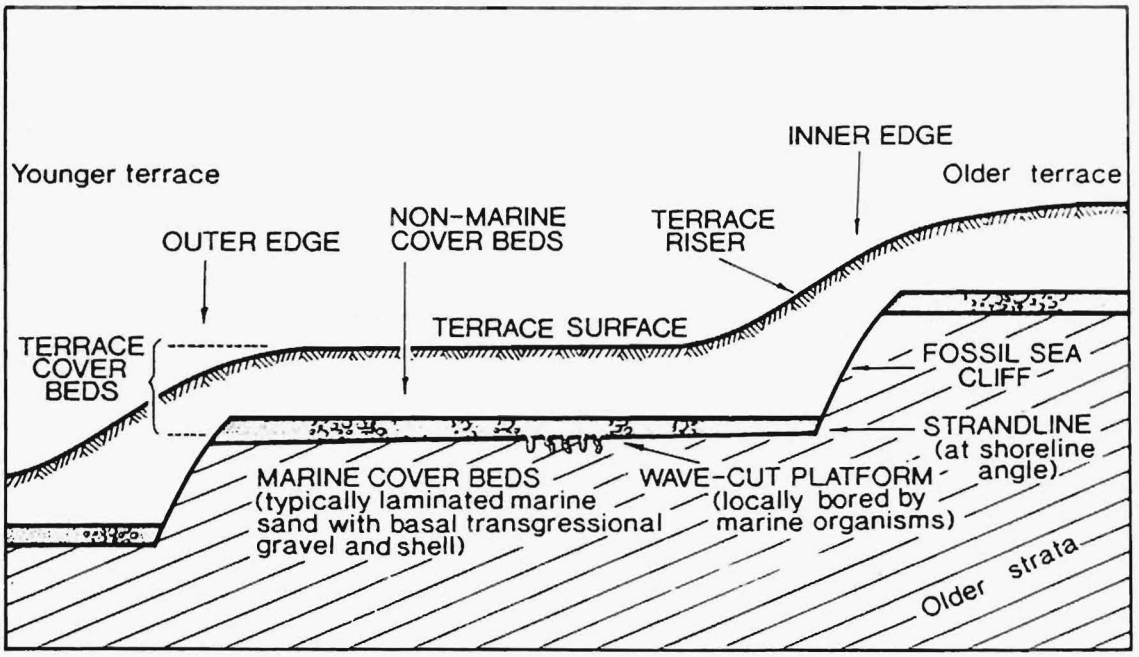
INNER EDGE
Younger terrace
Older terrace
OUTER EDGE
NON-MARINE COVER BEDS
TERRACE RISER
TERRACE SURFACE
TERRACE COVER BEDS
FOSSIL SEA CLIFF
STRANDLINE (at shoreline angle)
MARINE COVER BEDS (typically laminated marine sand with basal transgressional gravel and shell)
WAVE-CUT PLATFORM (locally bored by marine organisms)
Older strata

The altitudinal spacing of marine terraces along the North Canterbury coast has been described by Carr (1970); Yousif (1987) and Barrell (1989), from which ages and uplift rates have been inferred (Yousif, 1987; Barrell, 1989). Pillans (1990) summarised the information required to calculate an uplift rate from former marine terraces; one needs to know: 1) the age (T) of a marine terrace; 2) its present height (H); 3) the height (E) at which the strandline (Fig.3.23) was formed relative to sea-level; and 4) sea-level height (S) relative to present, at the time the terrace was formed. The uplift rate (U), is derived using the equation:

$$U = \frac{(H-E-S)}{T} \qquad (2)$$

The age of only one terrace is constrained by field relationships near the mouth of the Waipara River (M1 of Yousif, 1987) (Fig.3.17). The M1 terrace truncates an older fluvial terrace deposit which is capped by loess and interpreted as an aggradation surface of the last glaciation (Teviotdale Gravels: Wilson, 1963). The marine cover beds overlying the M1 terrace are capped by two loess sheets, separated by a weak paleosol, the upper of which contains a rhyolitic ash analogous to the central-North Island, Kawakawa Tephra, and returned a fission-track age of 20,300 ±7100 years. The age of the Kawakawa tephra (Oruanui eruption) has been revised to 22,500 years from radiocarbon dating of charcoal collected from a pyroclastic flow deposit near the source (Wilson et al. 1988).

From the thickness of loess on the M1 terrace, Yousif concluded that the wave-cut platform probably was formed during an interstadial high sea-level at about 60 kyr ago (oxygen-isotope stage 4a: Shackleton and Matthews, 1977). At a higher elevation than the fluvial terrace is an older marine terrace (M2 of Yousif), which Yousif inferred to be of last interglacial age (oxygen-isotope stage 5a: c.80 kyr), and a probable correlative of the Motunau coastal plain to the northeast, and the Amuri Bluff terrace at Conway Flat further north (Ota et al., 1984).

Yousif measured the height above present sea-level of the M1 and M2 wave-cut platforms, and calculated rates of uplift from the inferred terrace ages using the late Pleistocene sea-level curve of Shackleton and Matthews (1977). Yousif's uplift rates range from 0.5 m/kyr in the hinge of the Teviotdale Syncline, to 2.0 m/kyr at the termination of the Kate and Montserrat Anticlines (Fig.3.17). These values are comparable to uplift rates inferred for marine terraces further north (at Conway Flat: Sheet 18) (Ota et al. 1984).

If the revised sea-level curve of Chappell and Shackleton (1986) were used to estimate uplift from Yousif's oxygen-isotope stage and terrace height-terrace age correlations at the Waipara coast, the rate would increase slightly, but the terrace ages are not sufficiently precise to make stronger inferences about the rate of uplift, other than to say that the minimum regional uplift rate (assessed as net uplift along synclinal axes) probably varies from c.0.5-1.0 m/kyr, and the differential uplift may approach 2.7 m/kyr above anticlines (Cowan and Nicol, in prep.; Nicol and Alloway, in prep.). If the maximum differential uplift above the anticlines is c.2.7 m/kyr, then the estimated time of inception of uplift beneath the Cass Anticline (1200 m/.0027 m/yr = c.445,000 years) is similar to that obtained further west, by extrapolating the inferred post-glacial down-cutting rate at the Ashley River Gorge.

The available data indicate that uplift and unroofing of basement in the PPAFZ east of Waimakariri River has occurred within the last 1 million years, possibly within the last 500,000 years and for the first time since the late Cretaceous. Most importantly, the data constrain the rate of landscape evolution and structural development within the PPAFZ. The uplift rates are an order of magnitude higher than those estimated by Wellman (1979), but similar to data from southern North Island (Ghani, 1978; Pillans, 1986). Notwithstanding uncertainties about spatial and temporal variations in the rate of uplift, the estimated values used here cannot be lowered by more than a factor of 2 without requiring that uplift was occurring along the PPAFZ during the Pliocene, for which there is no evidence.

Just how recently the uplift began remains equivocal, but this question might be resolved by amino-acid racemisation dating of wood from the top of Kowai Formation - provided the top can be found. Absolute dating of late Pleistocene, fluvioglacial deposits preserved at high elevations (c.1000 m) in the Waimakariri Valley (Gage, 1958, 1970), would further constrain rates of uplift across the range-front at the western end of the PPAFZ.

3.10 SUMMARY

1. Geological mapping has identified three structural domains in which the geometry and kinematic style of late Quaternary deformation differ at the surface:

1) Strike-slip faulting characterises the western half of the study area, between the Waimakariri, Whistler and Glentui rivers, and centred

on Mt Oxford;

2) **Thrust and reverse faulting** characterises surface faulting east and southeast of Lees Valley, encompassing the Ashley and Okuku Ranges and the Esk Head Melange;

3) a **northwest-verging fold belt** is developing beneath the northern Canterbury Plains between Amberley and Cust. Quaternary conglomerates are folded, and Holocene surfaces are offset by faults.

2. One fault in the area (Boby's Creek Fault: Sheet 18; Maps 1 and 2) is a re-activated late Cretaceous structure, but there is no evidence of widespread late Cretaceous or Tertiary faulting. Although Miocene tectonic deformation was widespread in northern South Island, with the entire pre-Miocene cover sequence stripped from parts of northern North Canterbury, the intensity of deformation was weak in the south (this study area) because no unconformities on basement older than Pleistocene have been identified.

3. Between one and two kilometres of SE-directed post-Pliocene thrusting may be inferred at Mt Grey, from offset strike-ridges of Tertiary limestone and the presence of Plio-Pleistocene sediments beneath the Mt Grey thrust. East to southeast-directed thrusting is inferred from fault geometries at Mt Thomas, but there are no structural markers to constrain the amount of displacement.

In Lees Valley, the distribution of Tertiary igneous rocks on either side of the Lees Valley Fault indicates $\leq$4 km of right-lateral offset on that fault. A similar vertical offset is implied by juxtaposition across the fault, of mineralogically equivalent but texturally different Tertiary igneous rocks.

4. The total strike-slip offset across the PPAFZ is difficult to assess due to a lack of stratigraphic or geomorphic markers, but a right-lateral offset of approximately 3 km may be inferred from a deflection of the Waimakariri River along the strike of the Porter's Pass Fault.

5. Right-lateral offsets of up to 53 m on stream channels displaced by the Porter's Pass Fault, imply a Holocene slip-rate of 5-10 m/kyr for that fault (Coyle, 1988). This estimate probably represents a minimum rate for the wider PPAFZ, and is equivalent to 20-50 % of the Hope Fault slip-rate (20-25 m/kyr: Van Dissen and Yeats, 1991), which is the presently the most active element of the Marlborough fault system.

6. The thickness of basal cover sequence in the study area is relatively uniform, suggesting that the Torlesse-Cretaceous unconformity surface originally was sub-planar. Basement beneath the unconformity is strongly leached to a depth of 5-10 m. Localities where the leached unconformity surface is preserved have been documented and contoured, to calculate the total post-late Cretaceous uplift within the PPAFZ. The contoured unconformity surface corresponds closely to flat or gently inclined surfaces (ridge-crests and depressions) in the Okuku and Ashley Ranges, and reflects folding of the unconformity surface (wavelength c.6-8 km, amplitude c.400-600 m).

7. Preservation of the leached late Cretaceous unconformity surface in the Ashley and Okuku Ranges and only partially dissected fan deposits at high levels in the topography provide qualitative evidence of recent uplift and unroofing of basement in the study area. Differential uplift is estimated at different localities using the uniform thickness of cover sequence in the area (c.1000 m) and the height of the Torlesse-Cretaceous unconformity surface above the youngest elements of cover sequence.

Estimated differential uplift is greatest in the west and decreases from c.2600 m northwest of Waimakariri River, to c.1700 m above the Ashley Range; c.1450-1550 m above the Okuku Range and c.1100 above the Cass Anticline in the coastal fold belt northeast of Amberley.

8. A late Pleistocene-Holocene differential uplift rate of 2.5-3.3 m/kyr is calculated from a vertical offset of 40 m, between an aggradation terrace in the lower Ashley River Gorge and its inferred correlative, downstream from the range-front. Adopted as a first approximation to long-term uplift rates, this estimate suggests that initial uplift could have occurred within the range: (1700/0.0025 m/yr = 680,000 years) to (1700/0.033 m/yr = 515,000 years).

9. Uplifted Pleistocene marine terraces are preserved along the North Canterbury coast in the fold-belt at the eastern end of the PPAFZ. Uplift rates range from 0.5-2.1 m/kyr (Yousif, 1987), and are likely to be slightly higher at the hinges of anticlines. If the maximum differential uplift rate is c.2.5 m/kyr, then the time of inception of uplift beneath the Cass Anticline is (1200 m/.0027 m/yr = 445,000 years)

10. The available data indicate that uplift and unroofing of basement in the PPAFZ east of Waimakariri River has occurred within the last 1 million years and for the first time since the late Cretaceous. The

estimated rates of uplift are similar to uplift rates in southern North Island and constrain the rate of landscape and structural development in the PPAFZ.

CHAPTER 4. KINEMATICS OF CRUSTAL DEFORMATION IN NORTH CANTERBURY FROM MICROEARTHQUAKES

4.1 INTRODUCTION

Prior to this study the kinematics of crustal deformation in North Canterbury was poorly defined. The spacing of National Network seismographs did not permit focal mechanisms to be determined for small earthquakes in the region, and the nearest previous surveys of microseismicity were in Marlborough to the north (Arabasz and Robinson, 1976; Kieckhefer, 1977), and Southern Alps to the west (Scholz et al., 1973; Rynn and Scholz, 1978). Those studies had established the primacy of dextral strike-slip faulting in the upper crust, and the Marlborough survey identified pronounced differences in the orientation of strain axes between the upper and lower crust, that were tentatively attributed to the tectonic setting of Marlborough above an active subduction zone.

All of the large (M>7.0) historic earthquakes in North Canterbury from which estimates of slip and focal mechanism might be obtained, occurred during the pre-instrumental period prior to 1930 (Eiby, 1968), and with one exception (McKay 1890; Cowan 1991) these events cannot be attributed to specific faults. In this respect, the lack of seismological data on fault kinematics has been compounded by the fact that although many faults in the region show evidence of late Quaternary displacement (Wellman, 1953; Wilson, 1963; Gregg, 1964; Berryman, 1979), the mapped offsets are generally smaller and less well defined than those of Marlborough and the North Island (several of which have been associated with large historic earthquakes).

Paradoxically, the catalogue of North Canterbury seismicity since 1964 provides better definition of the trend of the Porters Pass-Amberley Fault Zone (PPAFZ), than any other surface fault zone in N.Z. (Reyners, 1989). The 1990 North Canterbury microearthquake survey was predicated on a need to acquire more detailed information on the mechanisms of deformation associated with this zone, and in a wider sense, to investigate the plate boundary transition from subduction in the northeast to collision tectonics in the west and south.

4.2 DATA

Network design and the logistics of deployment and operation of the North Canterbury microearthquake network were discussed in Chapter 2, and

summaries of the technical performance of the network and the derivation of the seismic velocity model are presented in Appendices 4.2 and 4.3.

The temporary North Canterbury network (Fig.1.5; Appendix 4.1) and supplementary National Network stations (Fig.1.6) recorded more than 200 earthquakes during the 12 week survey, from September 1-November 16, 1990 (Fig.4.1, Appendix 4.4). Locations, particularly focal depths, of events beneath the Southern Alps to the west of the network were poorly determined because of the azimuthal distribution of stations; these events were excluded from the analysis. Thus, only events located within the network are interpreted here. This includes a few deep events located off the Pacific coast, that lie just to the west of a line projected between Station OBE (Okains Bay, Banks Peninsula), and KHZ (Kahutara) (Fig. 1.5).

4.3 HYPOCENTRAL LOCATIONS (Appendix 4.4)

4.3.1 Regional seismicity

Two depth intervals of seismicity were identified: 1) a seismic zone in the upper crust (0-12 km) in which most activity clustered between 7 and 10 km, and; 2) a deeper zone of activity, between 17-40 km. Figures 4.2 and 4.3 illustrate the distribution of epicentres for events in each depth interval, and show that the majority of shallow events were located in the centre and west of the network, whereas deeper events were more common to the east and northeast.

Projected into cross-sections (A-B and C-D, Fig.4.4, Fig.4.5a and b), the shallow events define a zone of activity clustered between depths of 7-12 km. No events were recorded within the interval 12-17 km. Activity beneath a ceiling of 17-20 km defines a deeper seismic zone that broadens vertically to the northeast (Section A-B) and northwest (Section C-D), with a bottom edge which dips at 10° and 15°, respectively.

4.3.2 Porter's Pass-Amberley Fault Zone

Hypocentres in the area between Porters Pass and Amberley indicate predominately shallow seismicity (Fig.4.4: E-F; Fig.4.6a); only three deeper events were recorded in this area during the survey. A cross-section between the Esk Valley and Canterbury Plains (Fig.4.4: G-H; Fig.4.6b) shows that the shallow earthquakes were concentrated at depths of 5-11 km. The cluster of events beneath Townshend River represents aftershocks of an M4.2 event that occurred at 17h 07m U.T. on August 22,

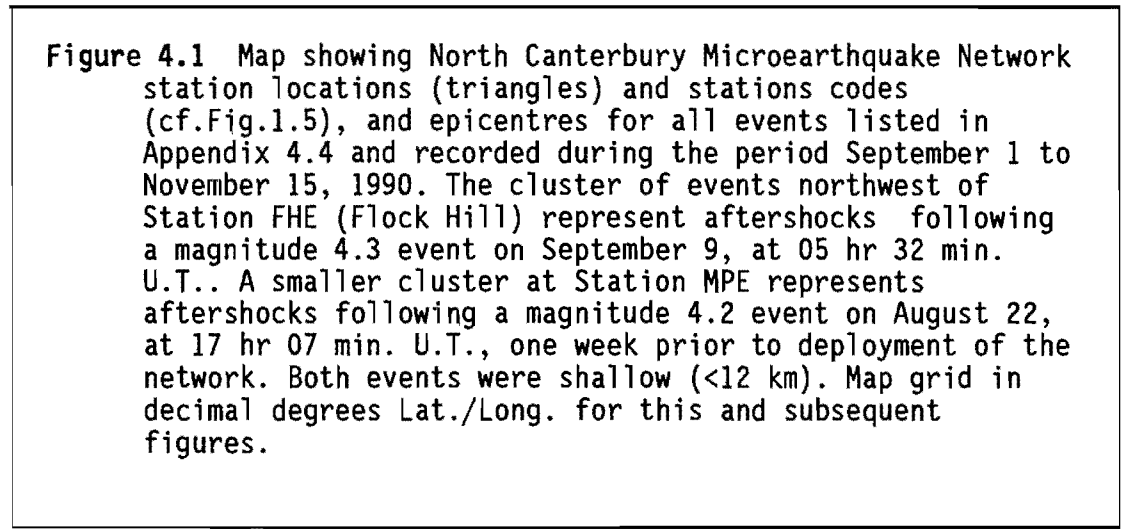

Figure 4.1 Map showing North Canterbury Microearthquake Network station locations (triangles) and stations codes (cf.Fig.1.5), and epicentres for all events listed in Appendix 4.4 and recorded during the period September 1 to November 15, 1990. The cluster of events northwest of Station FHE (Flock Hill) represent aftershocks following a magnitude 4.3 event on September 9, at 05 hr 32 min. U.T.. A smaller cluster at Station MPE represents aftershocks following a magnitude 4.2 event on August 22, at 17 hr 07 min. U.T., one week prior to deployment of the network. Both events were shallow (<12 km). Map grid in decimal degrees Lat./Long. for this and subsequent figures.

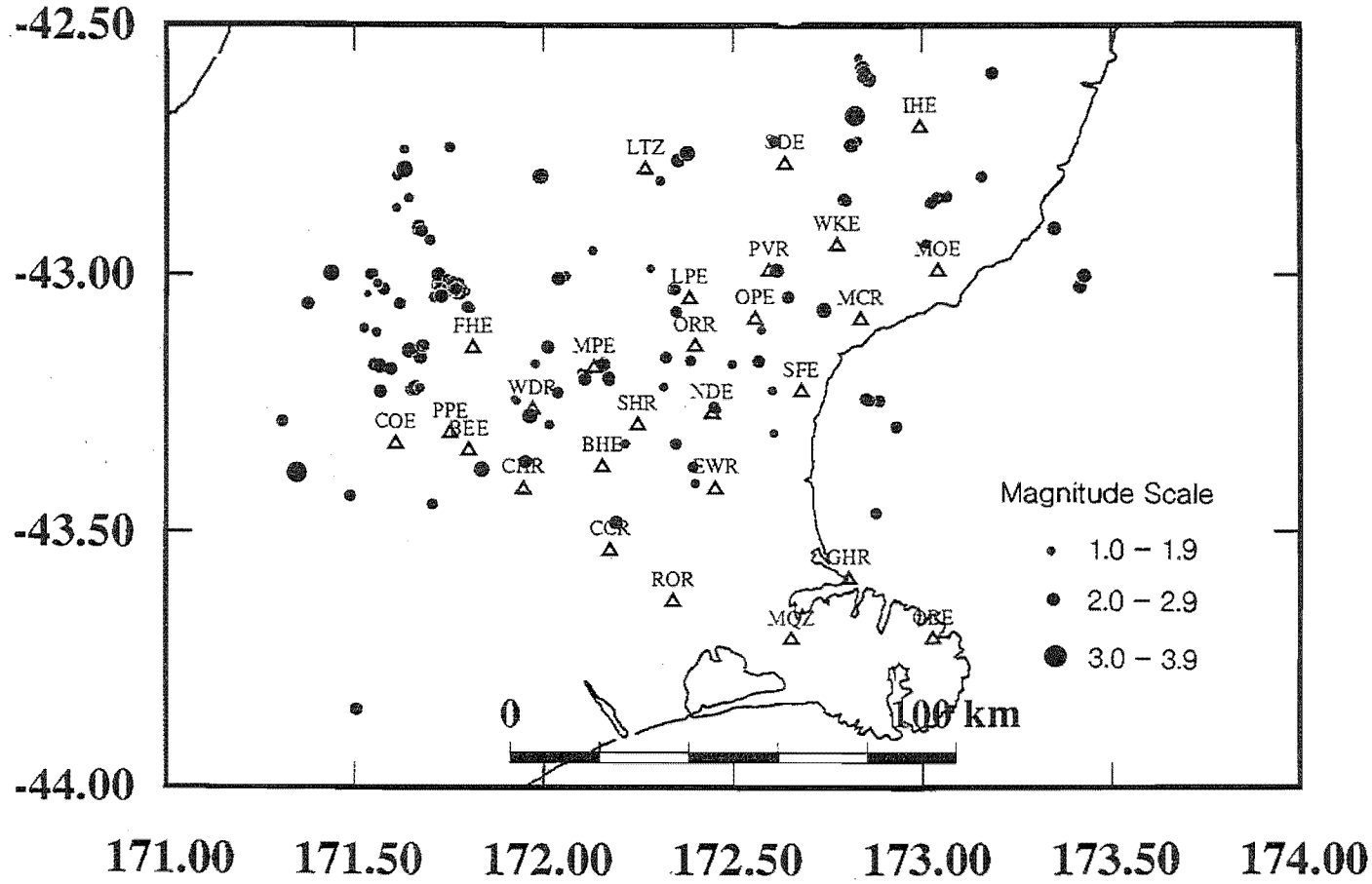
-42.50
-43.00
-43.50
-44.00
171.00
171.50
172.00
172.50
173.00
173.50
174.00
IHE
LTZ
SDE
WKE
PVR
MOE
LPE
OPE
MCR
FHE
ORR
MPE
SFE
WDR
NDE
SHR
PPE
COE
BEE
BHE
CMR
EWR
CCR
GHR
ROR
MQZ
ORE
Magnitude Scale
1.0 – 1.9
2.0 – 2.9
3.0 – 3.9
0
100 km

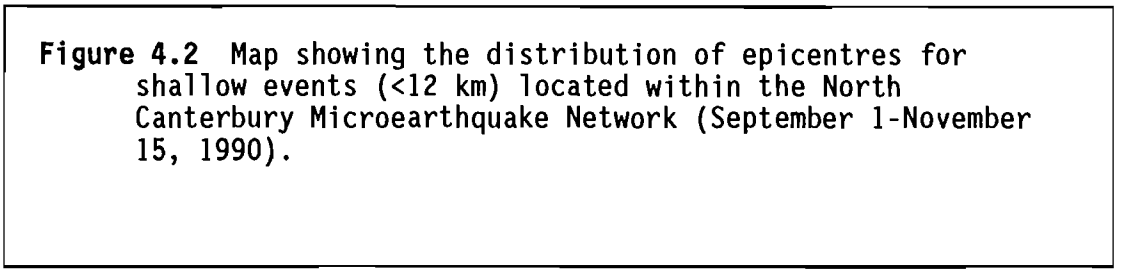

Figure 4.2 Map showing the distribution of epicentres for shallow events (<12 km) located within the North Canterbury Microearthquake Network (September 1-November 15, 1990).

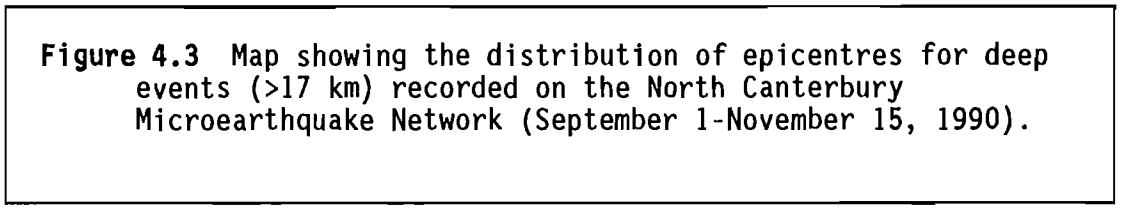

Figure 4.3 Map showing the distribution of epicentres for deep events (>17 km) recorded on the North Canterbury Microearthquake Network (September 1-November 15, 1990).

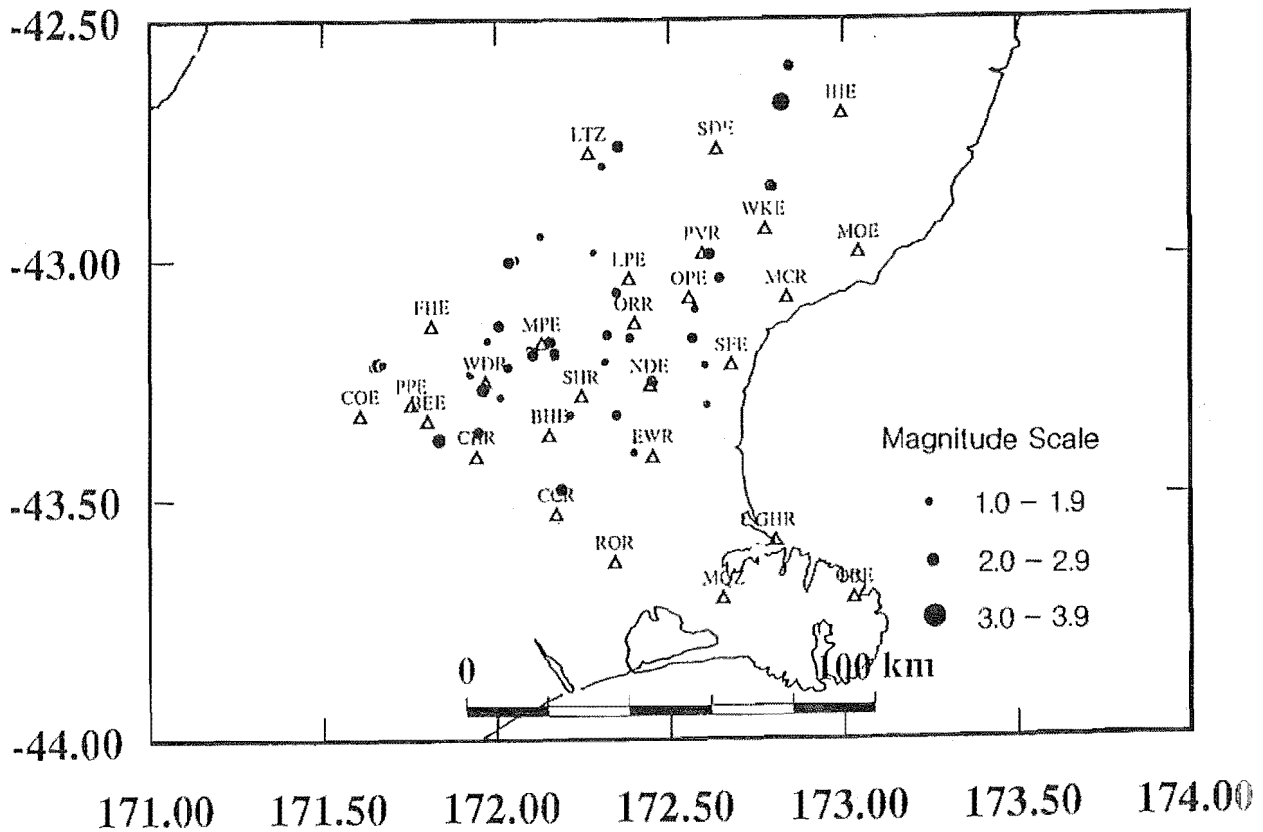
-42.50
-43.00
-43.50
-44.00
171.00
171.50
172.00
172.50
173.00
173.50
174.00
HIE
LTZ
SDE
WKE
PVR
MOE
LPE
OPE
MCR
ORR
FHE
MPE
SFE
WDR
NDE
SHR
COE
PPE
BEE
BHE
CHR
EWR
CCR
GHR
ROR
MQZ
DBE
Magnitude Scale
1.0 – 1.9
2.0 – 2.9
3.0 – 3.9
0
100 km

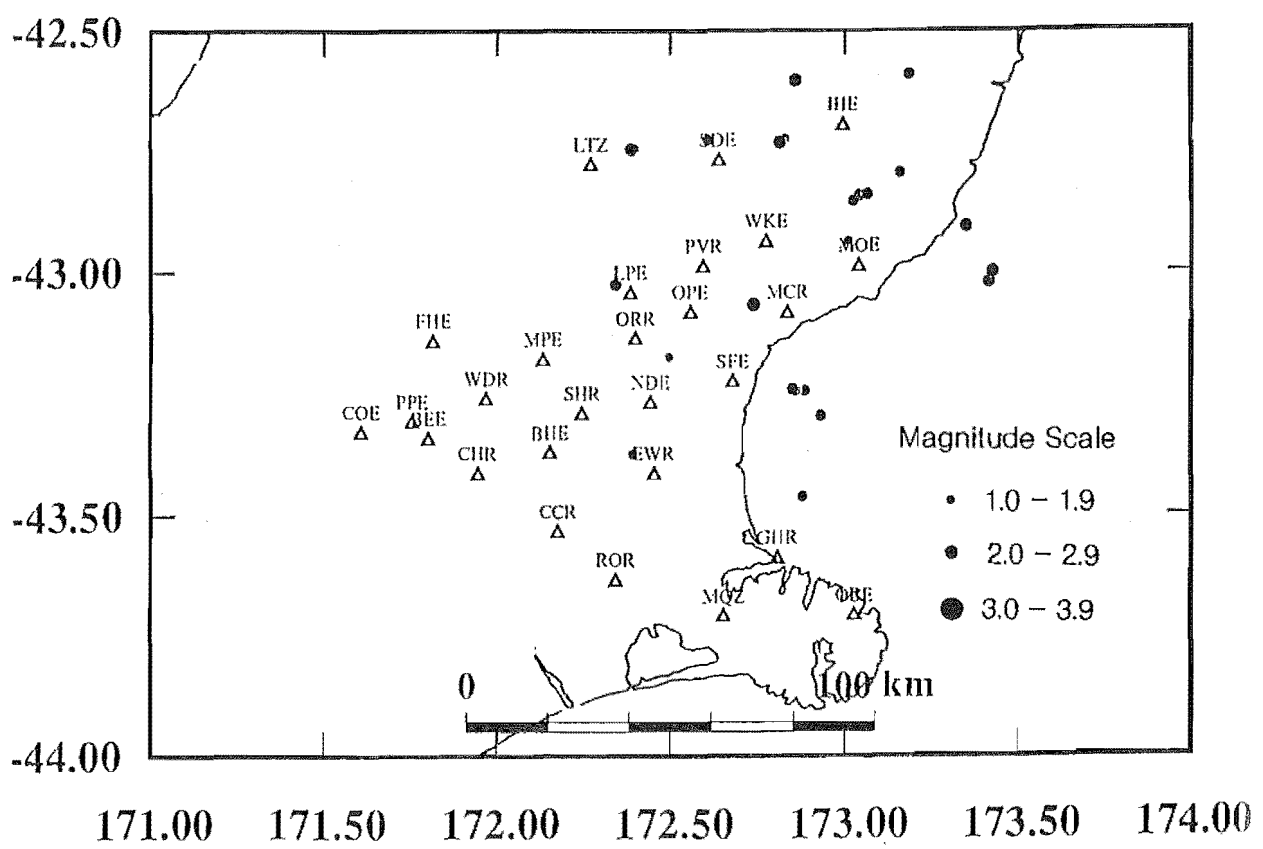
-42.50
-43.00
-43.50
-44.00
171.00
171.50
172.00
172.50
173.00
173.50
174.00
HIE
LTZ
SDE
WKE
PVR
MOE
LPE
OPE
MCR
ORR
FHE
MPE
SFE
WDR
NDE
SHR
COE
PPE
BEE
BHE
CHR
EWR
CCR
GHR
ROR
MQZ
DBE
Magnitude Scale
1.0 – 1.9
2.0 – 2.9
3.0 – 3.9
0
100 km

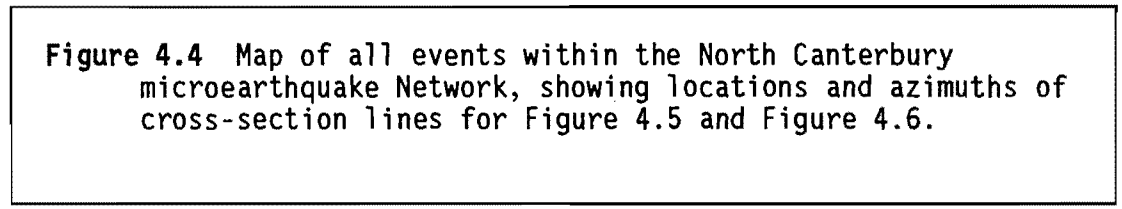

Figure 4.4 Map of all events within the North Canterbury microearthquake Network, showing locations and azimuths of cross-section lines for Figure 4.5 and Figure 4.6.

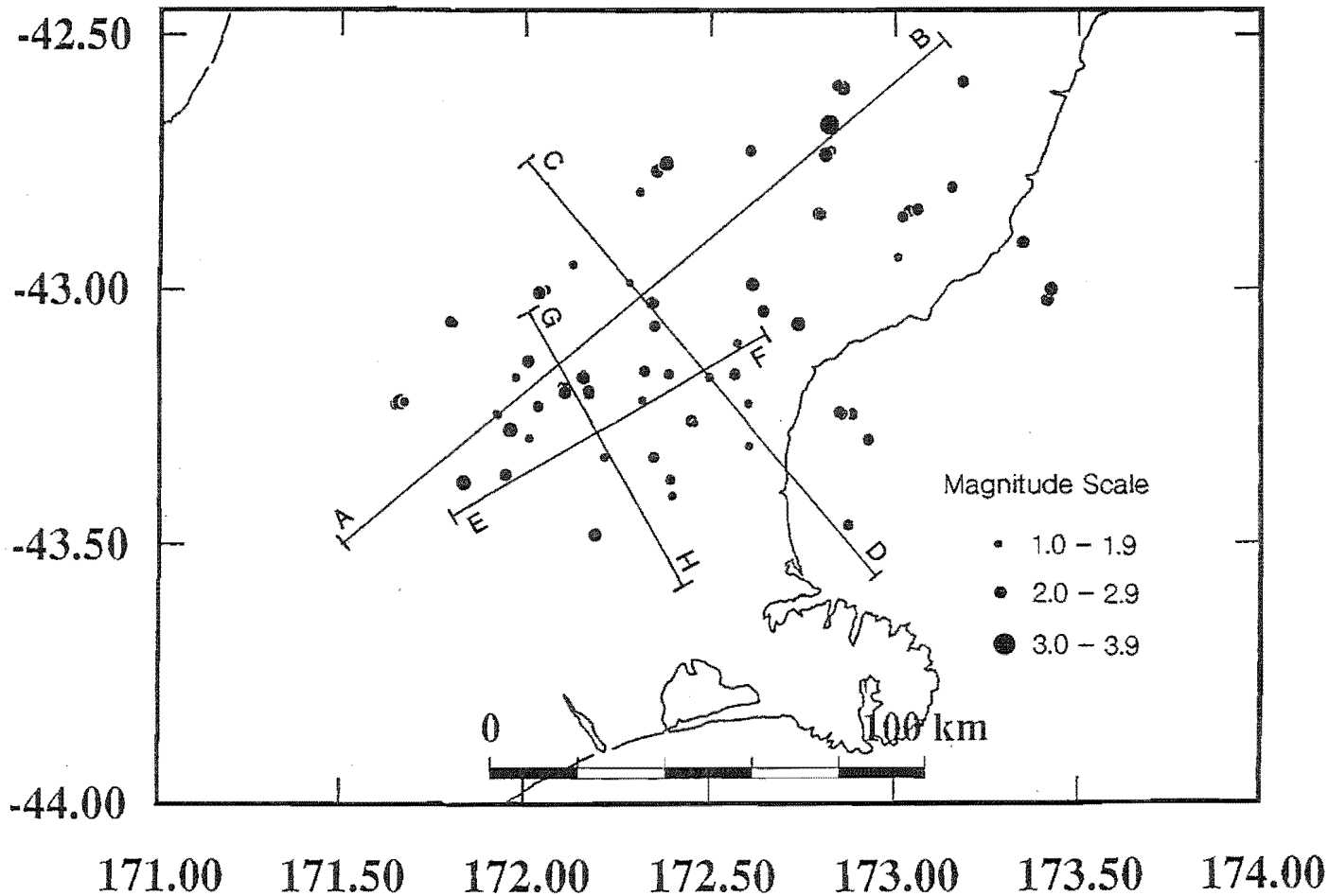
-42.50
-43.00
-43.50
-44.00
171.00
171.50
172.00
172.50
173.00
173.50
174.00
A
B
C
D
E
F
G
H
Magnitude Scale
1.0 – 1.9
2.0 – 2.9
3.0 – 3.9
0
100 km

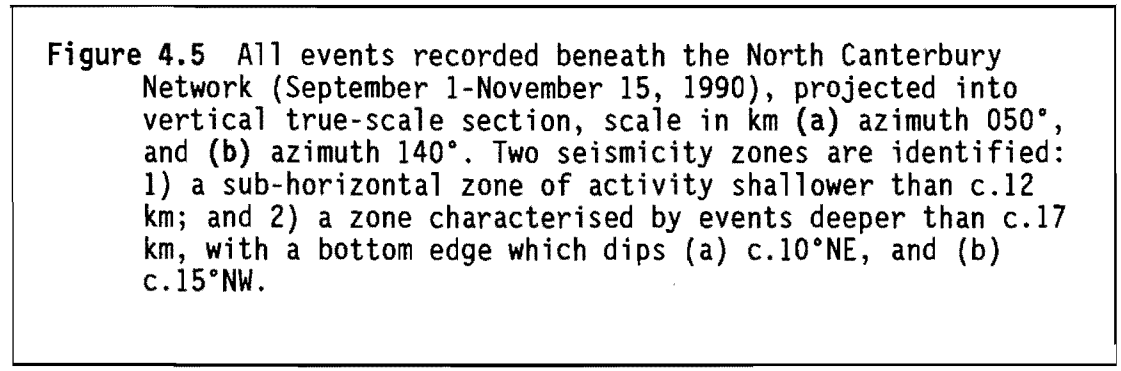

Figure 4.5 All events recorded beneath the North Canterbury Network (September 1-November 15, 1990), projected into vertical true-scale section, scale in km **(a)** azimuth 050°, and **(b)** azimuth 140°. Two seismicity zones are identified: 1) a sub-horizontal zone of activity shallower than c.12 km; and 2) a zone characterised by events deeper than c.17 km, with a bottom edge which dips (a) c.10°NE, and (b) c.15°NW.

a.

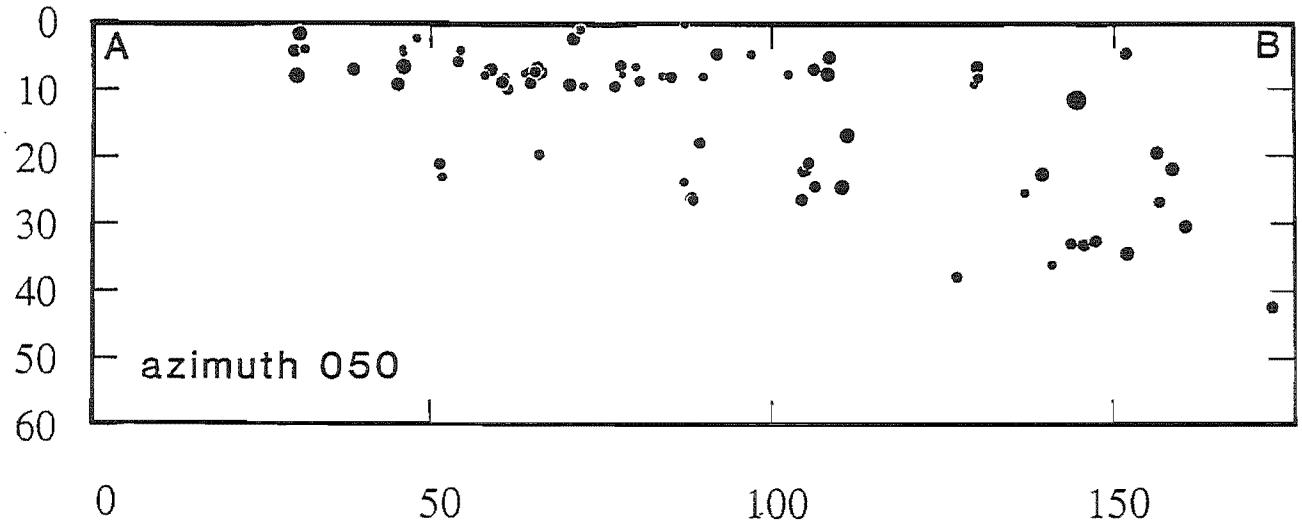
0
10
20
30
40
50
60
A
B
azimuth 050
0
50
100
150

b.

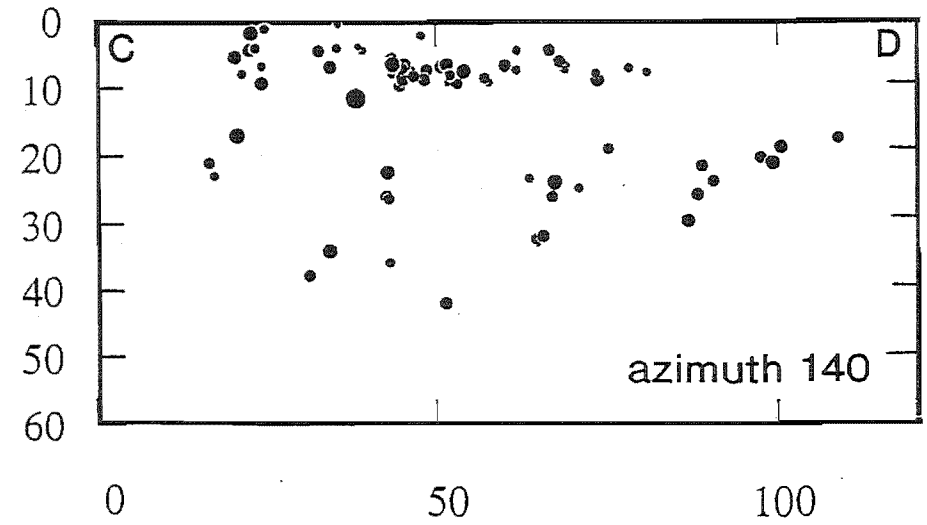
0
10
20
30
40
50
60
C
D
azimuth 140
0
50
100

Figure 4.6 Vertical true-scale sections (scale in km) of events located within the Porter's Pass-Amberley Fault Zone **(a)** azimuth 060°, and **(b)** azimuth 150°. Line locations from Figure 4.4, with events projected from 20 km either side of sections (cf. Sheet 18 for local geographic features). All but three recorded events are located shallower than 12 km and lie within the principal zone of Quaternary surface deformation.

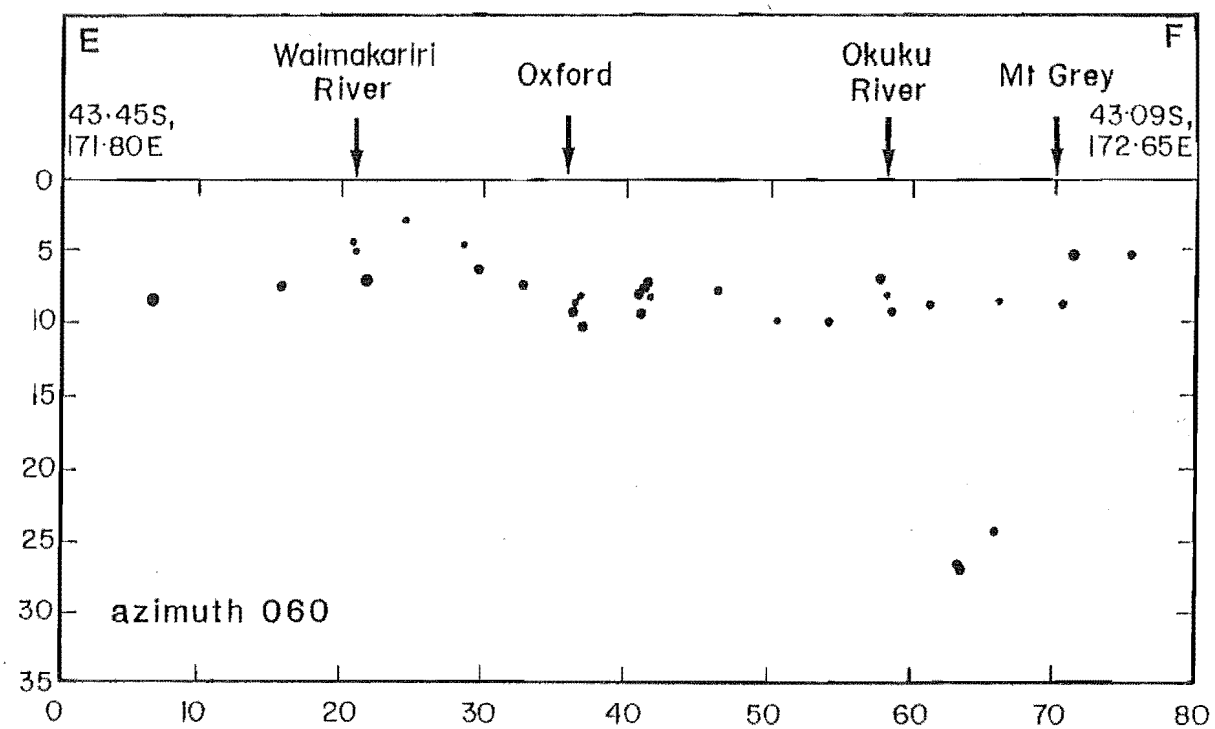
E
F
Waimakariri River
Oxford
Okuku River
Mt Grey
43·45S, 171·80E
43·09S, 172·65E
azimuth 060
0
5
10
15
20
25
30
35
0
10
20
30
40
50
60
70
80

a.

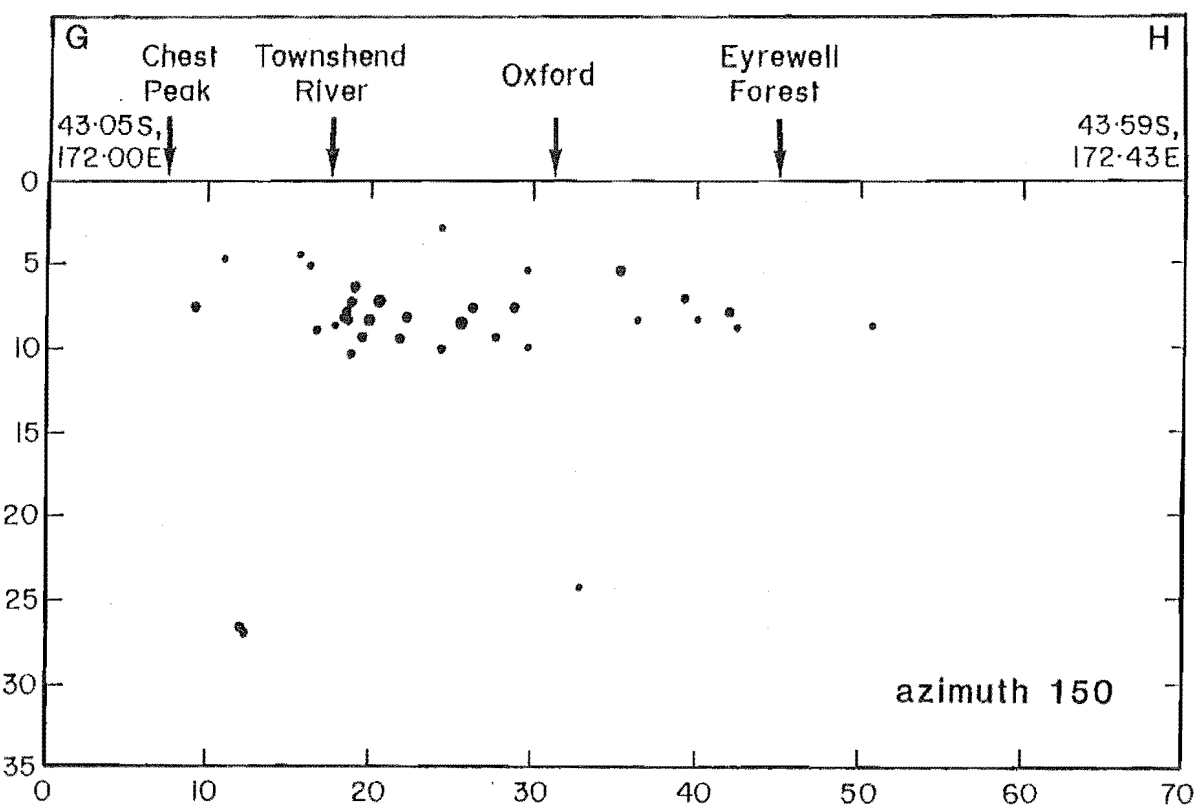
G
H
Chest Peak
Townshend River
Oxford
Eyrewell Forest
43·05S, 172·00E
43·59S, 172·43E
azimuth 150
0
5
10
15
20
25
30
35
0
10
20
30
40
50
60
70

b.

one week prior to deployment of the network.

4.4 FAULT-PLANE SOLUTIONS

4.4.1 Introduction

Forty four single-event and five composite fault-plane solutions have been derived from P-wave first-motions of the recorded earthquakes, from which inferences are made about regional tectonic structure and fault kinematics. Explanatory notes on the derivation and interpretation of fault-plane solutions are presented in Appendix 4.5. The fault-plane solutions are presented in Appendices 4.6 and 4.7, from which the quality of schematic results presented in discussion may be judged.

4.4.2 Upper seismic zone

Fault plane solutions for shallow events (Fig.4.7) indicate a predominance of strike-slip faulting in the upper crust. All strike-slip solutions include one nodal plane that is parallel to the E-NE structural grain of faults in North Canterbury. If this nodal plane represents the fault for these events, then the sense of displacement is consistently dextral.

Events within the PPAFZ provided the highest quality solutions (Fig.4.8) and almost all were located within fault zones that have been identified at the surface and mapped in this study (Fig.4.9). The majority of mechanisms imply strike-slip faulting, with one nodal plane parallel to the mapped surface faults. Those west of, and beneath Mt Thomas have strike-slip mechanisms consistent with steeply dipping faults observed at the surface, but the strike-slip mechanisms for events located in Lees Valley to the west, and to the east (Kowai Anticline) are at variance with the kinematic character of surface faults, which indicate predominately thrusting. The differences can be accounted for by a decrease in the dip of the faults as they approach the surface, and will be discussed further later.

Several oblique-slip and dip-slip mechanisms are located away from the central elements of the PPAFZ (Fig.4.9), principally at surface-fault terminations (sol.26), and fold structures - Cust Anticline (sol.10,20) and Doctors Anticline (sol.16,18). Two thrust events (sol.15,19) which appear on the regional map of shallow events but lie to the west of Figure 4.9 are located near the Mt Cheesman fault, beneath the Craigeburn Range at the western margin of the Castle Hill Basin (Fig.4.10 cf.

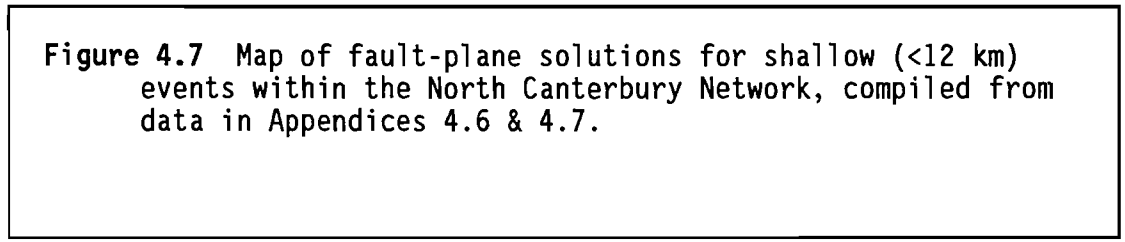

Figure 4.7 Map of fault-plane solutions for shallow (<12 km) events within the North Canterbury Network, compiled from data in Appendices 4.6 & 4.7.

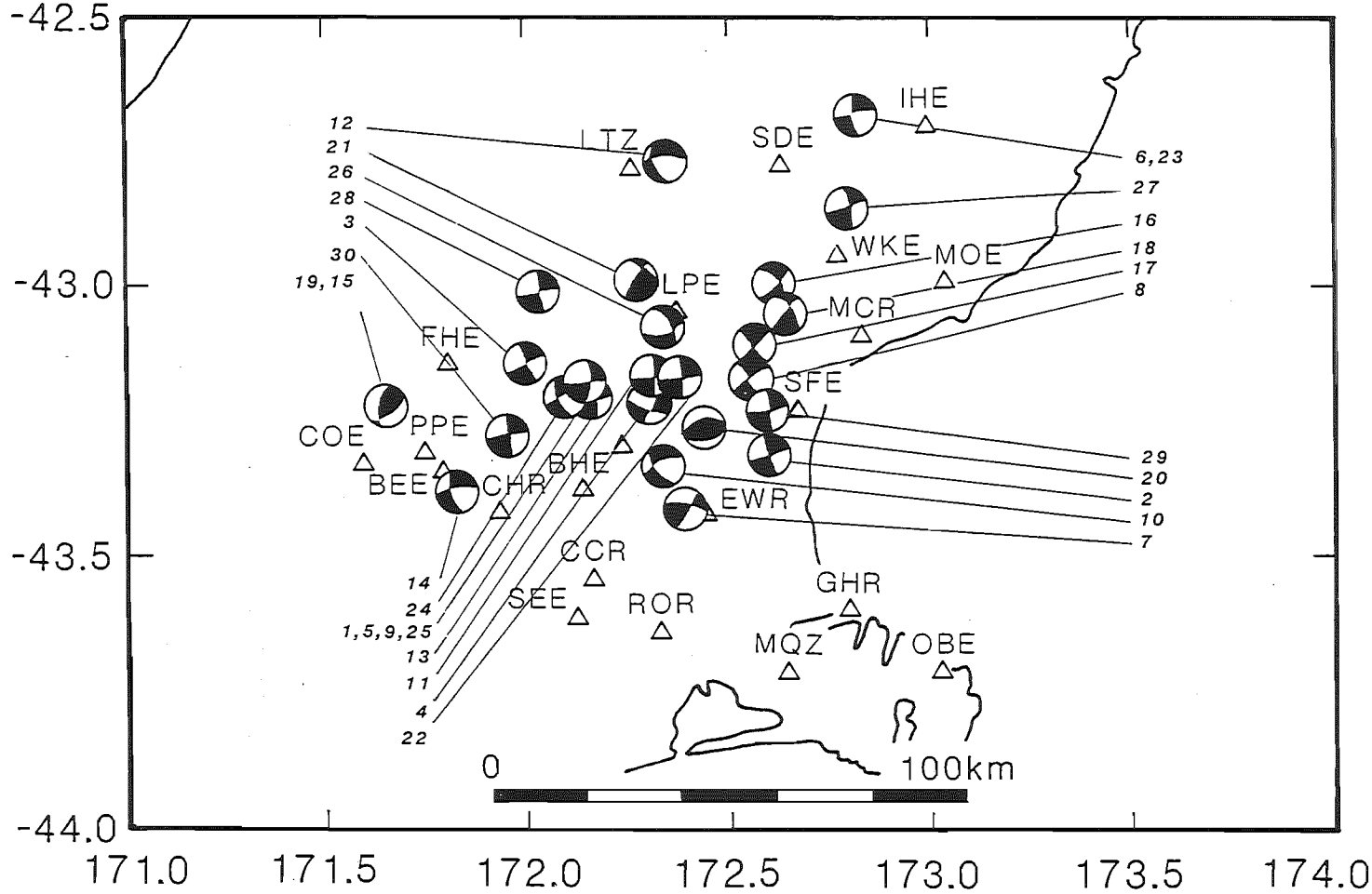
-42.5
-43.0
-43.5
-44.0
171.0
171.5
172.0
172.5
173.0
173.5
174.0
LTZ
SDE
IHE
LPE
WKE
MOE
MCR
FHE
SFE
COE
PPE
BEE
CHR
BHE
EWR
CCR
SEE
ROR
GHR
MQZ
OBE
12
21
26
28
3
30
19,15
14
24
1,5,9,25
13
11
4
22
6,23
27
16
18
17
8
29
20
2
10
7
0
100km

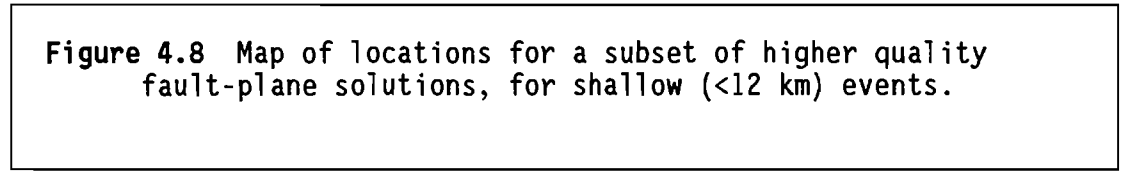

Figure 4.8 Map of locations for a subset of higher quality fault-plane solutions, for shallow (<12 km) events.

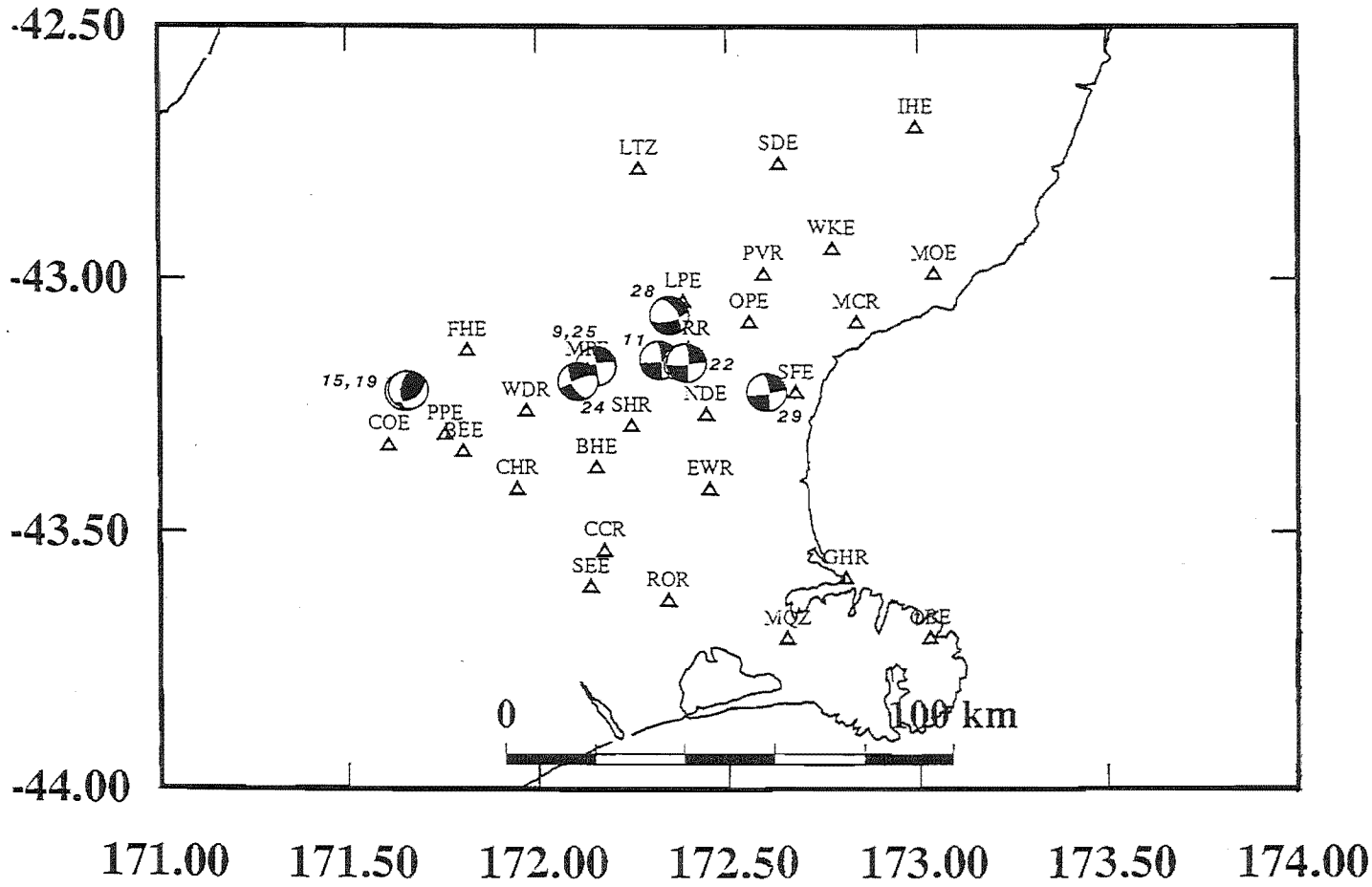
-42.50
-43.00
-43.50
-44.00
171.00
171.50
172.00
172.50
173.00
173.50
174.00
IHE
LTZ
SDE
WKE
PVR
MOE
LPE
28
OPE
MCR
FHE
9,25
11
22
15, 19
WDR
24
SHR
NDE
SFE
29
COE
PPE
BEE
BHE
CHR
EWR
CCR
SEE
ROR
GHR
MQZ
OBE
0
100 km

Figure 4.9 Map of locations and fault-plane solutions for recorded shallow events, superimposed on surface faults and fold structures of the Porter's Pass-Amberley Fault Zone, mapped in this study (cf. Maps 1 and 2: map pocket). Strike-slip mechanisms are consistent with kinematics of surface faults in the west, but at variance with thrust or hybrid oblique-slip geometries of surface faults and fold structures to the east.

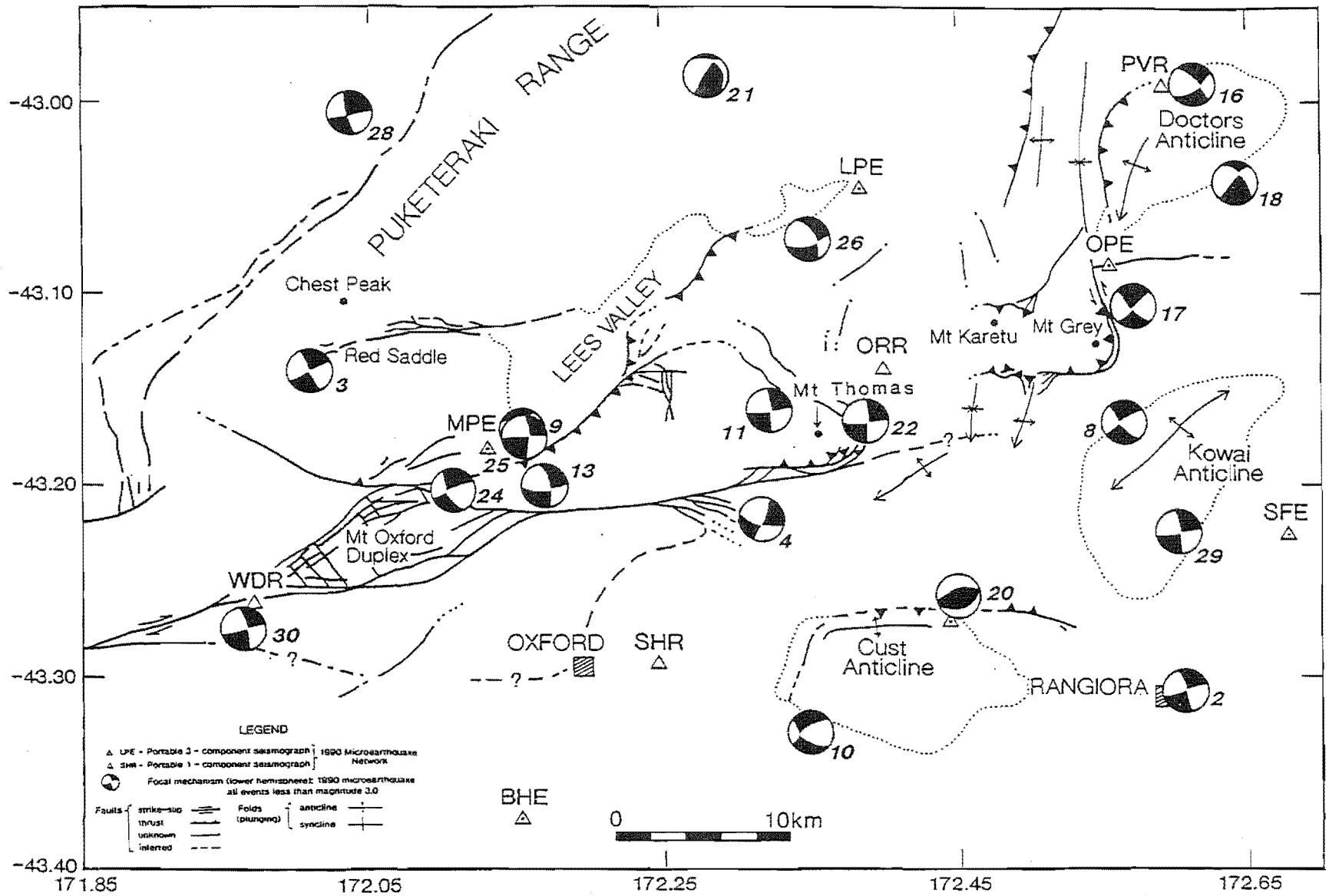
PUKETERAKI RANGE
Chest Peak
Red Saddle
LEES VALLEY
LPE
ORR
Mt Thomas
Mt Karetu
Mt Grey
PVR
Doctors Anticline
OPE
Kowai Anticline
SFE
MPE
Mt Oxford Duplex
WDR
OXFORD
SHR
Cust Anticline
RANGIORA
BHE
28
21
26
18
16
17
3
11
22
9
25
13
24
8
4
29
30
20
10
2
-43.00
-43.10
-43.20
-43.30
-43.40
171.85
172.05
172.25
172.45
172.65
0
10km
LEGEND

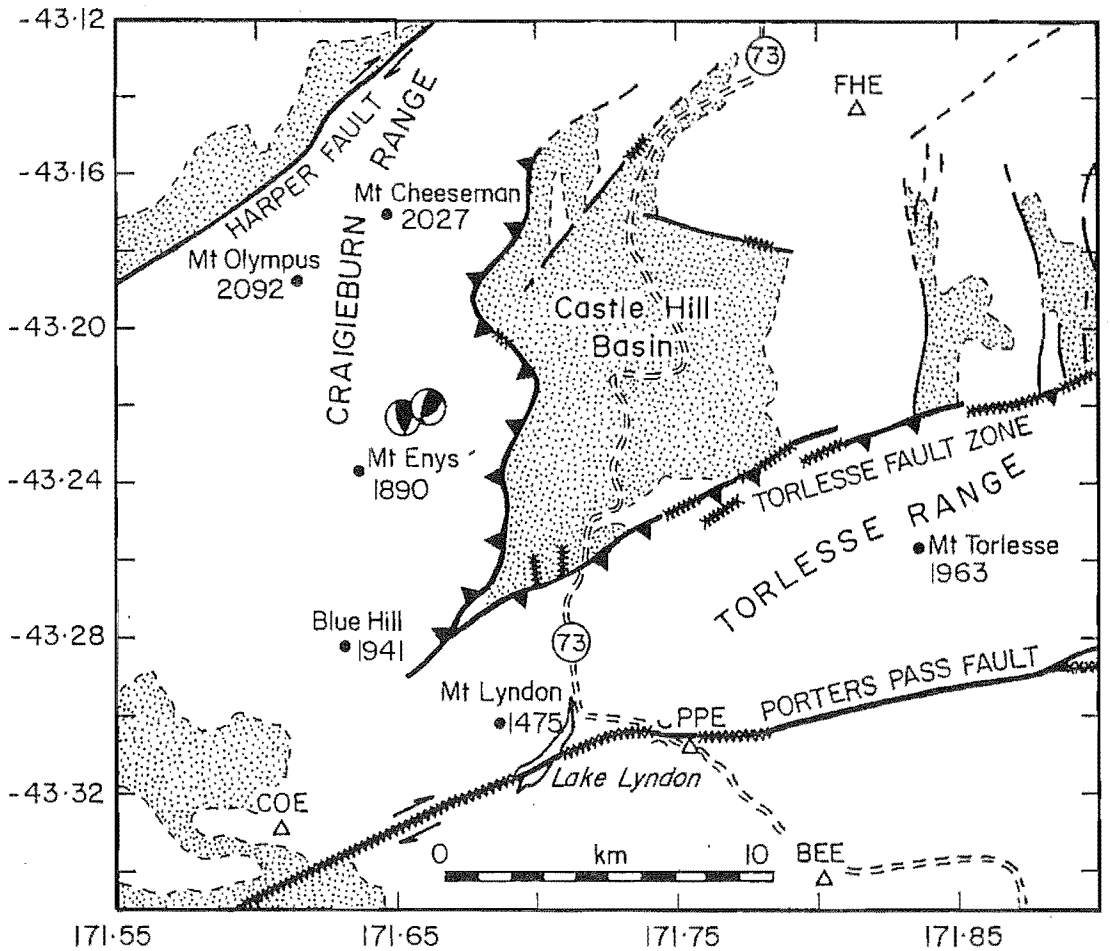

Figure 4.10 Map of the principal faults bounding the Castle Hill Basin at the western end of the North Canterbury Microearthquake Network, showing the locations of two pure thrust events beneath the Craigeburn Range, near the Mt Cheeseman Fault. teeth shown on hanging-wall of major thrusts. The symbol 'xxxxx' along sections of the mapped faults indicates the presence of a late Quaternary trace. Spot heights are in metres (a.s.l.); Highway 73 (Canterbury to Westland), and microearthquake recording stations BEE, PPE, FHE are indicated. The Cretaceous-Cenozoic cover sequence is shaded.

Frontispiece 1).

4.4.3 Lower seismic zone

The focal mechanisms for deeper events generally are not as well-constrained as those of the shallow events, but nonetheless they show marked differences from the latter; namely, there are more dip-slip and oblique-slip solutions than there are strike-slip solutions (Figs. 4.11a, 4.11b). One of the features of the deeper events is the larger number of normal fault mechanisms relative to those of shallow events (cf. Figs 4.7 and 4.11a).

4.5 CONTRACTIONAL STRAIN AXES

The axes of maximum contractional strain (P-axes) for solutions of shallow and deeper events are plotted in Figure 4.12a and 4.12b, respectively; and those of shallow events in the PPAFZ are shown in Figure 4.13. The lengths of the axes are proportional to the cosine of the angle between the axes and the horizontal. The P-axes of shallow events have a nearly uniform WNW-NW trend; a few exceptions (sol. 5,8,15,17: Fig.4.7) trend E-W. The azimuthal range for the highest quality solutions (excluding no.15) is between 290° and 310°.

The P-axes for deeper events vary systematically from south to north across the region. The P-axes of the most southerly events (32,37,42 and 43: Fig.4.11a) trend WNW-NW and are comparable to those of the shallow events. Slightly further north, deeper events beneath the PPAFZ (34,36,49: Fig.4.11a) have P-axes that trend WSW; and those of events further to the north, trend southwest.

4.6 TENSILE STRAIN AXES

Axes of maximum tensile strain (T-axes) for shallow events are shown in Figure 4.14a and those of deeper events in Figure 4.14b. T-axes for shallow events in the PPAFZ are presented in Figure 4.15. The lengths of the axes are proportional to the cosine of the angle between the axes and the horizontal. With only one exception (sol.no.21: Fig.4.9) the shallow T-axes trend N-NE. In the south of the region, the T-axes of deeper events show a dominantly N-S trend, but north of the PPAFZ the majority of T-axes show a northwesterly trend. The patterns described above are more evident from a subset of higher quality solutions for the respective groups (Fig.4.16 a,b,c,d).

Figure 4.11 (a) Map of fault-plane solutions for all deep (>17 km) events beneath the North Canterbury Network, compiled from data in Appendices 4.6 & 4.7; **(b)** a subset of the higher quality solutions. N.B. solutions 42 and 32 are superimposed, but almost identical (Appendix 4.7).

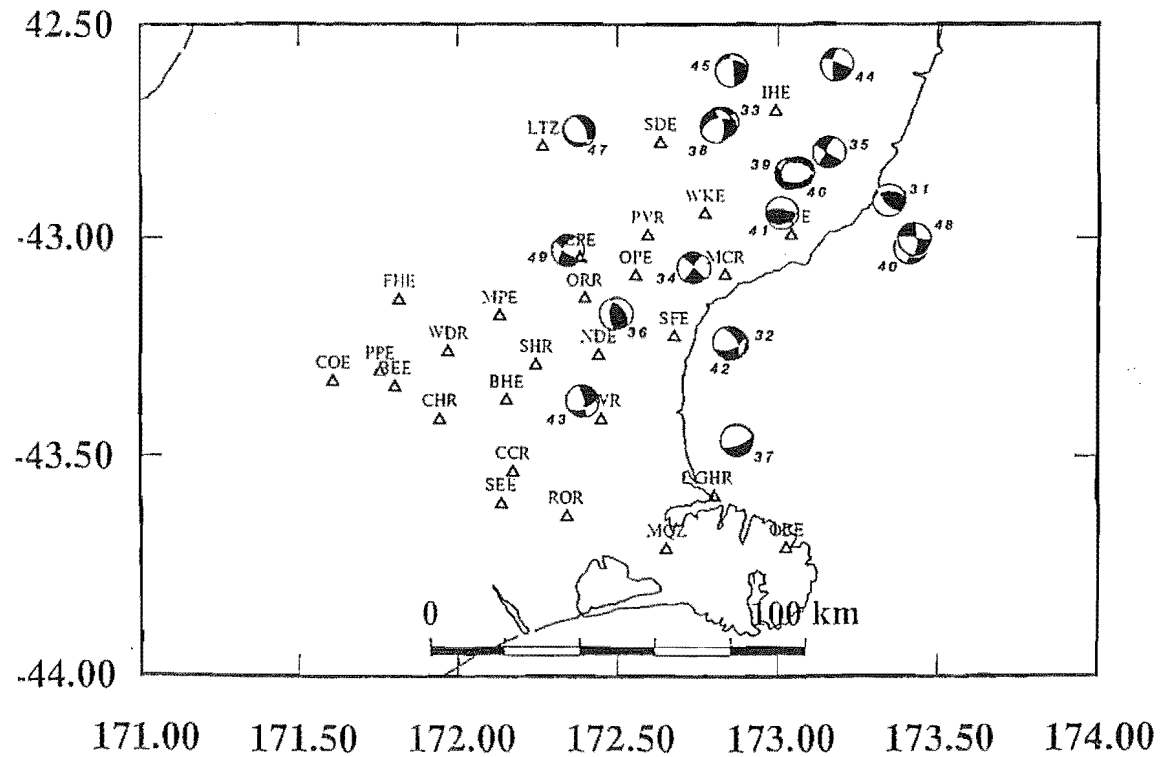
42.50
-43.00
-43.50
-44.00
171.00
171.50
172.00
172.50
173.00
173.50
174.00
IHE
LTZ
SDE
WKE
PVR
MOE
CRE
OPE
MCR
ORR
FHE
MPE
SFE
WDR
NDE
SHR
COE
PPE
BEE
BHE
CHR
VR
CCR
SEE
ROR
EGHR
MQZ
ORE
0
100 km

a.

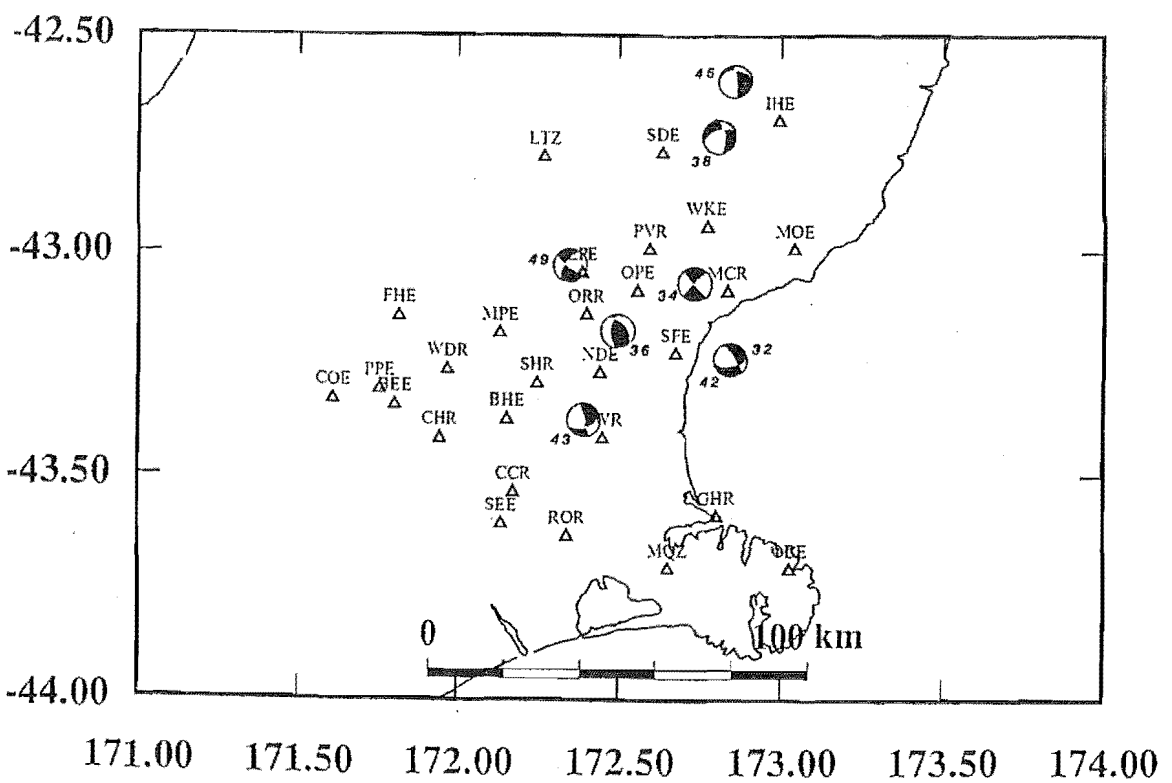
-42.50
-43.00
-43.50
-44.00
171.00
171.50
172.00
172.50
173.00
173.50
174.00
IHE
LTZ
SDE
WKE
PVR
MOE
CRE
OPE
MCR
ORR
FHE
MPE
SFE
WDR
NDE
SHR
COE
PPE
BEE
BHE
CHR
VR
CCR
SEE
ROR
EGHR
MQZ
ORE
0
100 km

b.

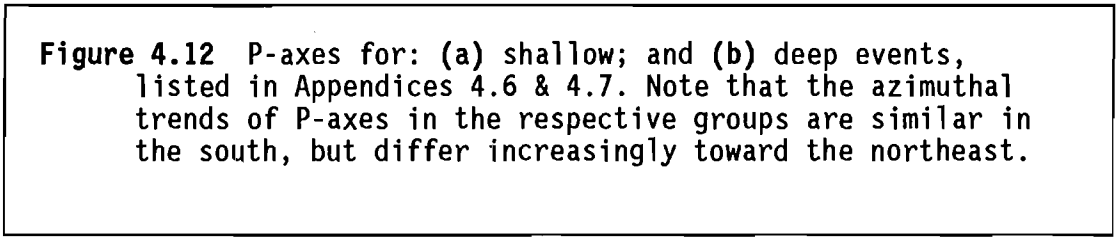

Figure 4.12 P-axes for: (a) shallow; and (b) deep events, listed in Appendices 4.6 & 4.7. Note that the azimuthal trends of P-axes in the respective groups are similar in the south, but differ increasingly toward the northeast.

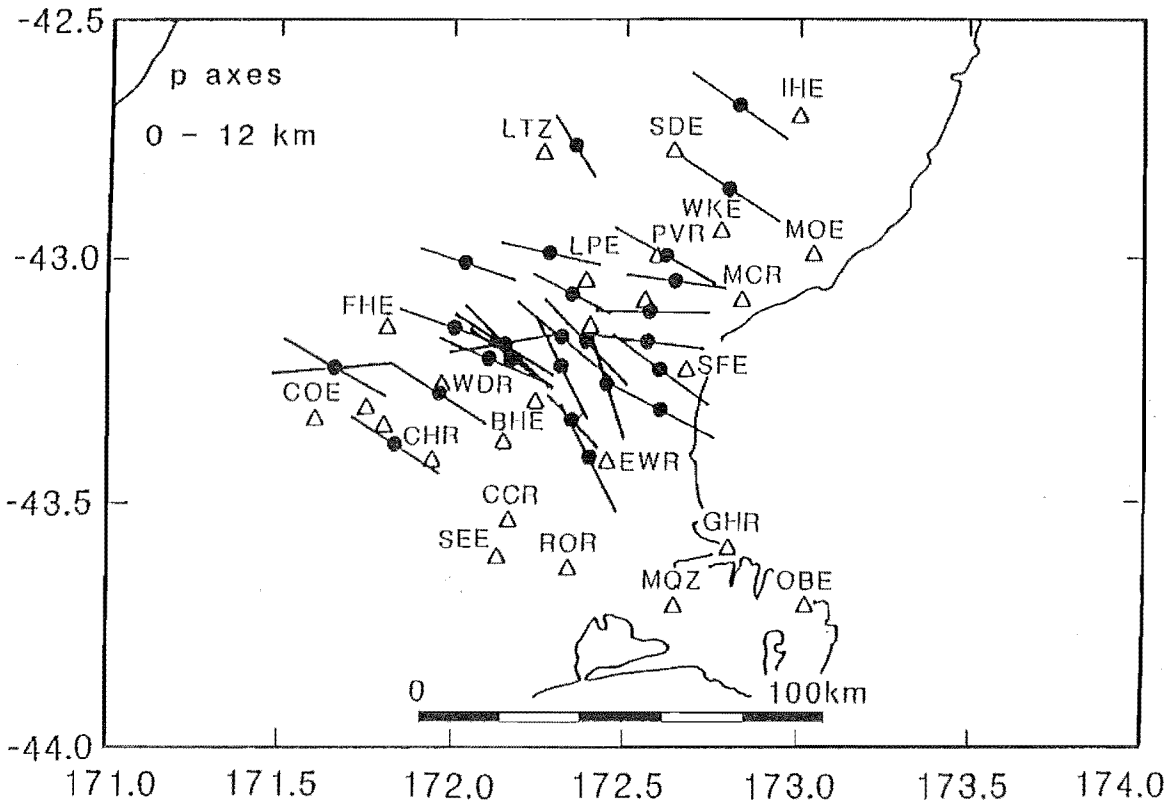
p axes
0 - 12 km
-42.5
-43.0
-43.5
-44.0
171.0
171.5
172.0
172.5
173.0
173.5
174.0
IHE
LTZ
SDE
WKE
PVR
MOE
LPE
MCR
FHE
SFE
COE
WDR
BHE
CHR
EWR
CCR
GHR
SEE
ROR
MQZ
OBE
0
100km

a.

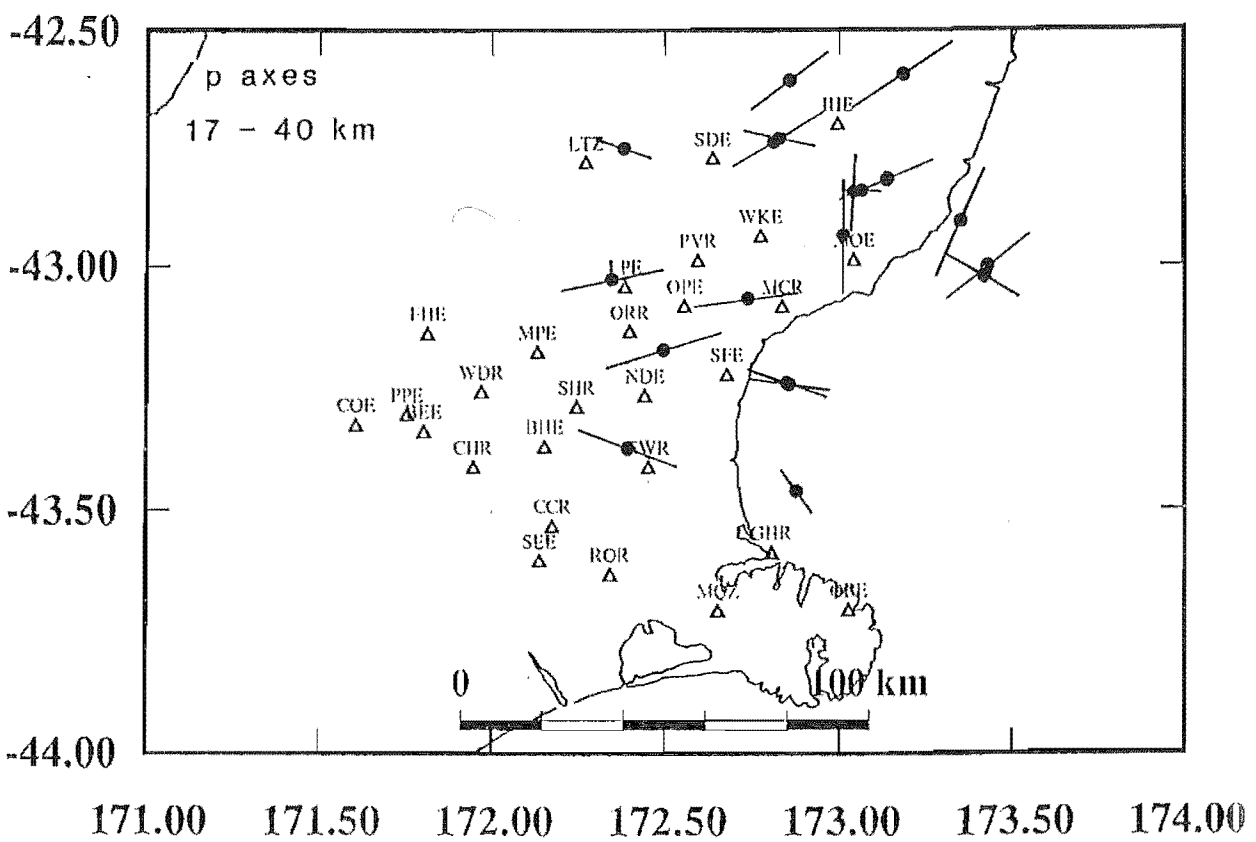
p axes
17 - 40 km
-42.50
-43.00
-43.50
-44.00
171.00
171.50
172.00
172.50
173.00
173.50
174.00
IHE
LTZ
SDE
WKE
PVR
MOE
LPE
OPE
MCR
FHE
ORR
MPE
SFE
WDR
NDE
SHR
COE
PPE
BEE
BHE
CHR
EWR
CCR
SEE
ROR
GHR
MQZ
OBE
0
100 km

b.

Figure 4.13 P-axes for shallow events (<12 km) in the Porter's Pass-Amberley Fault Zone, superimposed on faults and fold structures mapped in this study and that of Nicol (1991). Numbered P-axes correspond to fault-plane solutions in Appendices 4.6 & 4.7. See text for discussion.

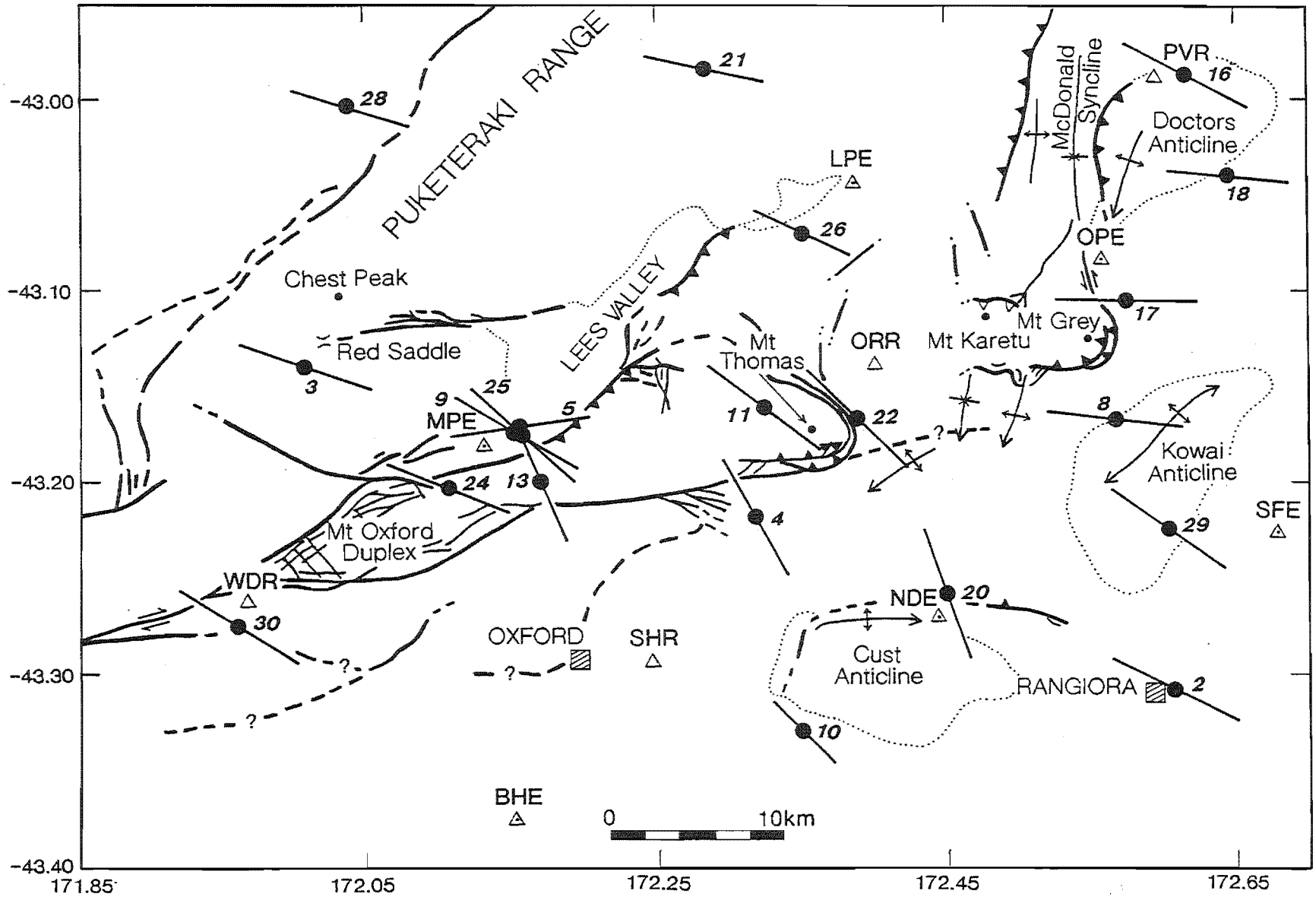
PUKETERAKI RANGE
LEES VALLEY
McDonald Syncline
Doctors Anticline
Kowai Anticline
Cust Anticline
Mt Oxford Duplex
Chest Peak
Red Saddle
Mt Thomas
Mt Karetu
Mt Grey
LPE
PVR
OPE
MPE
ORR
WDR
NDE
SHR
SFE
OXFORD
RANGIORA
BHE
0
10km
-43.00
-43.10
-43.20
-43.30
-43.40
171.85
172.05
172.25
172.45
172.65

Figure 4.14 T-axes for: **(a)** shallow; and **(b)** deep events, listed in Appendices 4.6 & 4.7. Note that the azimuthal trends of T-axes in the respective groups are similar in the south, but differ increasingly toward the northeast.

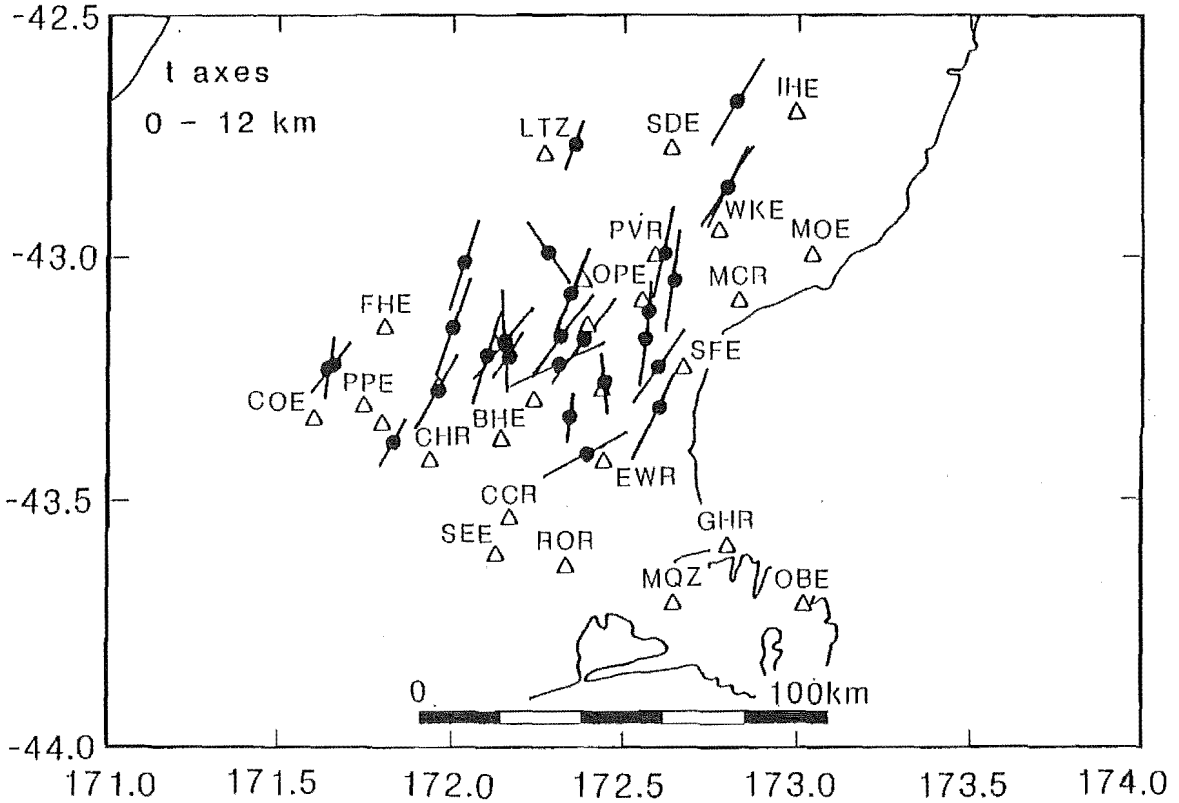
t axes
0 - 12 km
-42.5
-43.0
-43.5
-44.0
171.0
171.5
172.0
172.5
173.0
173.5
174.0
IHE
LTZ
SDE
WKE
MOE
PVR
OPE
MCR
FHE
SFE
COE
PPE
CHR
BHE
EWR
CCR
SEE
ROR
GHR
MQZ
OBE
0
100km

a.

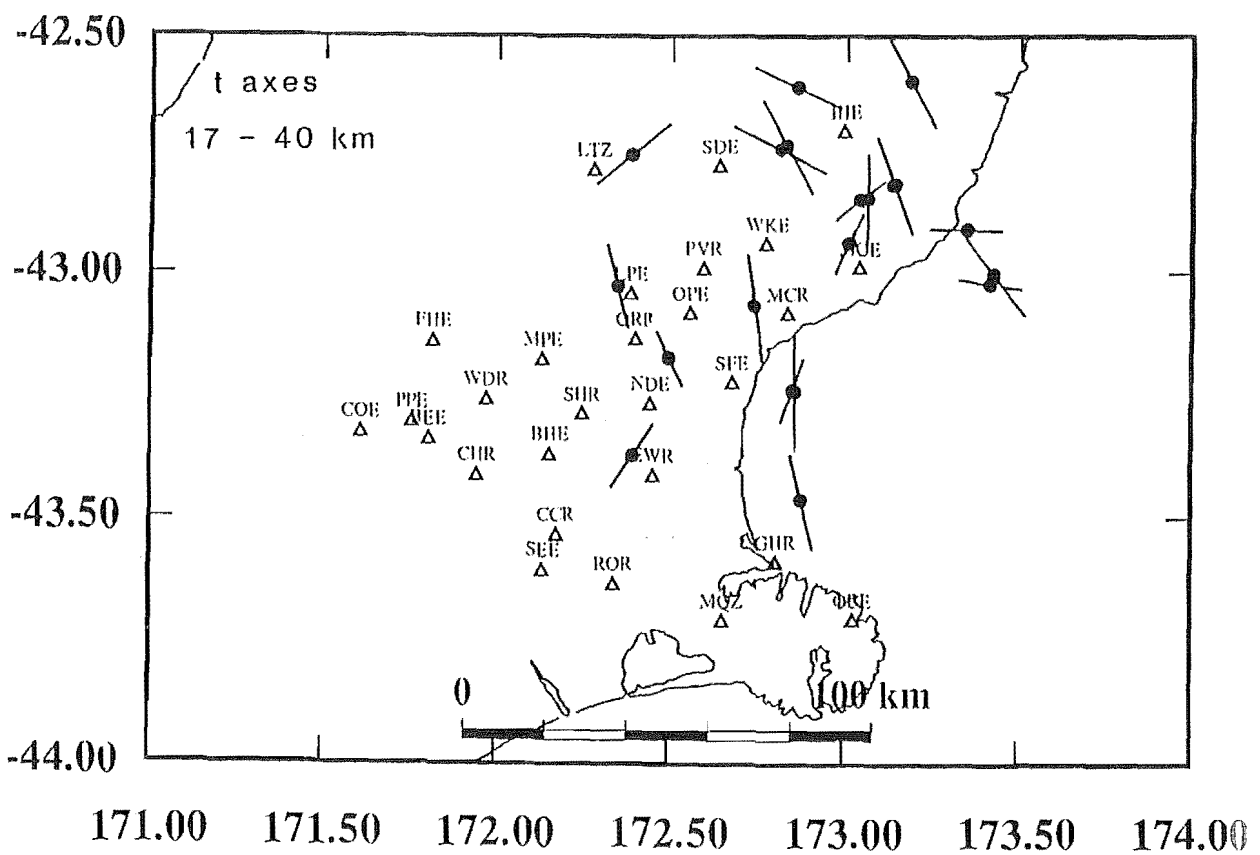
t axes
17 - 40 km
-42.50
-43.00
-43.50
-44.00
171.00
171.50
172.00
172.50
173.00
173.50
174.00
IHE
LTZ
SDE
WKE
PVR
OPE
MCR
FHE
MPE
SFE
WDR
NDE
SHR
COE
PPE
BHE
CHR
EWR
CCR
SEE
ROR
GHR
MQZ
0
100 km

b.

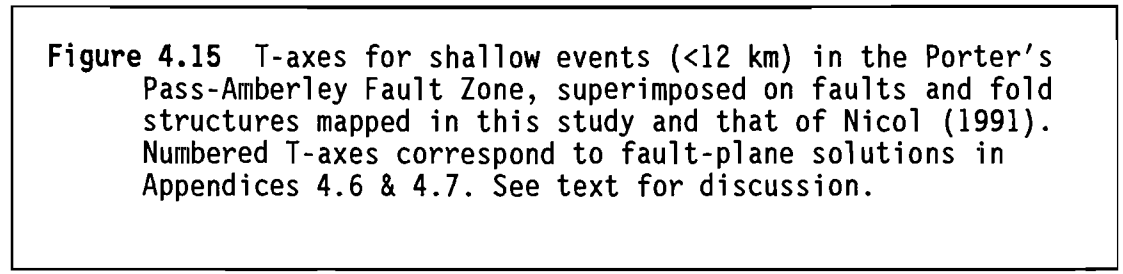

Figure 4.15 T-axes for shallow events (<12 km) in the Porter's Pass-Amberley Fault Zone, superimposed on faults and fold structures mapped in this study and that of Nicol (1991). Numbered T-axes correspond to fault-plane solutions in Appendices 4.6 & 4.7. See text for discussion.

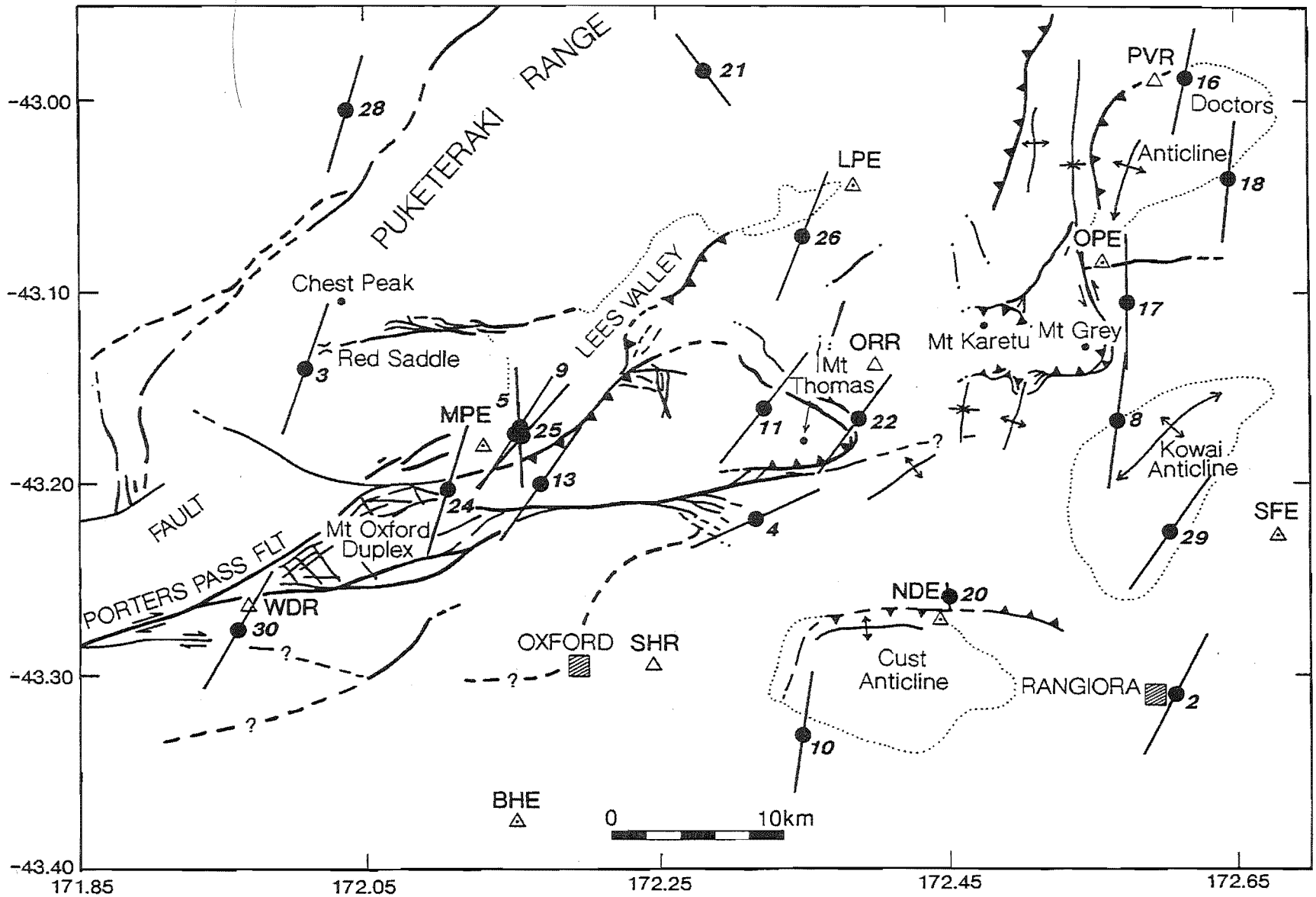
PUKETERAKI RANGE
LEES VALLEY
Chest Peak
Red Saddle
FAULT
PORTERS PASS FLT
Mt Oxford
Duplex
MPE
LPE
ORR
Mt
Thomas
Mt Karetu
Mt Grey
PVR
Doctors
Anticline
OPE
Kowai
Anticline
SFE
NDE
Cust
Anticline
RANGIORA
WDR
OXFORD
SHR
BHE
0
10km
-43.00
-43.10
-43.20
-43.30
-43.40
171.85
172.05
172.25
172.45
172.65

Figure 4.16 Comparison of a subset of P-axes (a & b); and T-axes (c & d) for higher quality solutions of shallow and deep events shown in Figs. 4.8 and 4.11(b), respectively, and listed in Appendices 4.6 & 4.7. Strain axes of the respective groups are similar in the south, but differ increasingly toward the northeast.

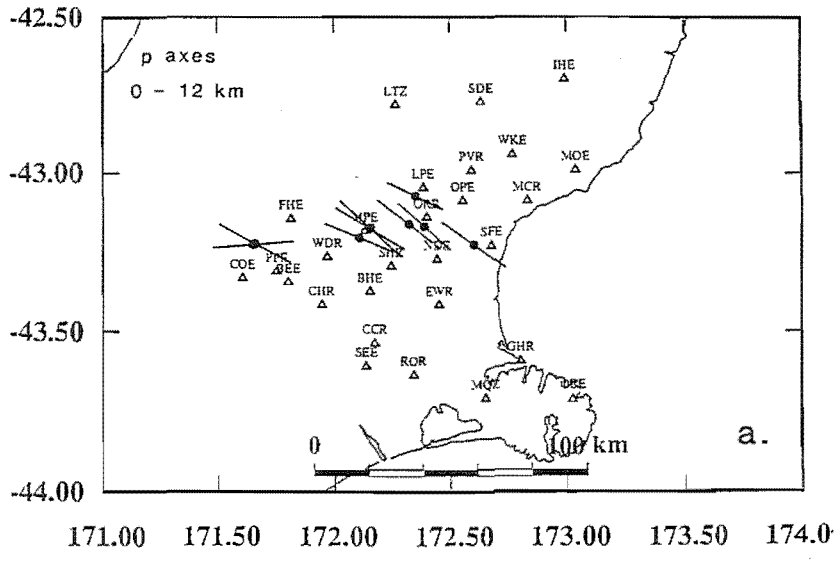
p axes
0 - 12 km
a.
0
100 km
-42.50
-43.00
-43.50
-44.00
171.00
171.50
172.00
172.50
173.00
173.50
174.0
LTZ
SDE
IHE
WKE
PVR
MOE
LPE
OPE
MCR
FHE
MPE
ORR
SFE
WDR
SHR
NDE
COE
PPE
BEE
BHE
CHR
EWR
CCR
SEE
ROR
GHR
MQZ
DBE

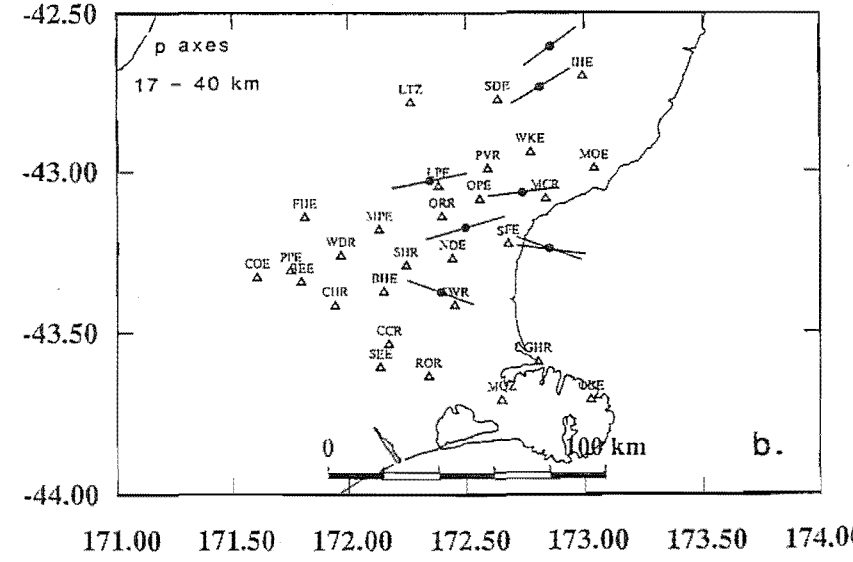
p axes
17 - 40 km
b.
0
100 km
-42.50
-43.00
-43.50
-44.00
171.00
171.50
172.00
172.50
173.00
173.50
174.00
LTZ
SDE
IHE
WKE
PVR
MOE
LPE
OPE
MCR
FHE
MPE
ORR
SFE
WDR
SHR
NDE
COE
PPE
BEE
BHE
CHR
EWR
CCR
SEE
ROR
GHR
MQZ
DBE

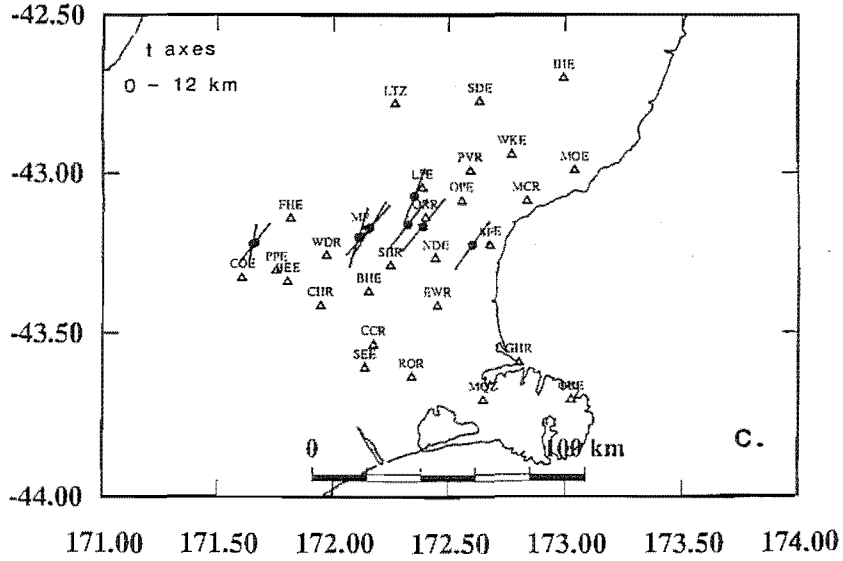
t axes
0 - 12 km
c.
0
100 km
-42.50
-43.00
-43.50
-44.00
171.00
171.50
172.00
172.50
173.00
173.50
174.00
LTZ
SDE
IHE
WKE
PVR
MOE
LPE
OPE
MCR
FHE
MPE
ORR
SFE
WDR
SHR
NDE
COE
PPE
BEE
BHE
CHR
EWR
CCR
SEE
ROR
GHR
MQZ
DBE

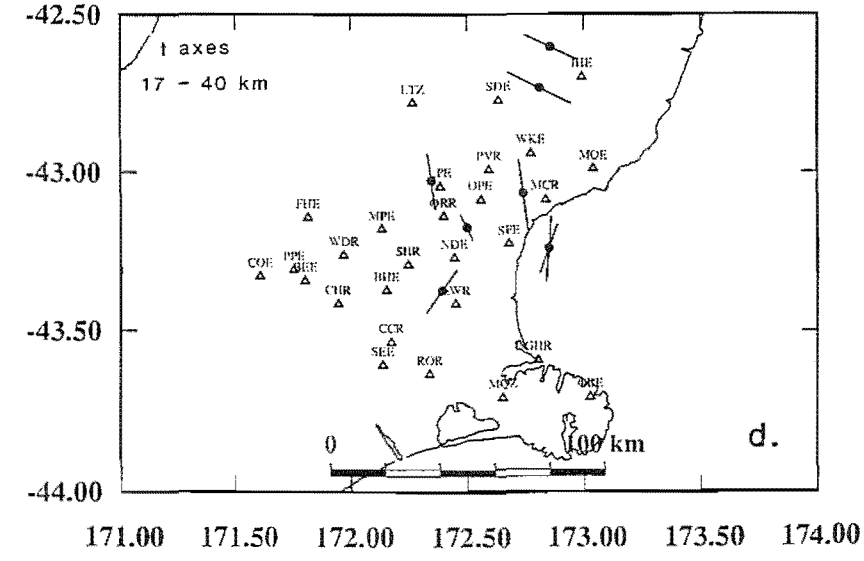
t axes
17 - 40 km
d.
0
100 km
-42.50
-43.00
-43.50
-44.00
171.00
171.50
172.00
172.50
173.00
173.50
174.00
LTZ
SDE
IHE
WKE
PVR
MOE
LPE
OPE
MCR
FHE
MPE
ORR
SFE
WDR
SHR
NDE
COE
PPE
BEE
BHE
CHR
EWR
CCR
SEE
ROR
GHR
MQZ
DBE

4.8 SLIP VECTORS

Slip vectors (the poles to auxiliary planes), for higher quality solutions in the upper seismic zone are shown in Fig.4.17 and those for all shallow events in the PPAFZ are shown in Fig.4.18. The length of the arrow is not the absolute motion, but is proportional to the cosine of its dip. The arrow points in the direction of motion of the east or south side of the fault relative to the north or west side. The nodal plane closest to the observed or projected trend of surface faults is inferred to be the fault plane. Poles to both nodal planes are plotted for solution 18 (Fig.4.18) which bears no obvious relationship to faults at the surface.

The majority of slip vectors trend W-WSW, and closely parallel the instantaneous plate motion vector. Two disparate solutions (Fig.4.17: sol.19 and Fig.4.18: sol.17) are for events associated with the Mt Grey and Mt Cheeseman Faults, respectively. These faults trend N-S, at a high angle to the regional structural grain. A third disparate solution (Fig.4.18: sol.20) is poorly constrained.

4.9 DISCUSSION

4.9.1 Regional seismicity

The distribution of hypocentres for the earthquakes recorded in this study show clear separation into two groups: 1) shallower than 12 km; and 2) deeper than 17 km. The shallow seismicity is concentrated chiefly between depths of 8 and 12 km. The absence of activity between 12 and 17 km is consistent with patterns observed elsewhere in continental regions, and indicative of a mid-crustal, brittle-ductile transition (Sibson, 1983). The zone of deeper earthquakes probably represents seismic activity within the oceanic crust on which the Mesozoic basement (submarine fan-facies greywacke) was laid down. The southward tapering of the deeper seismic zone suggests that the transition from oceanic subduction to continental collision is gradual, not abrupt.

Comparison of the focal mechanisms from above and below the mid-crustal aseismic zone indicates a difference in the pattern of strain release between the upper and lower crust, similar to that observed beneath the Marlborough region of northeastern South Island (Arabasz and Robinson, 1976) and southern California (Nicholson et al., 1986). The deeper mechanisms also are similar to that of an M_s 5.8 event which occurred on April 11, 1965 at a depth of 16 km (-5 or +9 km) beneath the

Figure 4.17 Horizontal projections of slip vectors for highest quality solutions of shallow events (<12 km) in the Porter's Pass-Amberley Fault Zone. Large arrow represents the instantaneous plate motion vector of DeMets et al. (1990).

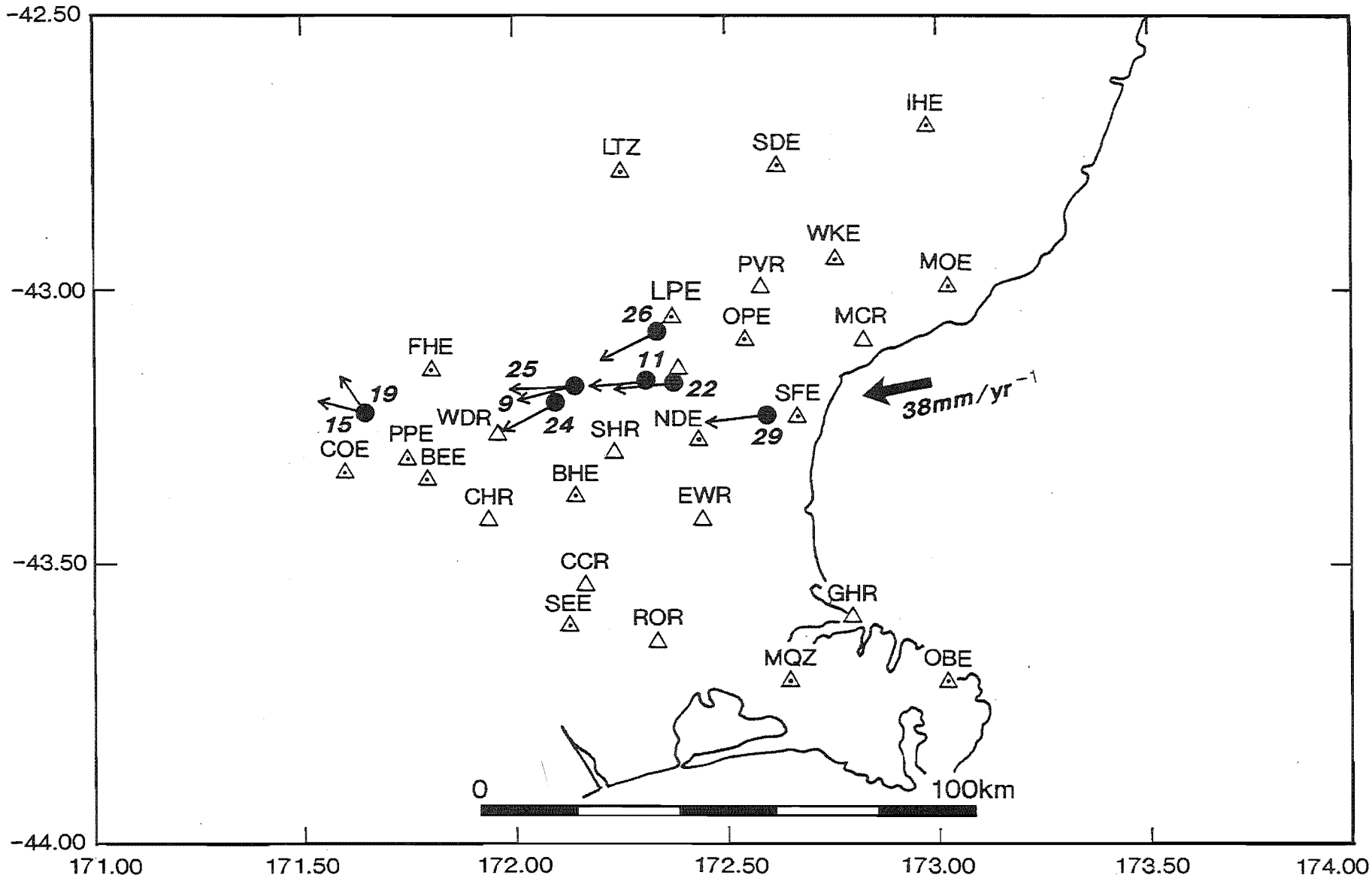
-42.50
-43.00
-43.50
-44.00
171.00
171.50
172.00
172.50
173.00
173.50
174.00
IHE
LTZ
SDE
WKE
PVR
MOE
LPE
OPE
MCR
FHE
SFE
WDR
PPE
BEE
COE
SHR
NDE
BHE
CHR
EWR
CCR
SEE
ROR
GHR
MQZ
OBE
26
11
25
22
19
9
15
24
29
38mm/yr⁻¹
0
100km

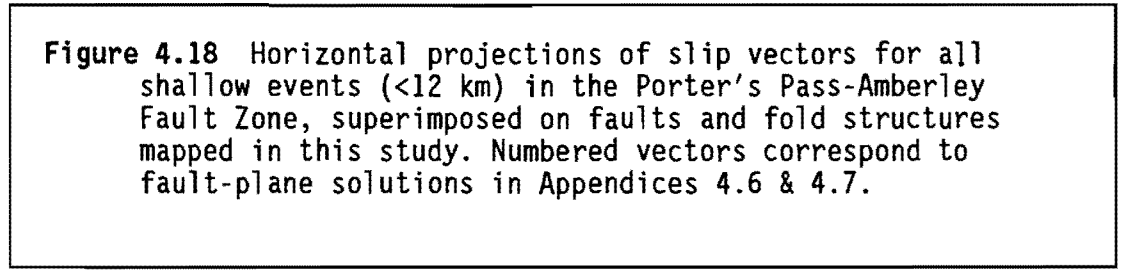

Figure 4.18 Horizontal projections of slip vectors for all shallow events (<12 km) in the Porter's Pass-Amberley Fault Zone, superimposed on faults and fold structures mapped in this study. Numbered vectors correspond to fault-plane solutions in Appendices 4.6 & 4.7.

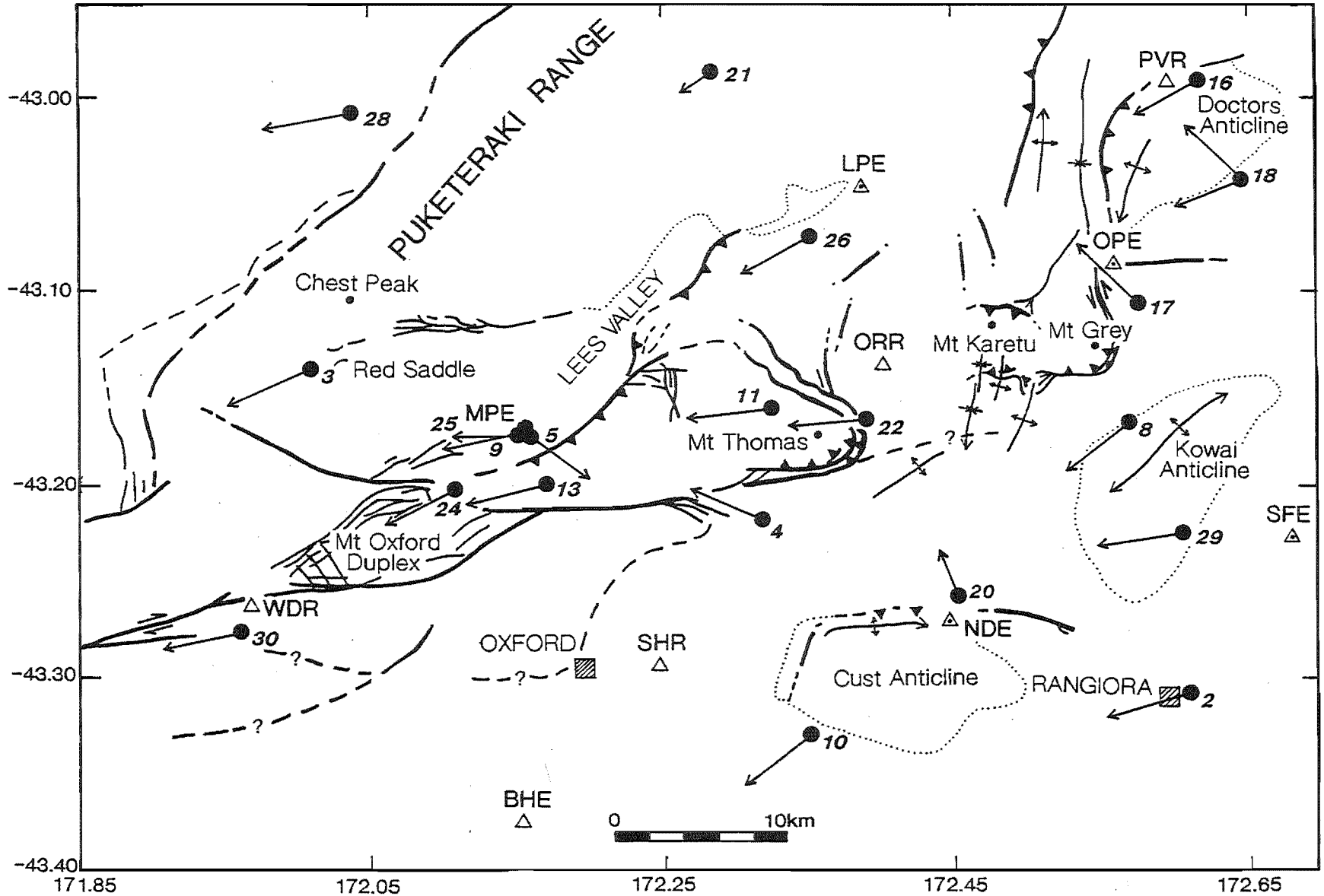
PUKETERAKI RANGE
Chest Peak
LEES VALLEY
Red Saddle
MPE
LPE
ORR
Mt Thomas
Mt Karetu
Mt Grey
PVR
Doctors Anticline
OPE
Kowai Anticline
SFE
Mt Oxford Duplex
WDR
OXFORD
SHR
NDE
Cust Anticline
RANGIORA
BHE
0
10km
-43.00
-43.10
-43.20
-43.30
-43.40
171.85
172.05
172.25
172.45
172.65

north Chatham continental slope (Fig.4.19).

The uniform NW-SE trend of sub-horizontal P-axes for shallow earthquakes (Fig.4.12a) is similar to those of Marlborough and consistent with previous estimates of principal horizontal shortening and relative contraction from fault slip vectors (Berryman, 1979; Nicol and Wise, 1992), and geodesy (Bibby, 1981), respectively. P-axes for deeper events in the north are rotated c.60° counterclockwise relative to those of shallow events (Fig.4.16a and b). This contrast also is evident for events beneath the PPAFZ further south, but there the relative rotation is c.35°. South of the PPAFZ, beneath Pegasus Bay and the Canterbury Plains, the azimuthal trend of P and T axes for deep and shallow events are similar. T-axes for the deeper events (Fig.4.16d) mirror the azimuthal change of P-axes from north to south and imply N-NW tension within the lower crust, north of the PPAFZ. This is consistent with a change in the dip-direction of the subduction beneath North Canterbury, reflecting the southwestward transition from subduction to continental collision.

4.9.2 Seismicity and geological structure of the PPAFZ

Figure 4.20 shows the location and focal mechanisms of 1990 microearthquakes in the PPAFZ, and the location of events recorded by the National Seismograph Network for the period 1964-1991 (N.Z. Seismological Observatory, 1992). Errors in the locations of the National Network events may amount to several kilometres, but three events of magnitude 5-5.2 were located along the main axis of the PPAFZ during this period, and more than half of the recorded events greater than magnitude 4 also lie within this central zone.

A majority of events less than magnitude 4 lie close to or within the mapped fault zones, but none have been located at, or near to localities where major late Holocene surface traces are preserved, namely: northern Lees Valley, Cust Anticline and Ashley Fault; and the Mt Grey Fault and Doctors Anticline. It is unclear whether the absence of seismicity during the last 28 years in areas of late Holocene surface faulting is due to a reduction of stress associated with recent (last few centuries) larger earthquakes, or indicative of accumulating elastic strain.

In Chapter 3, the kinematics of deformation in the PPAFZ was described from the results of mapping. An eastward transition from strike-slip to thrust and reverse faulting is evident - the latter being accompanied by folding in basement and cover, without evidence of

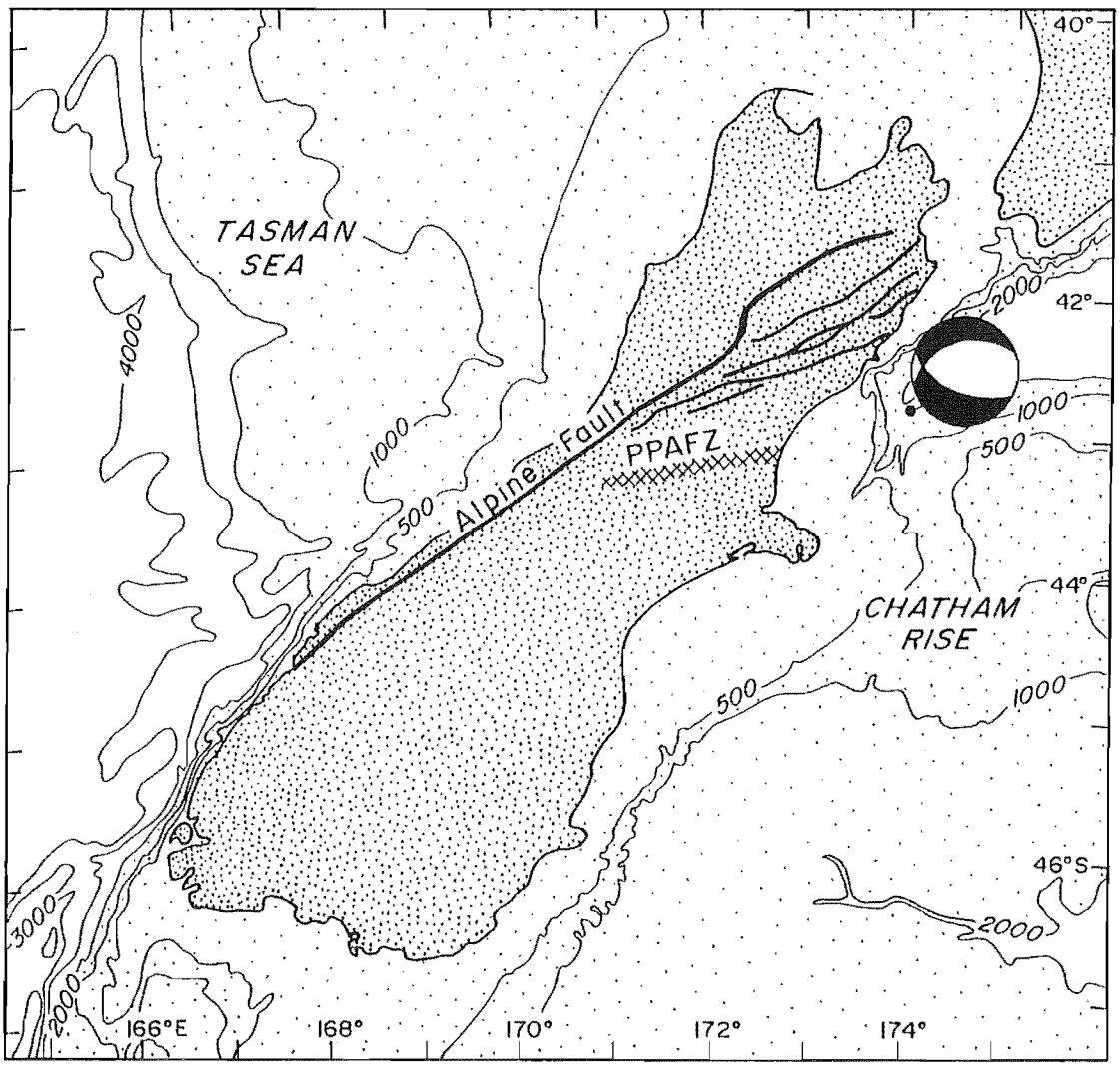

Figure 4.19 Map of South Island and offshore continental crust (light stipple), showing the Porter's Pass-Amberley Fault Zone and the normal fault-plane solution for an M_s5.8 event located beneath the northern Chatham slope at the western end of the Mernoo (normal) Fault Zone. The event occurred at a depth of 16 km (-5 or +9 km) on April 11, 1965 (H. Anderson pers.comm. 1991). Its relationship to the landward continental structures is uncertain, but the solution is similar to those of several deep (>17 km) microearthquakes recorded in northeastern Canterbury during this study.

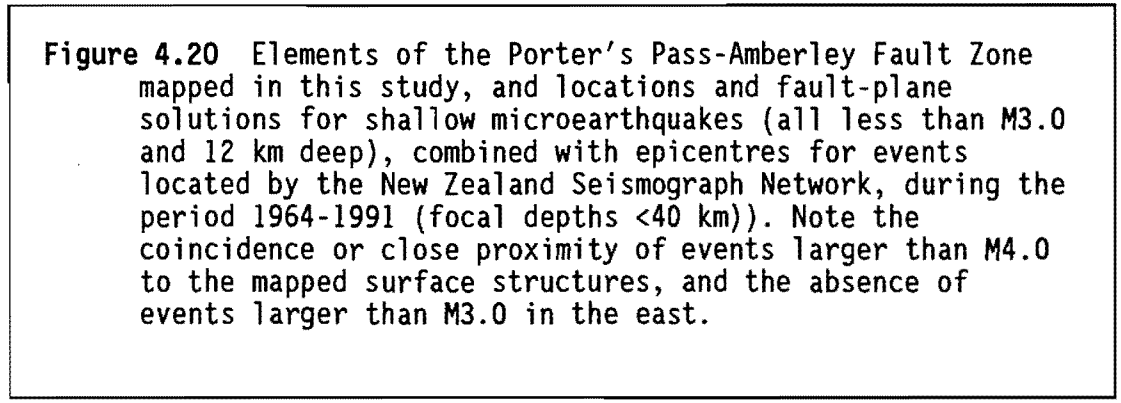

Figure 4.20 Elements of the Porter's Pass-Amberley Fault Zone mapped in this study, and locations and fault-plane solutions for shallow microearthquakes (all less than M3.0 and 12 km deep), combined with epicentres for events located by the New Zealand Seismograph Network, during the period 1964-1991 (focal depths <40 km)). Note the coincidence or close proximity of events larger than M4.0 to the mapped surface structures, and the absence of events larger than M3.0 in the east.

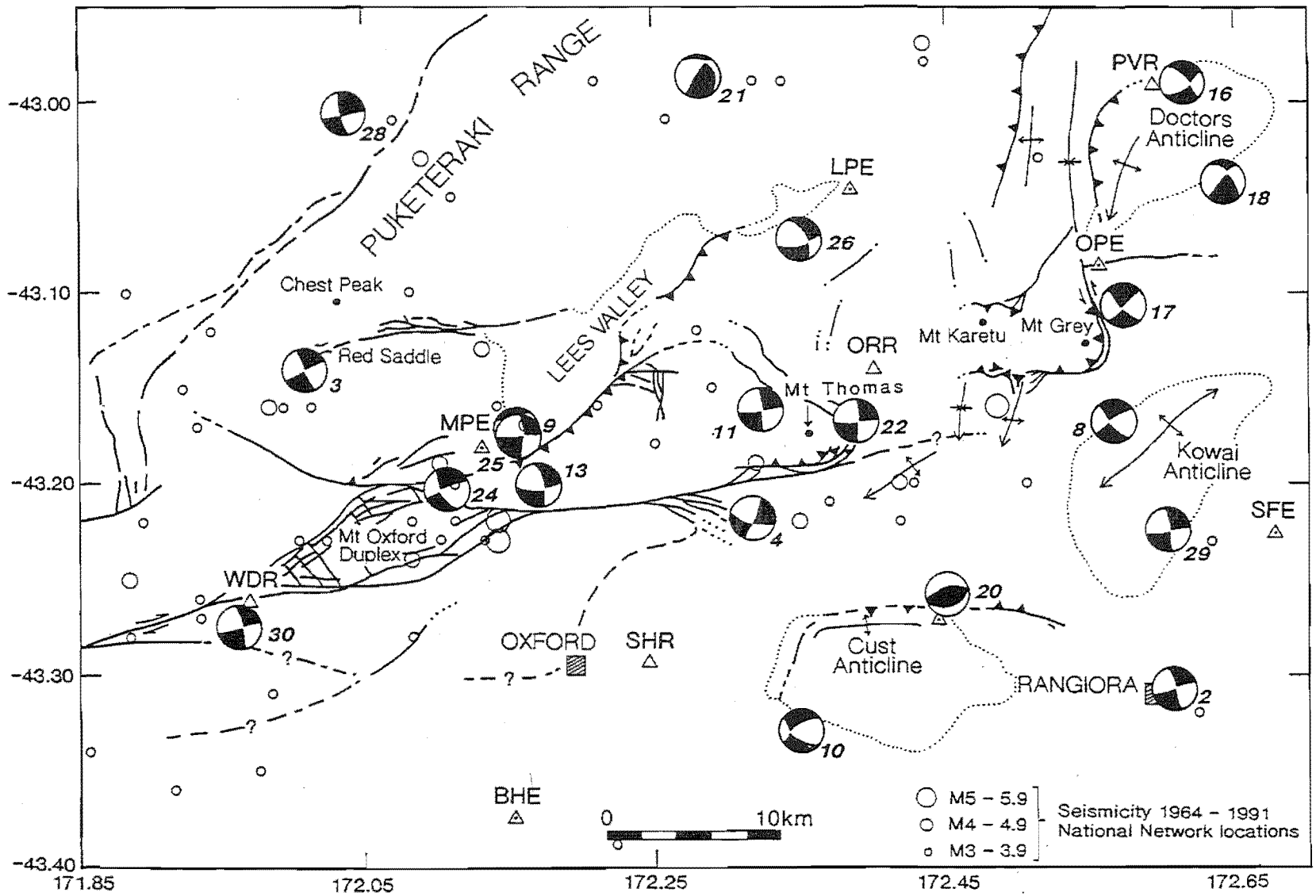
-43.00
-43.10
-43.20
-43.30
-43.40
171.85
172.05
172.25
172.45
172.65
PUKETERAKI RANGE
Chest Peak
Red Saddle
LEES VALLEY
LPE
ORR
Mt Thomas
MPE
Mt Oxford Duplex
WDR
OXFORD
SHR
BHE
PVR
Doctors Anticline
OPE
Mt Karetu
Mt Grey
Kowai Anticline
SFE
Cust Anticline
RANGIORA
28
21
26
3
9
25
24
13
11
22
4
16
18
17
8
29
20
30
2
10
0
10km
M5 - 5.9
M4 - 4.9
M3 - 3.9
Seismicity 1964 - 1991
National Network locations

decollement between the two. Recorded seismicity shows a strong correlation with surface faults and fold structures, and is low or absent in areas that have been mapped comprehensively, but in which few active faults have been identified (Fig.4.20). The main such area encompasses the Esk Head Melange, NNW of a line between Mt Thomas and Mt Grey, suggesting that the Esk Head Melange may be deforming relatively aseismically.

Focal mechanisms indicate predominately strike-slip faulting, with one nodal plane parallel to the observed strike of surface faults. Slip vectors for almost all events are closely parallel to the instantaneous plate motion vector (Figs. 4.17, 4.18), and strain axes closely match the geometries of geological structures, with P-axes oriented at a high angle to the axial surfaces of short-wavelength folds in cover (for example, between Mt Thomas and Mt Grey), and longer wavelength folds such as the Puketeraki Range; T-axes are oriented sub-parallel to fold axial surfaces (compare Fig.4.13, 4.15 with Frontispiece 1).

Strike-slip mechanisms for microearthquakes in the west, are consistent with steeply dipping faults observed at the surface. However, other strike-slip mechanisms are at variance with the dominantly thrust geometries of surface faults (Lees Valley), and those inferred from near-surface (<2 km deep) drillhole and seismic reflection data (Kowai Anticline: Hoolihan, 1978; Katz, 1982). Comparison of the near-surface dips of these faults and the nodal planes of focal mechanisms, suggests that in vertical cross-section (Maps 1 and 2; Cross-sections A-B, C-D, E-F: map pocket,) the faults splay upwards and are analogous to structures described from transpressional strike-slip zones elsewhere (e.g Wilcox et al., 1973; Sylvester and Smith, 1976; Sylvester, 1988).

4.10 SUMMARY

1. The 1990 North Canterbury microearthquake survey was predicated on a need to acquire detailed information on crustal deformation in the transition between subduction of oceanic Pacific Plate at the Hikurangi Trough and continental collision in the central Southern Alps.

2. Two depth intervals of seismicity are identified from events located within the network: 1) an upper seismic zone (0-12 km), and; 2) a lower seismic zone (17-40 km). The base of the upper seismic zone is horizontal; the lower seismic zone has a bottom edge which dips to the NE at 10°, and to the NW at 15°. No earthquakes were recorded in the interval 12-17 km, which probably represents a mid-crustal aseismic

ductile layer.

3. Forty-four single-event focal mechanisms and five composite mechanisms were obtained from events located within the network. The majority of shallow (<12 km) events were strike-slip, with one nodal plane parallel to the E-NE strike of mapped surface faults. If these nodal planes represent the fault-plane, then the sense of displacement is consistently right-lateral.

4. The lower seismic zone is interpreted as activity in old oceanic crust on which the Torlesse terrane greywackes were laid down. Hypocentres of events located in this zone to the north are consistent with the inferred depth of the subducted Pacific Plate. Mechanisms for events located in the deeper seismic zone (>17 km) were less well constrained, and included a greater number of dip-slip mechanisms that imply tensional faulting in the dip-direction of the subducted slab.

5. With few exceptions, contractional strain axes (P-axes) for shallow events are uniformly oriented WNW-NW, consistent with previous estimates of principal horizontal shortening and relative compression, from fault slip vectors and geodesy. Slip-vectors for most shallow events in the PPAFZ are parallel to the instantaneous plate-motion vector.

6. South of the PPAFZ, the azimuthal trend of P axes for deeper events is similar to that of shallow events, but north of the PPAFZ the P axes of deep events are rotated counter-clockwise relative to those of shallow events. The relative rotation is c.35° just north of PPAFZ, and c.60° in the far north of the region. The azimuthal trends of T axes for deeper events also change from south to north, and are consistent with tensional faulting in the dip-direction of the subducted plate.

7. The differences in azimuthal trend of shallow and deeper P and T axes are similar to those observed by Arabasz and Robinson (1976) in Marlborough. The pattern is interpreted here as evidence that the lower crust is being pulled down and detached from the upper crust above the ductile layer (12-17 km). The crust above the detachment is being shortened, but the across-strike spacing of the major faults and half-wavelengths of associated folds (10-15 km) are comparable to, and probably governed by, the depth of the ductile layer. South of the PPAFZ, the P and T axes of shallow and deeper events are similar, suggesting there, that the upper crust is coupled to the lower crust.

8. Locations of microearthquakes and historic (1964-1991) seismicity in the PPAFZ are remarkably similar, with most events located near mapped surface faults. No historic events (including microearthquakes) have been located beneath sites of known late Holocene surface rupture, but there are insufficient data to determine whether the low seismicity reflects a recent (last few centuries) reduction of stress following large prehistoric earthquakes, or presently accumulating elastic strain.

9. Few historic events (including microearthquakes) are located in the area of Esk Head Melange, suggesting that the melange may be deforming relatively aseismically. Almost all microearthquakes recorded in the PPAFZ were shallow (<12 km) and most were located near mapped surface faults. Strike-slip mechanisms of events in the west (around the Mt Oxford Duplex) are consistent with steeply-dipping faults at the surface, but several of those further east (beneath the Kowai Anticline) are at variance with near-surface structures, indicative of thrusting. These differences may be explained by the dip of the faults increasing with depth and converging within steeply-dipping zones of strike-slip faulting.

CHAPTER 5. SEISMIC HAZARD ASSESSMENT FROM FAULT RUPTURE AND LANDSLIDES ALONG THE PORTERS PASS-AMBERLEY FAULT ZONE

5.1 INTRODUCTION

Despite the location of the New Zealand astride the active, obliquely-convergent Pacific-Australia plate boundary, large earthquakes (>M7.0) occur relatively infrequently (Eiby, 1968), and our historic record (post-1850 A.D.) is too short to constrain the recurrence frequency of large earthquakes for individual fault zones. Studies of paleoseismicity have used landslides or evidence of fault displacement to infer the magnitude and timing of prehistoric earthquakes (Adams, 1980, 1981; Hull and Berryman, 1986; Cooper and Norris, 1990; Cowan and McGlone, 1991; Van Dissen et al.,1992; Crozier, 1991).

In this chapter, evidence of fault displacement and co-seismic landsliding is used to estimate the timing and magnitude of the largest earthquakes that have occurred in the Porter's Pass-Amberley Fault Zone (PPAFZ) of eastern South Island, during the last 2500 years. There have been no historic surface ruptures of the PPAFZ but several faults have late Quaternary displacements (Wellman, 1953; Gregg, 1964; Berryman, 1979). Since 1964, the zone has been better defined by seismicity (earthquakes of magnitude 3.0-5.3) than many other surface faults in New Zealand (Reyners, 1989).

The data used to infer prehistoric earthquakes in this study include: 1) dated landslides, and; 2) time-bracketed displacements on fault traces within the PPAFZ (Fig.5.1). Data were gathered during fieldwork between 1989 and 1992, and compiled from previously published (Burrows, 1975; Whitehouse, 1983) and unpublished sources (Coyle, 1988; Molloy and Tonkin pers.comm., 1992; McSaveney pers.comm. 1992).

5.2 TIMING OF SURFACE RUPTURES

5.2.1 Porters Pass Fault

At Porters Pass, buried soils each containing charcoal, have been offset by the Porters Pass fault in a road-side batter, where the fault crosses Highway 73 (Fig.5.2). The charcoals have been dated and the ages (Table 5.1) together with the stratigraphy suggest at least two rupture events. Fault 1 (Fig.5.2) displaces the lower of the two soils but not the upper horizon, and is inferred to have moved between 7000 and 9000 years ago. Both soils are displaced by Faults 2 and 3, indicating surface

Figure 5.1 Map showing the major structural elements of the Porter's Pass-Amberley Fault Zone and the distribution of prehistoric landslides. The locations of Figs. 5.2; 5.3; 5.5 and 5.6, and localities mentioned in the text are indicated.

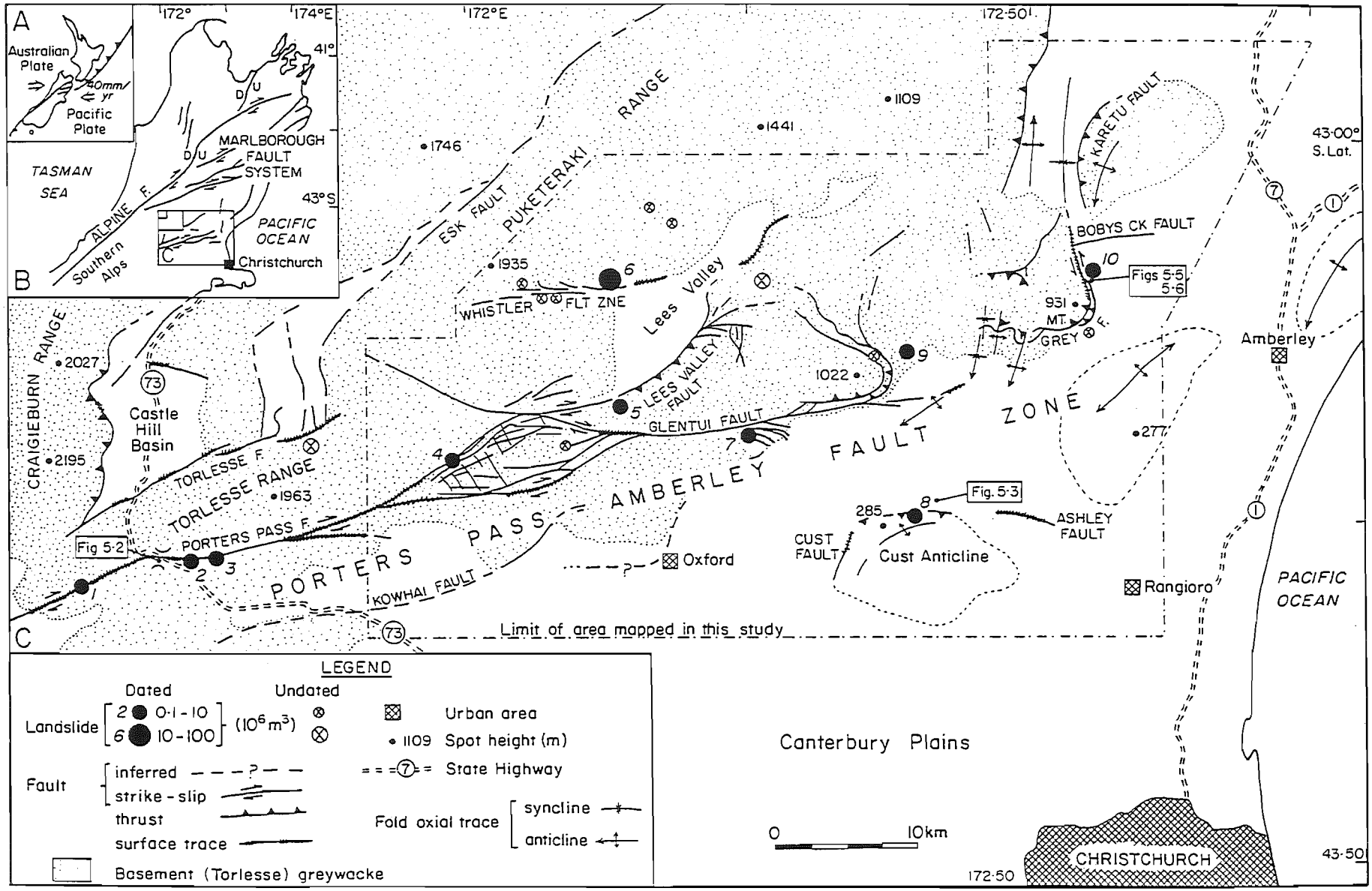
A
Australian Plate
40mm/yr
Pacific Plate
172°
174°E
41°
MARLBOROUGH FAULT SYSTEM
TASMAN SEA
ALPINE F.
Southern Alps
43°S
PACIFIC OCEAN
Christchurch
B
172°E
172·50'
1109
1441
1746
RANGE
PUKETERAKI
ESK FAULT
KARETU FAULT
43·00° S.Lat.
BOBYS CK FAULT
10
Figs 5·5 5·6
1935
6
WHISTLER FLT ZNE
Lees Valley
931
MT. GREY F.
Amberley
CRAIGIEBURN RANGE
2027
73
Castle Hill Basin
LEES VALLEY FAULT
1022
9
5
GLENTUI FAULT
7
ZONE
277
2195
TORLESSE F.
TORLESSE RANGE
1963
4
AMBERLEY
FAULT
Fig. 5·3
285
8
ASHLEY FAULT
CUST FAULT
Cust Anticline
Fig 5·2
PORTERS PASS F.
2
3
PORTERS PASS
Oxford
Rangioro
PACIFIC OCEAN
KOWHAI FAULT
C
Limit of area mapped in this study
LEGEND
Dated
Undated
Landslide
2 0·1 - 10
6 10 - 100
(10⁶m³)
Urban area
1109 Spot height (m)
State Highway
Fault
inferred
strike - slip
thrust
surface trace
Fold axial trace
syncline
anticline
Basement (Torlesse) greywacke
Canterbury Plains
0
10km
CHRISTCHURCH
172·50
43·50

TABLE 5.1 Evidence for prehistoric fault ruptures in the Porters Pass-Amberley Fault Zone

Fault & Locality	N.Z. Metric Grid (Geodetic Datum (1949)	Lat. Long. (Decimal degrees)	Site Description [1]	Timing of Surface Rupture [1]
Porters Pass Fault				
Porters Pass	2407900E 5767100N	43.2983 171.7414	Fault offsets buried soils containing charcoal in road batter on south side of State Highway 73. Youngest offset soil 500 - 700 yr B.P.* (Goh & Molloy, 1979). Older offset soils are 6900 ± 90 yr B.P. and 8900 ± 110 yr B.P. (Tonkin & Basher 1990).	One or more events between 7000 and 9000 years ago. One or more events since 7000 years; one younger than 500 - 700 years B.P. (c.1300 - 1500 A.D.) Refer Fig. 5.2.
Porters Pass Fault				
Porters Pass	2408020E 5767100N	43.2983 171.7429	Peat impounded behind fault trace on slopes NE of State Highway 73. Charcoal in peat at -1.30m defines transition from forest to grassland (N. Moar pers. comm. 1992). Interval -1.30 - 1.40 dated 1720 ± 60 yr B.P. (NZ 5235) Rate of peat accumulation for the interval (under forest) - 1.81 - 1.30m: 0.50_{min} - 0.64_{max} mm/yr. Inferred age for base of peat at 2.0 - 2.2m: c.2000 - 2500 years B.P.	Formation of fault trace pre-dates onset of peat accumulation.
Porters Pass Fault				
Acheron River	2401400E 5764800N	43.3181 171.6609	Rock avalanches bury fault trace (Burrows, 1975; Coyle, 1988) and provide minimum age for surface rupture (Table 5.2).	Rock avalanches presumably triggered by fault rupture, between c.1300 A.D. and 1500 A.D.
Kowai River	2411200E 5768100N	43.2897 171.7823		
Ashley Fault				
Ashley River	2460000E 5771650N	43.2626 172.3839	Strath terrace of Ashley River, 13 ± 2m above active floodplain on north limb of Cust Anticline. Strath dated: 2345 ± 58 yr B.P. (NZ 7857). Calibrated radiocarbon age ** (90% confidence interval) 533 B.C. to 201 B.C.	Strath terrace age = age of Mairaki landslide No. 8 (Table 5.2). River incision post-dates these events which are interpreted as a response to rupture and differential uplift in north limb of Cust Anticline.

Okuku River	2468500E 5771900N	43.2609 172.4886	Fault trace vertically offsets a Holocene terrace of the Okuku River by 1 - 1.5m. Terrace is same height above the active floodplain as a dated strath terrace on the south bank of Ashley River (above).	The fault trace scarp has not been degraded by river action. Last rupture inferred to post-date river incision below 11 - 15m level. (refer Ashley River site above). Fault trace truncated by Okuku River terrace riser (age unknown), 4 - 10m above active flood plain.
<u>Mt. Grey Fault</u> Mt. Grey	2473300E 5789850N	43.0995 172.5489	Stream bank exposure of fault, 3m below surface trace. Wood dated at 2330 ± 40 yr B.P. (NZ 7852), impounded with peat behind fault scarp, and disrupted by fault. Wood buried by debris flows from stream catchment. Two (buried) soils formed on debris flows: One flow faulted, one not. Tree stump in growth position in soil on unfaulted debris flow (182 ± 60 yr B.P. (NZ 7853). Calibrated age: 1661 A.D. - 1955 A.D.	Calibrated radiocarbon age of wood (463 B.C. to 205 B.C.) inferred to represent the timing of a seismic event that knocked a tree into the fault trench. Second rupture event disrupted wood and overlying debris flow, prior to formation of soil and growth of tree on younger unfaulted debris flow, and prior to 1850 A.D. (historic record begins). Modal weathering rind ages inferred to represent timing of surface ruptures. The ages are consistent with evidence for surface rupture in the stream bank exposure.
	2473300E 5789850N to 2472900E 5791500N	43.0995 172.5489 43.0847 172.5441	Weathering rinds on boulders and cobbles along fault trace indicate two modal ages for site disturbance: 1970 ± 340 and 390 ± 50 years (320 B.C. to 360 A.D., and 1550 A.D. to 1650 A.D.) (69, 1991). †	

(1) * Conventional radiocarbon age in years B.P. (1950 A.D.) Libby half-life (5568 years). N.Z. Radiocarbon Dating Laboratory number in brackets.

** Calibrated radiocarbon ages (95% confidence intervals unless otherwise stated) based on a compilation by Stuiver and Reimer (1986) of 20 year tree ring data for the period 7210 B.C. to 1950 A.D., with offset of -30 radiocarbon years as recommended by Stuiver and Pearson (1986) and Pearson and Stuiver (1986)

† Modal age (deducted from year of observation) from thickness of weathering rinds on surface clasts, using method of Chinn (1981) and calibration curve of McSaveney (1992). Number and year of observations, respectively in brackets.

ruptures younger than 7000 years ago. At the top of the batter, *Nothofagus* charcoal, derived from a fire between 500 and 700 years ago (c.1300 A.D. and 1500 A.D.) (Goh and Molloy, 1979, Molloy, pers.comm. 1992) is preserved only on the apparently down-thrown side of Fault 3. The last displacement on this fault is inferred to post-date the fire. Two landslides (1 and 2: Fig.5.1) bury the surface trace of the Porters Pass fault within a few kilometres of the exposure at Porters Pass. The landslides are the same age (Table 5.2) and constrain the timing of the younger rupture, which must lie within the range c.1300-1500 A.D.

A few hundred metres north of the highway at Porters Pass, peat has accumulated behind a surface trace of the fault. A radiocarbon date from the lower part of the peat column (Table 5.1) indicates that the base of the bog is probably about 2000-2500 years old. The surface trace formed prior to the onset of peat accumulation.

5.2.2 Cust Anticline and Ashley Fault

On the northern flank of the Cust Anticline (Figs.5.1; 5.3) consolidated Plio-Pleistocene siltstone is exposed in the south bank of the Ashley River. A terrace is bevelled into the siltstone and the strath is 13 ±2 m above the active Ashley River floodplain. Wood from the strath is between 2100 and 2500 calibrated radiocarbon years old (c.200-500 B.C., Table 5.1), implying that the river has incised at an averaged rate of 5.5 ±1.2 m/kyr over that period, including the period of deposition of the gravel veneer. The thickness of gravels beneath the active floodplain is unknown, so the calculated rate represents a minimum value.

The presence of consolidated siltstone at the surface of the Canterbury Plains, combined with the abrupt rise of topographic relief (150 m above the Ashley River (Fig.5.3), and a steep north-south gradient of bouguer gravity anomalies across the Ashley River (Thomas, 1963) implies the presence of an E-W trending fault. Displacement on this fault has contributed to growth of the Cust Anticline and is inferred to have controlled the rate of incision of the Ashley River along its southern bank. This fault probably connects beneath the Plains, to the Glentui Fault section of the PPAFZ (Fig.5.1) and is presumably also related to the Cust (Fig.5.3) and Ashley Faults (Fig.5.1; Maps 3 and 4).

The height of the terrace above the Ashley River probably indicates more than one increment of uplift and fold growth. The first increment of down-cutting below the strath is unlikely to have been older than the strath itself, which represents the local base-level of river erosion at

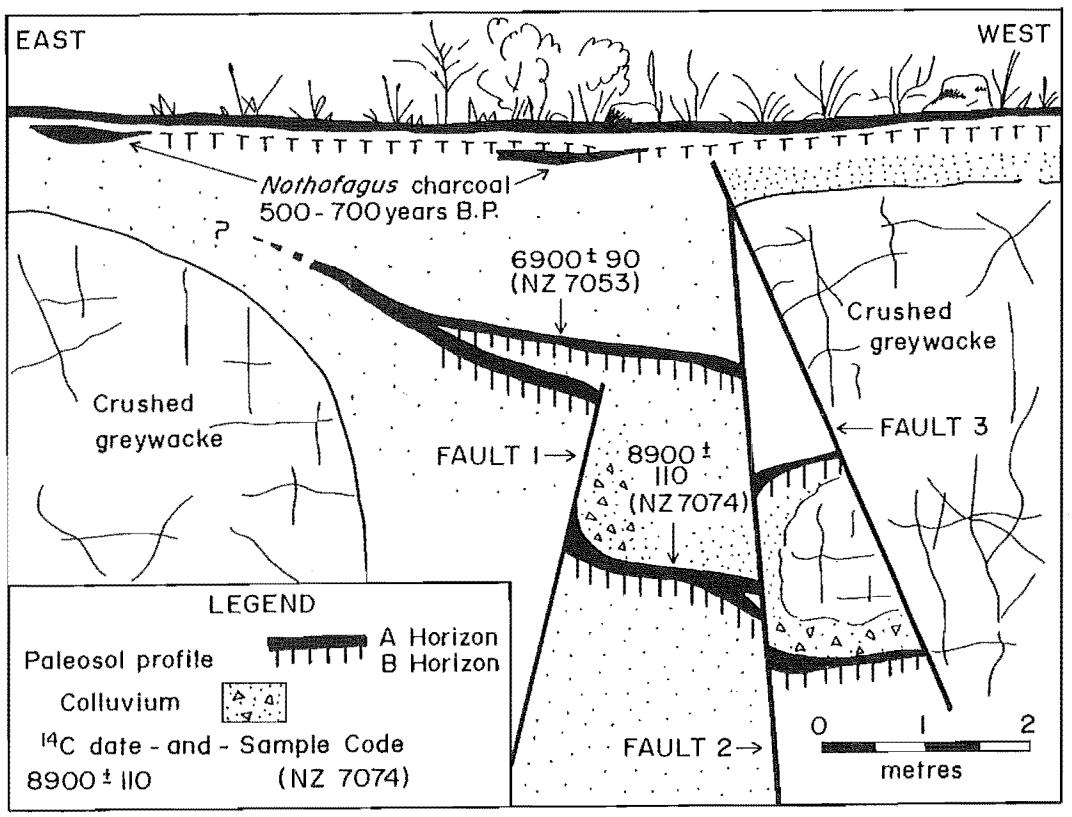

Figure 5.2 Holocene cross-cutting relationships of faults within the crushed zone associated with the Porter's Pass Fault at Porter's Pass, exposed in a batter on the south side of Highway 73. Buried soils containing charcoal of early-mid Holocene age are offset by Faults 1 and 2. Fault 2 is truncated by Fault 3. *Nothofagus* charcoal 500-700 radiocarbon years old, dated from several localities in the surrounding area, is preserved c.30 cm below ground surface on the downthrown side of Fault 3 and wedges out against the fault.

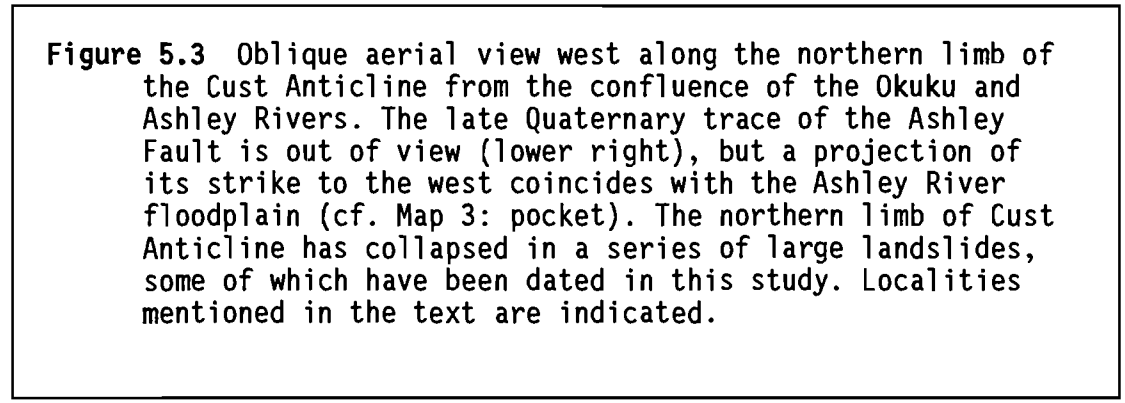

Figure 5.3 Oblique aerial view west along the northern limb of the Cust Anticline from the confluence of the Okuku and Ashley Rivers. The late Quaternary trace of the Ashley Fault is out of view (lower right), but a projection of its strike to the west coincides with the Ashley River floodplain (cf. Map 3: pocket). The northern limb of Cust Anticline has collapsed in a series of large landslides, some of which have been dated in this study. Localities mentioned in the text are indicated.


Canterbury Plains
Cust Fault
Cúst Anticline
Landslide 8a
Landslide 8b
strath terrace
Lower Pleistocene conglomerate
Ashley River
Okuku River

that time. The wood from which the age of the strath is inferred, is the same age as wood collected from a large landslide a few hundred metres upstream (Fig.5.3, Table 5.2). The landslide contains whole trees and included an articulated skeleton of the largest species of the extinct moa, *Diornis giganteus* (Fig.5.4). The landslide clearly incorporated abundant living matter, and the ages of the wood samples are presumably close to the age of both the landsliding event and the formation of terrace strath. These events are surmised to represent the product of coseismic surface rupture within the PPAFZ.

Further east, between Okuku and Makerikeri Rivers the Ashley Fault vertically offsets an inferred late Pleistocene aggradation terrace and one Holocene degradation terrace of the Okuku River (Maps 3 and 4). The offset varies between one and four metres on the late Pleistocene surface, and between 0.5 and 1.5 metres on the Holocene surface (Map 4). An average offset on all of the terraces is 1.5-2 metres; the variations accompany changes in the strike of the fault. The sense of the change is systematic and indicative of a minor right-lateral component of displacement, but no unequivocal right-lateral offsets have been measured.

The height of the youngest offset terrace above the confluence of Ashley and Okuku Rivers, is the same as that of the dated terrace strath above Ashley River, and the terraces may be of near equal age. The Ashley Fault scarp is not significantly degraded, so Okuku River had presumably incised to a lower level at the time the surface was offset. The oldest Okuku River terrace <u>not</u> offset by the Ashley Fault (the riser of which truncates the fault trace) is about 4 m above the active floodplain (Map 4). The age of the 4 m terrace is unknown. No datable material has been found and the terrace age can not be inferred from its height above the floodplain, (because the rate of river down-cutting cannot be assumed uniform at this locality, and very likely was not).

The conclusion drawn (from the available data) is that landsliding may have accompanied growth of the Cust Anticline and rupture of the Ashley Fault, probably during the period between c.200-500 B.C.. The 1.0-1.5 m offset across the Ashley Fault on the former terrace of the Okuku River indicates a younger surface rupture event, that is older than the undated +4 m Okuku River terrace.

5.2.3 Mt Grey Fault

Mt Grey is located at the eastern end of the PPAFZ (Fig.5.1), and is bounded by the Mt Grey Fault which comprises an east-striking (north-

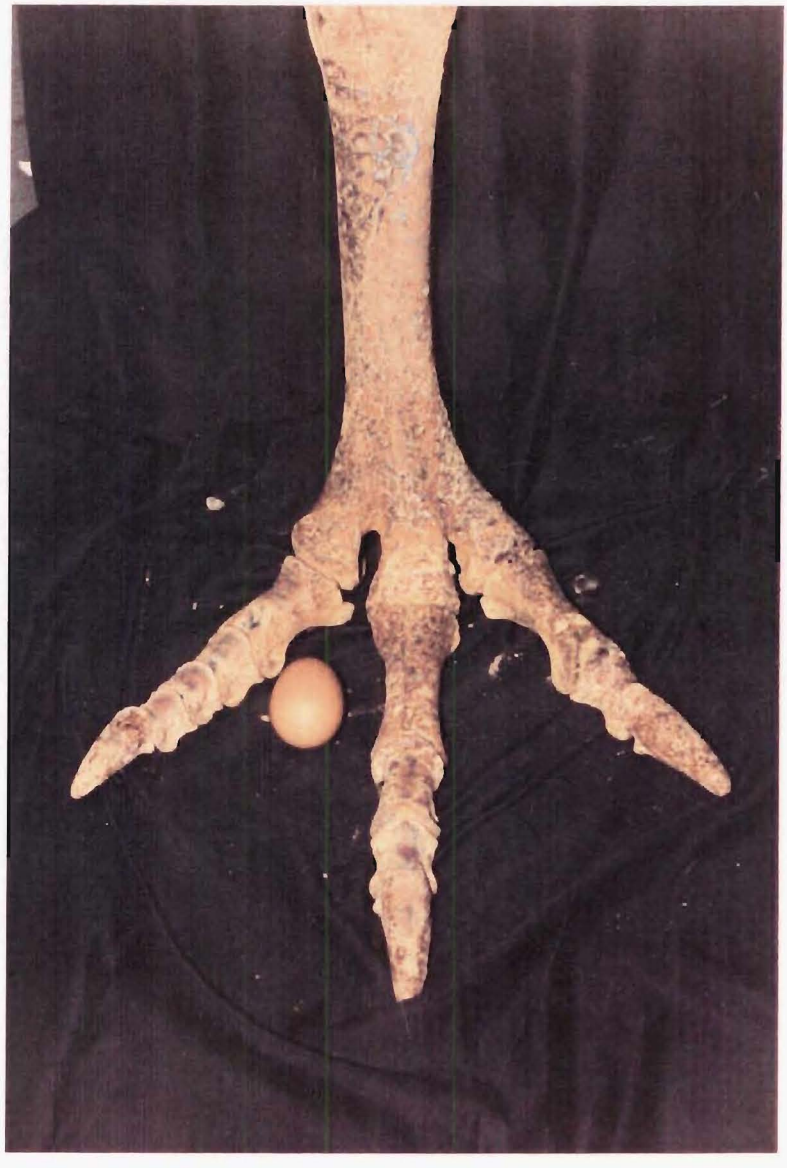

Figure 5.4 Meta-tarsus and toe bones of an articulated skeleton of *Diornis giganteus* (a giant moa), recovered from a landslide on the northern limb of Cust Anticline. The egg of a domestic hen provides scale.

dipping) thrust beneath its southern margin, that bends northward and steepens along the eastern slopes to form a north-striking, oblique-left lateral tear fault that dips to the west. The fault is exposed in a number of streams draining northeast from Mt Grey and forms a prominent surface trace and bench-hollow, behind which scree and boulders have accumulated (Fig.5.5).

The timing of prehistoric surface ruptures on the Mt Grey Fault are estimated from radiocarbon and weathering rind dates that indicate several events within the last 2500 years (Table 5.1). Evidence for the older event was collected from a stream-bank exposure of the fault (Fig.5.6), where wood and peat have been preserved on the surface of an older debris flow, offset across the fault scarp about three metres below the present ground surface. The wood was not in growth position.

The peat and wood are buried by younger colluvium which in turn has been offset by the fault (Fig.5.6). An A-C soil profile containing trace charcoal of unknown age is developed on the debris flow and defines an apparent vertical offset (downthrown to the west) across the fault. We could not discern from the field relationships, whether this buried soil had been deformed or merely developed on the exposed fault scarp at a later date. The soil is buried by a third debris flow capped by a younger A-C soil profile and a tree stump in growth position. A radiocarbon date for the tree stump (Table 5.1) merely provided an indicative age, but the buried soil clearly post-dates the last rupture which is prehistoric (older than 1850 A.D.).

Chips were collected from Torlesse sandstone boulders and cobbles exposed along the fault trace north of the stream bank locality (Fig.5.5, 5.6) and weathering rind ages were calculated using the method of Chinn (1981) and calibration curve of McSaveney (1992), to evaluate the timing of site disturbance. Two modal rind thicknesses were obtained and the ages (Table 5.1) are in good agreement with the time intervals for which surface rupture is inferred from the radiocarbon ages. The available data imply surface rupture on the Mt Grey Fault, between approximately 320 B.C.- 360 A.D. and 1550-1650 A.D.

5.3 LANDSLIDES

The evidence for surface rupture on three elements of the PPAFZ, between c. 2000-2500 years ago (Porters Pass, Ashley River, Mt Grey); between c. 500-700 years ago (Porters Pass, possibly Ashley River); and c. 300-500 years ago (Mt Grey) has been described above. Twenty landslides have been identified within the region of the PPAFZ (Fig.5.1).

Figure 5.5 View south along the surface trace of the Mt Grey Fault at Onepunga Station (foreground and arrows at distance), where it forms a trench more than two metres deep. Surface clasts of Torlesse sandstone preserved in the trench, provided weathering rinds for dating of past site disturbance.

Figure 5.6 Trench log of cross-cutting relationships associated with the Mt Grey Fault, exposed in a stream at Onepunga Station c.400 m south of observer in Figure 5.5. Wood and peat ponded behind the scarp three metres below present ground surface, are more than 2000 radiocarbon years old. They have been displaced by a younger rupture event, which formed a scarp in an overlying debris flow (Unit 2). A paleosol is developed on the scarp, but it is not clear whether soil development preceded or post-dated the rupture event. A younger debris flow (unit 3) also is capped by a paleosol and contained a tree stump in growth position. Units 3 and 4 which are not deformed are inferred to post-date the last rupture.

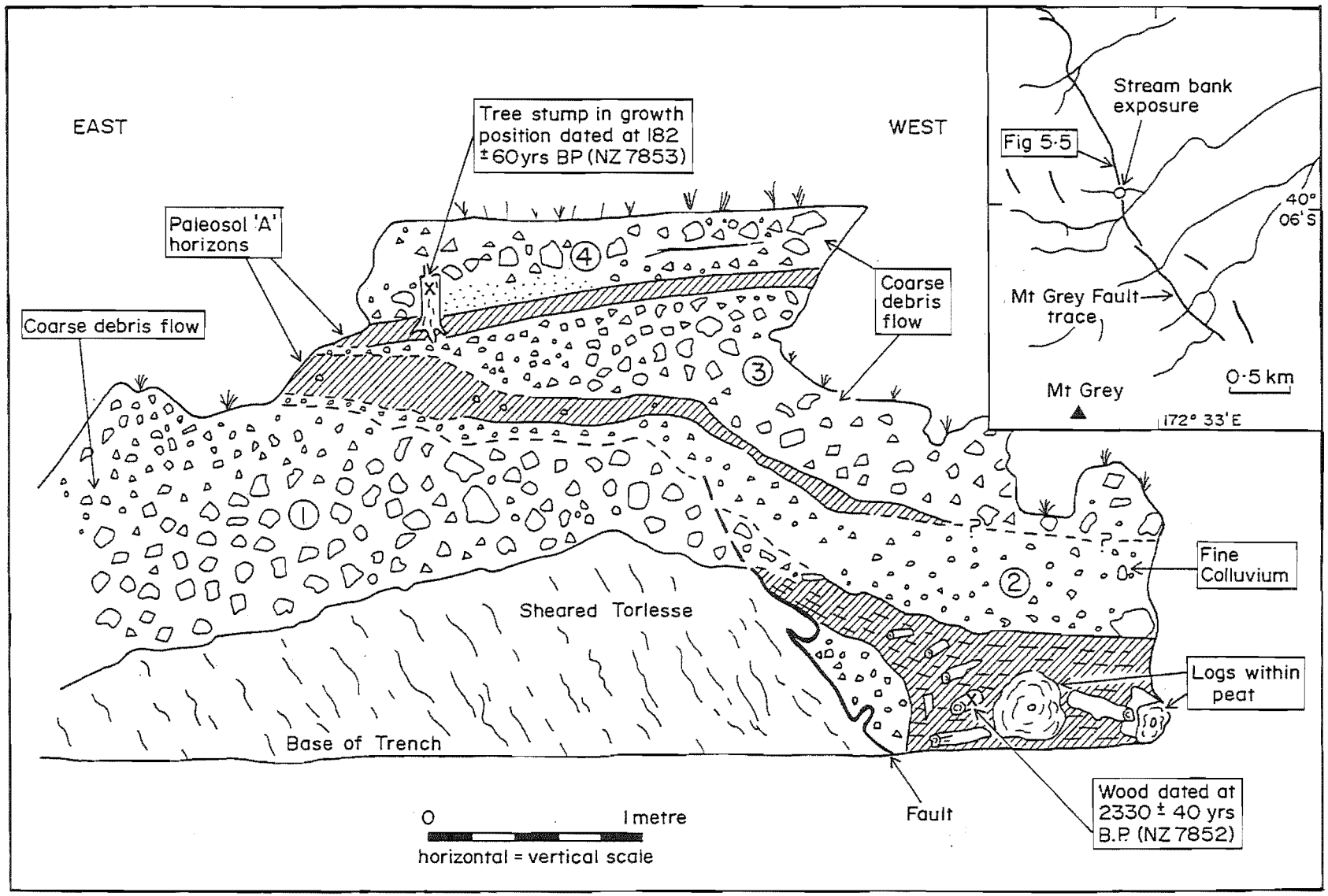
EAST
WEST
Tree stump in growth position dated at 182 ± 60 yrs BP (NZ 7853)
Paleosol 'A' horizons
Coarse debris flow
Coarse debris flow
Fine Colluvium
Sheared Torlesse
Logs within peat
Base of Trench
Fault
Wood dated at 2330 ± 40 yrs B.P. (NZ 7852)
0 1 metre
horizontal = vertical scale
Stream bank exposure
Fig 5·5
40° 06'S
Mt Grey Fault trace
0·5 km
Mt Grey
172° 33'E

Ages of ten of these have been determined, by radiocarbon dating, or from weathering rind dating (Table 5.2).

The landslides are large (0.2-10 x 10^6 m^3) rock avalanches derived from rock of the Torlesse terrane. Landslides on the north limb of the Cust Anticline are formed in Plio-Pleistocene conglomerates. Landslides (6,7 and 10) have multiple failures although it was not always possible to quantify them. A notable feature of the data is the clustering of landslide ages between about 1300 A.D. and 1500 A.D. (Fig.5.7) for those landslides in the western two-thirds of the area mapped (Fig.5.1); other landslides scatter in age back to more than 5000 B.C..

5.4 RELATIONSHIP BETWEEN SURFACE RUPTURES AND LANDSLIDES

One period of significant overlap emerges when the modal ages of landslides are compared with the timing of surface rupture inferred from fault data (Fig.5.7). From this it is inferred that the last large magnitude (>M7.0) event on the Porters Pass Fault occurred between 1300 A.D. and 1500 A.D.

To assess whether the effects of this event extended beyond the geographic limits of the PPAFZ study, the ages of regional rock avalanche data from the central Southern Alps (Whitehouse, 1983) were re-calculated and plotted the results on Figure 5.7. The two modal ages implied by Southern Alps data (580-940 A.D. and 100 B.C. - 300 A.D.) do not coincide with modal ages documented in the PPAFZ. Ages of three landslides from the central Southern Alps overlap with those from the PPAFZ, in the range 200-450 B.C. Faulting data indicate rupture of the PPAFZ during this period.

5.5 MAGNITUDES

The timing of earthquakes associated with surface rupture in the PPAFZ is not significantly different from the ages of large landslides. Landslides in the range 1300-1500 A.D. are well preserved, but there are insufficient data to confirm the spatial pattern of rupture events older than 2000-2500 years. This presumably reflects either the in-filling and concealment of fault traces by scree on steep slopes, or their removal by erosion.

Estimating the magnitude of prehistoric earthquakes from distribution of landslides, rests on two un-testable assumptions: 1) that landslides were triggered co-seismically; and 2) that all landslides of a similar age were co-seismic with the same event. The relationship between

Table 5.2 DATED LANDSLIDES OF THE PORTERS PASS - AMBERLEY FAULT ZONE

	LANDSLIDE LOCALITY location no.s Fig. 1		NZ Map Grid (m) Geodetic Datum 1949	Lat./Long. (decimal degrees)	Landslide Volume ($10^6 m^3$)	AGE [1]	AGE CALENDAR YEARS [1]
1	Acheron River [2]		2401400E 5764800N	43.3181 171.6609	6	* 500 ± 69 (NZ 547)	1290 A.D. - 1515 A.D. **
2	Kowai River I [3]		2411200E 5768100N	43.2897 171.7823	2	† 560 ± 90 (60, 1988)	1340 A.D. - 1520 A.D. †
3	Kowai River II [3]		2412900E 5768800N	43.2836 171.8034	0.2	† 590 ± 100 (40, 1988)	1300 A.D. - 1500 A.D. †
4	Coal Creek		2429600E 5755000N	43.4098 172.0071	0.02	* 5600 ± 62 (NZ 7918)	4575 B.C. - 4335 B.C. **
5	Ashley Gorge		2440300E 5779200N	43.1931 172.1422	0.3	† 490 ± 70 (75, 1991)	1430 A.D. - 1570 A.D. †
6	Whistler River		2438900E 5788100N	43.1128 172.1262	10	† 580 ± 90 (62, 1991)	1320 A.D. - 1500 A.D. †
7	Glentui River		2449900E 5777100N	43.2128 172.2601	4	† 600 ± 100 (70, 1991) † 1210 ± 190 (45, 1991)	1290 A.D. - 1490 A.D. † 590 A.D. - 970 A.D. †
8	Mairaki Downs	a	2459300E 5771450N	43.2643 172.3753	0.1	* 7400 ± 90 (NZ 7854)	6425 B.C. - 6000 B.C. **
		b	2459600E 5771500N	43.2639 172.3790	3	* 2300 ± 60 (NZ 7855) * 2270 ± 82 (NZ 7856)	(x) 200 B.C. - 400 B.C. **
9	Okuku River		2461300E 5783900N	43.1524 172.4010	4	* 2467 ± 66 (NZ 7895)	400 B.C. - 765 B.C. **
10	Mt. Grey		2473400E 5790400N	43.0946 172.5502	0.2	† 3430 ± 470 (99, 1991) † 4580 ± 660	970 B.C. - 1400 B.C. † 1930 B.C. - 3250 B.C. †

(1) * Conventional ^{14}C age: years B.P. (1950)
** Calibrated ^{14}C age: calendar years A.D./B.C.)
† Modal weathering rind age.) Rounded to nearest 5 years. Refer footer (1) Table 5.1

(2) Burrows (1975)

(3) Coyle (1988)

Figure 5.7 Temporal distribution of landslides and fault ruptures in the Porter's Pass-Amberley Fault Zone compared with dated landslides from the Southern Alps. Numbered landslides correspond to locations on Fig.5.1. A = Ashley Fault; MG = Mt Grey Fault; PP = Porter's Pass Fault; asterisk's denote weathering rind ages. Refer to Table 5.1 and 5.2 for further details.

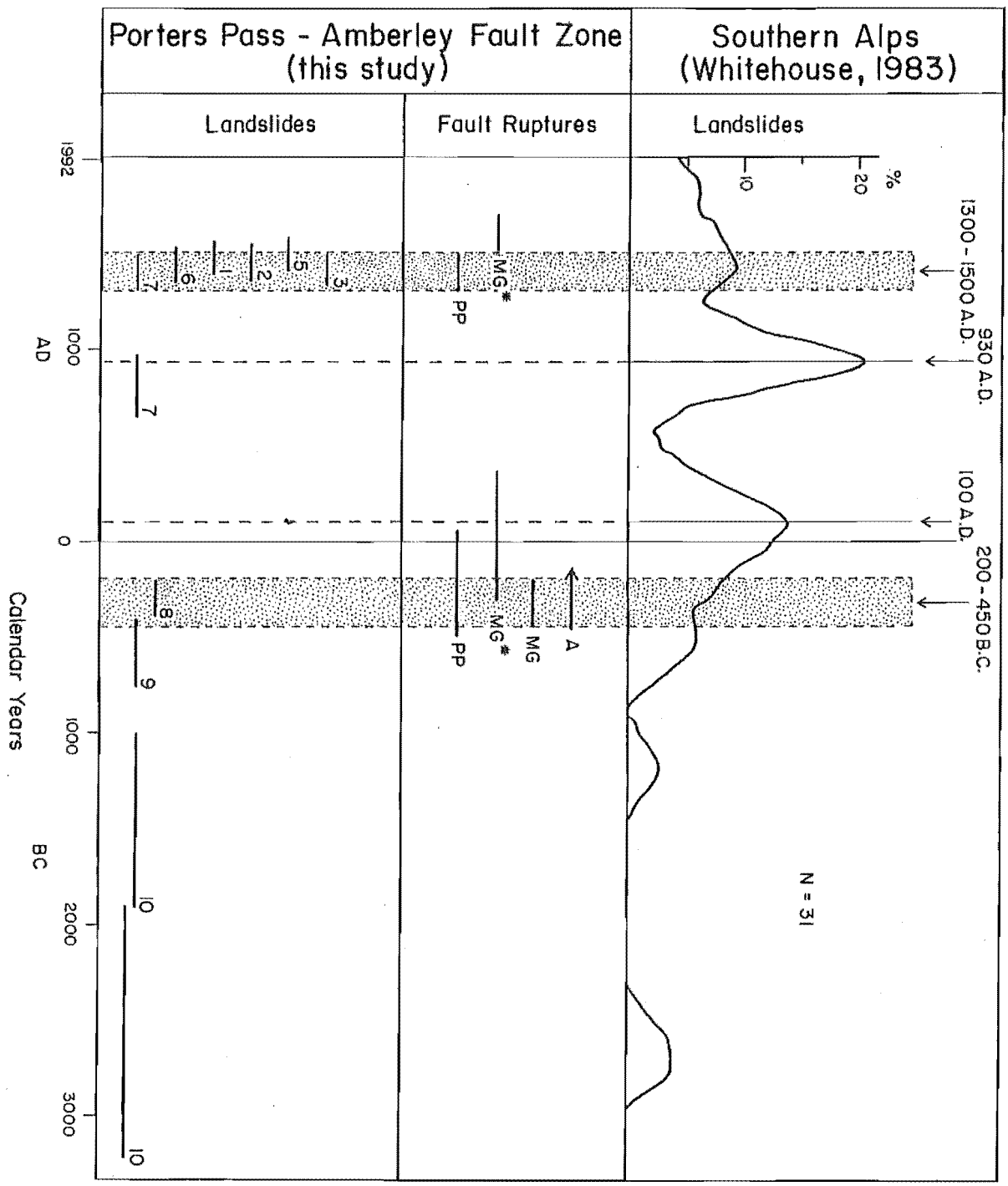
Porters Pass - Amberley Fault Zone
(this study)
Southern Alps
(Whitehouse, 1983)
Landslides
Fault Ruptures
Landslides
1992
1000
0
1000
2000
3000
AD
BC
Calendar Years
10
20
%
1300 - 1500 A.D.
930 A.D.
100 A.D.
200 - 450 B.C.
N = 31
MG*
PP
MG*
PP
MG
A
1
2
3
5
6
7
7
8
9
10
10

earthquake magnitude and landsliding, and the completeness of data for a given event must be inferred. Likewise, older landslides may have been buried by younger events from the same source, or removed by erosion.

Keefer (1984) analysed relationships between landslides and earthquake magnitude for 40 global earthquakes of varying focal depth and surface effects. The 1968 Inangahua earthquake was referenced in this study (Keefer 1984: his Table 1), but not included with data used to define threshold magnitude for landslides. Keefer fitted a lower-bound curve to the data, which significantly under-predicts the threshold magnitude for historic co-seismic landslides in northern South Island (Fig.5.8a, 5.8b); and a similar discrepency also has been noted for several North Island earthquakes (Crozier, 1991).

Keefer's catalogue included numerous small regolith failures and rock-falls triggered at large epicentral distances, and does not provide an appropriate basis for estimating the magnitude of prehistoric earthquakes in the mountainous topography of South Island.

Adams (1981) estimated the area of large rock avalanches triggered by two historic earthquakes in northern South Island (1929 Buller and 1968 Inangahua), and derived an equation:

$$M = 0.5 \text{ Log}_{10}(\text{area in km}^2 \text{ of MM X shaking}) + 5.9 \qquad (1)$$

using intensity-magnitude attenuation curves of Smith (1978). Adams' method provided a good 'hind-cast' estimate of the historic magnitudes, but was based only on two earthquakes.

In this study, data from the 1929 Arthurs Pass earthquake (central South Island) and new magnitude estimates for the Buller and Inangahua earthquakes, have been combined to revise Adams' equation (Table 5.3, Appendix 5.1) such that:

$$M = 6.03 + 0.51 \text{ Log}_{10} (\text{area km}^2 \text{ of landslides}) \qquad (2)$$

Equation (2) represents only a minor modification of equation (1), which is consistent with strong similarities between the historic earthquakes: all were shallow focii events (<15 km) (Dowrick and Smith, 1990) located in mountainous areas of northern South Island.

Magnitudes for the prehistoric earthquakes in the PPAFZ have been estimated from Figure 5.9, using equation (2) (Table 5.3). A coseismic origin of landslides in the Southern Alps is unsupported by evidence of faulting, so the interpretation of those as seismic events is speculative. If a coseismic origin is surmised then the distribution of

TABLE 5.3 Magnitude estimates for prehistoric earthquakes (inferred and surmised)

REGION	AGES (T) OF INFERRED EVENTS	SURFACE RUPTURE LENGTH (1) (km)	MINIMUM AREA OF LANDSLIDES (Ellipse area km (2) = π ab	MAGNITUDE ESTIMATES		ELAPSED TIME
				Rupture Length (2)	Landslides (3)	590 ± 100 years at 1992 A.D.
PPAFZ	T_1 1300 A.D. - 1500 A.D.	50 - 70	920	7.3 - 7.4	7.5	T_2 - T_1 (1725 ± 225)
	T_2 200 B.C. - 450 B.C.	70 - 100	1140	7.4 - 7.5	7.6	
SOUTHERN	T_3 580 A.D. - 940 A.D.	-	5880	-	7.9	T_4 - T_3 (700 ± 420)
ALPS	T_4 100 B.C. - 300 A.D.	-	1160	-	7.6	

(1) Rupture length surmised from fault geometries and evidence of surface displacement:
Event T_1 - 50 - 70km from Rakaia Valley (west) to Lees Valley (east)
Event T_2 - 70 - 100km from Rakaia Valley (west) to Mt. Grey (east).

(2) Estimated surface wave magnitude (M_s) using equation $M_s = 6.24 + 0.619$ (Log $_{10}$ Rupture Length), (Bonilla et al., 1984).

(3) Estimate using equation $M_s = 6.03 + 0.51$ (Log $_{10}$ Area of landslides (km^2), derived by least squares regression of landslide distribution on magnitude, (after Adams, 1981) from data in Appendix 5.1.

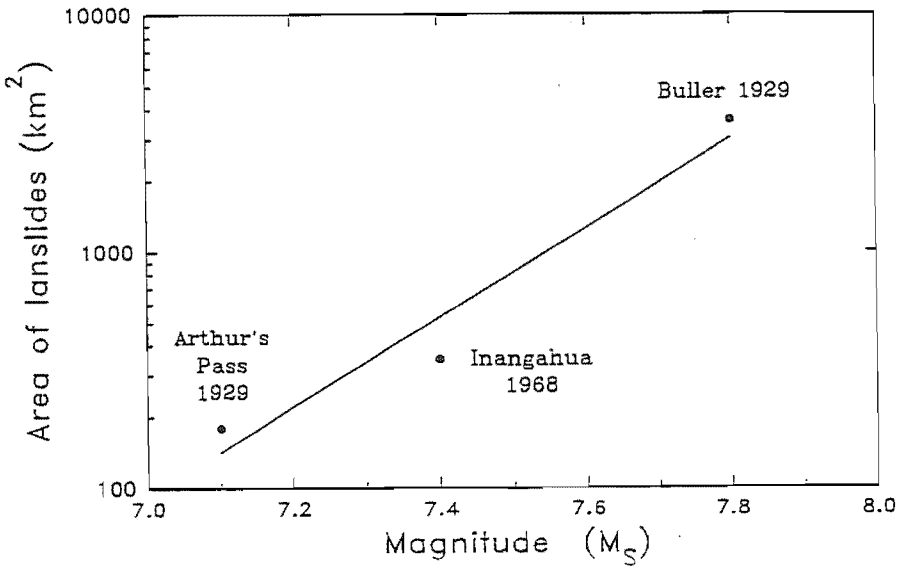

Figure 5.8(a & b) Comparison of landslide data for large historic earthquakes in northern South Island (Table 5.3, Appendix 5.1) with a compilation of global data by Keefer (1984). The data suggest a higher threshold magnitude for coseismic landsliding in South Island, than the areas from which Keefer gathered data.

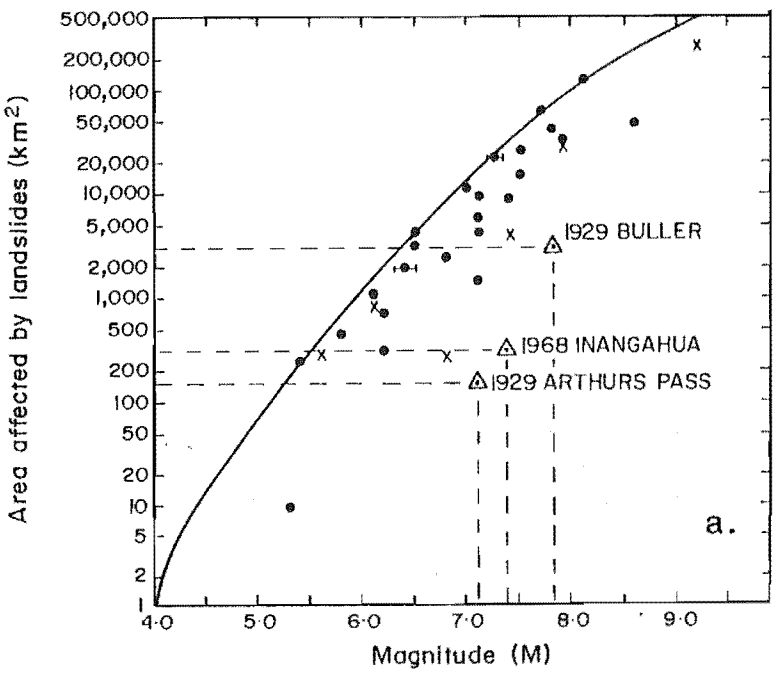
Area affected by landslides (km²)
500,000
200,000
100,000
50,000
20,000
10,000
5,000
2,000
1,000
500
200
100
50
20
10
5
2
1
1929 BULLER
1968 INANGAHUA
1929 ARTHURS PASS
a.
4·0
5·0
6·0
7·0
8·0
9·0
Magnitude (M)

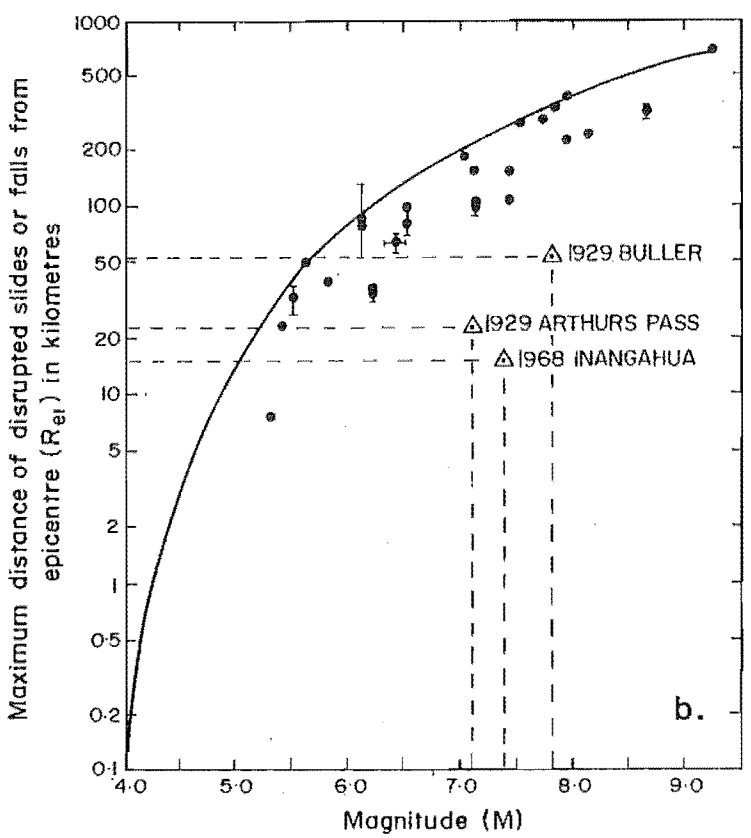
Maximum distance of disrupted slides or falls from epicentre (R_{el}) in kilometres
1000
500
200
100
50
20
10
5
2
1
0·5
0·2
0·1
1929 BULLER
1929 ARTHURS PASS
1968 INANGAHUA
b.
4·0
5·0
6·0
7·0
8·0
9·0
Magnitude (M)

Figure 5.9 Map of central South Island illustrating the spatial distribution of landslides in respective modal age groups (from Fig.5.7). Lake Chalice and Lake Waikaremoana (inset) represent large landslide- dammed lakes that formed during the interval 200-400 B.C.. Ellipses have been fitted to each group of South Island data for the purpose of estimating first-order magnitudes for inferred and surmised coseismic events, based on landsliding-magnitude relationships for historic South Island earthquakes (see Table 5.3). Data for the 1929 Arthurs Pass earthquake from Speight (1933); Southern Alps data from Whitehouse (1983). The polygon defines boundaries of a 5.08×10^3 km^2, Porter's Pass seismicity zone (from Elder et al. 1991).

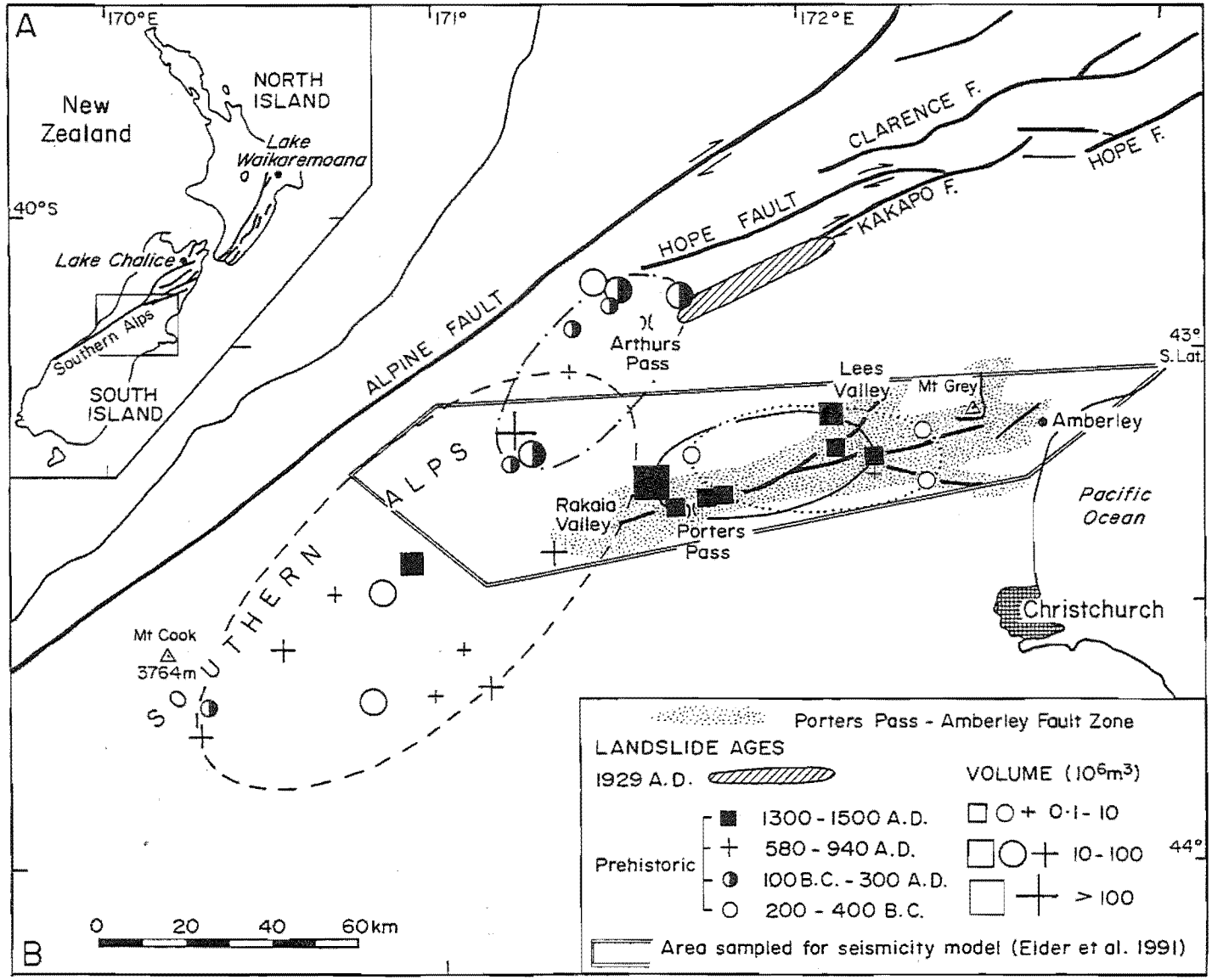
A
170°E
171°
172°E
New Zealand
NORTH ISLAND
Lake Waikaremoana
40°S
Lake Chalice
Southern Alps
SOUTH ISLAND
ALPINE FAULT
HOPE FAULT
CLARENCE F.
HOPE F.
KAKAPO F.
Arthurs Pass
43° S.Lat.
Lees Valley
Mt Grey
Amberley
ALPS
Rakaia Valley
Porters Pass
Pacific Ocean
SOUTHERN
Mt Cook 3764m
Christchurch
B
0 20 40 60km
Porters Pass - Amberley Fault Zone
LANDSLIDE AGES
1929 A.D.
VOLUME ($10^6 m^3$)
Prehistoric
1300 - 1500 A.D.
580 - 940 A.D.
100 B.C. - 300 A.D.
200 - 400 B.C.
0·1 - 10
10 - 100
> 100
44°
Area sampled for seismicity model (Elder et al. 1991)

landslides indicates an event of M7.9 at about 580-940 A.D., and an event of M7.6 slightly further north at about 100 B.C. - 300 A.D. (Table 5.3). The M7.9 event could be on the Alpine Fault, but the more northerly event (M7.4) could be on any number of faults including the Alpine Fault.

The computed magnitude estimates for the prehistoric events may be liberal, because landslides far removed from the main concentration of data for each group have been excluded. For example, the 1300-1500 A.D. landslides are limited to the PPAFZ with the exception of one landslide far to the south near Mt Cook (Fig.5.9). If this landslide were to be included the magnitude estimate would rise to M7.7, but in the absence of additional data closer to the main group this does not seem justified.

The major axes of the ellipses are presumed to be relatively well-defined in the PPAFZ, because this area has been mapped in some detail (Burrows, 1975; Marden, 1976; Coyle, 1988; this study). The minor axes may be too narrow because they are defined by the northern limits of mapping (approximately Lat.43°S) and by the southern limit of steep topography at the Canterbury Plains (Fig.5.1), but on balance, the distribution of landslides and orientations of inferred isoseismals for large historic earthquakes in North Canterbury are strongly elliptical, and parallel the strike of the causative faults (Speight, 1933; Yang, 1991; Cowan, 1991).

The amount of displacement associated with prehistoric rupture on the PPAFZ is poorly constrained, but the localities at which displacement is inferred provide a basis for surmising the rupture lengths. The 1300-1500 A.D. event ruptured the Porters Pass Fault, but not the Mt Grey Fault, and a rupture of 50-70 km between the Rakaia Valley and Lees Valley is surmised (Figs.5.7, 5.9). If displacements in the range 200-450 B.C., at Porters Pass and Mt Grey (and probably Ashley River) represent one event, then a rupture length of 70-100 km is probable. From these estimates, magnitudes not significantly different from those estimated from the distribution of landslides have been calculated using the expression: $Ms = 6.24 + 0.619 \log_{10}(\text{Rupture length})$, derived from a global compilation of historic co-seismic ruptures (Bonilla et al., 1984) (Table 5.3).

5.6 DISCUSSION

5.6.1 Implications for recurrence of large earthquakes

Landslides have been triggered by several large (>M7.0) historic earthquakes in New Zealand, and many elsewhere (e.g. Voight and Pariseau,

1978; Keefer, 1984), but there are examples of large landslides located in seismically active regions that have not been triggered by earthquakes (e.g. McSaveney, 1978; Plafker and Ericksen, 1978). In the absence of independent evidence, therefore, the co-seismic interpretation of prehistoric landslides is equivocal (Whitehouse and Griffiths, 1983).

At the northeastern end of the PPAFZ, the Mt Grey Fault shows evidence of surface rupture between 1500 A.D. and 1700 A.D., but no evidence of landsliding associated with this event has been documented (Fig.5.7). Nicol (1991, in prep.) has noted that this is the case also for the Karetu and Boby's Creek faults to the northeast (Fig.5.1); which have ruptured within the last 1000 years, but apparently without surface effects such as landsliding. The strike length of Boby's Creek and Karetu Faults is approximately 10 km, and it is inferred that surface rupture presumably accompanied earthquakes of lower magnitude ($M<7.0$) than that required to generate large landslides.

All of the historic earthquakes larger than magnitude 7.0 in northern South Island have been accompanied by large landslides (McKay, 1890, 1902; Henderson, 1937; Speight, 1933; Adams et al., 1968), so it is reasonable to infer from the preservation of only two major prehistoric events in the PPAFZ, that evidence of additional events would have been preserved had they occurred. Mathews (1979) observed that the zone of most intense landsliding that accompanied the 1946 Vancouver Island earthquake is offset from the epicentre by 50 km. The distribution of landslides attributed to the 1929 Buller earthquake also is offset by 15 km from the inferred area of shaking equal to MM X (Adams, 1981).

Similar effects associated with one or more prehistoric events in the PPAFZ, might explain the apparent absence of evidence for additional events in the local landscape, but such an offset presumably would have to be unidirectional to preclude landsliding in the PPAFZ, associated with rupture on other active faults in the mountains to the northwest (Gregg, 1964). There are other landslides in the PPAFZ which are undated (Fig.5.1), but the majority of the large ($>1 \times 10^6$ m^3) landslides are dated and their spatial distribution is reasonably uniform. It seems unlikely that the clustering of landslide ages in the PPAFZ merely is an artifact of under-sampling, so the absence of evidence for more large earthquakes may indicate the recurrence interval between the largest events in the PPAFZ, not withstanding the probability of more frequent earthquakes of moderate magnitude, such as the 1500-1700 A.D. event reported on the Mt Grey Fault (Fig.5.7).

If all of the landslides in the range 200-450 B.C. were induced by shaking, their wide distribution would imply either a very large

earthquake in the PPAFZ, or more probably an additional event(s) elsewhere. Several landslides in the PPAFZ do not coincide with either of the inferred rupture events and these may be unrelated to seismicity. If the majority of the landslides in the PPAFZ and Southern Alps were co-seismic, then the interval 100 A.D. - 450 B.C. may represent a period of particularly large seismic-moment release on the New Zealand section of the Australia-Pacific plate boundary.

In addition to the landslides in Southern Alps the formation by large landslides, of Lake Chalice in northern South Island and Lake Waikaremoana in northeastern North Island during this period (Adams, 1981; Perrin and Hancox, 1992) may be no coincidence: the former is located 7 km north of the Wairau section of the Alpine Fault and the latter is located at the northern end of the North Island shear belt (Fig.5.9). In a recent compilation of earthquake clustering from the east coast of North Island (Berryman and Beanland, 1991), the period 2000-2500 years B.P. is characterised by several large earthquakes, which together ruptured most of the length of the east coast.

5.6.2 Implications for seismic hazard assessment

The instrumental approach to seismic hazard assessment is to assume a uniform spatial distribution of earthquakes and an exponential distribution of magnitudes, of the Gutenburg-Richter (Richter, 1958) form:

$$\log N(m) = a - bm \qquad (3)$$

where N(m) is the cumulative number of earthquakes of magnitude equal to or greater than (m); 'a' defines the rate of occurrence, and 'b' the exponential decay with increasing magnitude.

The parameters 'a' and 'b' are constants of the seismicity model and are computed from a catalogue of historical seismicity. Historical data can be supplemented by geological data on faulting. When combined with an appropriate attenuation expression, the seismicity model may be used to derive return periods or probabilities of exceedence for specified levels of ground motion. This classical hazard analysis was advanced by Cornell (1968), and has been applied to New Zealand by among others: Peek et al. (1980); Mulholland (1982); and Smith and Berryman (1983, 1986).

Recent studies of specific fault zones have indicated that earthquake recurrence at high magnitudes generally is under-predicted by the 'b'-value seismicity model, and a 'characteristic earthquake' model

provides a better match to the available observations (Wesnousky et al., 1983; Schwartz and Coppersmith, 1984; Youngs and Coppersmith, 1985; Davison and Scholz, 1985). Seismic hazard analyses for engineering and planning in New Zealand still remain dependent upon the 'b'-value seismicity models computed from historic seismicity because there are too many faults for which there are no paleoseismic data available.

The parameters of the Smith and Berryman (1983, 1986) seismicity model are not directly comparable with the paleoseismic data presented in this study, because the PPAFZ straddles a boundary between two of their seismic zones (I and J of their Fig.1) which encompass much larger regions of contrasting tectonic style. The most recent study of seismic hazard in North Canterbury (Elder et al., 1991) proposed a detailed subdivision of the region that included as much geological data on earthquake recurrence as was available at the time. Their results are relevant to this discussion because they evaluated the PPAFZ (Porters Pass Tectonic Zone of their study) as a distinct seismic zone.

In Figure 5.10 the model of Elder et al. (1991) is compared with the apparent interval between the prehistoric earthquakes, inferred from landslides and fault displacements. The comparison, for a constant seismicity rate (a_4 = 0.3), maximum magnitude of M7.5 and 'b' values of 0.8 and 1.0 (Appendix 5.2), illustrates the sensitivity of the predicted frequencies of large magnitude earthquakes to changes in b-value.

The paleoseismic data suggest that the assumed maximum-magnitude is about right, but the frequency of M>7.0 earthquakes is over-predicted, by a factor of 6 for b=0.8, and a factor of 1.8 for b=1.0. The near coincidence between the predicted frequency of M>7.4 and the paleoseismic data (for b=0.8), merely reflects the truncation of the probability distribution at the inferred maximum magnitude of M7.5.

5.7 CONCLUSIONS

An important implication from the historic and paleoseismic data is that the recurrence-frequency of small (M<6.0) earthquakes in the PPAFZ is adequately modelled by an exponential 'b-value' distribution, whereas the largest earthquakes belong to a different (?characteristic) population of events. Geological observations indicate that the largest of the population of exponentially distributed magnitudes is likely to be somewhat less than magnitude M7.0, although just where the threshold magnitude lies is unknown; the seismicity rate at magnitudes of less than M5.5 has been high within the PPAFZ during the last 30 years, but there have been no events larger than M6.4 during the last 150 years (Eiby,

Figure 5.10 Seismicity model for the 5.08 x 10^3 km^2 zone shown in Fig.5.9, based on parameters calculated from historic seismicity tabulated in Appendix 5.2 (after Elder et al. 1991), and paleoseismic data from Table 5.3. Note the assumed exponential distribution of magnitudes is unconstrained above magnitude 6.4, and changes in b-value strongly influence predicted frequencies of large earthquakes. A b-value of 0.8 coincides with the paleoseismic recurrence interval only because the distribution is truncated at a maximum magnitude of M7.5. A b-value of 1.0 is more consistent with available geological data, which indicate that earthquakes above the threshold magnitude for widespread landsliding ($M_{prehistoric}$ - c.M7), are less frequent in the Porter's Pass-Amberley Fault Zone than predicted by an exponential distribution (see text for qualification).

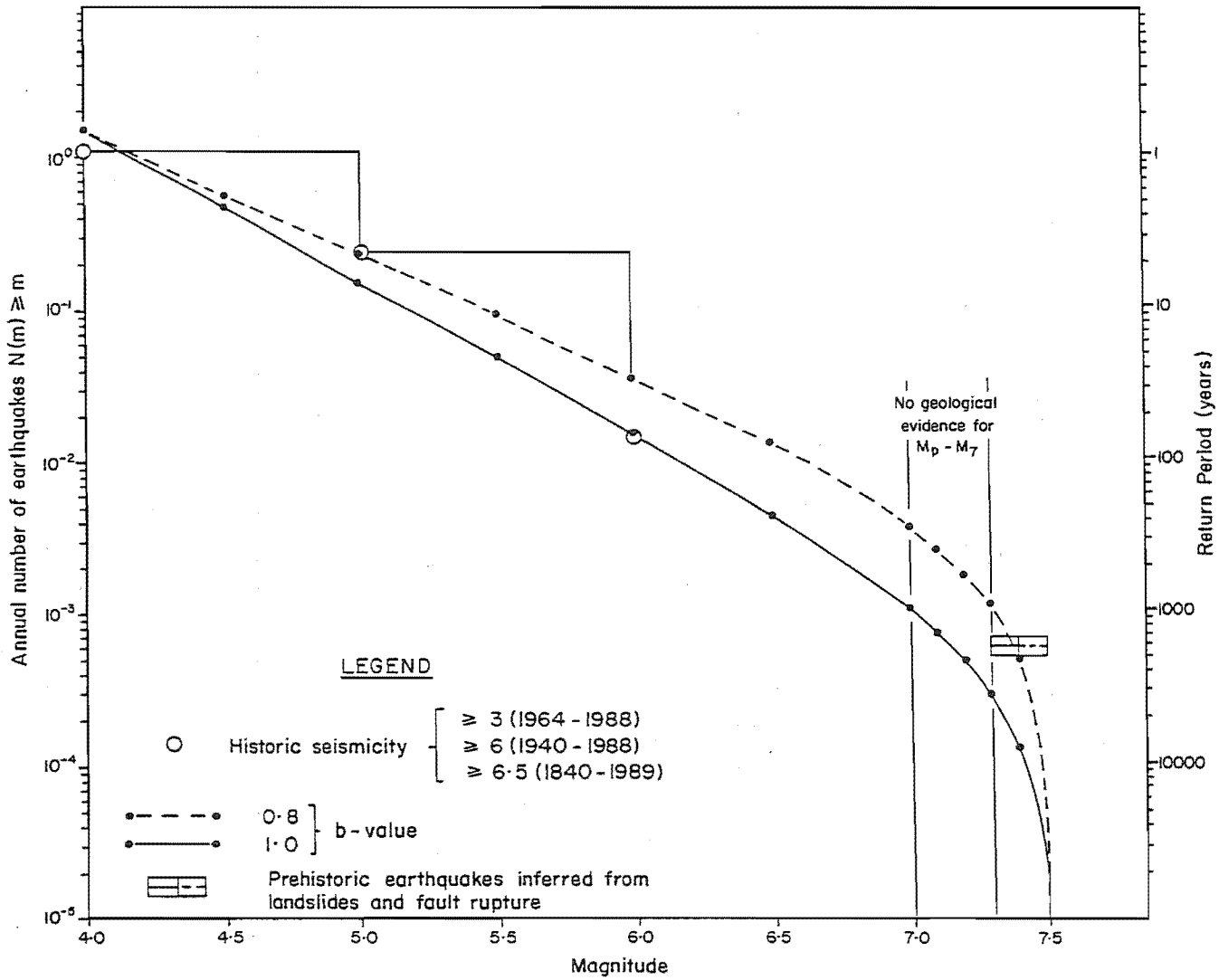
Annual number of earthquakes N(m) ≥ m
Return Period (years)
Magnitude
No geological evidence for $M_p - M_7$
LEGEND
Historic seismicity
≥ 3 (1964 - 1988)
≥ 6 (1940 - 1988)
≥ 6·5 (1840 - 1989)
0·8
1·0
b - value
Prehistoric earthquakes inferred from landslides and fault rupture

1968, 1990).

One of the inferences drawn from these results is that the seismic hazard at a site within a few kilometres of the PPAFZ - where the effects of smaller, but perhaps more frequent earthquakes are likely to be most pronounced - may be described realistically using a b-value of 0.8 (for M_{max}=7.5). At larger distances (40-60 km, say Christchurch), the infrequent large earthquakes pose the greater hazard, and a b-value of about 1.0 would provide a more realistic estimate of their frequency (Fig.5.10), while retaining a conservative margin to accommodate temporal variations and the possibility that the geological database is incomplete.

The paleoseismic data presented in this study indicate repeated rupture of the PPAFZ during the late Holocene, but the return period between the last two recognised events is 1500-1900 years - much less than predicted by log-linear modelling of historic seismicity. On the basis of these results there is a case for reassessing the PPAFZ's contribution to probabilities of exceedence of specified ground motion in Christchurch city. Such work lies beyond the immediate scope of this study.

CHAPTER 6. SYNTHESIS AND CONCLUSIONS

6.1 INTRODUCTION

North Canterbury straddles the eastern margin of late Cenozoic deformation associated with oblique-convergence between the Australia and Pacific plates. This zone is generally agreed to represent a westward transition from subduction of Pacific Plate beneath northern South Island, to continental collision across the Southern Alps (e.g. Scholz et al., 1973; Arabasz and Robinson, 1976; Walcott, 1978; Reyners, 1989; Lamb and Bibby, 1989) (refer to Fig.1.1).

Considerable attention has focused on the seismicity and geological structure of Marlborough and the Southern Alps, where data indicate historically high rates of shear strain (Walcott, 1979; Bibby, 1981), and large finite rotations of crustal blocks since the Miocene (Walcott and Mumme, 1981; Lamb and Bibby, 1989). Fewer data from North Canterbury, imply negligible late Cenozoic rotation and historically low rates of shear strain (Walcott and Mumme, 1981; Walcott, 1984 and Reilly, 1987, respectively). Consequently, the tectonics of this region have received less attention, and the structural styles and kinematics of deformation has remained enigmatic (but see Rynn and Scholz, 1978).

Carter and Carter (1982) postulated that the Porter's Pass Fault and its inferred extension along the northern margin of the Canterbury Plains, represents a southern element of the Marlborough Fault System connected to the Hikurangi subduction zone. Their inference rested on evidence derived from a limited number of marine seismic-reflection profiles, for a major NE-trending, strike-slip fault (Motunau Fault) on the continental shelf, along the projected strike of the Porter's Pass Fault (Frontispiece 1). Aspects of their data and interpretation were challenged by Herzer and Bradshaw (1985), who expressed reservations about the nature of interpreted features on the seismic lines and

cautioned that the pattern of deformation on-land to the southwest is complex, and not consistent with the existence of a single, through-going fault.

Results from recent mapping of the area northeast of Mt Grey (Nicol, 1991), and newly acquired seismic reflection data from the continental shelf further east (P. Barnes, pers.comm. 1990, 1991), have cast doubt on the existence of a "Motunau Fault" as proposed by Carter and Carter (1982). Rather, faults near the surface in those areas are predominately west-verging thrusts, with strike-lengths generally no greater than 15 km. The fold and thrust belt extends SE from near the Hope Fault (Frontispiece 1; Nicol, 1991; Syme, 1991), to the continental shelf off-shore, where Barnes (pers.comm. 1990) has documented thrust deformation within a NE-NNE trending zone, 10-15 km wide, parallel to the North Canterbury coast, to the east of which the cover sequence is flat-lying and undisturbed.

Notwithstanding the great complexity of faulting and the predominance of west-vergent thrust geometries identified in recent work, the strike of the fold belt at its southeastern margin coincides with, and is parallel to the PPAFZ, which defines the SE edge of the plate-boundary deformation front. No shallow earthquakes (<12 km) were located off-shore during the 1990 microearthquake survey, so the interpretation of upper crustal structure in that region, and its relationship to the Hikurangi subduction zone remains equivocal. However, the seismological and geological data documented on land, clarify both the structural styles and kinematics of late Cenozoic deformation, and provide new insights into the evolution of the plate boundary zone in North Canterbury.

6.2 CRUSTAL STRUCTURE IN NORTH CANTERBURY: THE TRANSITION FROM SUBDUCTION TO CONTINENTAL COLLISION

6.2.1 Crustal structure from earthquake hypocentres

In Chapter 4, seismicity recorded on the North Canterbury Microearthquake Network was presented and from the distribution of hypocentres, two seismic zones were identified: 1) a sub-horizontal zone of activity restricted to the upper crust (<12 km); and 2) a seismic zone in the lower crust (below a ceiling of c.17 km) that broadens vertically to the north and northwest to a depth of c.40 km, with a bottom edge which dips 10°N and 15°NW, respectively. No events were recorded at depths between 12 km and 17 km, which is interpreted as a relatively aseismic, mid-crustal ductile layer.

A similar pattern was observed in an earlier survey of microseismicity in Marlborough (Arabasz and Robinson, 1976), but the depth distribution of deeper events was much greater, reflecting the presence of the subducted Pacific Plate beneath that region. The lower-crustal seismic zone identified in this study is inferred to represent activity in old (Mesozoic) oceanic crust on which the submarine-fan complex of Torlesse basement was deposited. The southward tapering of activity that defines this zone, suggests that incipient subduction of lower crust is occurring as far south as the PPAFZ.

6.2.2 Strain axes and evidence for a mid-crustal detachment beneath North Canterbury

The strain axes for upper crustal events beneath North Canterbury trend NW-SE and are remarkably uniform throughout the region (Fig.4.12a). Their trends are similar to those determined in earlier studies of seismicity in adjacent regions to the west and north (Rynn and Scholz,

1978; Arabasz and Robinson, 1976, respectively); similar to axes of relative compression derived from measurements of geodetic strain (Bibby, 1981), and similar to principal horizontal shortening directions estimated from surface fault traces (Berryman, 1979) and faults (Nicol and Wise, in press), and joint sets and stylolite seams in Tertiary limestones (Nicol, in press).

Arabasz and Robinson (1976) observed marked differences in the trends of P and T axes for events in the upper and lower crust above the subducted plate in Marlborough. Such differences also are observed for fault-plane solutions above and below the inferred ductile layer in this study, but only to the north of the PPAFZ - upper and lower crustal events located beneath the Canterbury Plains to the south, have similar P and T axes (Fig.4.16).

Strain axes for lower crustal events show a systematic counter-clockwise rotation (relative to those of upper crustal events), from south to north across the PPAFZ: the similar trends of strain axes for the respective groups south of the PPAFZ, suggests that the upper crust beneath the Canterbury Plains may be coupled to the lower crust, whereas the upper crust further north is not.

6.2.3 Geological evidence for a mid-crustal detachment

Corroborative geological evidence for a mid-crustal detachment north of the PPAFZ includes the pronounced change in wavelength of major geological structures that occurs across the PPAFZ (refer to Frontispiece 1 and Sheet 18).

Firstly, geological structure to the north of the PPAFZ is characterised by narrow linear basins separated by anticlinal ridges of similar across-strike width, that are bounded by thrust faults (Nicol, 1991) and curve in strike from c.060°in the south, to c.020° further north. The absolute amplitude of these structures is uncertain, but

gravity data suggest that depth to basement in the Culverden Basin is probably no greater than 1.5 km (Hicks, 1989), and the topography associated with the basement ridges is relatively uniform, with remnants of cover sequence preserved on the flanks of the anticlines. The strike-normal width of the Culverden Basin (the distance between the principal bounding faults), is approximately 15 km and the ridges and basins further east - including the Conway Trough offshore (Carter et al. 1982) are c.10-12 km wide.

In contrast, geological structure south of the PPAFZ is dominated by the northeastern end of the Canterbury Basin, a broad synclinal trough, between the northern Canterbury Plain and Banks Peninsula to the south, where Torlesse basement is exposed in the eroded core of Lyttelton Volcano (Speight, 1917; Sewell, et al., 1988). Seismic reflection data (Kirkaldy and Thomas, 1963; Brown, 1975), and gravity data (Thomas, 1963; Hicks, 1989), indicate that the greatest thickness of Cenozoic sediment (c.2.4 km) coincides with the lowest topographic elevation of the basin, at the inner margin of Pegasus Bay near the mouth of the Waimakariri River.

The important point is that the half-wavelengths of structures north of the PPAFZ ($\lambda/_2$ = ridge or basin width), are relatively uniform and no greater than the thickness of crust above the ductile layer inferred from the distribution of earthquake hypocentres. The half-wavelength of the Canterbury Basin is comparable to the focal depths of events in the lower crust, recorded beneath the Plains and Pegasus Bay. The focal mechanisms of those events (Fig.4.11a: 32,37,42; Appendix 4.7) imply normal faulting on nodal planes sub-parallel to the basin axis.

The notion of a mid-crustal detachment beneath South Island is not new (Wellman, 1979; Norris et al. 1990; Nicol and Wise, in press), and similar structures have been inferred elsewhere in recent years (e.g. Turcotte et al., 1984; Nicholson et al., 1986; Namson and Davis, 1988; Burchfiel et al., 1989). However, the coincidence between the SE edge of

the inferred detachment and that of the plate-boundary deformation front in North Canterbury, could form the basis for future research into the role of intra-crustal detachments, in facilitating the propagation of new faults in the upper crust and the control such a detachment may have on the kinematics of near-surface deformation.

6.3 SEISMICITY, STRUCTURE AND QUATERNARY TECTONICS OF THE PORTER'S PASS-AMBERLEY FAULT ZONE

6.3.1 Structural domains and kinematics of near-surface deformation

In Chapter 3, the structure and kinematics of the PPAFZ are described, based on the results of detailed and extensive geological mapping. Spatial differences in structural style were identified in the context of three structural domains: 1) a strike-slip domain (in the west); 2) a thrust and reverse fault domain (to the east); and 3) a northwest-verging fold belt on the northern Canterbury Plains (Fig.3.1). This simple subdivision is appropriate for introducing the local structures, but it is clear from consideration of the gross geometry of the PPAFZ and the wavelengths and relative locations of basins and uplifted blocks, and patterns of drainage, that a fundamental relationship exists between topography and structure in all domains, and is repetitive on a scale of several kilometres.

With reference to Map 2 and Frontispiece 1, compare Castle Hill Basin with Lees Valley; the step-over embayments of the Oxford to Mt Grey range-front (see also Frontispiece 3); and the dominant SE trend of the major rivers. Compare also, the geometry of the modern and ancestral channels of Ashley River at Mairaki Downs (Cust Anticline) (Map 2). These similarities, although not rigorously defined in this study, imply deeper-seated structural controls on landscape evolution, of which SE-tilting and short-wavelength (c.6-8 km) cross-folding probably are the

most significant (cf. Map 2 and Fig.3.17).

6.3.3 Relationship between seismicity and geological structure of the PPAFZ

Focal mechanisms for shallow microearthquakes (<12 km), located beneath the western end of the PPAFZ are consistent with the kinematics of faults mapped at the surface (Fig.4.9). However, a number of those located in the east (e.g. solutions: 8, 22, 29), are at variance with the geometries of near-surface structures that imply thrusting. The surface structures can be reconciled with those implied by focal mechanisms, if the causative faults splay upwards in the manner of structures described from zones of transpression elsewhere (e.g Wilcox et al., 1973; Sylvester and Smith, 1976; Naylor et al., 1986; Sylvester, 1988).

The conclusion drawn from these data is that strike-slip faults are developing at depth in basement, beneath the eastern end of the PPAFZ, but have yet to propagate directly to the surface. Consequently, the Kowai Anticline is interpreted to represent the surface expression of a juvenile strike-slip duplex analogous to the uplifted, and more deeply dissected, Mt Oxford Duplex to the west (refer to Maps 1 and 2). A corollary to this interpretation is that differential uplift within the PPAFZ represents conservation of volume within a zone of dextral transpression at an early stage in its development.

The eastward divergence of fault terminations and east vergence of major thrust wedges in the PPAFZ suggests that the zone has propagated from west to east. Refer to the Lees Valley Fault (at Ashley Hill and in the headwaters of the Garry River and Pioneer Stream); the Glentui Fault Zone (at Glentui River); and the Mt Thomas and Mt Grey Fault Zones (Maps 1 and 2). These features are consistent with an eastward decrease in Quaternary uplift (next section), and the surficial transition from strike-slip to thrust faulting, which is accompanied by an increase in

the width of the zone and a decrease in the length (and presumably the offset), of individual structures.

The apparent west-to-east, diachronous nature of the PPAFZ provides an example of the rate at which tectonic structures (and landscape) can evolve within a zone of transpression. This has important implications for the interpretation of structures in older fault zones, where evidence of the early stages of development may be missing, overprinted, or attributed to a separate deformation event on the basis of contrasting geometry or kinematics. It is probable that the observed variations in the surface styles of deformation in the PPAFZ are related to the relative ages and/or stages of evolution of the structures, and their degree of dissection: the most evolved are expressed at the surface in the west, while the youngest are reflected by subdued topography and are only weakly dissected further east.

The outer (southeastern) limits of the PPAFZ are defined at the surface by the Cust Anticline and Ashley Fault, and by probable correlatives mapped offshore to the east (Pegasus Bay Fault - discussion in 6.4.1). The true edge of the plate-boundary deformation front is poorly defined at depth, because of the large thickness of cover. However, the southeastern limit to the distribution of microearthquakes recorded in this study, approximately coincides with the limit of late Quaternary surface structures (cf. Sheet 18 with Fig.4.1 and Fig.4.6b), and a similar correlation could be inferred from historic (1964-1991) seismicity (Fig.1.3).

6.3.2 Amount and rate of Quaternary uplift

Apatite and zircon fission-track dates of outcrop samples from a transect across the Southern Alps between Porter's Pass and Arthur's Pass (Kamp et al., 1989), indicate 12-15 km of uplift adjacent to the Alpine Fault since the Pliocene (c.5 Ma). Biotite schist is exposed adjacent to

the Alpine Fault, but metamorphic grade decreases to prehnite-pumpellyite at Porter's Pass (Coombs et al., 1959), where fission-track ages are gretaer than ≥100 Ma (Kamp et al., 1989).

Outliers of Cretaceous-Cenozoic cover sequence preserved in Castle Hill Basin attest to late Cenozoic uplift (Bradshaw, 1975), but the absence of unconformities older than Pleistocene on Torlesse basement in the PPAFZ and the widespread preservation of a leached zone beneath the Torlesse-Cretaceous unconformity (Appendix 3.1), indicates that not since the early-middle Cretaceous has this area been subjected to intense tectonic deformation. Structure contouring of the unconformity surface in the PPAFZ (Fig.3.17) has enabled the Quaternary differential uplift at the eastern margin of the Southern Alps to be estimated. The available data indicate maximum differential uplift of c.2600 m in the west (above the Torlesse and Puketeraki Ranges), decreasing to ≤1500 m above the Okuku Range to the east, and c.1200 m adjacent to the Cass and Black Anticlines near the east coast. Much lower rates (or a reversal) of uplift are evident within a few kilometres of the range-front escarpment. Basement is at a depth of c.1200 m below sea-level in the core of the Kowai Anticline (Hoolihan, 1978), and Pliocene shallow-marine sediments are exposed only 200 m above sea-level.

Late Pleistocene (<100 kyr) differential uplift rates of c.0.5-2.7 m/kyr have been estimated from marine terraces, uplifted on the flanks of folds at the east coast (Yousif, 1987; Barrell, 1989; Nicol pers.comm., 1992), and in the west a latest Pleistocene or Holocene rate of c.2.5-3.3 m/kyr is inferred from an offset fluvial terrace at Ashley Gorge (Fig.3.22). These rates are an order of magnitude higher than previous estimates in this area (Wellman, 1979), but are comparable to rates inferred from more detailed studies in northern North Canterbury (Ota et al., 1984) and southern North Island (Ghani, 1978, Pillans, 1986). If the late Pleistocene uplift rates estimated in this study represent long-term average values, then uplift commenced locally during the last 1 Ma, and

possibly within the last 0.5 Ma (refer to Chapter 3: sections 3.8 and 3.9 for full discussion).

6.4 SEISMIC HAZARD

6.4.1 Proximity of seismogenic structures to Christchurch

The most southerly element of the PPAFZ, and the closest recognised seismogenic structure to Christchurch is the Pegasus Bay Fault (Carter and Carter, 1982), which has an ENE strike and length of c.20 km, and approaches the shore between the Waimakariri and Ashley Rivers (P. Barnes pers.comm. 1991; Frontispiece 1). Carter and Carter (1982) reported that the anticline associated with the hanging-wall of the fault displaced the sea-floor, but the results of detailed re-surveying (Barnes, pers.comm. 1991) indicate no bathymetric expression.

However, as noted by Carter and Carter (1982), the Pegasus Bay Fault is delineated by small historic earthquakes (Fig.1.3), and the absence of a bathymetric scarp may reflect burial by sediment discharged from the Waimakariri River rather than seismic quiescence. The potential of this structure to generate large earthquakes is unknown. But, given the thickness of cover sequence in this area (c.2.4 km), its strike-length in basement may be underestimated.

Drillhole data in the area between Waimakariri River and Christchurch indicate subsidence of up to 67 m since the late Pleistocene (Suggate, 1958; Brown et al. 1988), but it is unclear whether this should be attributed to compaction of Pleistocene outwash gravels, during the fall of sea-level (and water-table) that accompanied the last glaciation, or to tectonic deepening of the Canterbury Basin. Several moderate-magnitude earthquakes occurred in this area during the late nineteenth century (Fig.1.2), but no active faults have been recognised in seismic reflection profiles or inferred from gravity data, south of the Pegasus

Bay Fault (Kirkaldy and Thomas, 1963; Hicks, 1989; Barnes, pers.comm.1991; Frontispiece 1), and no large Holocene landslides are known from Banks Peninsula (J.R. Pettinga, pers.comm., 1992). Consequently, it is reasonable to infer that the PPAFZ, including the Pegasus Bay Fault, represent the closest source of potential M>7 earthquakes to Christchurch.

6.4.2 Proximity of seismogenic faults to towns on the northern Canterbury Plains

The townships of Oxford, Rangiora and Amberley, and a large milling and timber processing facility at Ashley Forest (NE of Rangiora) lie within the PPAFZ. The late Quaternary trace of the Ashley Fault terminates approximately 5 km northwest of Rangiora township (Map 2, Map 4), but the absence of a surface trace further east is more likely to reflect river aggradation and burial of the fault scarp, rather than a termination of the structure in basement (note the change in bed-form of the Ashley River that occurs downstream from the western end of the Ashley Fault trace and the confluence of the Okuku River - Map 2).

Furthermore, an earthquake with a strike-slip solution and one nodal plane sub-parallel to the Ashley Fault (solution 2: Fig.4.9, Appendix 4.7), was located close to Rangiora during the 1990 microearthquake survey, suggesting the presence of an active structure beneath the township. A few kilometres further east, a fault with a similar strike extends ENE from the Ashley River mouth and probably is related to, if not directly connected with, the Ashley Fault (Herzer and Bradshaw, 1985).

In the northeast of the study area, the settlement of Amberley is located at the south-plunging termination of the Cass Anticline (Frontispiece 1). To the southwest, Oxford township is located adjacent to the Ashley Range escarpment, where the presence of faults is implied

by warped fans and springs along the lower slopes between Oxford and Glentui (Maps 1 and 2), and confirmed by a seismic reflection profile normal to the range-front, located c. 2 km northeast of Oxford (Kirkaldy and Thomas, 1963: Vax Line 2).

6.4.3 Maximum magnitudes

The PPAFZ has been characterised historically by frequent small earthquakes (Fig.1.3), but available paleoseismic data indicate a return period of 1500-1900 years between the last two M>7-7.5 earthquakes, and 500-700 years have elapsed since the last (Table 5.3). The magnitudes of these events are estimated from inferred maximum rupture lengths, and the distribution of dated landslides (mainly large rock avalanches) corresponding to each event (Fig.5.7, 5.8). An upper bound magnitude of M7.5 for the PPAFZ is surmised.

6.4.4 Seismicity model for PPAFZ

Comparison of the paleoseismicity data with the short historic record of seismicity suggests that the magnitudes of the largest earthquakes in this zone are not exponentially distributed (Fig.5.10), but there are insufficient data to determine whether their frequency conforms to a recognised model of behaviour (e.g. characteristic earthquake or time-variable slip models - refer to Berryman and Beanland, 1991; Schwartz, 1989).

The frequency of large prehistoric earthquakes inferred for the PPAFZ in this study, is consistent with a small geological offset (c.$\leq$4 km) and a lower slip-rate (c. 5-10 m/kyr), than for example the Hope Fault to the north (cf. relationships illustrated by Wesnousky, 1988). The PPAFZ is at an earlier stage in its development than the Hope Fault, which has accumulated c.20 km of offset (Freund, 1971), and is

characterised by frequent large earthquakes and a slip-rate of 20-25 m/kyr (Cowan and McGlone, 1991; Van Dissen and Yeats, 1991).

Although the late Holocene frequency of earthquakes greater than magnitude M7 in the PPAFZ, is indicated by data gathered in this study, the frequency of moderate-magnitude earthquakes in the PPAFZ (M6-6.5) is poorly understood and warrants further study. The upper limit to the population of exponentially-distributed magnitudes is unknown, but a b-value of 1.0 for this fault zone is more consistent with the available geological data, than the b-value of 0.8 adopted by Elder et al. (1991) (see Fig.5.9 and Appendix 5.2).

The proposed revision of the seismicity model, from b=0.8 to b=1.0 (Fig.5.10), reduces the predicted frequency of large earthquakes ($M \geq 7.0$) in this zone by a factor of 3.5, but retains a margin of 1.8 x (interval between the last two events), which allows for temporal variations in the frequency of large events and the possibility that the geological database is incomplete. If the proposed revision of parameters for the PPAFZ seismicity model is accepted, the contribution of this zone to the hazard at Christchurch will be reduced, and the hazard model should be revised.

6.5 FINAL STATEMENT AND RECOMMENDATIONS FOR FUTURE WORK

The Porter's Pass-Amberley Fault Zone represents the deformation front associated with the Australia-Pacific plate-boundary zone in northeastern South Island and is not a simple structure (such as described by Carter and Carter (1982)), but a complex system of interconnected faults and folds that is evolving in response to dextral transpression at depth.

In this study of the PPAFZ, I have attempted to integrate seismological, geological and geomorphological data in a way hitherto not attempted in this region, and the data have been used to assess the

seismic hazard of the zone. The project was an inter-disciplinary study that touched on a diversity of topics. Any one of these could have been explored in greater detail, but were not attempted because they fell outside the immediate scope and funding constraints of the study.

A considerable amount of time has been devoted to comprehensive field-mapping at an appropriate level of detail, in order to establish the geometry and kinematics of surface structures in the PPAFZ and provide a framework for the study of seismicity, as well as local (site-specific) studies of individual fault traces that may follow. Future work arising from the results of this study fall into two categories: 1) The general application or extension of methods adopted in this study, to similar problems over a wider area, and; 2) further studies of Quaternary deformation and related topics in the Porter's Pass-Amberley Fault Zone. Some of these possibilties include:

1) more extensive mapping of the axial ranges of New Zealand, to locate seismogenic faults and define their architecture in basement. Although existing regional geological maps illustrate a wealth of geological data they generally do not provide adequate information on this topic.

2) more extensive documentation of the spatial (altitudinal) distribution of the Torlesse-Cretaceous unconformity surface in North Canterbury and elsewhere, to identify variations in uplift and facilitate data-based modelling of crustal structure and dynamics. Because the late-Cretaceous unconformity surface in Central Canterbury has been unroofed for the first time during the Late Quaternary and at several localities is not seriously disrupted, the possibility may exist to study aspects of the Cretaceous land surface.

3) further study of seismicity, particularly at the eastern end of the zone (east of Mt Grey), where no upper crustal earthquakes were recorded during the 2.5 month survey in 1990. It is recommended that a future seismograph network be extended south of the PPAFZ, to enhance the prospect of locating deeper (lower crustal) events for the purpose of comparing kinematics of deformation above and below the inferred mid-crustal ductile layer.

4) detailed studies such as trenching across individual fault traces, to refine the paleoseismic history of the zone. The Ashley Fault represents a high priority target because of its proximity to the town of Rangiora. Other fault traces where trenching is warranted, include: Lees Valley, Mt Lawry, Mt Grey, Cust, Glentui and Cooper's Creek Faults.

5) analysis of tectonic geomorphologic indices, such as strath and cut-and-fill terraces of the Waimakariri, Ashley, Okuku and other rivers should be studied in detail to establish (where possible) the ages of surfaces and deposits, and their relationships to differential tectonic movements. Erosional knick-points (waterfalls and other abrupt changes in stream gradient) should be documented for the same purpose. An outcome of such work would be an improved understanding of the nature and rate of differential displacement within the PPAFZ, as well as a greater knowledge of rates of landform development, soil genesis and perhaps past climatic change.

6) high-resolution shallow (upper crust) seismic reflection profiling and detailed gravity surveys are recommended to obtain a better understanding of Quaternary deformation history and clarify the presence/absence of active structures beneath the Canterbury Plains. Priority targets include, the Oxford-Mt Thomas range-front and the Cust Anticline-Ashley Fault complex. Minimum penetration of at least 1 second

would be required to image structures in basement.

7) review of available geodetic data and re-calculate shear strain rates between Banks Peninsula and the Hope Fault. Re-occupy key stations and establish new GPS arrays across the PPAFZ.

8) conduct a deep (mid-lower crustal) seismic reflection traverse across North Canterbury, to test the validity of crustal models based on seismicity data, and assess the relationship between surface structures (long and short-wavelength) and deep structure.

REFERENCES

REFERENCES

Adams, J., 1980. Paleoseismicity of the Alpine Fault seismic gap, New Zealand. *Geology*, v.8: 72-76.

_____ 1981. Earthquake-dammed lakes in New Zealand. *Geology*, v.9: 215-219

Adams, R.D.; Eiby, G.A.; Lowry, M.A.; Lensen, G.J.; Suggate, R.P., and Stephenson, W.P., 1968. Preliminary reports on the Inangahua earthquake, New Zealand, May 1968. *DSIR Bulletin 193.*

Aki, K., and Richards, P.G. 1980. *Quantitative seismology: theory and methods*. W.H. Freeman and Co., San Fransisco.

Andrews, P.B., 1968. Patterns of sedimentation during early Otaian (Early Miocene) time in North Canterbury, New Zealand. *N.Z. Journal of Geology and Geophysics* 11: 711-752.

Arabasz, W.J.; Robinson, R., 1976. Microseismicity and geologic structure in the northern South Island, New Zealand. *N.Z. Journal of Geology and Geophysics* 19:569-601.

Barrell, D., 1989. *Geomorphic evolution and engineering geology studies at coastal Motunau, North Canterbury*. Unpublished M.Sc. Engineering Geology thesis, University of Canterbury Library.

Berryman, K., 1979. Active faulting and derived PHS directions in the South Island, New Zealand. *In*: The Origin of the Southern Alps (edited by Walcott, R.I. & Cresswell, M.M.). *Bulletin of the Royal Society of N.Z.* 18.

----------; Beanland, S., 1991. Variation in fault behaviour in different tectonic provinces of New Zealand. *Journal of Structural Geology* 13: 177-189.

Bibby, H.M., 1981. Geodetically determined strain across the southern end of the Tonga-Kermadec-Hikurangi subduction zone. *Geophysical Journal of the Royal astronomical Society* 66:513-533.

Bishop, D.G.; Bradshaw, J.D.; Landis, C.A., 1985. Provisional terrane map of South Island, New Zealand. *Circum-Pacific Council for Energy Minerals and Earth Sciences Series* 1. Houston.

Bonilla, M.G.; Mark, R.K.; Lienkaemper, J.J., 1984. Statistical relations among earthquake magnitude, surface rupture length, and surface fault displacement. *Bulletin of the Seismological Society of America* **74**: 2379-2411.

Botsford, J.W., 1983. *The Esk Head Melange in the Esk Head-Okuku area, North Canterbury*. Unpublished M.Sc. thesis, University of Canterbury Library.

Bradshaw, J.D., 1972. Stratigraphy and structure of the Torlesse Supergroup (Triassic-Jurassic) in the foothills of the Southern Alps near Hawarden (S60-61), Canterbury. *N.Z. Journal of Geology and Geophysics* **15**:71-87.

----------, 1975. The folds at Castle Hill (Canterbury) and their bearing on Kaikouran deformation style in the Canterbury Basin. *Journal of the Royal Society of N.Z.* **5**:209-217.

----------, 1989. Cretaceous geotectonic patterns in the New Zealand region. *Tectonics* **8**: 803-820.

----------; Adams, C.J.; Andrews, P.B., 1981. Carboniferous to Cretaceous on the Pacific margin of Gondwana: the Rangitata phase of New Zealand. *In*: Cresswell, M.M.; Vella, P. (eds). Fifth International Gondwana Symposium. Balkema, Amsterdam:217-221.

Brown, L.J., 1973. Geological Map of New Zealand 1:63,360. Sheet S76 *"Kaiapoi"* (1st Ed.). NZ DSIR, Wellington.

----------; Wilson, D.D., 1988. Stratigraphy of the late Quaternary deposits of the northern Canterbury Plains, New Zealand. *N.Z. Journal of Geology and Geophysics* **31**: 305-335.

Brown, L.N., 1975. Tenement review PPL's 1029/1043, Canterbury Plains Area, South Island, New Zealand: Associated Australian Resources N.L. N.Z. Geological Survey unpublished *open-file Petroleum Report* **637**. NZ DSIR, Wellington.

Browne, G.H.; Field, B.D., 1985. The lithostratigraphy of Late Cretaceous to early Pleistocene rocks of northern Canterbury, New Zealand. *N.Z. Geological Survey Record* **6**.

Burchfiel, B.C.; Deng, Q.; Molnar, P.; Royden, L.; Wang, Y.; Zhang, P.; Zhang, W., 1989. Intracrustal detachment within zones of continental deformation. *Geology* **17**: 448-452.

Burrows, C.J., 1975. A 500-year old landslide in the Acheron River valley, Canterbury. *N.Z. Journal of Geology and Geophysics* **18**:357-360.

Carlson, J.R.; Grant-Mackie, J.A.; Rodgers, K.A., 1980. Stratigraphy and sedimentology of the Coalgate area, Canterbury, New Zealand. *N.Z. Journal of Geology and Geophysics* **23**: 179-192.

Carr, M.J., 1970. *The stratigraphy and chronology of the Hawera Series. marginal succession of the North Canterbury coast.* Unpublished Ph.D. thesis, University of Canterbury Library.

Carter, L.; Carter, R.M.; Griggs, G.B., 1982. Sedimentation in the Conway Trough, a deep nearshore marine basin at the junction of the Alpine transform and Hikurangi subduction plate boundary, New Zealand. *Sedimentology* **29**:475-497.

Carter, R.M.; Carter, L., 1982. The Motunau Fault and other structures at the southern edge of the Australian-Pacific plate boundary, offshore Marlborough, New Zealand. *Tectonophysics* **88**: 133-159.

Chappell, J.; Shackleton, N.J., 1986. Oxygen isotopes and sea level. *Nature* **324**: 137-140.

Chinn, T.J.H., 1981. Use of rock weathering-rind thickness for Holocene absolute age-dating in New Zealand. *Arctic and Alpine Research* **13**: 33-45.

Coombs, D.S.; Ellis, A.J.; Fyffe, W.S.; Taylor, A.M., 1959. The zeolite facies, with comments on the interpretation of hydrothermal syntheses. *Geochimica et Cosmochimica Acta* **17**: 53-107.

Cooper, A.F.; Norris, R.J., 1990. Estimates for the timing of the last coseismic displacement on the Alpine Fault, northern Fiordland, New Zealand. *N.Z. Journal of Geology and Geophysics* **33**: 303-307.

Coote, J.A.R., 1987. *Cenozoic volcanism in the Waiau area, North Canterbury.* Unpublished M.Sc. thesis, University of Canterbury Library.

Cornell, C.A., 1968. Engineering seismic risk analysis. *Bulletin of the Seismological Society of America* **58**: 1583-1606.

Cotton, C.A., 1917. Block mountains of New Zealand. *American Journal of Science* **44**: 249-293.

Cowan, H.A., 1989. *An evaluation of the late Quaternary displacements and seismic hazard associated with the Hope and Kakapo Faults, Amuri District, North Canterbury.* Unpublished M.Sc. Engineering Geology thesis, University of Canterbury Library.

----------, 1990. Late Quaternary displacements on the Hope Fault at Glynn Wye, North Canterbury. *N.Z. Journal of Geology and Geophysics* **33**: 285-293.

----------, 1991. The North Canterbury earthquake of September 1, 1888. *Journal of the Royal Society of N.Z.* **21**: 1-12.

----------; Pettinga, J.R., 1990. Seismic Hazards. *In*: Bell, D.H., (Ed.) Analysis of natural hazards in the Canterbury Civil Defence Region. Report to Canterbury Regional Council, R90/8. ISBN 1-86937-110-0.

----------; McGlone, M.S., 1991. Late Holocene displacements and characteristic earthquakes on the Hope River segment of the Hope Fault, New Zealand. *Journal of the Royal Society of N.Z.* **21**: 373-384.

Coyle, S., 1988. *The Porter's Pass Fault.* Unpublished M.Sc. thesis, University of Canterbury Library.

Crossan, R.S., 1976. Crustal structure modelling of earthquake data, 1: Simultaneous least squares estimation of hypocenter and velocity parameters. *Journal of Geophysical Research* **81**: 3036-3046.

Crozier, M.J., 1991. Determination of paleoseismicity from landslides. *In*: Landslides (edited by Bell, D.). Proceedings of the Sixth International Symposium: 10-14 February, 1992, Christchurch. pp 1173-1180.

Cutten, H.N.C., 1979. Rappahannock Group: Late Cenozoic sedimentation and tectonics contemporaneous with Alpine Fault movement. *N.Z. Journal of Geology and Geophysics* **22**: 535-553.

Davison, F.C.; Scholz, C.H., 1985. Frequency-moment distribution of earthquakes in the Aleutian Arc: A test of the characteristic earthquake model. *Bulletin of the Seismological Society of America* **75**: 1349-1361.

DeMets, C.; Gordon, R.G.; Argus, D.F.; Stein, S., 1990. Current plate motions. *Geophysical Journal International* **101**: 425-478.

Department of Survey and Land Information, 1983. New Zealand Topographical Map 1:50,000. NZMS 260 Sheet L35 *"Waimakariri"*. Government Printer, Wellington.

----------, 1984. New Zealand Topographical Map 1:50,000. NZMS 260 Sheet M35 *"Christchurch"*. Government Printer, Wellington.

----------, 1990. New Zealand Topographical Map 1:50,000. NZMS 260 Sheet L34 *"Puketeraki"*. Government Printer, Wellington.

----------, 1991. New Zealand Topographical Map 1:50,000. NZMS 260 Sheet M34 *"Amberley"*. Government Printer, Wellington.

Dibble, R.R.; Ansell, J.H.; Berrill, J.B., 1980. Report on a study of seismic risk for B.P. New Zealand Ltd sites at Woolston and Lyttelton. Unpublished report to B.P. New Zealand Ltd.

Dowrick, D.J.; Smith, E.G.C., 1990. Surface wave magnitudes of some New Zealand earthquakes: 1901-1988. *Bulletin of the N.Z. National Society of Earthquake Engineering* 23: 198-210.

Eiby, G.A., 1968. An annotated list of New Zealand earthquakes, 1460-1965. *N.Z. Journal of Geology and Geophysics* 11: 630-647.

----------, 1990. The Lake Coleridge earthquakes of 1946. *Bulletin of the N.Z. National Society for Earthquake Engineering* 23: 150-158.

Elder, D. McG.; McCahon, I.F.; Yetton, M.D., (Soils and Foundations Ltd) 1991. The earthquake hazard in Christchurch: a detailed evaluation. Report to Earthquake and War Damages Commission.

Field, B.D.; Browne, G.H., 1986. Lithostratigraphy of Cretaceous and Tertiary sediments, South Canterbury, New Zealand. *N.Z. Geological Survey Record* 14.

----------; and others 1989. Cretaceous and Cenozoic sedimentary basins and geological evolution of the Canterbury Region, South Island, New Zealand. *N.Z. Geological Survey Basin Studies* 2.

Freund, R., 1971. The Hope Fault: A strike-slip fault in New Zealand. *N.Z. Geological Survey Bulletin* 86.

Gage, M., 1958. Late Pleistocene glaciations of the Waimakariri Valley, Canterbury, New Zealand. *N.Z. Journal of Geology and Geophysics* 1: 123-155.

--------, 1970. Late Cretaceous and Tertiary rocks of Broken River, Canterbury. *N.Z. Journal of Geology and Geophysics* 13: 507-559.

Gair, H.S., 1967. *The question of Post-Rangitata peneplanation in New Zealand. An investigation of Cretaceous peneplanation in relation to unconformities in Upper Jurassic and Cretaceous sequences.* Unpublished Ph.D. thesis, University of Canterbury Library.

Garlick, R., 1992. *Lees Valley Fault.* Unpublished B.Sc.(Hons) dissertation, University of Canterbury Library.

Ghani, M.A., 1978. Late Cenozoic vertical crustal movements in the Southern North Island. *N.Z. Journal of Geology and Geophysics* 21: 117-126.

Gledhill, K.R., 1991. EARSS users' manual. *Geophysics Division Technical Report* 109. NZ DSIR, Wellington. ISSN 0113-3055

----------; Randall, M.J., and Chadwick, M.P., 1991. The EARSS digital seismograph: system description and field trials. *Bulletin of the Seismological Society of America* 81: 1380-1390.

----------, 1992. *Shear-wave splitting and seismic anisotropy in the Wellington region, New Zealand.* Unpublished Ph.D. thesis, Victoria University of Wellington Library.

Goh, K.M.; Molloy, B.P.J., 1979. Contaminants in charcoals used for radiocarbon dating. *N.Z. Journal of Science* 22: 39-47.

Gregg, D.R., 1964. Geological Map of New Zealand 1:250,000. Sheet 18, *"Hurunui"*. N.Z. DSIR, Wellington.

Haast, J. von 1872. Report on the geology of the Malvern Hills, Canterbury. *N.Z. Geological Survey report of geological exploration* 1871-72: 1-88.

Henderson, J., 1937. West Nelson earthquake of 1929. *N.Z. Journal of Science and Technology* 19: 66-144.

Herzer, R.H.; Bradshaw, J.D., 1985. The Motunau Fault and other structures at the southern edge of the Australian-Pacific plate boundary, offshore Marlborough, New Zealand - discussion. *Tectonophysics* 115: 161-166.

Hicks, S.R., 1989. Structure of the Canterbury Plains, New Zealand, from Gravity Modelling. *Geophysics Division Research Report* 222. NZ DSIR, Wellington. ISSN 0113-2903.

Hoolihan, K., 1978. Kowai No.1 well completion report. Offshore Mining Co. Ltd. DSIR Geology & Geophysics unpublished open-file petroleum report 722.

Hull, A.G.; Berryman, K.R., 1986. Holocene tectonism in the region of the Alpine Fault at Lake McKerrow, Fiordland, New Zealand. *Royal Society of N.Z. Bulletin* 24: 317-331.

Kamp, P.J.J.; Green, P.F.; White, S.H., 1989. Fission track analysis reveals character of collisional tectonics in New Zealand. *Tectonics* 8: 169-195.

Katz, H.R., 1982. Petroleum prospects in North Canterbury, South Island, New Zealand. *N.Z. Journal of Geology and Geophysics* 25: 201-207.

Keefer, D.K., 1984. Landslides caused by earthquakes. *Geological Society of America Bulletin* 95: 406-421

Kieckhefer, R.M., 1977. Microseismicity in the vicinity of the Clarence Fault, New Zealand. *N.Z. Journal of Geology and Geophysics* 20: 165-177.

Kirkaldy, P.H.S.; Thomas, E.G., 1963. Final report on a seismic survey in the Canterbury Plains area of New Zealand. BP Shell and Todd Petroleum Development Ltd. N.Z. Geological Survey unpublished *open-file Petroleum Report* 328.

Lamb, S.H.; Bibby, H.M., 1989. The last 25 Ma of rotational deformation in part of the New Zealand plate-boundary zone. *Journal of Structural Geology* 11: 473-492.

Lee, W.H.K.; Stewart, S.W., 1981. Principles and applications of microearthquake networks. *Advances in Geophysics (Supplement 2).* Academic Press, New York.

McKay, A., 1890. On the earthquakes of September 1888, in the Amuri and Marlborough districts of the South Island. *N.Z. Geological Survey report of geological explorations* 20: 1-16.

_____ 1902. *Report on the recent seismic disturbances within Cheviot County in Northern Canterbury and the Amuri District of Nelson, New Zealand.* Government Printer, Wellington.

McKenzie, D.P., 1969. The relation between fault-plane solutions for earthquakes and the directions of the principal stresses. *Bulletin of the Seismological Society of America* **59**: 591-601.

McLennan, J.M., 1981. *The Cretaceous-Tertiary rocks of Avoca, Oxford and Burnt Hill, Central Canterbury*. Unpublished M.Sc. thesis, University of Canterbury Library.

----------; Bradshaw, J.D., 1984. Angular unconformity between Oligocene and older Cenozoic rocks at Avoca, Canterbury. *N.Z. Journal of Geology and Geophysics* **27**: 299-303.

----------; Weaver, S.D., 1984. Olivine-nephelinite at Mounseys Creek, Oxford, Canterbury (Note). *N.Z. Journal of Geology and Geophysics* **27**: 389-390.

McMorran, T.J., 1991. *The Hope Fault at Hossack Station east of Hanmer Basin, North Canterbury*. Unpublished M.Sc. Engineering Geology thesis, University of Canterbury Library.

McSaveney, M.J., 1978. Sherman Glacier rock avalanche, Alaska, U.S.A.. *In*: Rockslides and Avalanches 1 (edited by Voight, B.), Elsevier Scientific Publishing, New York. pp 197-258.

---------, 1992. A manual of weathering-rind dating for sandstone of the Torlesse Supergroup. *N.Z. DSIR Geology & Geophysics Technical Report* (in preparation).

Marden, M., 1976. *Late Pleistocene geology of the Kowai River catchment, Mid-Canterbury*. Unpublished M.Sc. thesis, University of Canterbury Library.

Mason, B.H., 1941. The geology of the Mount Grey district, North Canterbury. *Transactions of the Royal Society of N.Z.* **71**: 103-127.

Mathews, W.H., 1979. Landslides of central Vancouver Island and the 1946 earthquake. *Bulletin of the Seismological Society of America* **69**: 445-450.

Mendenhall, W., 1975. *Introduction to Probability and Statistics* (4th Ed.). Wadsworth Publishing, Belmont, California.

Molnar, P.; Chen, W.P., 1982. Seismicity and mountain building *In*: Mountain Building Processes (edited by Briegel, V., and Hsu, K.J.), Academic Press, London. pp.41-57.

Mould, R.J., 1992. *Structure and kinematics of Late Cenozoic deformation along the western margin of the Culverden Basin, North Canterbury, New Zealand.* Unpublished M.Sc. thesis, University of Canterbury Library.

Mulholland, M., 1982. *Estimation of design earthquake motions for New Zealand.* Unpublished M.E. thesis, University of Canterbury Library.

Namson, J.S.; Davis, T.L., 1988. Seismically active fold and thrust belt in the San Joaquin Valley, central California. *Geological Society of America Bulletin* 100: 257-273.

Naylor, M.A.; Mandl, G.; Siypestieyn, C.H.K., 1986. Fault geometries in basement-induced wrench faulting under different initial stress states. *Journal of Structural Geology* 8: 737-752.

New Zealand Seismological Observatory, 1992. New Zealand earthquakes: 1460-January, 1992. Observatory Master File. DSIR Geology and Geophysics, N.Z. Department of Scientific and Industrial Research.

Nicholson, C.; Seeber, L.; Williams, P.; Sykes, L.R., 1986. Seismicity and fault kinematics through the eastern Transverse Ranges, California: Block rotation, strike-slip faulting and low-angle thrusts. *Journal of Geophysical Research* 91(B5): 4891-4908.

Nicol, A., 1991. *Structural styles and kinematics of deformation on the edge of the New Zealand plate boundary zone, mid-Waipara region, North Canterbury.* Unpublished Ph.D. Thesis, University of Canterbury Library.

---------, 1992. Tectonic structures developed in Oligocene limestones: implications for New Zealand plate boundary deformation in North Canterbury. *N.Z. Journal of Geology and Geophysics* 35: 353-362.

---------, in press. Conical folds produced by dome and basin fold interference and their application to determining strain: examples from North Canterbury, New Zealand. *Journal of Structural Geology.*

---------; Wise, D.U., in press. Paleostress adjacent to the Alpine Fault of New Zealand: fault, vein and stylolite data from the Doctors Dome area. *Journal of Geophysical Research.*

Norris, R.J.; Craw, D., 1987. Aspiring terrane: an oceanic assemblage from New Zealand and its implications from terrane accretion in the southwest Pacific. *In*: Leitch, E.C.; Scheibner, E., (Eds.) Terrane accretion and orogenic belts. Geodynamics Series 19: 169-177.

----------; Koons, P.O.; Cooper, A.F., 1990. The obliquely-convergent plate boundary in the South Island of New Zealand: implications for ancient collision zones. *Journal of Structural Geology* **12**: 715-725.

NZ DSIR, Division of Information Technology, 1991. LANDSAT image of North Canterbury-South Marlborough (02 August, 1975). (E - 2192-21265) MSS Band 4.

Officers of the New Zealand Geological Survey 1983. Late Quaternary tectonic map of New Zealand 1:2,000,000. (2nd Ed.). *N.Z. Geological Survey miscellaneous series map* **12**. NZ DSIR, Wellington.

Ota, Y.; Yoshikawa, T; Iso, N.; Okada, A.; Yonekura, N., 1984. Marine terraces of the Conway coast, South Island, New Zealand. *N.Z. Journal of Geology and Geophysics* **27**: 313-326.

Pearson, G.W.; Stuiver, M., 1986. High-precision calibration of the radiocarbon time scale, 500-2500 BC. *Radiocarbon* **28**: 839-862.

Peek, R.; Berrill, J.B.; Davis, R.O., 1980. A seismicity model for New Zealand. *Bulletin of the N.Z. National Society of Earthquake Engineering* **13**: 355-364.

Perrin, N.D.; Hancox, G.T., 1991. Landslide-dammed lakes in New Zealand - Preliminary studies on their distribution, causes and effects. **In**: Landslides (edited by Bell, D.). Proceedings of the Sixth International Symposium: 10-14 February, 1992, Christchurch. pp 1457-1466.

Pillans, B., 1986. A Late Quaternary uplift map for North Island, New Zealand. *Royal Society of N.Z. Bulletin* **24**: 409-417.

----------, 1990. Pleistocene marine terraces in New Zealand: a review. *N.Z. Journal of Geology and Geophysics* **33**: 219-231.

Plafker, G.; Ericksen, G.E., 1978. Nevados Huascaran avalanches, Peru. *In*: Rockslides and avalanches 1 (edited by Voight, B.). Elsevier Scientific Publishing, New York, pp. 277-314.

Reyners, M.E., 1989. (Hochstetter review) New Zealand seismicity 1964-87: an interpretation. *N.Z. Journal of Geology and Geophysics* **32**: 307-315.

----------; Cowan, H.A. in preparation. The transition from subduction to continental collision: crustal structure in the North Canterbury region, New Zealand.

Richter, C.F., 1958. *Elementary seismology*. W.H. Freeman and Co., San Fransisco, 768 p.

Robinson, R., 1983. Velocity structure of the Wellington region, New Zealand, from local earthquake data and its implications for subduction tectonics. *Geophysical Journal of the Royal astronomical Society* 75: 335-359.

----------, 1986. Seismicity, structure and tectonics of the Wellington region, New Zealand. *Geophysical Journal of the Royal astronomical Society* 87: 379-409.

----------, 1987. Temporal variations in coda duration of local earthquakes in the Wellington Region, New Zealand. *Geophysical Journal of the Royal astronomical Society* 87: 379-409.

----------, 1988. "RATS": an inexpensive portable earthquake recorder (abs.) *Seismological Research Letters* 59: 21.

----------, 1991. Extent and geometry of subduction in the Northern South Island and Wellington Regions. *Geological Society of N.Z. miscellaneous publication* 56: 44-46.

Rynn, J.M.W.; Scholz, C.H., 1978. Seismotectonics of the Arthur's Pass region, south Island, New Zealand. *Geological Society of America Bulletin* 89: 1373-1388.

Scholz, C.H.; Rynn, J.M.W.; Weed, R.W.; Frolich, C., 1973. Detailed seismicity of the Alpine Fault Zone and Fiordland region, New Zealand. *Geological Society of America Bulletin* 84: 3297-3316.

Schwartz, D.P., 1989. Paleoseismicity, persistence of segments, and temporal clusterin of large earthquakes - examples from the San Andreas, Wasatch, and Lost River fault zones. *In*: Proceedings of Conference XLV. Fault Segmentation and Controls of Rupture Initiation and Termination (edited by Schwartz, D.P.; Sibson, R.H.). U.S. Geological Survey Open File Report 89-315: 361-375.

----------; Coppersmith, K.J., 1984. Fault behaviour and characteristic earthquakes: examples from Wasatch and San Andreas Faults. *Journal of Geophysical Research* 89: 5681-5698.

Sewell, R.J.; Gibson, I.L., 1988. Petrology and geochemistry of Tertiary volcanic rocks from inland Central and South Canterbury, South Island, New Zealand. *N.Z. Journal of Geology and Geophysics* 31: 477-492.

----------; Weaver, S.D.; Thiele, B.W., 1988. Sheet M36BD *"Lyttelton"*. Geological Map of New Zealand, 1:50,000. Map (1 sheet) and notes. NZ DSIR, Wellington.

Shackleton, N.J.; Matthews, R.K., 1977. Oxygen isotope stratigraphy of Late Pleistocene coral terraces in Barbadoes. *Nature* **268**: 618-620.

Sibson, R.H., 1983. Continental fault structure and the shallow earthquake source. *Journal of the Geological Society of London* **140**: 741-767.

Silberling, N.J.; Nichols, K.M.; Bradshaw, J.D.; Blome, C.D., 1988. Limestone and chert in tectonic blocks from the Esk Head subterrane, South Island, New Zealand. *Geological Society of America Bulletin* **100**: 1213-1223.

Smale, D., 1989. Leaching of heavy minerals above and below the mid-Cretaceous unconformity in the Ohuriawa Gorge area of the Waipara River, North Canterbury, New Zealand. *Journal of Sedimentary Petrology* **59**: 1011-1021.

Smith, W.D., 1978. Spatial distribution of felt intensities for New Zealand earthquakes. *N.Z. Journal of Geology and Geophysics* **21**: 293-311.

----------, 1979. Documentation for earthquake location programs LOCAL and MICRO and supporting software. *Geophysics Division Technical Note* **80**. NZ DSIR, Wellington.

Smith, W.D.; Berryman, K.R., 1983. Revised estimates of earthquake hazard in New Zealand. *Bulletin of the N.Z. National Society for Earthquake Engineering* **16**: 259-272.

_____ 1986. Earthquake hazard in New Zealand: inferences from seismology and geology. *Royal Society of N.Z. Bulletin* **24**: 223-242.

Speight, R., 1917. The geology of Banks Peninsula. *Transactions of the New Zealand Institute* **49**: 365-392.

----------, 1924. The Benmore coal area of the Malvern Hills. *Transactions of the N.Z. Institute* **55**: 619-626.

----------, 1933. The Arthur's Pass earthquake of 9th March, 1929. *N.Z. Journal of Science and Technology* **XV(3)**: 173-182.

----------, 1938. Recent faulting in the Southern Alps. *N.Z. Journal of Science and Technology* **19**: 701-708.

----------; Wild, L.J., 1918. The stratigraphical relationship of the Weka Pass Stone and the Amuri Limestone. *Transactions of the N.Z. Institute* 50: 65-93.

Stirling, M.W., 1990. The Old Man Range and Garvie Mountains: tectonic geomorphology of the Central Otago peneplain, New Zealand. *N.Z. Journal of Geology and Geophysics* 33: 233-243.

Stuiver, M.; Pearson, G.W., 1986. High-precision calibration of the radiocarbon time scale AD 1950-500 BC. *Radiocarbon* 28: 805-838.

----------; Reimer, P.J., 1986. A computer program for radiocarbon age calibration. *Radiocarbon* 28: 1022-1030.

Suggate, R.P., 1958. Late Quaternary deposits of the Christchurch metropolitan area. *N.Z. Journal of Geology and Geophysics* 1: 103-122.

----------, 1965. Late Pleistocene geology of the northern part of the South Island, New Zealand. *N.Z. Geological Survey Bulletin* 77.

----------, 1988. Quaternary deposition and deformation in the Buller and tributary valleys. *N.Z. Geological Survey Record* 25.

Sylvester, A.G., 1988. Strike-slip faults. *Geological Society of America Bulletin* 100: 1666-1703.

----------; Smith, R.R., 1976. Tectonic transpression and basement-controlled deformation in the San Andreas fault zone, Salton Trough, California. *Bulletin of the American Association of Petroleum Geologists* 60(12): 2081-2102.

Syme, A.R., 1991. *Structural analysis of the deformation of the Marble Point Outlier, Waiau River, North Canterbury*. Unpublished B.Sc.(Hons) dissertation, University of Canterbury Library.

Thomas, E.G., 1963. Review of gravity results, Canterbury Plains area, South Island, New Zealand. N.Z. Geological Survey unpublished *open-file Petroleum Report* 709. NZ DSIR, Wellington.

Tonkin, P.J.; Basher, L.R., 1990. Soil-stratigraphic techniques in the study of soil and landform evolution across the Southern Alps, New Zealand. *Geomorphology* 3: 547-575.

Trangmar, B.B., 1987. Overview of Canterbury Loess Deposits: Tour guide for International Symposium on Loess: 14-21 February, 1987. Third meeting of the Western Pacific Working Group of the INQUA Loess Commission.

Turcotte, D.L.; Liu, J.Y.; Kulhawy, F.H., 1984. The role of an intercrustal asthenosphere on the behaviour of major strike-slip faults. *Journal of Geophysical Research* 89: 5801-5816.

Van Dissen, R.; Yeats, R.S., 1991. Hope Fault, Jordan thrust, and uplift of the Seaward Kaikoura Range, New Zealand. *Geology* 19: 393-396.

----------; Berryman, K.R.; Pettinga, J.R.; Hill, N.L., 1992. Paleoseismicity of the Wellington-Hutt Valley Segment of the Wellington Fault, North Island, New Zealand. *N.Z. Journal of Geology and Geophysics* 35: 165-176.

Voight, B.; Pariseau, W.G., 1978. Rockslides and Avalanches: An Introduction. *In*: Rockslides and Avalanches 1 (edited by Voight, B.). Elsevier Scientific Publishing, New York. pp 1-67.

Walcott, R.I., 1978. Present tectonics and Late Cainozoic evolution of New Zealand. *Geophysical Journal of the Royal astronomical Society* 52: 137-164.

----------, 1979. Plate motion and shear strain rates in the vicinity of the Southern Alps. *In*: The Origin of the Southern Alps (edited by Walcott, R.I.; Cresswell, M.M.). *Royal Society of N.Z. Bulletin* 18: 5-12.

----------, 1984. The kinematics of the plate-boundary zone through New Zealand: a comparison of short and long-term deformation. *Geophysical Journal of the Royal astronomical Society* 79: 613-633.

----------, 1987. Geodetic strain and the deformational history of the North Island of New Zealand during the late Cainozoic. *Philosophical Transactions of the Royal Society of London* A321: 163-181.

----------; Christoffel, D.A.; Mumme, T.C., 1981. Bending within the axial tectonic belt of New Zealand during the last 9 myr from paleomagnetic data. *Earth and planetary science letters* 52: 427-434.

Weaver, S.D.; Smith, I.E.M., 1989. New Zealand Intraplate Volcanism. *In*: Johnson, R.W.; Knutson, J.; Taylor, S.R. (eds), Intraplate Volcanism in Eastern Australia and New Zealand, Cambridge University Press, 157-188.

Wellman, H.W., 1953. Data for the study of Recent and late Pleistocene faulting in the South Island of New Zealand. *N.Z. Journal of Science and Technology* B34: 270-288.

----------, 1979. An uplift map for the South Island of New Zealand, and a model for the uplift of the Southern Alps. *In*: The Origin of the Southern Alps (edited by Walcott, R.I. & Cresswell, M.M.). Bulletin of the Royal Society of N.Z. 18.

Wesnousky, S.G., 1988. Seismological and structural evolution of strike-slip faults. *Nature* 335: 340-343.

----------; Scholz, C.H.; Shimazaki, K.; Matsuda, T., 1983. Earthquake frequency distribution and the mechanics of faulting. *Journal of Geophysical Research* 88(B11): 9331-9340.

Whitehouse, I.E., 1983. Distribution of large rock avalanche deposits in the central Southern Alps, New Zealand. *N.Z. Journal of Geology and Geophysics* 26: 271-279.

----------; Griffiths, G.A., 1983. Frequency and hazard of large rock avalanches in the central Southern Alps, New Zealand. *Geology* 11: 331-334.

Wilcox, R.E.; Harding, T.P.; Seely, D.R., 1973. Basic wrench tectonics. *Bulletin of the American Association of Petroleum Geologists* 57: 74-96.

Wilson, C.J.N.; Switsur, R.V.; Ward, A.P., 1988. A new 14C age for the Oruanui (Wairakei) eruption, New Zealand. *Geological Magazine* 125: 297-300.

Wilson, D.D., 1963. Geology of Waipara Subdivision. *N.Z. Geological Survey Bulletin* 64.

----------, 1989. Quaternary geology of northwestern Canterbury Plains (NZMS 260 Sheets L35 and parts sheets L36, M35 and M36) 1:100,000. *N.Z. Geological Survey miscellaneous series map 14*. Map (1 sheet) and notes. N.Z. DSIR, Wellington.

Yang, J.S., 1991. The Kakapo Fault - a major active dextral fault in the central North Canterbury - Buller regions of New Zealand. *N.Z. Journal of Geology and Geophysics* 34: 137-143.

Youngs, R.R.; Coppersmith, K.J., 1985. Implications of fault slip-rates and earthquake recurrence models to probabilistic seismic hazard estimates. *Bulletin of the Seismological Society of America* 75(4): 939-964.

Yousif, H.S., 1987. *The applications of remote sensing to geomorphological neotectonic mapping in North Canterbury, New Zealand.* Unpublished PhD thesis, University of Canterbury Library.

Zoback, M.D.; Zoback, M.L., 1991. Tectonic stress field of North America and relative plate motions. *In*: Neotectonics of North America (edited by Slemmons, D.B.; Engdahl, E.R.; Zoback, M.D.; Blackwell, D.D.) Geological Society of America, Decade Map Volume 1.

APPENDICES

APPENDIX 3.1 LOCATIONS OF SPOT HEIGHTS ON, OR CLOSE TO THE TORLESSE-CRETACEOUS UNCONFORMITY

Explanatory notes

Spot heights (metres a.s.l.) on the Torlesse-Cretaceous unconformity have been used to contour the unconformity surface and assess its relationship to local topography and structure (Fig. 3.17). Data on the height of the unconformity surface consist of the following:

1) exposures of basal cover sequence - Late Cretaceous quartzose coal measures of the Broken River Formation - in sedimentary contact with strongly leached Torlesse;

2) exposures of strongly leached Torlesse below the inferred unconformity surface from which the cover sequence has been stripped.

3) exposures of basal cover sequence above the unconformity surface which is not exposed; the unconformity surface is inferred to lie within a few metres of the exposure, because the Broken River Formation generally is ≤40 m thick in the study area (Field and Browne, 1986: p.17).

The three categories of observation are denoted by the superscripts: (1) (2) and (3), respectively. Grid references are from the New Zealand Metric Grid (Geodetic Datum 1949) and prefixed by sheet numbers of the NZ Map Series 260 (1:50,000) (Department of Survey and Land Information, Wellington).

Locality	NZMG (Datum 1949) (m)	Altitude (metres a.s.l.)
(1)1. West bank, Waimakariri River	L35/. 2424550,5769300	340
(1)2. Coal Creek	L34/. 2430500,5776000	620
(2)3. Townshend Valley	L34/. 2431000,5778750	580
(3)4. Dobson Stream	L34/. 2431600,5777150	640
(1)5. Feary's Farm, Cooper's Ck	L34/. 2433650,5770750	380

[2]6. The Grange, Oxford.	L34/. 2443200,5770800	360
[3]7. Bay Road, Oxford.	L35/. 2443700,5769500	300
[2]8. Blowhard Track, Bald Hills.	M34/. 2451700,5780155	540
[2]9. Blowhard Track, Bald Hills.	M34/. 2451650,5780100	520
[3]10. Lees Valley	L34/. 2446100,5784500	400
[3]11. Lees Valley	L34/. 2444800,5783550	400
[2]12. Lees Valley Airstrip road, Richon	L34/. 2449400,5789600	500
[2]13. Pinchgut Road, Mt Thomas.	M34/. 2458150,5783900	660
[2]14. Round Hill, Okuku River.	M34/. 2458100,5786300	500
[2]15. Flat Tops, Okuku Hills Station.	M34/. 2457650,5787100	500
[2]16. Whiterock Downs, North Loburn.	M34/. 2462600,5784450	340
[1]17. Demmocks Road, Ashley Forest.	M34/. 2465200,5785100	350
[1]18. Marshall Road, Ashley Forest.	M34/. 2466500,5785558	330
[2]19. Karetu Road, Ashley Forest.	M34/. 2467650,5786650	420
[2]20. Horsford Downs Road, Ashley Forest.	M34/. 2469050,5787400	560
[1]21. Grey River (west branch).	M34/. 2469400,5785150	300
[2]22. Okuku Road, Ashley Forest.	M34/. 2469000,5788650	730

[3]23. Okuku Road, Ashley Forest.	M34/. 2466250,5789700	660
[3]24. Birdseye Stream, Ashley Forest.	M34/. 2465350,5791350	400
[1]25. Okuku Pass Road, Ashley Forest.	M34/. 2465165,5792150	380
[1]26. Birdseye Stream, Ashley Forest.	M34/. 2466900,5792905	320
[1]27. Birdseye Stream, Ashley Forest.	M34/. 2467100,5793905	300
[1]28. Rocky Road, Ashley Forest.	M34/. 2463000,5793800	440
[1]29. Field Road, Ashley Forest.	M34/. 2462900,5794450	460
[2]30. Lees Pass, Okuku Pass Road.	M34/. 2458800,5797000	570
[2]31. McDonald Downs Private Road.	M34/. 2459450,5798650	520
[1]32. McDonald Downs Private Road.	M34/. 2462050,5799250	520

N.B. Okuku Pass Road is a public right of way, but access to other roads in Ashley Forest and Mt Thomas Forest is by permit (and keys) only (contact Ashley Forest Headquarters).

Appendix 4.1 Station locations for the North Canterbury microearthquake network

SITE	DEGREES		NZMG	
	LATITUDE	LONGITUDE	mE	mN
BEE	43.34215	171.80221	2412900.	5762300.
BHE	43.37318	172.15328	2441400.	5759200.
COE	43.32915	171.60812	2397140.	5763500.
* COE0	43.32605	171.60511	2396890.	5763840.
* COE2	43.33172	171.61225	2397480.	5763220.
CCR	43.53536	172.17453	2443300.	5741200.
CHR	43.41557	171.94524	2424600.	5754300.
** ELE	43.73866	172.37076	2459330.	5718750.
EWR	43.41551	172.45274	2465700.	5754700.
FHE	43.14242	171.81410	2413550.	5784500.
* FHEA	43.14204	171.81239	2413410.	5784540.
* FHEB	43.14185	171.81104	2413300.	5784560.
GHR	43.59035	172.80407	2494200.	5735400.
IHE	42.70032	172.99368	2509500.	5834300.
LPE	43.04520	172.38487	2459900.	5795800.
* LPEA	43.04699	172.38239	2459700.	5795600.
* LPEB	43.04788	172.37993	2459500.	5795500.
MCR	43.08610	172.83513	2496597.	5791429.
MOE	42.99062	173.04082	2513350.	5802050.
* MOEA	42.99107	173.03775	2513100.	5802000.
* MOEB	42.99197	173.03530	2512900.	5801900.
MPE	43.17994	172.13197	2439450.	5780650.
NDE	43.26919	172.44358	2464850.	5770950.
* NDEA	43.26964	172.44235	2464750.	5770900.
* NDEB	43.26990	172.44111	2464650.	5770870.
OBE	43.70661	173.02700	2512200.	5722500.
OPE	43.08525	172.55701	2473950.	5791440.
ORR	43.13845	172.39929	2461150.	5785450.
PPE	43.30776	171.75414	2408946.	5766063.
PVR	42.99168	172.59387	2476900.	5801850.
** ROE	43.32609	172.01670	2430270.	5764310.
ROR	43.63455	172.34172	2456900.	5730300.
SDE	42.77353	172.63625	2480250.	5826100.
** SEE0	43.60683	172.13702	2440350.	5733230.
* SEE1	43.60839	172.14109	2440680.	5733060.
* SEE2	43.60994	172.14429	2440940.	5732890.
SFE	43.22644	172.67785	2483850.	5775800.
SHR	43.29192	172.24683	2448900.	5768300.
WDR	43.26185	171.96945	2426350.	5771400.
WKE	42.94113	172.77263	2491463.	5807522.

* Portable 2-geophone spread deployed from EARSS stations for explosions.

** Portable EARSS seismograph deployed for explosions.

contd./

Location of explosions and geophone spreads for the crustal structure experiment

EXPLOSION	NZMG (m)
Coleridge Shot	2385575, 5772465
Akaroa Shot	2504498, 5694919
Motunau Shot	2520500, 5789803

SERCEL 48-channel Geophone Spread	NZMG (m)
Coleridge Shot	
SA01	2460660.,5717420
SA24	2459840.,5718230
SA25	2459100.,5719020
SA48	2458320.,5719800
Akaroa Shot	
SB01	2430945.,5741460
SB24	2430360.,5742400
SB25	2429800.,5743325
SB48	2429230.,5744250
Motunau Shot	
SC01	2431930.,5764140
SC24	2430780.,5764260
SC25	2429710.,5764380
SC48	2428610.,5764500

Appendix 4.2

NORTH CANTERBURY MICROEARTHQUAKE SURVEY: NETWORK PERFORMANCE

INTRODUCTION

During the first week of September 1990 ten RATS and eleven EARSS were deployed in North Canterbury to monitor microearthquakes for a period of 2-3 months. A further three EARSS were deployed to boost network coverage during a complementary crustal velocity structure experiment in late September. These additional instruments were subsequently redeployed as permanent stations until the entire network was withdrawn in mid-November 1990.

Instruments were located on average between 10 and 20 km apart, on geology which varied from indurated metamorphic basement (Torlesse) or basaltic volcanics, to weakly consolidated river gravels and loess. Care was taken to find quiet sites, and only two instruments were subsequently relocated because of excessive wind noise. Overall the experiment was a great success: more than 100 local earthquakes were detected on three or more stations during the ~1800 hours of monitoring, and a number of these offer good potential for determining unambiguous focal mechanisms.

However, from time to time there were problems which compromised data quality, or resulted in loss of power to various instruments. Most of these problems can be put down to 'experience' and avoided in future studies by adopting a few simple precautions, and by implementing relatively minor modifications to equipment. The purpose of this brief report is to ensure that the problems encountered during the Canterbury experiment are documented for future reference.

FACTORS AFFECTING THE PERFORMANCE OF EARSS

Climatic conditions

All portable EARSS stations were battery powered (2 per station) and installed outdoors, shielded from the elements only by plastic bags and jute sacking. During September, a number of southerly fronts brought snow to low levels in Canterbury, followed by sharp frosts. Diurnal temperature fluctuations of as much as 30 deg C occurred during this period and resulted in numerous tape errors and several power failures, as tapedrives hunted continuously around bad sectors. More tape errors occurred at the start of successive strings, than were correlated with probable diurnal minima (i.e. 0000 to 0700 hrs local time). The number of tape errors and temperature related power failures dropped to a very low level from early October onwards, presumably in response to warming temperatures. Better insulation of EARSS during periods of cold weather would probably eliminate these problems.

Physical interference by animals

When the sites were selected care was taken to ensure that cattle, horses, deer and goats were excluded. Only goats were perceived to pose a direct threat to the equipment and more emphasis was placed on the noise-generating potential of large animals. Sheep were not avoided where the stocking rate was light, but this proved to be a costly error of judgement. More power failures and loss of time-marks were due to sheep chewing power cables and radio aerials than to any other cause.

Hardware Failures

A factor contributing to numerous power failures was the ease with which power cables and jumper leads could be pulled off, because in many cases the clip jaws were too small to ensure adequate purchase on the battery posts. It is probably worth noting that jumper clips slipped off at least twice without any obvious interference by animals. A simple change from clips to clamps is probably all that is required to correct the problem. Other problems resulting in power failure or degradation of data quality included:
1) noisy channel boards, (channels 1 and 2: EARSS #155, and EARSS #106);
2) fault in multiplexer (EARSS #104).
3) fault in pip detector board (EARSS #106; EARSS #102).
4) burnt out power supply board (EARSS #110).
5) fault in CH1 on SEIS #650: only high frequencies recorded despite accurate levelling of the seismometer.
6) broken tuning armature in radio (EARSS #109).
7) DC offset unstable on CH1 (EARSS #151), and CH0 (EARSS #107).

FACTORS AFFECTING THE PERFORMANCE OF RATS

Gain settings

Compared with EARSS stations, significantly fewer local events were captured by RATS. This was a rather disappointing feature of the RATS component of the Canterbury network, and raises the question as to whether gain settings were sufficiently high. However, one pleasing feature was a higher than expected rate of event capture at sites on the Canterbury Plains indicating possible amplification of shaking within the deep alluvium.

Timing Errors

All RATS stations displayed diminishing clock drift rates during the experiment. However, RATS #2 and RATS #24 displayed a drift rate of 0.14 s/day and 0.18 s/day respectively, thus severely limiting the period of service-free monitoring by these stations. Pip detectors failed progressively in two instruments (#24 and #22), and RATS #23 suffered some kind of mix-up between event detection and pip detection, the cause of which has (at the time of writing), yet to be determined.

RADIO RECEPTION

Poor radio reception is typical of mountainous parts of New Zealand, and serious difficulties were experienced in obtaining adequate reception at several sites in Canterbury. Up to 70 metres of aerial was required to achieve this at each of two stations in the Alps (COE and FHE), yet most instruments were supplied with as little as 2-4 metres of aerial wire beyond the shielded coax. To avoid this potential source of frustration in the future, staff working in remote or rugged areas should ensure that additional true-rip is carried at all times. Quite apart from problems which may be encountered when initially deploying stations, repairs may need to be effected during routine servicing. During the Canterbury experiment aerials were severed repeatedly by possums, hares and sheep, and in several cases the entire aerial (including coax and plug) had to be replaced. One aerial attached to a small tree nearby was pulled out of its socket by high winds, emphasising the need to tape down

or otherwise immobilise the cable near the socket. Considering the time and distances that may be involved in servicing remote stations, it would be prudent to ensure that such precautions are taken at the outset, and that spares are carried at all times.

CONCLUSIONS

It is unlikely that any experiment involving the deployment of high-tech equipment under rigorous field conditions will conclude without some disappointments. Overall, the performance of equipment during the Canterbury experiment was very good; considering the size of the network (24 portable and 6 National Network stations), and the often extreme weather conditions, the number of failures was perhaps surprisingly small. Many of the problems encountered arose from an inadequate knowledge of the operating limitations of the equipment, and a failure to appreciate that plastic cable of less than 5 mm thick is highly palatable to sheep (at no time was the thicker L4-3D coaxial cable chewed).

The majority of these problems can be avoided in the future by ensuring that: 1) all stock are excluded from around the instruments; 2) insulation is provided where EARSS is to be operated in temperatures below 5 deg C (N.B. plastic bags and jute sacks do not constitute adequate insulation); 3) componentry, particularly channel boards and clocks are thoroughly tested BEFORE being deployed; 4) power cable and jumper lead clips are modified to guarantee reliable purchase on battery posts.

ACKNOWLEDGEMENTS

I am grateful to Martin Reyners and John Taber for assistance during the deployment and initial servicing of the Canterbury network, and to Ken Gledhill, Jim Millar and Tim O'Neill for further help in diagnosing and correcting subsequent equipment failures.

Hugh Cowan,
Department of Geology,
University of Canterbury,
90/11/22

APPENDIX 4.3 DERIVATION OF THE SEISMIC VELOCITY MODEL

In recent years a technique for the simultaneous inversion of earthquake arrival time data for both hypocentres and velocity structure has been developed (e.g. Crossan, 1976). For the technique to be successful, both a dense seismograph network and a reasonable distribution of local earthquakes are required. Both these conditions are met in the current microearthquake survey. However, to establish a fixed reference point for the inversion, it is important to include data from accurately-timed explosions. To this end, three 200 kg explosions were detonated at the corners of the microearthquake network, as shown in Figure 1.5.

These explosions were well recorded, not only on the microearthquake network, but also on a 48-channel seismic spread deployed for each explosion. The locations of the explosions resulted in two reversed refraction profiles, one between Lake Coleridge and Banks Peninsula, the other between Lake Coleridge and Motunau Beach. Even though the number of recorders along these profiles fell well short of that normally employed for a refraction survey, the data recorded were sufficient to define a 4-layer initial crustal structure model for the arrival time inversion.

The inversion technique used was that of Robinson (1983, 1986). A subset of 42 well-recorded and well-distributed earthquakes was used together with the three explosions. After numerous inversions of the data, it was found that the best fit to both the arrival times and the earthquake distribution was achieved with the five layer velocity model shown in the the Table.

Layer	Depth to top of layer (km)	P-wave velocity (km/sec)
1	0.00	4.50*
2	1.92	5.70 ±0.03
3	10.85	6.24 ±0.04
4	20.00	7.12 ±0.09
5	27.00	8.09 ±0.08

* = velocity fixed during inversion

A constant ratio of P-wave velocity to S-wave velocity of 1.73 was used for all layers.

A detailed description of the inversion process is given in Reyners and Cowan (in prep.). It should be noted that there is a significant reduction in the root mean square of the weighted travel-time residuals of earthquakes using the new model, compared with the standard New Zealand crustal model. For the 42 earthquakes used in the inversion this RMS is 0.09 seconds for the new model, compared with 0.19 seconds for the standard model.

APPENDIX: 4.4 HYPOCENTRE LISTING OF EVENTS RECORDED BY THE NORTH CANTERBURY MICROEARTHQUAKE NETWORK

List of event headers:

YR	=	Year (1990)
EVT	=	Event No. in recorded sequence
DATE	=	Month and Day
HRMN, SEC	=	Origin time in U.T.
LAT	=	Latitude (°)
LONG	=	Longitude (°)
DEPTH	=	Hypocentral Depth (km)
MAG	=	Richter Magnitude
SE	=	Standard Error of Residuals (Sec)
NP	=	No. of Phases used for location
NS	=	No. of stations at which event was recorded
ERT	=	Standard error in origin time (sec)
ERY	=	Standard error in Latitude (°)
ERX	=	Standard error in Longitude (°)
ERZ	=	Standard error in depth (km) (R - restricted depth)

YR	EVT	DATE	HR	MN	SEC	LAT.	LONG.	DEPTH	MAG.	SE	NP	NS	ERT	ERY	ERX	ERZ
90/	001	SEP 02	1112		25.99	43.363S	171.950E	7.5	2.3	0.12	10	7	0.18	.004	.014	0.8
90/	002	SEP 02	1835		44.20	43.386S	171.346E	1.5	3.6	0.25	18	13	0.29	.013	.010	1.5
90/	003	SEP 04	0730		14.33	43.203S	172.171E	8.0	2.1	0.10	16	9	0.03	.002	.003	0.5
90/	004	SEP 04	1734		12.69	42.908S	173.349E	30.0	2.4	0.21	15	9	0.14	.008	.016	2.8
90/	005	SEP 04	1957		03.91	43.286S	171.307E	2.4	2.1	0.21	16	11	0.34	.013	.009	2.3
90/	006	SEP 05	0435		14.84	43.291S	172.018E	0.0	1.6	0.15	9	6	0.17	.006	.006	1.2
90/	007	SEP 05	0858		12.06	43.307S	172.606E	8.6	1.6	0.08	17	11	0.03	.002	.003	0.4
90/	008	SEP 05	2052		42.45	43.140S	172.009E	7.4	2.3	0.10	14	9	0.05	.003	.003	1.0
90/	009	SEP 07	2214		36.40	43.244S	172.884E	24.3	2.1	0.02	6	5	0.06	.001	.005	0.9
90/	010	SEP 07	2220		21.60	43.242S	172.858E	22.1	2.2	0.08	14	11	0.06	.003	.005	1.1
90/	011	SEP 07	2221		41.62	43.243S	172.856E	22.1	2.1	0.08	15	10	0.06	.003	.005	1.1
90/	012	SEP 08	0202		34.75	43.175S	171.552E	5.0R	2.2	0.15	9	5	0.09	.006	.007	R
90/	013	SEP 09	0434		29.32	43.019S	171.743E	3.2	2.5	0.19	22	16	0.13	.006	.007	1.3
90/	014	SEP 09	0532		56.40	43.021S	171.737E	0.8	4.3	0.18	32	24	0.19	.004	.005	1.2
90/	015	SEP 09	0538		12.42	43.034S	171.769E	2.1	1.9	0.06	10	6	0.13	.004	.007	0.9
90/	016	SEP 09	0543		01.84	43.031S	171.772E	3.2	1.8	0.08	13	8	0.09	.004	.007	0.7
90/	017	SEP 09	0547		27.63	43.035S	171.782E	2.2	2.5	0.16	19	12	0.22	.007	.013	1.4
90/	018	SEP 09	0552		18.10	43.033S	171.766E	5.9	1.8	0.13	11	6	0.18	.006	.014	1.2
90/	019	SEP 09	0553		33.99	43.030S	171.768E	3.9	1.8	0.06	12	6	0.07	.003	.005	0.7
90/	020	SEP 09	0559		58.91	43.034S	171.779E	1.1	1.7	0.07	13	8	0.11	.003	.005	0.8
90/	021	SEP 09	0601		04.94	43.029S	171.763E	6.2	1.6	0.09	7	4	0.13	.008	.013	2.4
90/	022	SEP 09	0609		56.05	43.024S	171.738E	6.0	2.5	0.17	24	15	0.09	.005	.005	1.0
90/	023	SEP 09	0615		31.54	43.025S	171.770E	2.1	2.1	0.06	9	5	0.11	.004	.008	0.9
90/	024	SEP 09	0619		46.70	43.025S	171.759E	2.3	2.1	0.18	15	11	0.20	.006	.012	1.7
90/	025	SEP 09	0633		11.04	43.028S	171.764E	1.1	1.7	0.03	7	4	0.05	.002	.005	0.4
90/	026	SEP 09	0643		06.60	43.031S	171.770E	5.1	1.8	0.06	9	5	0.08	.004	.006	1.7
90/	027	SEP 09	0645		52.96	42.727S	172.827E	35.7	1.8	0.11	15	8	0.13	.006	.007	1.1
90/	028	SEP 09	0648		13.39	43.028S	171.760E	3.0	1.8	0.04	7	4	0.06	.003	.005	4.7
90/	029	SEP 09	0653		05.67	43.018S	171.730E	2.8	2.4	0.17	24	16	0.08	.005	.005	1.3
90/	030	SEP 09	0700		39.66	43.026S	171.757E	1.5	1.7	0.04	6	3	0.08	.003	.009	0.8
90/	031	SEP 09	0728		41.75	43.031S	171.767E	5.3	1.6	0.06	7	4	0.14	.004	.009	2.3
90/	032	SEP 09	0807		49.30	43.030S	171.770E	2.7	2.0	0.07	16	10	0.06	.002	.004	0.5
90/	033	SEP 09	0811		49.39	43.031S	171.774E	0.9	2.1	0.04	16	10	0.06	.002	.003	0.5
90/	034	SEP 09	0819		35.83	43.032S	171.773E	3.7	1.8	0.07	15	8	0.07	.003	.005	0.4
90/	035	SEP 09	0827		45.08	43.030S	171.768E	2.8	2.1	0.07	16	9	0.07	.003	.005	0.5
90/	036	SEP 09	0907		53.51	43.030S	171.763E	6.6	1.6	0.07	8	4	0.08	.004	.007	1.5
90/	037	SEP 09	0943		27.28	43.029S	171.773E	5.0R	1.9	0.05	4	3	0.09	.004	.006	R
90/	038	SEP 09	1029		55.32	43.033S	171.768E	6.7	1.7	0.05	8	6	0.06	.003	.005	1.0
90/	039	SEP 09	1313		20.03	43.029S	171.763E	3.5	1.6	0.04	8	5	0.05	.002	.004	2.5
90/	040	SEP 09	1343		38.96	43.022S	171.761E	4.5	1.8	0.05	6	3	0.09	.005	.006	2.2
90/	041	SEP 09	1428		11.01	43.028S	171.766E	0.5	1.7	0.03	5	3	0.08	.003	.010	1.0
90/	042	SEP 09	1500		35.71	43.030S	171.765E	3.1	1.7	0.06	7	4	0.08	.003	.008	0.9
90/	043	SEP 09	1535		00.40	43.030S	171.763E	5.5	1.6	0.05	7	4	0.07	.003	.007	1.3
90/	044	SEP 09	1639		43.50	43.030S	171.759E	1.7	1.6	0.05	6	3	0.09	.004	.011	0.9
90/	045	SEP 09	1955		01.70	43.018S	171.729E	3.3	2.4	0.16	20	13	0.09	.004	.005	0.9
90/	046	SEP 09	2007		42.23	43.034S	171.777E	0.2	1.5	0.01	5	3	0.02	.001	.002	0.2
90/	047	SEP 09	2009		25.60	43.030S	171.763E	3.1	1.9	0.05	11	6	0.06	.002	.005	0.3
90/	048	SEP 09	2200		05.69	43.020S	171.728E	2.7	2.3	0.20	25	18	0.09	.005	.006	1.4
90/	049	SEP 09	2334		56.38	43.028S	171.750E	1.1	2.9	0.24	30	20	0.22	.005	.007	1.3
90/	050	SEP 10	0218		44.50	43.031S	171.772E	4.4	1.7	0.02	8	4	0.03	.001	.002	1.0
90/	051	SEP 10	0223		55.07	43.228S	172.035E	6.3	2.0	0.11	11	6	0.04	.003	.004	1.0
90/	052	SEP 10	0458		14.93	43.030S	171.767E	3.5	1.6	0.08	7	5	0.13	.005	.011	1.5
90/	053	SEP 10	0734		11.33	43.026S	171.780E	1.5	2.3	0.06	10	7	0.10	.004	.009	0.8
90/	054	SEP 10	1244		46.44	42.564S	172.831E	5.0R	1.6	0.11	6	3	0.16	.009	.005	R
90/	055	SEP 10	1943		27.22	43.017S	171.740E	4.3	2.0	0.20	20	14	0.10	.006	.006	1.0
90/	056	SEP 10	2005		12.81	43.019S	171.755E	2.5	2.2	0.04	8	5	0.07	.005	.005	5.9
90/	057	SEP 10	2032		57.32	43.021S	171.734E	2.5	2.8	0.20	28	23	0.09	.005	.006	0.9
90/	058	SEP 11	0727		46.02	43.067S	172.738E	24.4	2.7	0.14	31	20	0.04	.004	.005	0.5
90/	059	SEP 11	0734		09.81	43.020S	171.741E	3.3	1.9	0.19	19	13	0.13	.007	.008	1.2
90/	060	SEP 11	0909		32.20	43.035S	171.769E	3.3	1.9	0.10	12	8	0.11	.005	.008	0.6
90/	061	SEP 11	1336		02.96	43.028S	171.725E	2.0	1.9	0.16	13	8	0.21	.006	.004	1.3
90/	062	SEP 11	2038		13.16	43.189S	172.099E	8.5	1.6	0.14	7	4	0.17	.004	.018	1.5
90/	063	SEP 12	0724		19.84	42.798S	173.157E	26.5	2.0	0.16	16	9	0.08	.007	.010	0.6
90/	064	SEP 12	0846		54.59	43.035S	171.779E	3.0	1.6	0.07	8	4	0.09	.004	.007	0.7
90/	065	SEP 15	1959		13.52	43.032S	171.785E	1.8	1.6	0.06	9	5	0.11	.003	.005	0.7

YR	EVT	DATE	HR	MN	SEC	LAT.	LONG.	DEPTH	MAG.	SE	NP	NS	ERT	ERY	ERX	ERZ
90/	066	SEP 15	2010	25	.08	43.022S	171.752E	3.1	2.8	0.21	25	20	0.10	.005	.006	0.9
90/	067	SEP 16	0146	05	.04	43.033S	171.780E	1.9	2.1	0.11	14	8	0.18	.005	.009	1.1
90/	068	SEP 16	0705	29	.30	43.024S	171.737E	1.8	2.2	0.20	25	17	0.22	.005	.006	1.4
90/	069	SEP 16	0823	52	.08	43.029S	171.753E	2.2	2.4	0.17	14	9	0.23	.006	.006	1.3
90/	070	SEP 16	0958	48	.00	43.027S	171.747E	1.8	2.8	0.15	21	16	0.16	.005	.004	0.9
90/	071	SEP 16	1023	02	.11	43.029S	171.785E	0.2	1.8	0.11	8	5	0.20	.004	.021	2.3
90/	072	SEP 16	2016	00	.65	43.194S	172.110E	10.2	2.0	0.10	6	4	0.14	.005	.016	0.5
90/	073	SEP 16	2103	36	.90	43.020S	171.734E	3.5	2.2	0.19	17	11	0.10	.006	.007	1.2
90/	074	SEP 16	2232	26	.66	43.031S	171.791E	0.7	2.0	0.09	14	8	0.13	.003	.007	1.0
90/	075	SEP 16	2327	29	.07	43.065S	171.808E	22.8	1.7	0.06	6	3	0.10	.008	.007	2.6
90/	076	SEP 17	0136	03	.73	43.062S	171.799E	20.9	2.0	0.03	6	3	0.05	.005	.004	2.2
90/	077	SEP 17	0856	40	.56	43.036S	171.773E	3.5	1.7	0.11	12	7	0.11	.004	.007	1.4
90/	078	SEP 17	1932	37	.77	43.028S	171.787E	0.8	1.8	0.04	9	5	0.07	.002	.003	0.5
90/	079	SEP 17	2332	19	.36	43.227S	171.568E	13.0	2.3	0.19	9	5	0.21	.026	.007	5.2
90/	080	SEP 17	2333	03	.62	43.179S	171.567E	4.7	2.2	0.23	11	6	0.13	.019	.007	2.0
90/	081	SEP 18	1300	40	.40	43.032S	171.786E	8.7	1.6	0.05	8	4	0.05	.002	.003	0.4
90/	082	SEP 19	1109	38	.60	43.016S	171.754E	3.1	2.0	0.20	21	14	0.11	.006	.006	1.3
90/	083	SEP 19	2202	07	.80	43.172S	171.976E	4.7	1.7	0.05	12	8	0.03	.002	.002	0.5
90/	084	SEP 20	0448	15	.13	43.217S	172.316E	9.8	1.6	0.09	13	8	0.03	.002	.003	0.3
90/	085	SEP 21	0311	53	.02	43.056S	171.620E	5.0R	2.1	0.15	15	14	0.21	.006	.015	R
90/	086	SEP 21	1440	13	.71	43.170S	172.156E	8.1	2.0	0.08	17	10	0.03	.002	.003	0.3
90/	087	SEP 21	1820	17	.05	43.445S	171.706E	15.0	1.9	0.04	5	3	0.09	.009	.007	0.6
90/	088	SEP 21	2233	31	.27	43.024S	171.766E	1.2	1.6	0.07	5	3	0.18	.004	.041	3.5
90/	089	SEP 22	0935	02	.36	42.677S	172.821E	11.9	3.5	0.19	32	23	0.07	.005	.006	0.7
90/	090	SEP 23	0346	57	.96	42.853S	172.791E	9.7	1.6	0.05	11	8	0.03	.002	.003	0.4
90/	091	SEP 23	1751	19	.41	43.892S	173.381E	8.1	2.3	0.22	19	15	0.55	.039	.028	3.6
90/	092	SEP 24	0731	40	.81	43.028S	171.774E	0.1	1.6	0.06	9	5	0.11	.003	.007	0.9
90/	093	SEP 24	1452	47	.73	43.029S	171.759E	5.0	1.6	0.05	7	4	0.11	.003	.006	2.7
90/	094	SEP 25	0005	16	.30	43.405S	172.399E	8.0	1.7	0.11	18	12	0.04	.002	.004	0.4
90/	095	SEP 25	0229	43	.81	43.608S	172.753E	3.0R	2.4	0.19	17	12	0.08	.004	.008	R
90/	096	SEP 25	1645	57	.30	43.167S	172.566E	5.4	2.2	0.13	20	16	0.04	.002	.005	1.0
90/	097	SEP 26	0054	09	.68	43.173S	172.497E	23.8	1.7	0.07	17	10	0.03	.002	.003	0.4
90/	098	SEP 26	0907	36	.95	43.026S	171.746E	1.6	1.9	0.06	8	4	0.10	.003	.007	0.8
90/	099	SEP 28	0132	22	.44	43.172S	172.158E	8.2	1.8	0.06	9	6	0.05	.002	.003	0.4
90/	100	SEP 28	2230	57	.65	43.016S	171.778E	5.8	1.9	0.05	6	3	0.11	.006	.004	1.6
90/	101	SEP 29	1354	00	.90	43.181S	171.581E	7.5	1.7	0.07	7	4	0.13	.004	.010	1.1
90/	102	SEP 30	0812	17	.86	43.462S	172.875E	18.2	2.0	0.16	9	5	0.08	.011	.011	2.2
90/	103	SEP 30	1701	32	.61	43.173S	172.153E	7.8	2.1	0.06	21	14	0.02	.001	.002	0.2
90/	104	OCT 01	0516	18	.54	42.999S	171.547E	9.6	2.1	0.12	9	5	0.17	.006	.012	0.9
90/	105	OCT 01	1213	06	.65	43.027S	171.767E	5.2	1.5	0.09	8	4	0.12	.004	.007	2.8
90/	106	OCT 01	1644	23	.40	43.328S	172.348E	7.8	2.0	0.08	22	12	0.02	.001	.002	0.3
90/	107	OCT 01	1752	04	.50	42.735S	172.811E	22.6	2.5	0.08	18	10	0.04	.003	.003	0.5
90/	108	OCT 02	1501	16	.27	42.999S	171.543E	8.2	2.0	0.08	9	5	0.13	.008	.009	1.5
90/	109	OCT 03	1124	44	.01	43.175S	171.568E	2.4	2.1	0.15	20	15	0.19	.005	.004	1.2
90/	110	OCT 04	0302	57	.61	43.160S	172.322E	9.9	2.0	0.07	26	16	0.02	.001	.002	0.2
90/	111	OCT 04	0428	43	.66	43.291S	172.013E	3.0R	1.7	0.16	15	11	0.05	.004	.005	R
90/	112	OCT 04	2248	56	.30	42.765S	172.355E	5.8	2.4	0.06	19	13	0.03	.002	.002	0.3
90/	113	OCT 05	0235	21	.63	43.020S	171.758E	3.6	1.5	0.10	8	4	0.13	.005	.010	4.9
90/	114	OCT 05	1416	18	.36	43.199S	172.170E	9.3	2.2	0.06	14	8	0.02	.002	.002	0.2
90/	115	OCT 06	2159	33	.45	43.378S	171.836E	8.4	2.8	0.11	14	9	0.08	.003	.007	0.5
90/	116	OCT 07	2123	53	.13	43.223S	171.652E	4.8	2.3	0.13	22	18	0.07	.003	.005	0.6
90/	117	OCT 08	1624	16	.06	42.990S	172.614E	8.2	2.5	0.10	22	13	0.03	.002	.002	0.3
90/	118	OCT 09	1056	19	.62	43.106S	172.573E	5.4	1.7	0.08	15	9	0.04	.002	.002	0.4
90/	119	OCT 10	0756	16	.90	43.042S	172.643E	7.5	2.2	0.12	19	11	0.05	.003	.003	0.5
90/	120	OCT 10	0842	58	.73	43.220S	171.661E	2.3	2.7	0.21	29	20	0.21	.005	.006	1.3
90/	121	OCT 10	0848	42	.72	43.220S	171.673E	4.6	1.8	0.06	8	4	0.07	.002	.003	1.4
90/	122	OCT 10	1319	21	.67	43.011S	171.754E	1.6	1.8	0.08	15	8	0.10	.003	.005	0.8
90/	123	OCT 10	1536	05	.87	43.257S	172.449E	7.0	2.1	0.05	10	6	0.03	.002	.002	0.3
90/	124	OCT 10	1831	59	.81	42.986S	172.282E	1.2	1.5	0.08	13	7	0.14	.002	.003	0.9
90/	125	OCT 11	1044	25	.13	43.043S	171.712E	7.0	1.9	0.08	7	4	0.17	.011	.007	1.9
90/	126	OCT 11	1634	49	.98	43.112S	171.558E	5.0R	1.8	0.08	10	5	0.08	.003	.005	R
90/	127	OCT 11	1804	16	.79	43.104S	171.525E	5.0R	1.8	0.21	15	8	0.09	.007	.006	R
90/	128	OCT 11	2232	51	.41	42.845S	173.040E	32.8	2.2	0.12	14	8	0.08	.006	.007	0.9
90/	129	OCT 12	1119	53	.85	43.022S	173.416E	19.4	2.4	0.17	15	9	0.19	.012	.014	0.9
90/	130	OCT 12	1400	50	.20	42.937S	173.010E	25.3	1.7	0.16	12	7	0.10	.010	.010	0.7

YR	EVT	DATE	HR	MN	SEC	LAT.	LONG.	DEPTH	MAG.	SE	NP	NS	ERT	ERY	ERX	ERZ
90/	131	OCT 13	0807	47	28	43.295S	172.930E	20.9	2.1	0.07	13	8	0.05	.002	.007	0.8
90/	132	OCT 13	1241	28	48	43.240S	172.849E	26.2	2.2	0.11	11	6	0.08	.007	.009	1.0
90/	133	OCT 13	1428	57	87	43.373S	172.393E	19.6	1.9	0.10	21	12	0.03	.002	.004	0.3
90/	134	OCT 15	1402	11	61	43.001S	172.057E	1.7	1.8	0.04	9	5	0.05	.001	.001	0.3
90/	135	OCT 17	0059	36	20	43.034S	171.777E	2.8	2.6	0.12	25	17	0.10	.003	.007	0.6
90/	136	OCT 17	0429	33	29	43.041S	171.731E	2.5	2.4	0.18	18	13	0.08	.007	.005	1.3
90/	137	OCT 17	1909	56	08	43.028S	171.578E	5.0R	2.2	0.30	10	6	0.15	.019	.009	R
90/	138	OCT 18	0152	27	30	43.481S	172.190E	9.6	2.4	0.06	6	4	0.11	.005	.006	0.8
90/	139	OCT 18	0956	38	98	43.166S	172.387E	9.2	1.9	0.07	32	19	0.02	.001	.001	0.2
90/	140	OCT 18	1815	15	77	42.997S	171.723E	2.2	2.1	0.17	23	15	0.19	.004	.005	1.2
90/	141	OCT 18	2148	34	85	42.594S	173.185E	41.6	2.2	0.23	14	8	0.25	.010	.023	4.1
90/	142	OCT 22	0316	15	40	42.583S	172.841E	2.5	2.5	0.16	12	7	0.12	.006	.006	1.8
90/	143	OCT 22	0331	00	10	43.183S	171.597E	4.4	2.2	0.16	18	14	0.14	.005	.010	0.8
90/	144	OCT 23	1042	38	72	42.728S	172.608E	37.5	2.0	0.16	11	6	0.20	.011	.011	1.9
90/	145	OCT 24	1817	48	77	43.021S	171.761E	1.4	2.0	0.03	8	4	0.06	.006	.004	0.9
90/	146	OCT 26	0959	27	16	43.261S	172.458E	8.2	1.4	0.08	17	9	0.03	.002	.003	0.4
90/	147	OCT 28	0440	16	15	42.796S	171.614E	9.4	1.9	0.30	11	7	0.36	.013	.021	2.7
90/	148	OCT 28	0835	27	84	43.154S	171.660E	5.0R	1.6	0.07	8	4	0.11	.006	.007	R
90/	149	OCT 28	1311	04	74	42.849S	172.793E	7.2	2.3	0.07	20	12	0.02	.002	.002	0.4
90/	150	OCT 28	2049	12	80	43.147S	171.645E	4.8	2.7	0.17	17	12	0.09	.005	.006	1.1
90/	151	OCT 29	0112	21	11	42.997S	171.438E	5.0R	2.9	0.21	16	14	0.10	.008	.006	R
90/	152	OCT 30	2313	55	91	43.032S	171.771E	5.8	1.8	0.04	13	7	0.03	.002	.002	0.7
90/	153	OCT 31	0722	00	65	43.149S	171.658E	5.0R	1.3	0.09	6	3	0.14	.006	.008	R
90/	154	OCT 31	0724	20	32	43.153S	171.662E	3.9	1.4	0.08	8	4	0.13	.005	.007	2.8
90/	155	OCT 31	0730	40	50	43.202S	172.107E	9.2	2.3	0.12	23	14	0.03	.003	.003	0.4
90/	156	OCT 31	1318	18	25	43.011S	171.754E	3.3	1.7	0.07	15	8	0.06	.003	.004	0.8
90/	157	OCT 31	1704	19	40	43.160S	171.674E	4.2	2.4	0.10	22	14	0.07	.003	.005	0.5
90/	158	OCT 31	2118	05	78	42.745S	171.633E	5.0R	1.8	0.28	6	4	0.42	.027	.037	R
90/	159	NOV 01	0042	22	19	42.454S	172.882E	2.8	2.5	0.24	24	15	0.09	.005	.009	1.2
90/	160	NOV 01	0512	34	05	42.931S	171.700E	10.6	1.9	0.18	11	6	0.19	.007	.013	1.2
90/	161	NOV 01	0529	36	50	42.444S	173.017E	5.0R	1.9	0.29	10	6	0.25	.018	.016	R
90/	162	NOV 01	0712	03	56	43.430S	171.488E	2.5	2.0	0.15	21	12	0.10	.006	.005	0.9
90/	163	NOV 01	0923	38	96	43.038S	171.535E	5.0R	1.3	0.24	9	5	0.31	.009	.021	R
90/	164	NOV 01	1039	26	66	42.910S	171.671E	2.3	2.5	0.21	30	19	0.20	.005	.008	1.2
90/	165	NOV 01	1411	58	93	43.148S	171.654E	2.2	1.5	0.05	7	4	0.09	.005	.007	1.0
90/	166	NOV 01	1424	12	03	42.951S	172.128E	7.2	1.6	0.06	10	5	0.09	.002	.004	1.5
90/	167	NOV 01	2008	49	98	42.905S	171.671E	2.7	2.4	0.19	22	14	0.14	.006	.009	1.2
90/	168	NOV 02	0041	18	68	42.848S	171.644E	5.0R	1.8	0.39	12	8	0.33	.016	.026	R
90/	169	NOV 02	0321	36	35	42.432S	172.797E	5.0R	2.1	0.24	7	4	0.38	.010	.045	R
90/	170	NOV 02	0616	24	50	42.099S	173.642E	18.0	2.3	0.26	9	5	0.48	.015	.058	2.6
90/	171	NOV 02	0858	12	71	42.221S	172.701E	0.8	2.4	0.37	19	12	0.59	.010	.019	3.8
90/	172	NOV 02	0904	43	01	42.221S	172.701E	2.4	2.3	0.32	18	13	0.54	.008	.015	3.5
90/	173	NOV 02	0921	42	87	43.174S	172.157E	7.2	2.3	0.08	17	12	0.04	.002	.004	0.3
90/	174	NOV 02	1032	11	03	42.606S	172.857E	34.0	2.6	0.17	11	6	0.14	.012	.010	2.3
90/	175	NOV 02	2132	10	45	42.592S	172.844E	5.3	2.4	0.17	27	19	0.07	.004	.005	0.8
90/	176	NOV 02	2311	44	08	42.999S	171.723E	2.4	2.5	0.18	32	21	0.16	.004	.005	1.0
90/	177	NOV 03	0226	48	47	43.014S	171.759E	2.3	2.2	0.11	27	17	0.13	.004	.006	0.9
90/	178	NOV 03	0329	25	27	43.007S	171.746E	5.0	1.7	0.05	10	5	0.05	.003	.005	1.9
90/	179	NOV 03	0610	27	45	42.856S	173.023E	32.6	2.1	0.16	8	5	0.26	.019	.026	1.9
90/	180	NOV 03	0804	07	88	42.230S	172.664E	5.0R	2.2	0.42	25	17	0.17	.010	.020	R
90/	181	NOV 04	0649	50	07	43.013S	171.754E	7.6	1.7	0.06	11	6	0.06	.003	.005	1.0
90/	182	NOV 04	0823	43	95	43.012S	171.758E	7.3	1.4	0.05	11	6	0.05	.002	.003	1.1
90/	183	NOV 05	2028	35	28	42.868S	171.612E	9.9	1.7	0.19	10	5	0.29	.011	.017	1.5
90/	184	NOV 06	0534	48	37	43.022S	171.767E	4.3	1.7	0.11	13	7	0.10	.004	.007	3.8
90/	185	NOV 06	0633	42	29	43.030S	171.770E	5.1	1.3	0.08	10	5	0.10	.005	.006	2.4
90/	186	NOV 06	0849	40	54	43.015S	171.756E	7.4	1.3	0.08	7	4	0.08	.005	.006	2.0
90/	187	NOV 06	1510	36	56	43.173S	172.152E	7.7	2.0	0.05	8	4	0.03	.003	.002	0.3
90/	188	NOV 07	0614	08	77	43.328S	172.214E	8.2	1.7	0.09	13	8	0.04	.002	.004	0.5
90/	189	NOV 07	0904	07	48	42.751S	172.380E	17.0	2.7	0.17	22	12	0.11	.009	.006	0.7
90/	190	NOV 07	1839	47	51	42.842S	173.063E	32.2	2.2	0.04	8	4	0.07	.002	.005	0.5
90/	191	NOV 07	2138	25	96	42.740S	171.753E	8.3	1.9	0.18	11	6	0.15	.006	.011	1.3
90/	192	NOV 09	1550	01	21	43.071S	172.349E	8.8	2.0	0.11	27	17	0.03	.002	.002	0.3
90/	193	NOV 09	1753	02	40	43.245S	171.928E	5.1	1.5	0.10	12	6	0.09	.003	.003	2.2
90/	194	NOV 09	1818	38	32	42.601S	172.843E	5.1	2.1	0.09	8	4	0.15	.009	.004	3.6
90/	195	NOV 09	1847	34	65	43.241S	171.922E	4.5	1.3	0.07	10	6	0.03	.002	.003	0.8

YR	EVT	DATE	HR	MN	SEC	LAT.	LONG.	DEPTH	MAG.	SE	NP	NS	ERT	ERY	ERX	ERZ
90/	196	NOV 09	2331		47.97	42.851S	172.798E	8.7	1.9	0.05	13	8	0.04	.002	.002	0.4
90/	197	NOV 09	2352		43.74	43.001S	173.427E	21.7	2.5	0.19	19	11	0.13	.008	.011	1.3
90/	198	NOV 11	0512		39.68	42.913S	171.678E	1.9	2.2	0.27	16	10	0.39	.012	.023	3.3
90/	199	NOV 11	1319		16.11	43.017S	171.561E	0.3	1.8	0.18	12	6	0.28	.009	.019	1.8
90/	200	NOV 12	0020		52.87	43.845S	171.505E	12.6	2.2	0.04	8	5	0.08	.004	.006	0.4
90/	201	NOV 12	0954		11.61	43.006S	172.038E	9.6	2.4	0.09	14	8	0.04	.003	.003	0.4
90/	202	NOV 12	0958		31.24	43.224S	172.602E	8.7	1.7	0.12	22	12	0.05	.002	.004	0.4
90/	203	NOV 12	1555		19.98	42.806S	172.308E	8.2	1.7	0.08	7	4	0.08	.004	.005	0.5
90/	204	NOV 12	1900		28.41	42.784S	171.633E	5.0R	3.0	0.43	31	20	0.26	.011	.021	R
90/	205	NOV 13	0903		10.46	42.797S	171.991E	2.6	2.8	0.20	26	15	0.14	.007	.007	1.1
90/	206	NOV 13	1442		14.64	43.027S	171.770E	5.4	2.1	0.04	8	4	0.06	.004	.003	1.1
90/	207	NOV 13	1735		08.38	43.057S	171.376E	1.6	2.3	0.36	17	10	0.53	.011	.011	3.3
90/	208	NOV 13	1939		08.83	43.138S	171.681E	4.2	2.3	0.09	13	7	0.10	.005	.006	0.6
90/	209	NOV 14	0324		58.60	43.274S	171.962E	7.1	2.7	0.14	20	10	0.04	.004	.004	0.7
90/	210	NOV 14	0547		35.20	41.958S	172.757E	39.7	2.0	2.85	21	12	2.90	.147	.210	45.7
90/	211	NOV 14	1837		09.62	42.207S	172.725E	3.9	2.0	0.60	15	8	0.28	.014	.028	6.1
90/	212	NOV 15	1236		35.23	43.026S	172.343E	26.1	2.2	0.13	21	11	0.04	.004	.005	0.4
90/	213	NOV 15	1242		47.05	43.027S	172.347E	26.4	1.9	0.11	18	9	0.04	.003	.004	0.3
90/	214	NOV 15	1654		35.02	42.202S	172.739E	0.7	2.3	0.48	20	11	0.65	.015	.025	3.8
90/	215	NOV 16	1852		31.85	43.140S	171.684E	5.0R	1.3	0.09	10	5	0.08	.004	.007	R

APPENDIX 4.5 FAULT-PLANE SOLUTIONS

Introduction

In this study, the principal references to the derivation and interpretation of P-wave first-motions and fault-plane solutions are: McKenzie (1969); Aki and Richards (1980); Lee and Stewart (1981); Molnar and Chen (1982); and Zoback and Zoback (1991). Only a brief outline of the methodology and principal assumptions is provided here.

P-wave first-motions

P-wave first motions are determined from vertical component seismograms (e.g. Fig.2.1). The rays are then traced back to the focal sphere, where the position of a given seismic station on the surface of the focal sphere is defined by two angles α and ß. Alpha (α) is the azimuthal angle (clockwise from north) from the earthquake epicentre to the station. Beta (ß) is the take-off angle (with respect to vertical) of the P-wave from the hypocentre to the station. The former is computed from the coordinates of the hypocentre and station; the latter from the travel time derivatives.

The set of first motion polarities are plotted on an equal-area projection - lower hemisphere projections of a focal mechanism program FM (in-house software at Institute of Geophysics, Victoria University, Wellington), were used in this study. For the lower hemisphere projection, direct arrivals (up-going rays: ß>90°) are plotted by substituting (180° + α) for α, and (180° - ß) for ß.

Fault-plane solution

Deriving a fault-plane solution amounts to finding the two orthogonal nodal planes which separate the first motions of P-waves into compressional and dilatational quadrants on the focal sphere. The fault-plane solution illustrated below is for an event of Ml.9 recorded on the North Canterbury Network, located about 9 km beneath Mt Thomas (solution no.22: Fig.4.9). Seismograms of the same event are illustrated in Figure 2.1. The solid dots and open circles represent compressions and dilatations, respectively.

The arc WABE represents the projection of a nodal plane that strikes 085° and dips 84°S. The pole to this nodal plane is point C, which is 90° from the arc WABE, and lies in the second nodal plane defined by the arc NCBS. The nodal plane NCBS strikes 353° and dips 72°E, and its pole (point A) lies in the first nodal plane (WABE). The line of

intersection between the two planes is point B, which is known as the null axis (no displacement). The plane normal to the null axis is represented by the arc CPAT, which contains the T-axis (T) and P-axis (P).

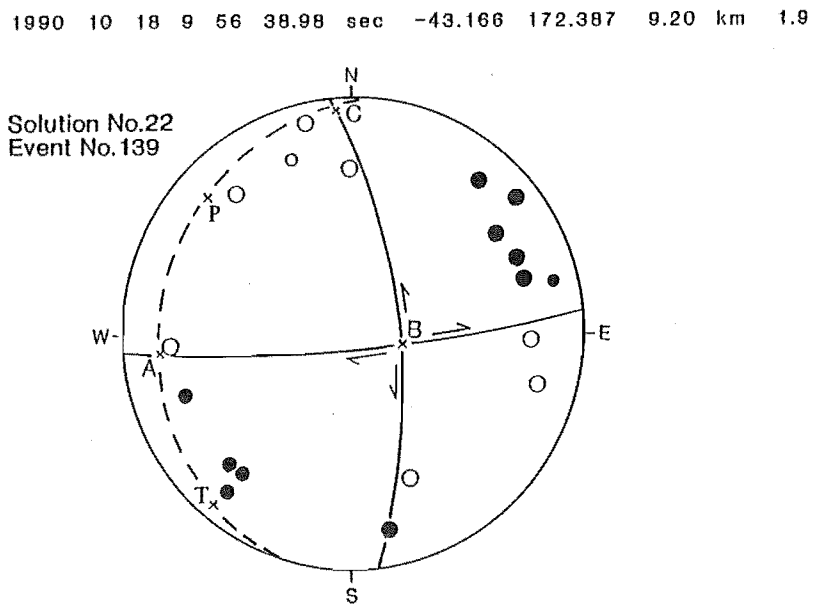

P and T axes

For shear failure in a homogeneous rock-mass the T-axis is c.45° from the A and C axes, and the P-axis is 90° from the T-axis. For this general case, the P and T axes are assumed to represent the maximum compressive and tensile stresses, respectively. The slip vector is assumed to be parallel to the resolved shearing stress in the fault-plane, and is defined as the pole to the auxiliary plane. In heterogeneous rocks with pre-existing faults, however, the slip vector is a function both of the orientation of the fault and the orientation and relative magnitude of the principal stresses. Consequently, the P and T axes of the focal mechanism will provide only an approximation of the principal stress directions. The P and T axes for shallow (<12 km) events recorded in this study are consistent with previous estimates of relative compression in North Canterbury, derived from geodetic measurements and stress tensor analysis of geological structures (Bibby, 1981; Nicol and Wise, in press, respectively). However, because P and T axes for focal mechanisms represent strain (not stress), the terms contractional and

tensile strain are used in this study.

Interpreting the fault-plane solution

It is not possible to determine from P-wave first motions alone, which nodal plane represents the fault-plane. For the example given above, the complexity of surface faulting at Mt Thomas is such that either nodal plane could be the fault-plane. However, the strike of the principal fault zone at this locality is approximately west-east, so the preferred fault plane is the arc WABE. The inferred mechanism thus indicates right-lateral strike-slip faulting and a slip vector (point A) of 264°/18°. However, when an event is recorded on fewer stations, the correct orientation of the nodal planes may be equivocal. This point is illustrated by the following example, an M2.0 event located in the lower crust beneath northern North Canterbury.

1990 9 12 7 24 19.84 sec -42.798 173.157 26.50 km 2.0

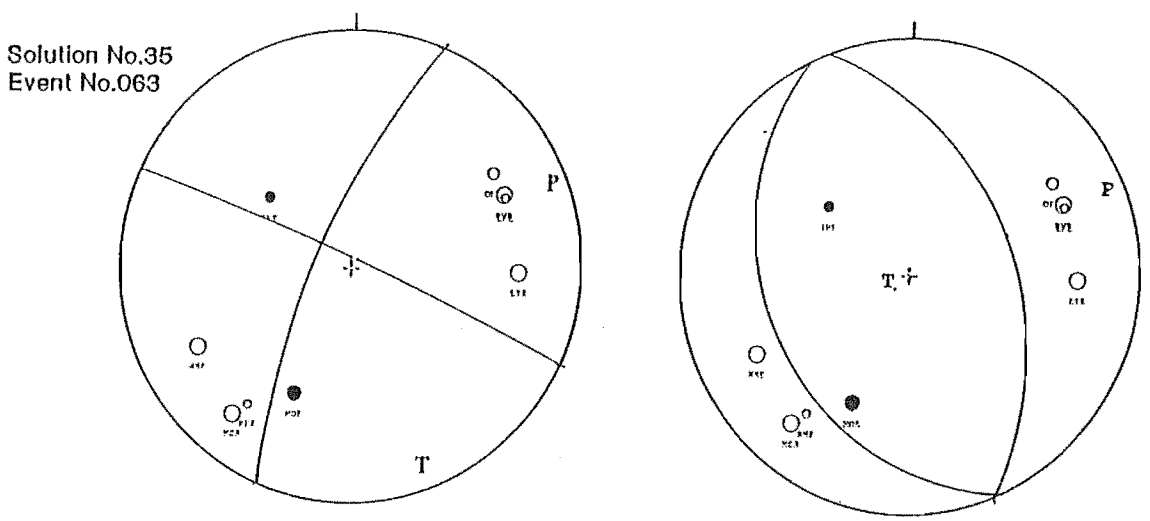

First-motion polarities for this event can be separated into compressional and dilatational quadrants, but the data are consistent with: 1) thrust faulting on one of two, NNW/SSE-striking nodal planes; or 2) strike-slip faulting on a NW-striking nodal plane (left-lateral), or NNE-striking nodal plane (right-lateral). The P-axes are similar for both solutions, but the T-axes are orthogonal. The mechanism is poorly constrained and is accorded a low-confidence weighting (Appendix 4.6).

Appendix 4.6 Listing of events used for fault-plane solutions (Appendix 4.7)

Solution[1] No	Date[2]	Time[2] Hr Mn	Sec	Event No.[3]	Location S.Lat.	E. Long.	Depth[4]	Mag.	Plane 1[5] Strike	Dip	Slip Vector[6]	Plane 2 Strike	Dip	Slip Vector	P-Axis[7]	T-Axis[7]
1(2)	19900904	0730	14.33	003	43.203	172.171	8.00	2.1	266	81N	084/09	174	81W	175/09	130/12	220/00
2(2)	19900905	0858	12.06	007	43.307	172.606	8.6	1.6	252	89N	252/07	342	83E	162/01	298/02	208/06
3(2)	19900905	2052	42.45	008	43.140	172.009	7.4	2.3	244	90	063/00	334	90	152/00	108/00	198/00
4(3)	19900920	0448	15.13	084	43.217	172.316	9.8	1.6	119	54S	293/08	023	82E	030/36	335/32	076/17
5(2)	19900921	1440	13.71	086	43.170	172.156	8.1	2.0	313	78E	126/29	216	61W	222/12	083/13	180/29
6(2)	19900922	0935	02.36	089	42.677	172.821	11.90	3.5	259	89N	078/16	169	74W	169/01	125/12	034/09
7(3)	19900925	0005	16.30	094	43.405	172.399	8.0	1.7	022	71E	193/23	283	67N	290/19	151/02	243/30
8(3)	19900925	1645	57.30	096	43.167	172.566	5.4	2.2	233	80N	051/12	141	78S	142/10	094/16	006/07
9(1)	19900930	1701	32.61	103	43.173	172.153	7.8	2.1	255	76N	258/06	347	84E	166/14	123/10	213/08
10(3)	19901001	1644	23.40	106	43.328	172.348	7.8	2.0	238	70N	052/20	141	70S	149/20	102/29	192/00
11(1)	19901004	0302	57.61	110	43.160	172.322	9.9	2.0	082	84S	263/06	352	84E	353/06	306/09	219/00
12(3)	19901004	2248	56.30	112	42.765	172.355	5.8	2.4	270	74N	064/57	154	33W	179/16	144/52	022/24
13(3)	19901005	1416	18.36	114	43.199	172.170	9.3	2.2	084	68S	256/23	345	67E	352/22	302/32	214/00
14(3)	19901006	2159	33.45	115	43.378	171.836	8.4	2.8	259	73N	043/21	163	69W	169/17	122/27	031/02
15(2)	19901007	2123	53.13	116	43.223	171.652	4.8	2.3	160	52W	285/47	014	43E	071/38	267/06	010/72
16(2)	19901008	1624	16.06	117	42.990	172.614	8.2	2.5	330	50E	336/09	067	80E	240/39	296/34	192/18
17(3)	19901009	1056	19.62	118	43.106	172.573	5.4	1.7	136	78SW	315/07	045	83SE	046/12	090/04	000/13
18(2)	19901010	0756	16.90	119	43.042	172.643	7.5	2.2	336	54E	132/31	220	60NW	247/34	278/01	188/50
19(2)	19901010	0842	58.73	120	43.220	171.661	2.3	2.7	185	56W	326/42	056	48SE	094/34	300/06	038/62
20(3)	19901010	1536	05.87	123	43.257	172.449	7.0	2.1	254	57N	338/56	068	34S	164/33	342/10	072/79
21(3)	19901010	1831	59.81	124	42.986	172.282	1.2	1.5	210	80W	238/66	326	24NE	119/10	283/30	140/50
22(1)	19901018	0956	38.98	139	43.166	172.387	9.2	1.9	085	84S	264/18	353	72E	356/06	312/17	219/06
23(2)	19901028	1311	04.74	149	42.849	172.793	7.2	2.3	349	83E	349/06	079	84S	260/07	303/10	214/00
24(1)	19901031	0730	40.50	155	43.202	172.107	9.2	2.3	246	83N	062/25	152	65W	155/07	110/22	018/12
25(1)	19901102	0921	42.87	173	43.174	172.157	7.2	2.3	086	90	267/18	356	72E	356/00	314/13	221/11
26(1)	19901109	1550	01.21	192	43.071	172.349	8.8	2.0	073	67S	241/32	330	58E	344/23	292/40	202/06
27(3)	19901109	2331	47.97	196	42.851	172.798	8.7	1.9	254	84N	257/22	347	68E	164/06	302/10	208/18
28(3)	19901112	0954	11.61	201	43.006	172.038	9.6	2.4	076	84S	079/12	169	78W	348/06	122/04	032/13
29(1)	19901112	0958	31.24	202	43.224	172.602	8.7	1.7	080	84S	261/09	350	81E	350/06	306/10	215/01
30(2)	19901114	0324	58.60	209	43.274	171.962	7.1	2.7	076	88S	257/14	346	76E	346/02	302/12	211/08
31(3)	19900904	1734	12.69	004	42.908	173.349	30	2.4	263	40N	045/30	136	63S	173/50	203/13	091/60
32(2)**	19900907	2220	21.60	010	43.242	172.858	22.1	2.2	057	65S	216/41	306	52E	327/25	277/43	180/02
	19900907	2221	41.62	011	43.243	172.856	22.1	2.1								
33(2)	19900909	0645	52.96	027	42.727	172.827	35.7	1.8	193	72W	196/10	284	80N	103/18	058/06	151/19
34(2)	19900911	0727	46.02	058	43.067	172.738	24.4	2.7	217	88W	216/04	307	86N	126/02	262/02	171/04

$35_{(3)}$	19900912	0724	19.84	063	42.798	173.157	26.5	2.0	203	76W	204/04	292	86N	112/14	067/04	160/14
$36_{(1)}$	19900926	0054	09.68	097	43.173	172.497	23.8	1.7	184	54W	230/46	320	44E	093/36	253/04	154/65
$37_{(3)}$	19900930	0812	17.86	102	43.462	172.875	18.2	2.0	274	22N	339/22	068	68S	183/68	324/64	165/24
$38_{(2)}$	19901001	1752	04.50	107	42.735	172.811	22.6	2.5	244	60N	262/30	352	60E	152/30	208/44	297/01
$39_{(3)}$	19901011	2232	51.41	128	42.845	173.040	32.8	2.2	121	79S	279/64	008	26E	031/11	003/50	231/30
$40_{(3)}$	19901012	1119	53.85	129	43.022	173.416	19.4	2.4	018	87E	032/80	124	10S	288/03	299/47	098/41
$41_{(3)}$	19901012	1400	50.20	130	42.937	173.010	25.3	1.7	277	67N	343/66	073	24S	188/23	000/22	205/66
$42_{(2)}$**	19901013	0807	47.28	131	43.295	172.930	20.9	2.1	075	59S	236/29	325	61E	346/36	289/46	020/02
	19901013	1241	28.48	132	43.240	172.849	26.2	2.2								
$43_{(1)}$	19901013	1428	57.87	133	43.373	172.393	19.6	1.9	074	50S	251/03	341	87E	345/40	290/29	035/25
$44_{(2)}$	19901018	2148	34.85	141	42.594	173.185	41.6	2.2	192	67W	197/14	287	76N	102/23	057/08	151/25
$45_{(2)}$**	19901023	1042	38.72	144	42.728	172.608	37.5	2.0	355	86E	170/53	260	37N	266/04	233/38	115/32
	19901102	1032	11.03	174	42.606	172.857	34.0	2.6								
$46_{(2)}$**	19901103	0610	27.45	179	42.856	173.023	32.6	2.1	289	48N	343/41	072	49S	200/42	272/69	180/01
	19901107	1839	47.51	190	42.842	173.063	32.2	2.2								
$47_{(2)}$	19901107	0904	07.48	189	42.751	172.380	17.0	2.7	340	66E	021/54	110	36S	252/24	295/64	052/18
$48_{(3)}$	19901109	2352	43.74	197	43.001	173.427	21.7	2.5	009	74E	184/20	272	70N	278/16	232/28	142/01
$49_{(2)}$**	19901115	1236	35.23	212	43.026	172.343	26.1	2.2	218	67NW	034/10	124	80S	128/23	078/24	173/10
	19901115	1242	47.05	213	43.027	172.347	26.4	1.9								

NOTES

(1) Lower focal hemisphere (schmidt) projections of P-wave first motions: Appendix 4.7
Subscripts denote relative robustness of fault-plane solution:
Confidence $_{(1)}$ max rotation of both nodal planes $\leq 10^o$
Confidence $_{(2)}$ " " one or both nodal planes $\leq 20^o$
Confidence $_{(3)}$ " " one or both " " $\geq 20^o$

(2) Date and time in U.T.

(3) Hypocentre list: Appendix 4.4

(4) See Appendix 4.4 for formal errors.

(5) Nodal planes from lower focal hemisphere projections in Appendix 4.7. Plane 1 represents the fault plane inferred from surface fault geometries.

(6) Slip vector for fault displacement expressed as trend and plunge normal to the auxiliary plane. Note that Plane 1 represents the preferred choice of fault plane.

(7) Trend and plunge of maximum contractional and tensile strain axes (P and T axes), respectively.

** indicates composite solution. Header for second event only on focal sphere: Appendix 4.7.

1990 9 4 7 30 14.33 sec -43.203 172.171 8.00 km 2.1

Solution No.1
Event No.003

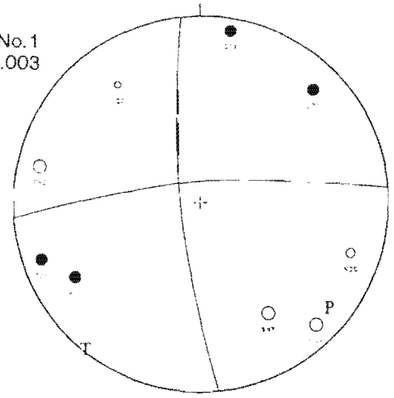

1990 9 5 8 58 12.06 sec -43.307 172.606 8.60 km 1.6

Solution No.2
Event No.007

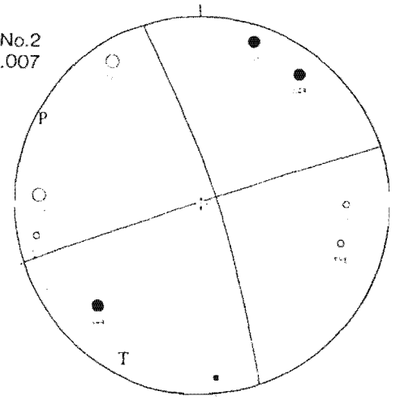

1990 9 5 20 52 42.45 sec -43.140 172.009 7.40 km 2.3

Solution No.3
Event No.008

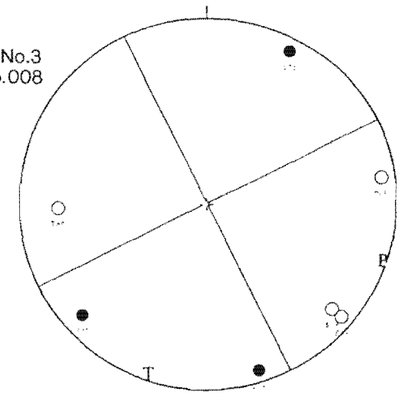

1990 9 20 4 48 15.13 sec -43.217 172.316 9.80 km 2.1

Solution No.4
Event No.084

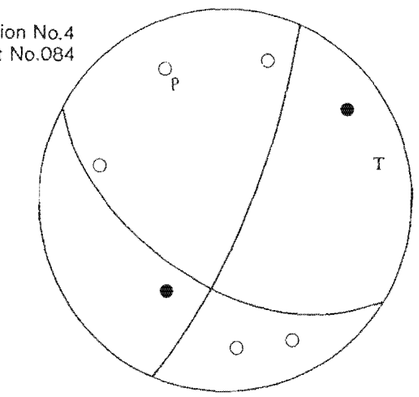

1990 9 21 14 40 13.71 sec -43.170 172.156 8.10 km 2.0

Solution No.5
Event No.086

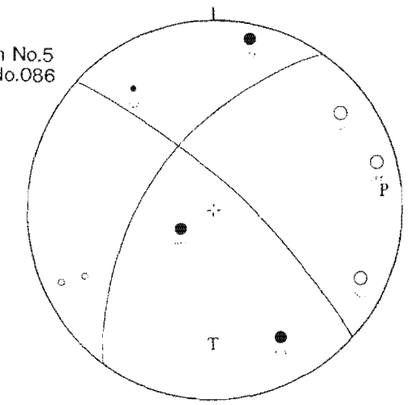

1990 9 22 9 35 2.36 sec -42.677 172.821 11.90 km 3.5

Solution No.6
Event No.089

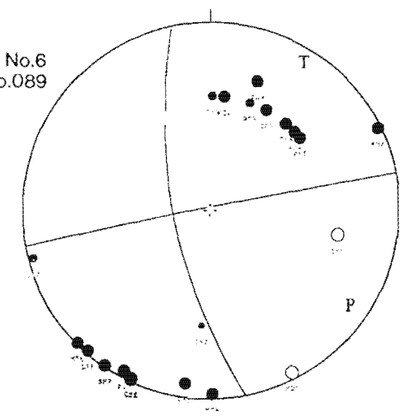

1990 9 25 0 5 16.30 sec -43.405 172.399 8.00 km 1.7

Solution No.7
Event No.094

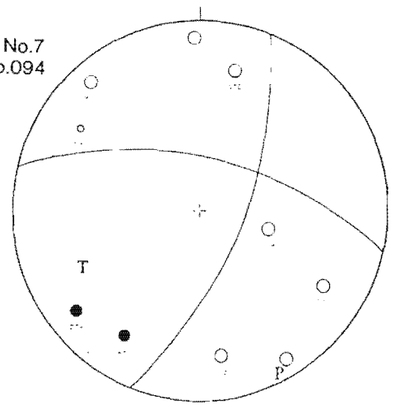

1990 9 25 16 45 57.30 sec -43.167 172.566 5.40 km 2.2

Solution No.8
Event No.096

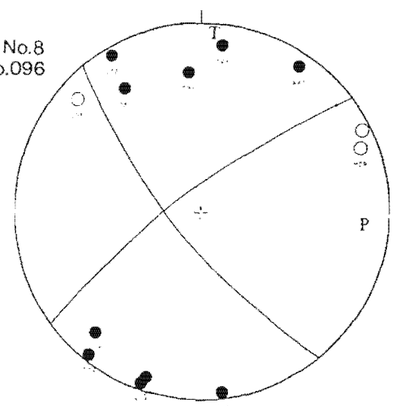

1990 9 30 17 1 32.61 sec -43.173 172.153 7.80 km 2.1

Solution No.9
Event No.103

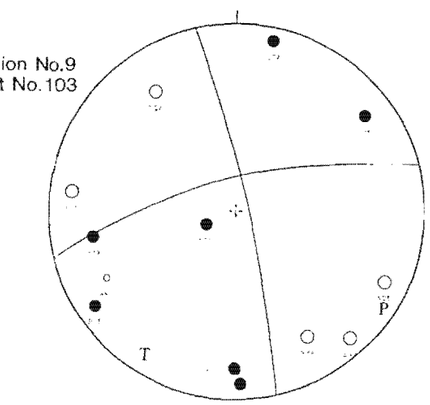

Solid dots are compressions
Open circles are dilatations

Larger symbols represent impulsive arrivals
Smaller symbols represent emergent arrivals

APPENDIX 4.7 Lower focal hemisphere fault plane solutions of events listed in Appendices 4.4 and 4.6

1990 10 1 16 44 23.40 sec -43.328 172.348 7.80 km 2.0

Solution No.10
Event No.106

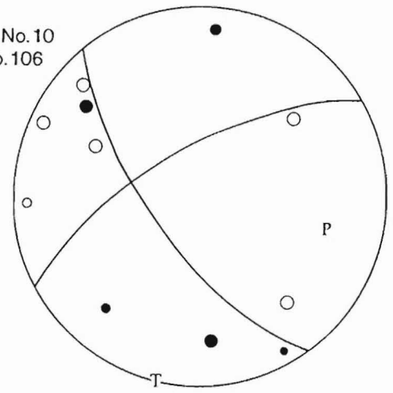

1990 10 4 3 2 57.61 sec -43.160 172.322 9.90 km 2.0

Solution No.11
Event No.110

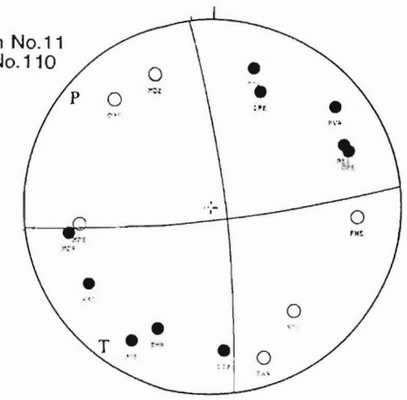

1990 10 4 22 48 56.30 sec -42.765 172.355 5.80 km 2.4

Solution No.12
Event No.112

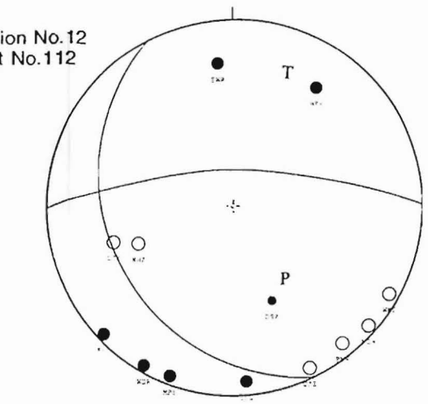

1990 10 5 14 16 18.36 sec -43.199 172.170 9.30 km 2.2

Solution No.13
Event No.114

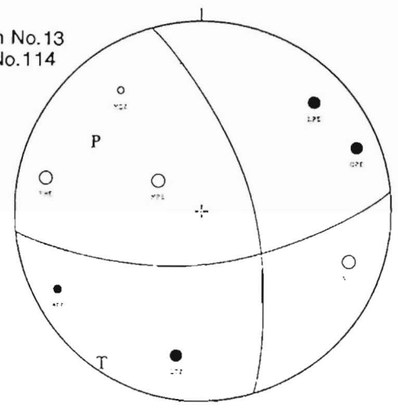

1990 10 6 21 59 33.45 sec -43.378 171.836 8.40 km 2.8

Solution No.14
Event No.115

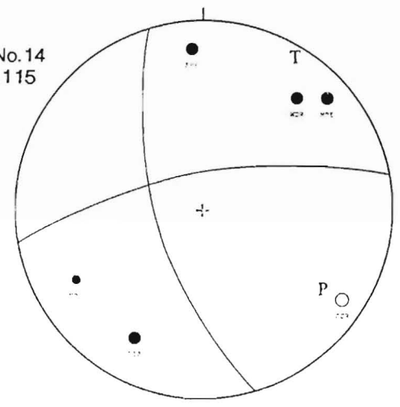

1990 10 7 21 23 53.13 sec -43.223 171.652 4.80 km 2.3

Solution No.15
Event No.116

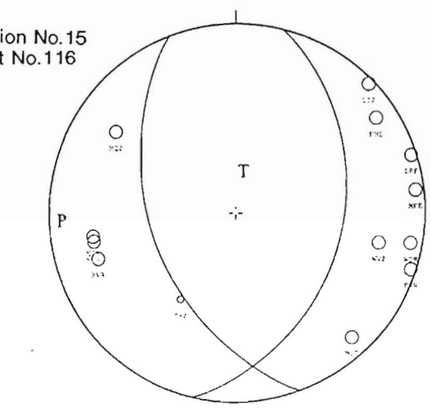

1990 10 8 16 24 16.06 sec -42.990 172.614 8.20 km 2.5

Solution No.16
Event No.117

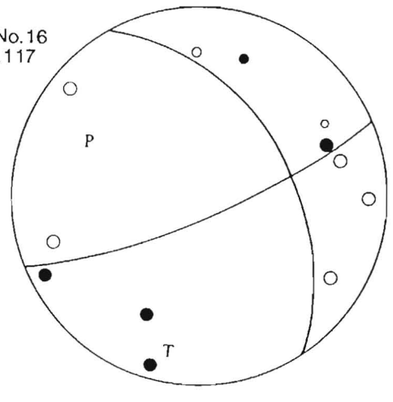

1990 10 9 10 56 19.62 sec -43.106 172.573 5.40 km 1.7

Solution No.17
Event No.118

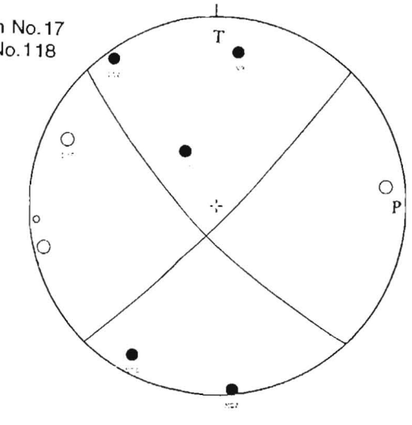

1990 10 10 7 56 16.90 sec -43.042 172.643 7.50 km 2.2

Solution No.18
Event No.119

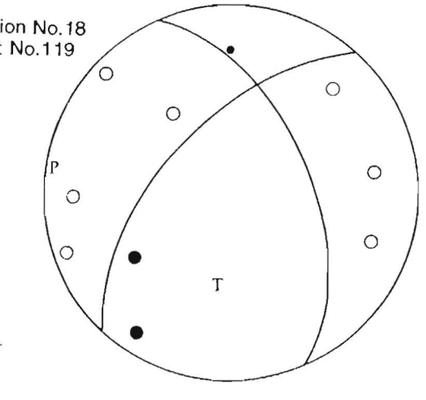

1990 10 10 8 42 58.73 sec -43.220 171.661 2.30 km 2.7

Solution No.19
Event No.120

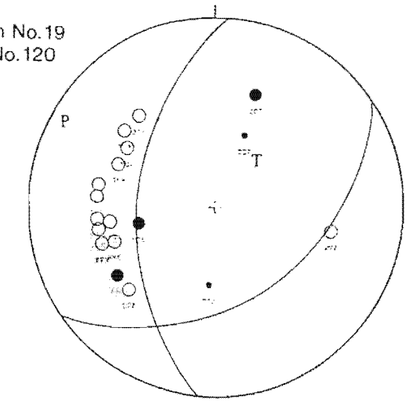

1990 10 10 15 36 5.87 sec -43.257 172.449 7.00 km 2.1

Solution No.20
Event No.123

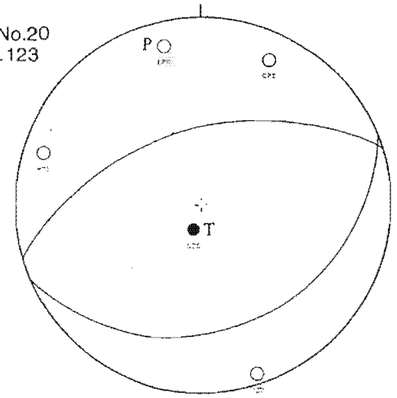

1990 10 10 18 31 59.81 sec -42.986 172.282 1.20 km 1.5

Solution No.21
Event No.124

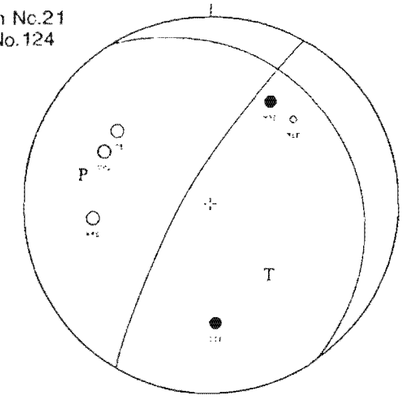

1990 10 18 9 56 38.98 sec -43.166 172.387 9.20 km 1.9

Solution No.22
Event No.139

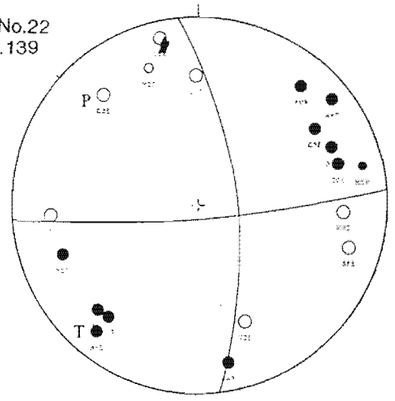

1990 10 28 13 11 4.74 sec -42.849 172.793 7.20 km 2.3

Solution No.23
Event No.149

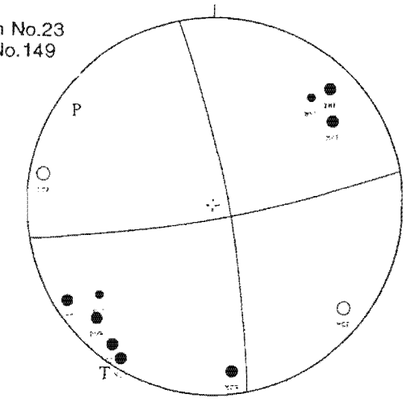

1990 10 31 7 30 40.50 sec -43.202 172.107 9.20 km 2.3

Solution No.24
Event No.155

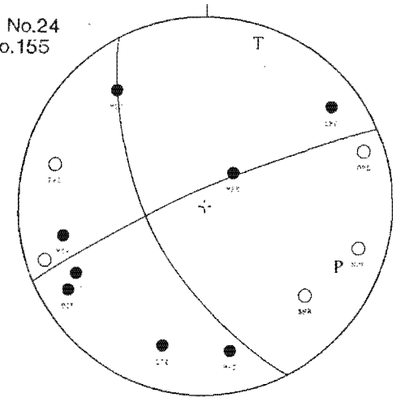

1990 11 2 9 21 42.87 sec -43.174 172.157 7.20 km 2.3

Solution No.25
Event No.173

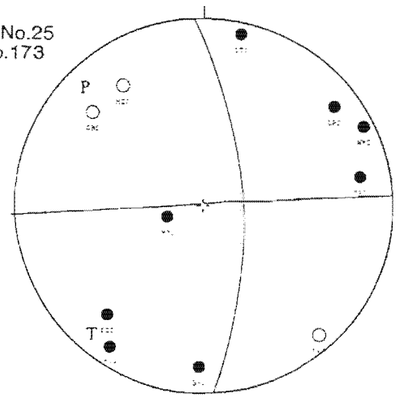

1990 11 9 15 50 1.21 sec -43.071 172.349 8.80 km 2.0

Solution No.26
Event No.192

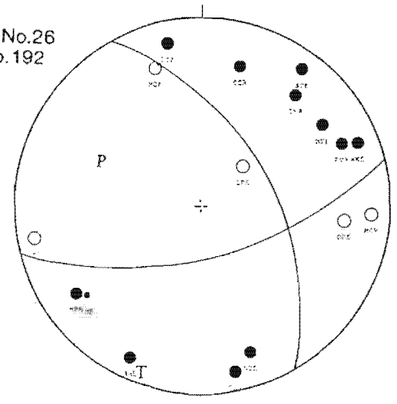

1990 11 9 23 31 47.97 sec -42.851 172.798 8.70 km 1.9

Solution No.27
Event No.196

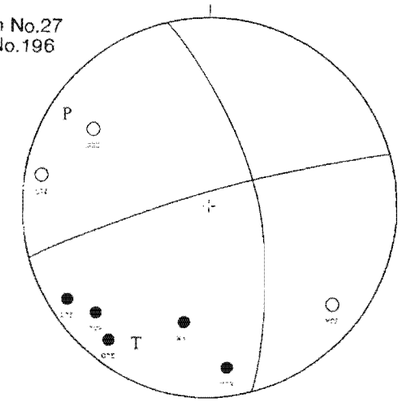

1990 11 12 9 54 11.61 sec -43.006 172.038 9.60 km 2.4

Solution No.28
Event No.201

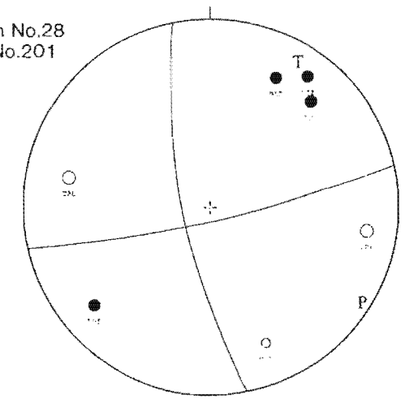

1990 11 12 9 58 31.24 sec -43.224 172.602 8.70 km 1.7

Solution No.29
Event No.202

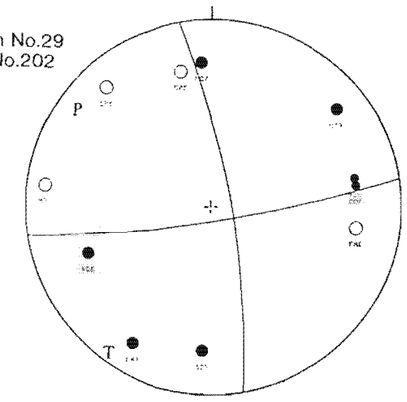

1990 11 14 3 24 58.60 sec -43.274 171.962 7.10 km 2.7

Solution No.30
Event No.209

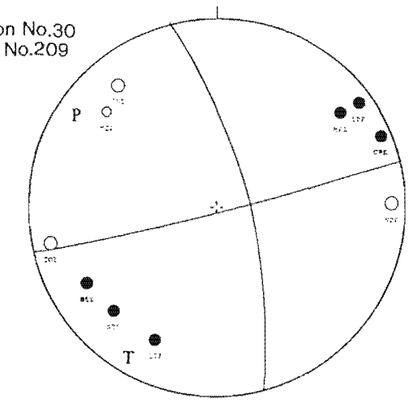

1990 9 4 17 34 12.69 sec -42.908 173.349 30.00 km 2.4

Solution No.31
Event No.004

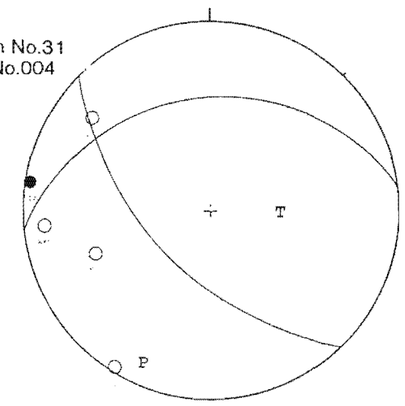

1990 9 7 22 21 41.62 sec -43.243 172.856 22.10 km 2.1

Solution No.32
Event No's.
010 and 011

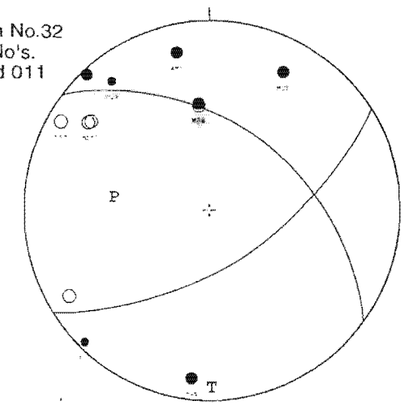

1990 9 9 6 45 52.96 sec -42.727 172.827 35.70 km 1.8

Solution No.33
Event No.027

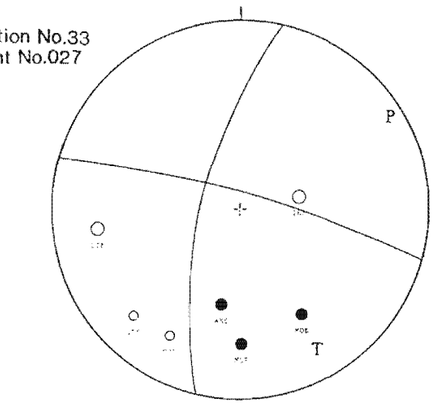

1990 9 11 7 27 46.02 sec -43.067 172.738 24.40 km 2.7

Solution No.34
Event No.058

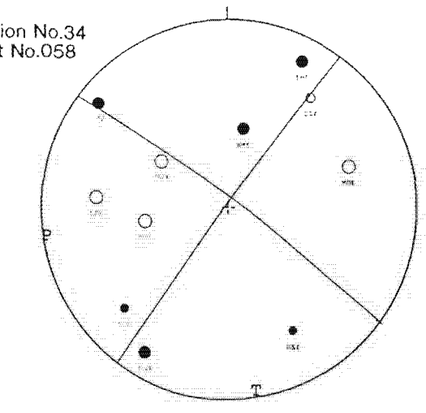

1990 9 12 7 24 19.84 sec -42.798 173.157 26.50 km 2.0

Solution No.35
Event No.063

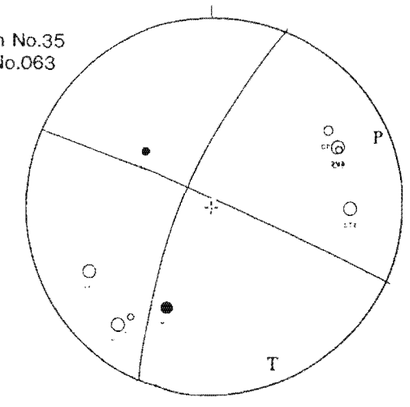

1990 9 26 0 54 9.68 sec -43.173 172.497 23.80 km 1.7

Solution No.36
Event No.097

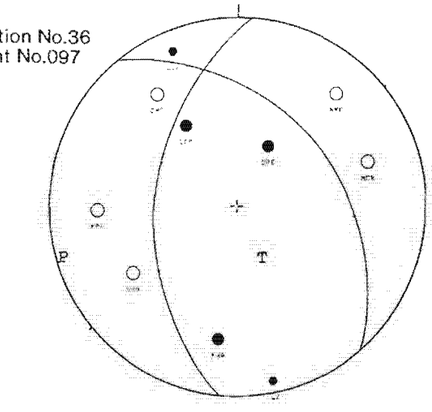

1990 9 30 8 12 17.86 sec -43.462 172.875 18.20 km 2.0

Solution No.37
Event No.102

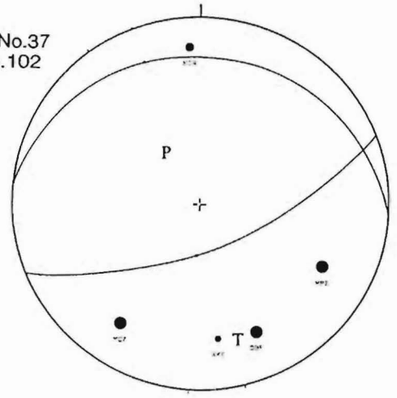

1990 10 1 17 52 4.50 sec -42.735 172.811 22.60 km 2.5

Solution No.38
Event No.107

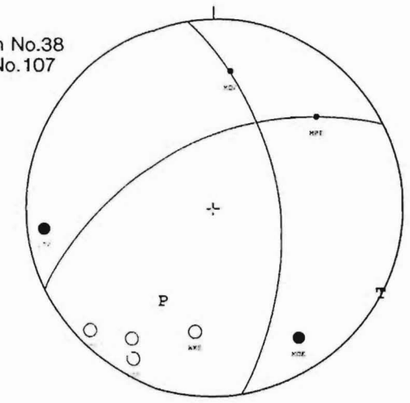

1990 10 11 22 32 51.41 sec -42.845 173.040 32.80 km 2.2

Solution No.39
Event No.128

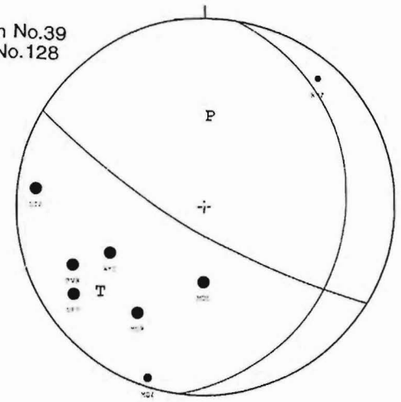

1990 10 12 11 19 53.85 sec -43.022 173.416 19.40 km 2.4

Solution No.40
Event No.129

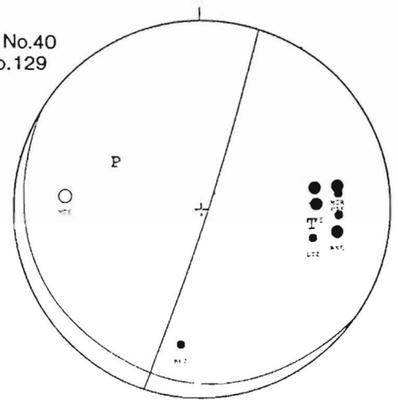

1990 10 12 14 0 50.20 sec -42.937 173.010 25.30 km 1.7

Solution No.41
Event No.130

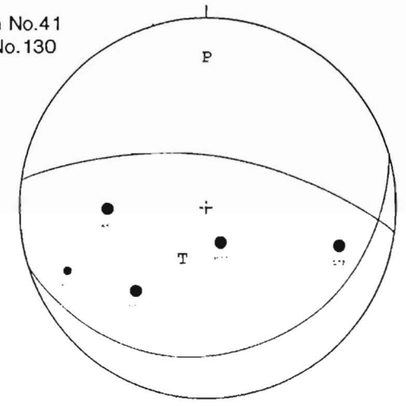

1990 10 13 12 41 28.48 sec -43.240 172.849 26.20 km 2.2

Solution No.42
Event No's.
131 and 132

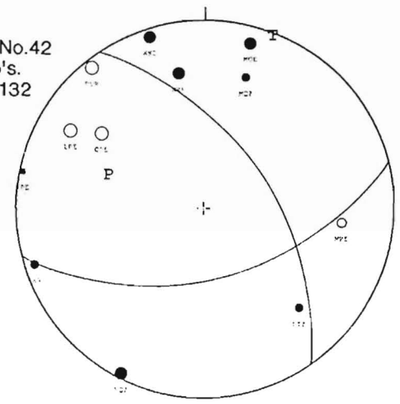

1990 10 13 14 28 57.87 sec -43.373 172.393 19.60 km 1.9

Solution No.43
Event No.133

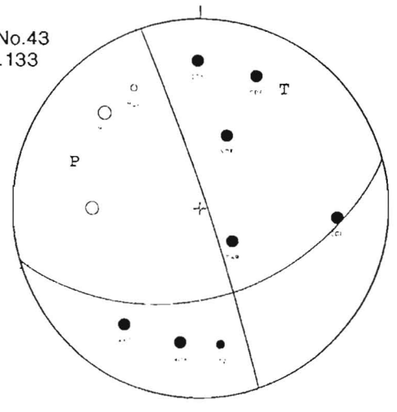

1990 10 18 21 48 34.85 sec -42.594 173.185 41.60 km 2.2

Solution No.44
Event No.141

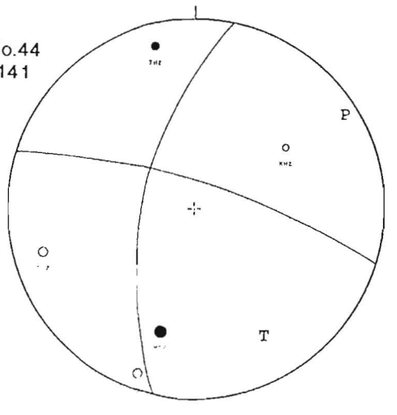

1990 11 2 10 32 11.03 sec -42.606 172.857 34.00 km 2.6

Solution No.45
Event No's.

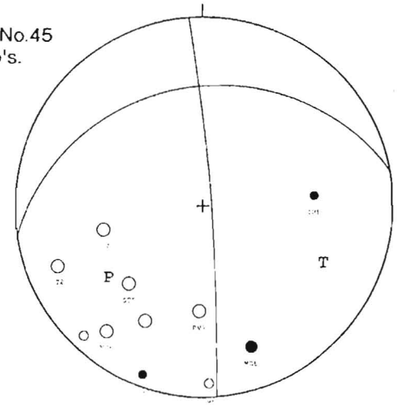

1990 11 7 18 39 47.51 sec -42.842 173.063 32.20 km 2.2

Solution No.46
Event No's.
179 and 190

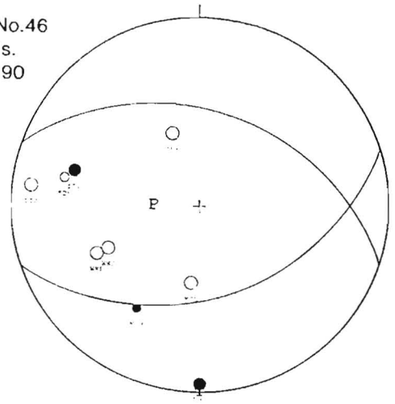

1990 11 7 9 4 7.48 sec -42.751 172.380 17.00 km 2.7

Solution No.47
Event No.189

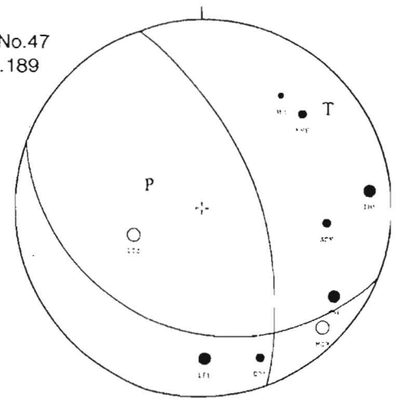

1990 11 9 23 52 43.74 sec -43.001 173.427 21.70 km 2.5

Solution No.48
Event No.197

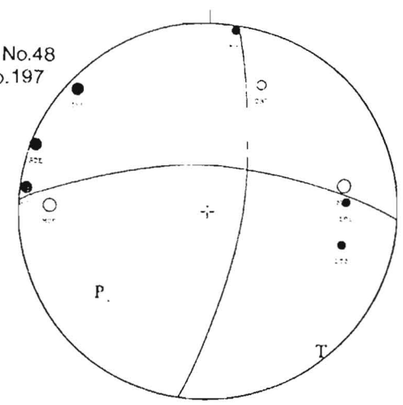

1990 11 15 12 42 47.05 sec -43.027 172.347 26.40 km 1.9

Solution No.49
Event No's.
212 and 213

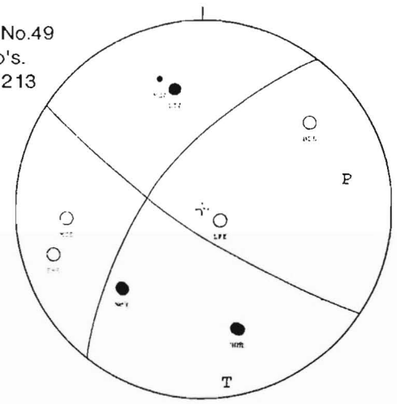

APPENDIX: 5.1 Historic earthquakes associated with rock slides in northern South Island compiled for least-squares regression (Mendenhall, 1975) of landslide area ($log_{10}km^2$) on magnitude revised after Adams (1981).

Earthquake	Area of landslides (km^2)	Magnitude (M_s)[1]
May, 1968 [2] Inangahua	350	7.4
June, 1929 [3] Buller	3600	7.8
March, 1929 [4] Arthurs Pass	180	7.1

(1) Surface wave magnitudes from Dowrick & Smith (1990)
(2) Adams et al. (1968)
(4) Henderson (1937); Adams (1981)
(4) Speight (1933)

Log Area (Xi)	Magnitude (Yi)	XiYi	Xi^2	Yi^2
2.54	7.4	18.796	6.45	54.76
3.55	7.8	27.690	12.60	60.84
2.25	7.1	15.975	5.06	50.41
$\Sigma Xi = 8.34$	$\Sigma Yi = 22.3$	$\Sigma XiYi = 62.461$	$\Sigma Xi^2 = 24.11$	$\Sigma Yi^2 = 166.01$
$\bar{x} = 2.78$	$\bar{y} = 7.43$			

$$Ssx = \sum_{i=1}^{n} Xi^2 - \frac{(\sum_{i=1}^{n} Xi)^2}{n} \rightarrow SSx = 0.9248$$

$$SSxy = \sum_{i=1}^{n} Xiyi - \frac{(\sum_{i=1}^{n} xi)(\sum_{i=1}^{n} yi)}{n} \rightarrow SSxy = 0.469$$

Slope of least squares line $\hat{\beta} = \frac{SSxy}{SSx} = 0.51$

y intercept of least squares line $\hat{\beta}_o = \bar{y} - \hat{\beta}_1 \bar{x} = 6.03$

least squares line $= \hat{y} = \hat{\beta}_o + \hat{\beta}_1 X \rightarrow M = 6.03 + 0.51$ (log area)

Coefficient of Determination

$$r^2 = \frac{SSy - SSE}{SSy} = \frac{\Sigma(Yi - \bar{y})^2 - SSE}{\Sigma (Yi - \bar{y})^2}$$

$$SSy = \sum_{i=1}^{n} yi^2 - \frac{(\sum_{i=1}^{n} Yi)^2}{n} \rightarrow SSy = 0.2466$$

$$SSE = SSy - \hat{\beta}_1 SSxy \rightarrow SSE = 0.0131$$

$$r^2 = \frac{SSy - SSE}{SSy} \rightarrow r^2 = 0.95$$

APPENDIX 5.2. DERIVATION OF SEISMICITY MODEL PARAMETERS FOR THE PORTER'S PASS-AMBERLEY FAULT ZONE

Introduction

The PPAFZ has been characterised historically by frequent small to moderate-magnitude (M<6.5) earthquakes (Reyners, 1989), but no large (M>7.0) earthquakes. Thus, probabilistic models of earthquake recurrence-frequency based on historic seismicity are dominated by the large number of small events in the catalogue, and it is difficult to assess the validity of the assumption that large earthquake magnitudes are exponentially distributed within the zone.

Exponential magnitude distribution

The classical form of the Gutenburg-Richter exponential frequency-magnitude relationship is given by Richter (1958) as:

$$\log N(m) = a - bm \qquad (1)$$

where N is the cumulative number of earthquakes of magnitude greater than or equal to m; a is the seismicity rate and b defines the exponential decay with increasing magnitude. Equation (1) may be integrated to obtain a cumulative exponential distribution, truncated at a maximum magnitude for a given set of faults or volume of crust, such that:

$$N = N_o[10^{b(Mo - M)} - 10^{b(Mo - Mmax)}] \qquad (2)$$

N_o is the number of earthquakes of magnitude Mo or greater, where Mo is an arbitrary threshold magnitude. By defining parameter a_4 to be the annual number of earthquakes of magnitude M≥4 in an area 1000 km^2, equation 2 becomes:

$$N = a_4\,[10^{b(4 - M)} - 10^{b(4 - Mmax)}] \qquad (3)$$

Porter's Pass-Amberley Fault Zone Seismicity Model

Elder et al. (1991) developed a seismicity model for analysis of seismic hazard in Christchurch, based on a detailed subdivision of North Canterbury. Their Porter's Pass Tectonic Zone (PPT: in Figure below) encompasses an area of 5.08 x 10^3 km^2, including the area mapped in this study. Parameters of the (PPT) zone, seismicity model (data supplied by the N.Z. Seismological Observatory) are as follows:

M≥3 1964-1988	M≥4 1964-1988	M≥5 1964-1988	M≥6 1848-1989	M≥6.5 1848-1989	Mmax b a4
N3 94 N3/At 0.74	N4 28 N4/At 0.22	N5 6 N5/At 0.047	N6 2 N6/At 0.0028	N6.5 0 ----	7.5 0.8 0.3

In Chapter 5, landslides and surface rupture are interpreted as evidence of two large prehistoric earthquakes (M~7.5) in the PPAFZ during the last 2500 years. These data are compared with historic seismicity, for b-values of 0.8 and 1.0, using the model parameters tabulated above (see Chapter 5: Section 5.6.2).